University of Southampton

Faculty of Medicine

Clinical and Experimental Sciences

Characterisation Of The Human Microglial Profile Identified With Translocator Protein (TSPO) And Its Role In The Pathophysiology And Progression Of Alzheimer's Disease

by

Emma Garland

ORCID ID: 0000-0002-8501-4326

Thesis for the degree of Doctor of Philosophy in Clinical Neurosciences

February 2024

University of Southampton

Abstract

Faculty of Medicine

Clinical and Experimental Sciences

Doctor of Philosophy in Clinical Neurosciences

Characterisation Of The Human Microglial Profile Identified With Translocator Protein (TSPO) And Its Role In The Pathophysiology And Progression Of Alzheimer's Disease

By

Emma Garland

Neuroinflammation is one of the pathological hallmarks of Alzheimer's disease (AD). Microglia are the main immune cell in the central nervous system and contribute to the development and severity of AD pathology. The need for novel methods to study reactive microglia are of the utmost importance, with accurate positron emission tomography (PET) methods becoming prevalent. Translocator protein (TSPO), expressed on microglial mitochondria, has been attributed to microglial reactivity and is commonly used as a PET ligand for this reason. However, clinicians' interpretation of this ligand is somewhat conflicting as it is not known which functional or morphological subtypes of microglia are being identified. Therefore, this project aims to characterise which microglia TSPO identifies, and its importance in the context of AD. Furthermore, the cerebellum is used as a pseudo-reference region for PET scans in AD and this will be compared to the temporal lobe, an area of high AD pathology, to assess whether the cerebellum is appropriate to use for baseline measurements.

Sixty cases from temporal lobe and cerebellum, split equally into three Braak groups (stages 0-II, stages III-IV and stages V-VI), were used for immunohistochemistry to assess TSPO expression, AD pathology (Aβ, hyperphosphorylated (p)Tau) and neuroinflammation (Iba1, HLA-DR and MSR-A), with half of the cases used for fluorescent double labelling of TSPO with microglial markers (Iba1, HLA-DR, CD68, MSR-A and CD64), astrocytes (GFAP), perivascular macrophages (CD163) and endothelial cells (CD31). Multiplex assays for thirty inflammatory proteins were performed to evaluate the neuroinflammatory microenvironment.

As expected, Aβ, pTau and TSPO load increased as the disease progressed in the temporal lobe. In the cerebellum, Iba1, a marker of microglial motility, was significantly increased as AD progressed. There was a positive association found between TSPO and pTau in the temporal lobe. The inflammatory microenvironment showed increased IL15 only in the temporal lobe. The double fluorescent staining showed no significant change in cell count over the course of the disease for each individual set of double labelling in either brain region. However, when comparing the double labelling cell counts, the highest in both brain regions was $CD68^{+}TSPO^{+}$. Double staining with non-microglial markers displayed the absence of TSPO expression by astrocytes and perivascular macrophages, with some endothelial cells expressing TSPO.

Overall, these findings suggest that TSPO expression may be related to a reactive/phagocytic phenotype with the higher expression in the more pathologically affected temporal lobe. The cerebellum exhibited a homeostatic environment with low levels of AD pathology, consistent lower TSPO expression, and presence of homeostatic microglia, meaning that this region remains appropriate to use as a pseudo-reference region for TSPO PET scans. Of note, the phagocytic profile of TSPO appeared to not be affected by disease stage or brain region.

Table of Contents

Contents

Table of Figures

Table of Figures

Table of Tables

Table of Tables

List of Accompanying Materials

Research Thesis: Declaration of Authorship

Print name: Emma Garland

Title of thesis: Characterisation Of The Human Microglial Profile Identified With Translocator Protein (TSPO) And Its Role In The Pathophysiology And Progression Of Alzheimer's Disease

I declare that this thesis and the work presented in it are my own and has been generated by me as the result of my own original research.

I confirm that:

1. This work was done wholly or mainly while in candidature for a research degree at this University;
2. Where any part of this thesis has previously been submitted for a degree or any other qualification at this University or any other institution, this has been clearly stated;
3. Where I have consulted the published work of others, this is always clearly attributed;
4. Where I have quoted from the work of others, the source is always given. With the exception of such quotations, this thesis is entirely my own work;
5. I have acknowledged all main sources of help;
6. Where the thesis is based on work done by myself jointly with others, I have made clear exactly what was done by others and what I have contributed myself;
7. Parts of this work have been published as:-

Garland EF, Hartnell IJ, Boche D. Microglia and Astrocyte Function and Communication: What Do We Know in Humans? Front Neurosci. 2022;16:824888

Garland EF, Dennett O, Lau LC, Chatelet DS, Bottlaender M, Nicoll JAR, and Boche D. The mitochondrial protein TSPO in Alzheimer's disease: relation to the severity of AD pathology and the neuroinflammatory environment. J Neuroinflammation. 2023;20(1):186.

Signature: ..... Date: 15/12/2023

Acknowledgements

Firstly, I would like to thank my supervisors Prof. Delphine Boche and Prof. James Nicoll for their support and guidance throughout my PhD. Their extensive knowledge has helped shape not only my research, but me as a scientist. Thank you also to our collaborator, Michel Bottlaender, for his expertise on TSPO.

I would also like to thank members of the Histochemistry Research Unit: Jon Ward and Jenny Norman for their knowledge on immunohistochemistry and their patience over my many questions. A big thank you to the Biomedical Imaging Unit members Dave Johnston, David Chatelet, Regan Doherty and Patricia Goggin for their help with all thing's microscopy and imaging. Thank you to Laurie Lau for his help with the mesoscale experiments.

I would not have been able to complete my PhD without my friends and family, especially my parents who have always pushed me to be the best I can be whilst giving me all the support I could need. I am very grateful to have a brother and sister who have believed in me from the beginning. To my best friend, Katie, thank you for always being there for me and for making me laugh when I needed it most; I couldn't have done this PhD without you. To my partner, James, thank you for your unwavering support and allowing me to vent to you about experiments not working. You never fail to make me feel better when I am stressed, which was a lot of the time when writing this thesis. To my friends from LD30 and B85, thank you for being amazing people and for all the help/procrastination time you have given me (including our debates on which animal would win in the Kelly-Brown-Kelly arena). Thank you to my longest friends from home, you have kept me sane and given me a reprieve from always talking about brains. To the students I have supervised on this project: Oliver, Laura, Henrike, Tom and Charlotte; I thoroughly enjoyed working together and you all added a great deal to the work in this thesis, thank you. Thank you to Iain Hartnell for all his help and for writing our review together.

Finally, I would like to show my appreciation to my funders, Alzheimer's Research UK, the tissue donors and their families, without whom this research would not have been possible.

Publications, Presentations and Conferences

Publications

- Garland EF, Hartnell IJ and Boche D. Microglia and Astrocyte Function and Communication: What do we know in humans? Front Neurosci. 2022;16:824888
- Garland EF, Dennett O, Lau LC, Chatelet DS, Bottlaender M, Nicoll JAR, and Boche D. The mitochondrial protein TSPO in Alzheimer's disease: relation to the severity of AD pathology and the neuroinflammatory environment. J Neuroinflammation. 2023;20(1):186.
- In preparation: Garland EF, Kulagowska L, Scott T, Antony H, Rogien C, Bottlaender M, Nicoll JAR, and Boche D.

Internal presentations

- Oral presentation at the Southampton Neuroscience Research Group (Southampton, UK), 5th May 2022.
- Oral presentation at the Southampton Neuroscience Research Group (Southampton, UK), 12th Jan 2023.
- Oral presentation at the Southampton Neuroscience Research Group (Southampton, UK), 30th Nov 2023.

Conferences

- Poster presentation at Alzheimer's Research UK (Brighton, UK), 28th Feb 2022.
- Oral presentation at the British Neuropathological Society (Online), 17th March 2022.
- Poster presentation at the Alzheimer's Association International Conference (San Diego, USA), 1st August 2022.
- Flash talk and poster presentation at the British Neuropathological Society (London, UK), 2nd March 2023.
- Oral presentation and poster presentation at Alzheimer's research UK (Aberdeen, UK), 14th March 2023.
- Poster presentation at the Alzheimer's Association International Conference (Amsterdam, NL), 17th July 2023.

Definitions and Abbreviations

Aβ..... Amyloid beta

AChE..... Acetylcholinesterase

AD ..... Alzheimer's disease

APP..... Amyloid precursor protein

APOE ..... Apolipoprotein E

ARIA..... Amyloid-related imaging abnormalities

BBB..... Blood-brain-barrier

BCA..... Bicinchoninic acid

BDNF ..... Brain-derived neurotrophic factor

BSA..... Bovine serum albumin

CAA..... Cerebral amyloid angiopathy

CB2R..... Cannabinoid receptor type 2

CD..... Cluster of differentiation

CNS..... Central nervous system

CSF ..... Cerebrospinal fluid

CSF1R ..... Colony-stimulating factor 1 receptor

CXC3R1..... C-X3-C motif chemokine receptor 1

DAM ..... Disease associated microglia

EOAD..... Early onset Alzheimer's disease

FACS ..... fluorescence-activated cell sorting

FITC ..... Fluorescein isothiocyanate

GFAP..... Glial fibrillary acidic protein

GWAS ..... Genome wide association studies

HD ..... Huntington's disease

HAB ..... High affinity binder

HLA..... Human leukocyte antigen

HRP..... Horseradish peroxidase

Iba1 ..... Ionized calcium binding adapter molecule 1

IL ..... Interleukin

LAB ..... Low affinity binders

LOX..... Lysyl oxidase

LPS..... Lipopolysaccharide

MAB ..... Mixed affinity binders

MCI..... Mild cognitive impairment

MDC ..... Macrophage derived chemokine

MGnD ..... Microglia associated with neurodegenerative disease

MRI..... Magnetic resonance imaging

MS ..... Multiple sclerosis

MSD..... Mesoscale discovery

MSR-A ..... Macrophage scavenging receptor-A

MMSE..... Mini-mental state exam

NADPH..... Nicotinamide adenine dinucleotide phosphate

NfL..... Neurofilament light

NFT..... neurofibrillary tangle

NMDA..... N-methyl-D-aspartate

NMR ..... Nuclear magnetic resonance spectroscopy

PBR..... Peripheral benzodiazepine receptor

PD..... Parkinson's disease

PECAM..... platelet endothelial cell adhesion molecule

PET ..... Positron emission tomography

P2RX7 ..... Purinergic receptor P2X7

P2RY12 ..... Purinergic receptor P2Y12

ROS..... Reactive oxygen species

SMA..... Smooth muscle actin

SNP ..... Single nucleotide polymorphism

SPM ..... Specialized pro-resolving lipid mediators

SUV ..... Standardized uptake value

TBI ..... Traumatic brain injury

TLR ..... Toll-like receptor

TMEM119 ..... Transmembrane protein 119

TNF ..... Tumour necrosis factor

TREM2 ..... Triggering receptor expressed on myeloid cells 2

TSPO ..... Translocator protein

Chapter 1 Introduction

1.1 Alzheimer's disease

1.1.1 Overview

Neurodegenerative diseases are characterised by the progressive worsening of symptoms. Alzheimer's disease (AD) is one such disease, which primarily affects people aged 65 years and over and impacts a range of cognitive abilities, notably memory (1). Due to the ageing population, the prevalence of AD is increasing with over 55 million people living with the disease worldwide as of 2020 (2). The disease was first discovered in 1906 by Alois Alzheimer (3) and since then the characteristics and neuropathology of AD have been explored in greater detail. The main pathologies used to define the disease by histology are extracellular amyloid beta (Aβ) plaques (4), intracellular tau tangles and neuropil threads (4). These pathological proteins cause neurons to become dysfunctional leading to neuronal death, cortical atrophy and cognitive decline. There are many other factors that have an impact in AD, which will be discussed further in this introduction.

As mentioned, Aβ plaques and tau tangles are hallmarks of the disease with neuronal death/brain atrophy and neuroinflammation also included in this category. As AD is primarily a grey matter disease (5), the hallmark proteins are found at higher levels in this area. Aβ forms when its precursor, amyloid precursor protein (APP) is cleaved (6). A theory that has been accepted as the primary cause of AD for many years, is known as the amyloid cascade hypothesis. This states that Aβ is the main causative protein of the disease as it is seen to accumulate first (6). Neurofibrillary tangles, brain atrophy and cell loss are all secondary and a consequence of this (6). Following on from the proposal of this theory, there has been supporting evidence in the form of APP transgenic mouse models, which have been somewhat successful in replicating AD symptoms (7). However, these models only express the disease form of Aβ and do not include tau or any other hallmark. Clinical trials that target Aβ with the aim to remove the protein, have been somewhat unsuccessful in reducing symptoms of AD despite effectively removing Aβ (8, 9). Therefore, this protein cannot be the sole cause of the disease. On the other hand, there is mounting evidence that the tau protein is equally important in causing AD. Braak staging is a way of tracking the progression of tau spread and suggests that it is the tau tangles that contribute heavily to the symptoms of AD (10). When tau becomes hyperphosphorylated it creates neurofibrillary tangles which can inhibit the binding of microtubules

within neurons, thus impacting transport along the axon, leading to neuronal dysfunction and death (11). Another key hallmark of AD is neuroinflammation. This aspect of the pathology has come to the forefront of AD research in recent years and is thought to play a significant role in aiding the disease severity. Cells such as microglia, the resident immune cell of the brain, and astrocytes are involved in the pathogenesis of AD, but their exact role in the disease is not fully understood. Although, it has been postulated that they may become dysfunctional or unable to cope with the pathological protein load present in AD, which has been discovered through methods such as positron emission tomography (PET) (12, 13) and genome wide association studies (GWAS) (14). The idea that chronic neuroinflammation plays a major role in the pathogenesis of AD will be the focus of this thesis.

Another aspect of AD pathogenesis that is now thought to be important is the role of mitochondrial dysfunction. Mitochondria are responsible for biochemical processes e.g., respiration needed for cellular functioning. In disease, these organelles can undergo several changes both morphologically and functionally that affect their performance. For example, excessive reactive oxygen species (ROS) accumulation has been seen in AD due to electron transport chain disruption (15) and can cause inhibition of kinases related to tau phosphorylation (16). Deficits in ATP production contribute to disrupted cell dynamics (17), and mitochondrial mitophagy is not as efficient resulting in higher levels of damaged mitochondria (17). As the brain requires the highest amount of energy of any organ in the body (20% of the metabolic energy daily) (18), with neurons and glia contributing to this extremely high energy burden, the effect of mitochondrial dysfunction is a significant detriment and may be a key feature of neurodegenerative disease.

It is also important to consider sex differences when studying AD, as not only is the frequency of the disease is regularly reported to be higher in females than males (19), but the risk of developing AD is also higher in females than males (21.1% vs 11.6% respectively, at the age of 65) (20). This may owe to a plethora of reasons, including longer life span in females (~4.5 years longer than males) (21) and other more mechanistic differences. For example, brain structure differs between sexes with males having larger ventral temporal and occipital lobes and females have increased volume in their prefrontal and superior parietal cortices (22). There are also hormonal differences, with the female hormone oestrogen currently thought one of the contributing factors for the sex difference in AD. During menopause, when oestrogen levels are lowered, this could initiate the development of AD due to this hormone's ability to regulate synaptic plasticity (19). Studies in both mice and humans have shown that replacement of oestrogen have lowered the levels of AD pathology and decreased the risk of developing the disease (23, 24).

1.1.2 Risk factors

The main risk factor for AD is ageing (1) but there are several other contributing factors such as genetics, repetitive traumatic brain injuries (TBI) (25), hearing loss, pollution and diabetes (26) (**Figure 1**). The genetic risk of AD is relatively low but certain genes can increase the risk of developing the disease. Apolipoprotein E (APOE) is a gene that has been highly studied in regard to AD with different allele variations contributing to the risk of developing the disease. This protein aids the transport of lipids in the body and within the central nervous system (CNS) it is mainly produced by astrocytic cells (27). The APOE ε4 allele contributes significantly to an increased genetic risk of developing AD, and having two copies of this allele may increase the risk twelve fold (28). Whereas APOE ε2 seems to provide a protective quality (28). This may be due to the lipid binding properties of the different alleles. For example, APOE ε4 preferentially binds to low density lipoproteins which reduces its stability, whereas the more protective APOE ε2 and neutral APOE ε3 preferentially bind to high density lipoproteins (29). The most common allele is the APOE ε3 variant (30). APOE ε4 could potentially hinder microglial cells by disrupting their lipid metabolism and ability to respond to neuronal activity (31). Recently, APOE ε4 carriers have been found to have an increased microglial reactivity in early stage disease, which correlated to increased Aβ and tau presence (32). Another genetic risk factor for AD is associated with microglial function and is attributed to the triggering receptor expressed on myeloid cells 2 (TREM2) microglial protein. TREM2 is a receptor that may aid in microglial phagocytosis, motility, cytokine production and proliferation (33). A loss of function mutation in this gene, termed R47H, has been proven to be linked to higher risk of AD in large cohort analysis (34, 35). However, much of the research conducted has used animal models. When TREM2 has been examined in human *post-mortem* tissue, the cells that express the protein are mostly monocytes (36), therefore making its importance in microglial function questionable.

In terms of 'modifiable risk factors' (i.e., risk factors that can be reduced via external sources) there are several that have a fairly high risk at different points in life. In early life, less education is a contributing factor (**Figure 1**), and this primarily affects low-and-middle income countries. This could be due to education providing increased cognitive stimulation, which is beneficial in reducing the risk of dementia (26, 37). In midlife, the largest risk factor is hearing loss (26) (**Figure 1**). Interestingly, a study using cognitively normal patients found that hearing impairment in midlife was associated with reduction in temporal lobe volume (38), which is a factor of AD. However, this study did not look extensively into cognitive decline but did find that 6.7% of patients had some sort of cognitive impairment after 19.5 years (38). The second highest modifiable risk factor at this time point is TBIs (26) (**Figure 1**). TBIs are most common in athletes such as rugby players, American football players and boxers but can also occur in the general population, where concussion or other head injuries (e.g., bleeds) have taken place. One TBI event is enough to cause extensive tau pathology, reactive

astrocytes, and amyloid plaques in humans (39). In later life, the highest risk factor is smoking (**Figure 1**). However, an interesting component for greater risk of AD is co-morbidity with diabetes (**Figure 1**). In fact, the correlation between imbalanced blood sugar and AD appears to be strong enough that some researchers refer to AD as type 3 diabetes (40, 41). There is an overlap between pathological features of diabetes and AD, with amyloid deposits being a large factor in both (42).

There is a variant of AD, termed 'early-onset Alzheimer's disease' (EOAD) which has a significant genetic component, with APP, presenilin 1 (PSEN1) and presenilin 2 (PSEN2) contributing to the earlier inception of the disease (28), causing age of onset between 30-65 (43). Having one or both copies of APOE ε4 has also been shown to lower the age of onset (44), but to a lesser extent than the aforementioned genes. There are many types of mutations in these genes that contribute to onset of EOAD. These include missense mutations, locus duplications and mutations in different domains of the gene (45). Only around 10% of AD patients are diagnosed with EOAD (45) and these patients share the same pathological hallmarks as late-onset AD. However, some research has shown a higher quantity of Aβ and tau in younger EOAD patients with both neuritic plaques and neurofibrillary tangles being increased in early onset compared to late onset AD (46). Additionally, the course of EOAD seems to have a faster progression than late onset AD (47), which, in conjunction with the increased hallmark proteins, suggests a more aggressive pathophysiology. The genetic component of EOAD is incredibly high with heritability around 92-100% in an autosomal recessive manner (48).

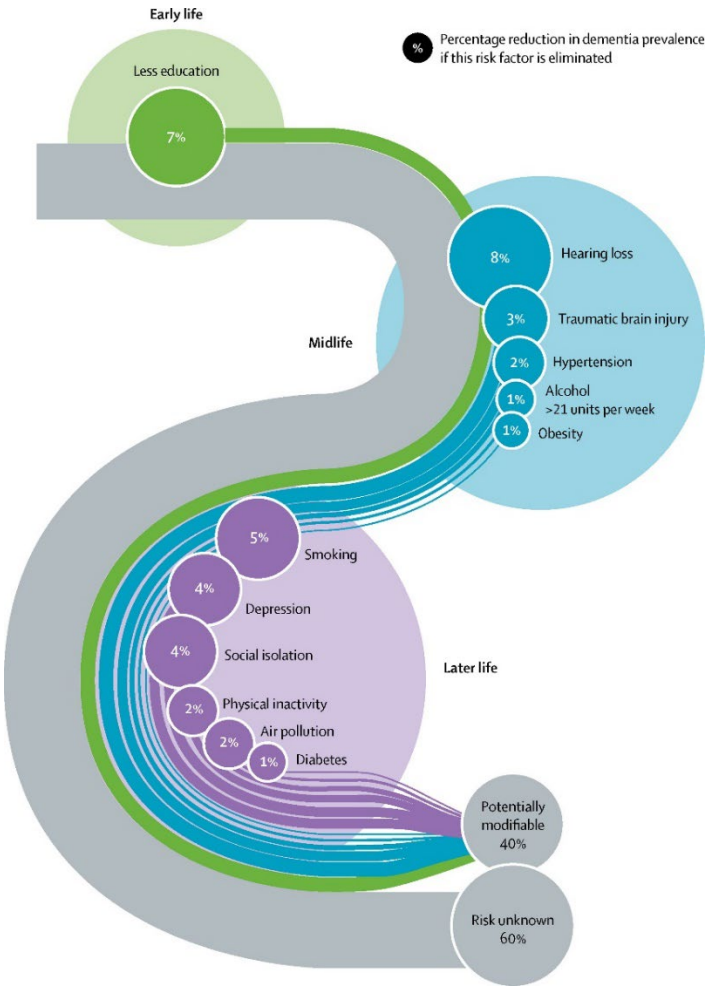

Figure 1 Diagram depicting potentially modifiable risk factors for AD at different life points and the percentage reduction of that risk if it was eliminated. Taken with permission from Livingston et al, Lancet (2020).

1.1.3 Diagnosis

There is evidence that the neuropathological markers of AD start to occur many years before any symptoms appear (49). This means that there is a great need for diagnostic tools that detect these biomarkers early in the disease progression in order to try and prevent as much damage as possible. Currently, the most common cognitive assessment used is a patient-based questionnaire that focuses on cognitive questions and memory tasks called a mini-mental state exam (MMSE) (50). The MMSE will often be used in conjunction with other investigative tests to aid in the accuracy of the diagnosis. One such test could be magnetic resonance imaging (MRI) scans. Cortical atrophy due to neuronal loss, particularly in the hippocampus, can be seen with MRI scans, which is a significant feature of AD (51). However, this characteristic is also shared by a range of other disorders, such as multiple sclerosis (MS) (52) and ischemic stroke (53), making this test inconclusive and further investigation

would be needed to give a definitive diagnosis of AD. An MRI test is usually used to rule out any other conditions rather than diagnose AD.

There have been recent developments in more accurate and reliable diagnostic methods for detecting levels of pathological proteins Aβ and pTau in the cerebrospinal fluid (CSF) (54, 55). CSF biomarkers are also being developed to target neuroinflammation. One such marker, YKL-40, is released by microglia and astrocytes (56) and has been shown, along with other glial markers, to be increased in AD (57). The same markers, including YKL-40, ICAM1, and VCAM1 were associated with pTau (57). This provides good evidence for inflammatory markers being reliable in a diagnostic capacity for AD. While CSF biomarkers are promising in their accuracy, the procedure is invasive and time consuming. Therefore, blood-based biomarkers have been postulated as an easier and less invasive method of detecting these proteins. It has been shown that ptau181, neurofilament light (NfL) and Aβ42/40 plasma markers were increased in AD compared to controls (58). Also, ptau181 appeared to have the best clinical performance and could be detected successfully in mild cognitive impairment (MCI) patients also (58). It is postulated that using a combination of markers for Aβ, pTau and inflammation could provide the most accurate diagnostic outcome for patients (59). Again, neuroinflammatory markers have also been developed using plasma. Using trophic factors such as brain-derived neurotrophic factor (BDNF) to identify neuronal injury, a meta-analysis of fifteen studies showed reduced serum levels of BDNF in AD (60) with increased levels of this trophic factor having a positive correlation with cognition and decreased risk of developing AD (61). Furthermore, an increase in astrocytic glial fibrillary acidic protein (GFAP) marker was seen in early onset AD individuals (58, 62). However, markers for inflammation such as tumour necrosis factor (TNF)-α and IL6 were not increased (58, 62). This is a surprising result as other research has shown and elevation in these molecules in AD (63). A downside of using blood-based biomarkers is the blood plasma does not come into direct contact with the CNS, due to the blood brain barrier (BBB), making this type of biomarker a less reliable tool for diagnosis. More work is being conducted to increase the efficacy of blood based biomarkers for AD, with promising results.

Currently, the only way to accurately diagnose AD is via *post-mortem* analysis. Immunohistochemical methods are used for Aβ to look at Thal phasing which shows the severity of spread of this protein. The progression starts in the neocortex, moving through the allocortex and the limbic system, spreading through the brainstem and finally there may be low levels of Aβ present in the cerebellum at the very last stages (64) (**Figure 2**). Also, as mentioned in Section **1.1.1**, Braak staging is used to analyse tau progression in a similar way. However, the pattern of spread is different from Thal staging. Tau spread starts in the entorhinal area, then spreads to the limbic region and finally the cortical area (10) (**Figure 2**). Often these two methods of AD diagnosis will be combined to make the 'ABC' score (65). 'A' stands for Amyloid and uses the Thal staging score. 'B' stands for Braak and uses

the tau progression score. Finally, 'C' stands for CERAD which is a measure of neuritic plaques (65, 66). A plaque is termed neuritic when it has a core of Aβ surrounded by degenerating neurites and possible immune cells such as microglia (67). Non-neuritic plaques are considered diffuse when they don't have these features and are typically associated with normal ageing.

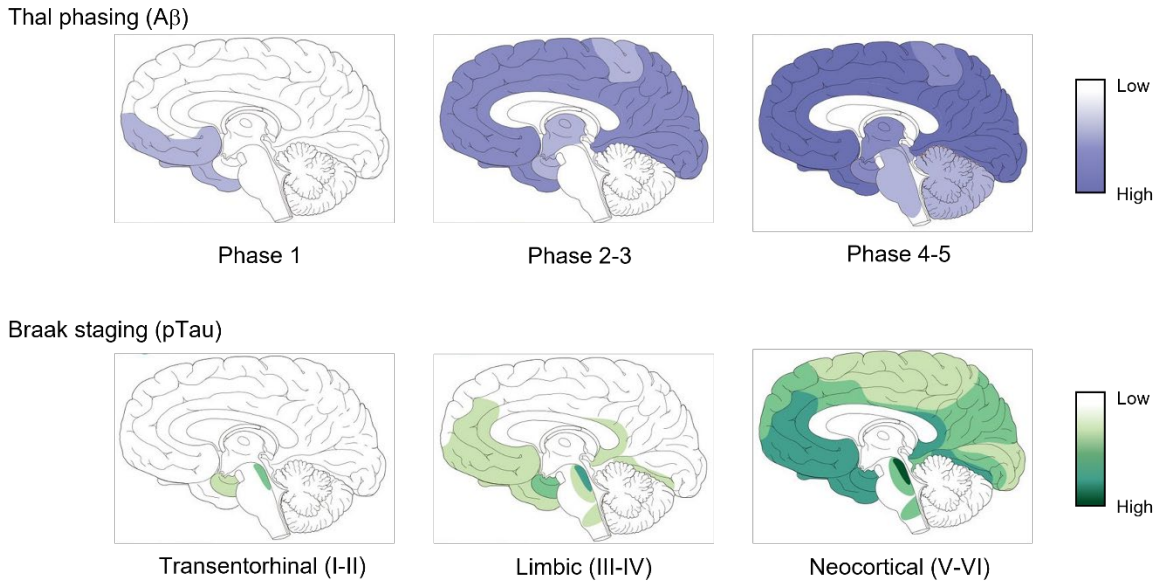

Figure 2 Thal phasing (Aβ) and Braak staging (pTau) in AD. Adapted with permission from Goedert, Science (2015); Braak and Braak, Acta Neuropathol (1991); Braak and Tredici, Acta Neuropathol (2010). Thal phasing exhibits a quicker cortical progression, whereas Braak staging progresses more in the limbic regions before moving to the cortex. Pale colours exhibit low levels and darker colours exhibit higher levels of pathological proteins.

1.1.4 Treatments

The majority of treatments currently used in AD target symptoms rather than the cause. These include acetylcholinesterase (AChE) inhibitors which work on the basis of blocking this enzyme from breaking down the neurotransmitter acetylcholine. This allows for a prolonged exposure of the neurotransmitter and therefore increased firing of neurons (68). One type of AChE inhibitor, Donepezil, has side effects such as insomnia and nausea (69) which may cause reluctance in taking the drug. Another class of drug targets N-methyl-D-aspartate (NMDA) receptors and can be used when a patient is intolerant to AChE inhibitors (70). Memantine is one such drug, which may improve symptoms such as mood and cognition in patients with moderate-to-severe AD (70). Because these

kinds of medications treat the symptoms and do not target the pathology of AD, research is being conducted on both Aβ and tau removal strategies.

The first human clinical trial actively immunising against Aβ (AN1792) showed successful removal of the amyloid plaques but proved unsuccessful in improving cognitive symptoms and caused meningoencephalitis (inflammation of the brain and meninges) in 6% of patients (71, 72). This trial was subsequently terminated due to this side effect, but it paved the way for future studies. Furthermore, in a neuropathological follow up study of patients from the AN1792 trial, it was discovered that the vaccine had effectively cleared Aβ plaques, even up to 15 years later, but failed to reduce the presence of tau (72). Further monoclonal antibodies were tested with the aim of removing Aβ deposits. An early trial using Bapineuzumab showed little effectiveness in improving cognition despite clearing the protein (73). However, recently, an Aβ monoclonal antibody has been approved in the United States for clinical use on AD patients called Aducanumab (Aduhelm®). This drug has shown to reduce amyloid plaques in the brains of AD patients but failed to significantly improve cognitive symptoms compared to the placebo (74). Thus, making the use of aducanumab controversial. Also, amyloid-related imaging abnormalities (ARIA) were a fairly common feature of Aducanumab treatment, with 41.3% of participants experiencing this phenomenon (75). *Post-mortem* data from a patient who was administered with aducanumab showed reduced Aβ but substantial tau accumulation (Braak stage V), however this was lower than placebo cases (76). Also, the patient continued to exhibit cognitive decline despite taking aducanumab (76), therefore the sole use of amyloid removal drugs may not be the best form of treatment for AD. However, two other Aβ targeting monoclonal antibodies appear to be more promising than Aducanumab and have been shown to reduce the levels of the protein and also improving cognitive decline in early AD: Lecanemab (LEQEMBI®) and Donanemab. Lecanemab has been approved by the FDA in the United States for the treatment of AD as it reported a 27% reduction in cognitive decline over an 18 month phase 3 trial (77). However, there were side effects seen when taking this drug, with 26.4% of patients experiencing an adverse effect (77). Donanemab showed a slightly better reduction in cognitive decline at 35% over 18 months and, infusion related adverse effects were lower with 8.7% of participants experiencing these (78). These recent developments in anti-Aβ therapies show promising results but there is still more research to be conducted about their efficacy.

Current tau targeted therapies are aiming to stop hyperphosphorylation (79) and aggregation of the protein. Tau aggregation inhibitor, Methylthioninium, has shown minor improvements in patient cognition over a 24 week period (80). Further research needs to be conducted into this type of treatment. Anti-tau therapies are in earlier stages than anti-Aβ therapies, with most only in phase 2 trials currently. The monoclonal anti-tau drug, Semorinemab, failed to reduce tau accumulation and improve cognitive symptoms in a phase 2 clinical trial (81). A new approach to target tau is to use an

antisense oligonucleotide to silence the MAPT gene, in order to reduce the amount of protein being produced (82). A phase 1 trial showed a 50% reduction in total tau and pTau after 24 weeks and no adverse effects were seen (82). Tau therapies could prove to be beneficial for the treatment of AD, however more large scale trials need to be conducted.

Finally, there has been a recent interest in targeting inflammation for the treatment of AD. Microglia and astrocytes are affected in the disease and possible restoration of these cells could help improve the disease state. By inhibiting cytokine release or their expression, the immune response can be modulated (83). Also, the use of specialized pro-resolving lipid mediators (SPMs) has shown to improve the phagocytic function of microglia in AD leading to reduction of Aβ *in vitro* (84). Further therapeutic strategies targeting inflammation and microglia will be discussed in Section **1.3.1**. It is most likely that a combination of targeted therapies, including Aβ, tau and inflammation, will show the most effectiveness when treating AD due to the diseases' multi-faceted nature.

1.2 Microglia

1.2.1 Origin

Microglia are the resident immune cells of the brain and make up about 10-16% of all cells in the CNS subject to brain region and developmental stage etc., (85, 86). They originate from the mesodermal yolk sac and proliferate from here; there is no participation from bone marrow stem cells (87). However, this concept was originally debated. Microglia were first named by Río-Hortega in 1919 (88), where it was proposed that these cells shared similarities with monocytes and therefore, their origins must be the same, which was from the ectoderm. It is true that monocytes can assume a microglia-like morphology when introduced to inflammatory stimuli (89). However, most microglia develop in early neonatal stages (87), whereas monocytes are continually renewed. Colony stimulating factor (CSF-1) plays a role in microglial development but may not impact monocytes as its depletion in mouse models reduced the development of microglia, but monocytes continued to be renewed (87), showcasing the differences between these cell types. In humans, mesodermal microglia appear very early in development, from 13 weeks gestation, and the most variability in the morphologies of these cells occur from here until 18 weeks (90). After this developmental period, the cell population begin to stabilise in morphology and number.

During adulthood, microglia replenish themselves rather than new cells developing from the bone marrow or blood. Examining the cells *in vivo* using a CX3CR1^{gfp} mouse line which express the fluorescent protein in microglia only, it was found that microglia are long lived cells that circulate for

several months (91). In humans, microglia have an average lifespan of over four years which is a turnover rate of 28% per year (92) or 0.05% per hour (93). However, this rate may have been underestimated as another group more recently found a turnover rate of 0.69% in human microglia (94). Using proliferation marker, Ki-67, and microglial marker, Iba1, it was estimated that only 2% of microglial cells are dividing at any one point in the human brain (94). This is a relatively low proliferation rate compared to other immune cells such as T cells, which proliferate at a rate of 60% per year (95).

1.2.2 Function and classification

Microglia are highly plastic cells that are able to change their morphology and function depending on what is required of them. When in a homeostatic state they exhibit a ramified morphology with many finger-like processes, whereas when these cells become reactive, their processes shorten and they exhibit a more amoeboid shape (**Figure 3**). Some of the normal physiological functions of microglia include synaptic pruning and plasticity, phagocytosis, surveillance of the brain parenchyma and stimulating and inflammatory response (96-99) (**Figure 4**). They contribute to normal acute neuroinflammatory processes by release of chemokines, cytokines (**Figure 4**), which can be pro- or anti-inflammatory to initiate or stop an immune response, and by protecting against ROS (100). They are often referred to as macrophage-derived cells, which is due to the crossover between markers present on the cells (101). For example, microglia and macrophages share markers for cluster of differentiation 11b (CD11b), cluster of differentiation 68 (CD68), C-X3-C motif chemokine receptor 1 (CXC3R1) and ionized calcium binding adaptor molecule 1 (Iba1) (101) (**Table 1**). However, there are possible microglia specific markers which include purinergic receptor P2Y12 (P2RY12), transmembrane protein 119 (TMEM119) and cluster of differentiation 45 (CD45); and macrophage specific markers such as cluster of differentiation 163 (CD163) and cluster of differentiation 206 (CD206) (101) (**Table 1**). Microglia are essential to maintain normal brain functionality and health. It is approximated that microglia can survey the whole brain in just a few hours (102) and they work in conjugation with several other cells in the brain, namely astrocytes and neurons (86).

Microglia can be described as ‘resting’ or ‘activated’, although these terms may not be a completely accurate. The ‘resting’ state allows the microglia to scan or survey the microenvironment of the brain parenchyma using finger-like processes (103). This, therefore, is why the term ‘resting’ may not be accurate terminology as they are still performing a function. While in this state, the cells have a highly ramified morphology (**Figure 3**) (103). Previously, when microglia became ‘activated’, they were classified into two different conditions based on the macrophage model: classical activation (M1) and alternative activation (M2) (104). It was thought that M1 induced a pro-inflammatory response and allowed the cell to kill foreign bodies in the brain, perform phagocytosis and present

antigens to other immune cells (105), whereas, M2 activation caused the microglia to initiate tissue repair and the remodelling of the extracellular matrix as well as phagocytosis by being anti-inflammatory (105). This phenotype appears more amoeboid in morphology (**Figure 3**) (103). The more appropriate term for previously 'activated' microglia are now called 'reactive'. The term reactive is thought to be more appropriate when describing the change in microglial function due to the nature of that change. The term 'activated' indicates that there is 'inactivated' state, which is untrue. Therefore, 'reactive' is more appropriate as the cells are reacting to a stimuli. Furthermore, while it is difficult to fully group a dynamic cell such as microglia, a different and possibly more robust classification system for microglial cells in disease has been proposed. This terms microglia as M0, which refers to a homeostatic phenotype, and microglia associated with neurodegenerative disease (MGnD) (106) or disease associated microglia (DAM), which have been established using mouse models but have yet to be substantially proven in humans (107, 108). M0 microglia have a transcriptomic signal that expresses a number of genes including *P2RY12* and *TMEM119* (109, 110), which are thought to keep the microglia in homeostatic state (**Table 1**). There are also a number of cell surface makers associated with this homeostatic phenotype in order to maintain normal functioning of microglia; including CD11b which is involved in cell adhesion, CD45 aids the regulation of T-cell activation and CX3CR1 which is associated with cell adhesion and migration etc., (101) (**Table 1**). On the other hand, when microglia become reactive and show attributes of the MGnD/DAM phenotype, they express genes such as *APOE* and *TREM2*, which are both found to be AD risk factors from GWAS studies (111). Discriminating markers present in reactive microglia include human leukocyte antigen (HLA-DR/DQ/DP) which is an antigen presenting marker that is highly increased in AD (112-114), CD16 and CD68 which are both involved in phagocytosis (101, 115) and macrophage scavenging receptor-A (MSR-A) which is associated with scavenging activity (115) (**Table 1**). TREM2 is also an interesting marker and is further discussed in Section **1.3.1**, but it could be important for not only microglial function but risk of developing neurodegenerative disease. Classifying microglia into subgroups is highly complex and it may be the case that there are specific phenotypes associated with each neurodegenerative disease rather than blanket groupings for every condition.

Table 1 Common microglial markers and their roles in physiology and disease conditions

Marker	*Name*	*In physiology*	*In pathology*
TSPO/PBR	Translocator protein/Peripheral benzodiazepine receptor	Involved in cholesterol transport, steroid synthesis and protection from ROS (116).	Suggested to be increased in human AD (12). A potential marker of reactive microglia/neuroinflammation.
Iba1	Ionized calcium binding adaptor molecule 1	Involved in cytoskeleton organisation, membrane ruffling and phagocytosis (117). Associated with all microglia (118). Aids modification of actin in	Decrease in this protein as AD progresses, indicating a loss in motility (115). Some argument for increase in expression of this marker but not

		processes of microglia for motility (119).	number of cells present in human AD (120).
MHCII/HLA-DR/DQ/DP	Major histocompatibility complex II/Human leukocyte antigen	Antigen presentation and recognition. Generally thought of as a marker for microglial activation. Responds strongly to $CD4^+$ T cells (121).	Associated with Aβ plaques and shown to increase in human AD (112).
MSR-A	Macrophage scavenging receptor	Lipoprotein scavenging receptor involved in endocytosis of foreign particles (122, 123).	Positively associated with dementia and AD pathology in humans (115). May cause immobilisation of microglia when they encounter Aβ plaques (115).
P2RY12	Purinergic receptor P2Y12	Homeostatic marker of microglia involved in motility due to activation of potassium channels (124).	Decreased expression in AD mouse models, linked with Aβ response which is reduced in the disease (107, 124).
TMEM119	Transmembrane protein 119	Thought to associate with all microglial subsets. Exact function unknown.	No increase in expression when exposed to infection or inflammatory molecules (109). Expressed by microglia that have both ramified ($Iba1^+$) and amoeboid ($CD68^+$) cells in AD (109).
TREM2	Triggering receptor expressed on myeloid cells 2	Microglial-specific. Forms complex with Tyrobp for phagocytic activity (107).	Loss of function mutations (R47H) thought to be associated with AD in human and iPSC (33, 35).
CX3CR1 (Fractalkine)	C-X3-C motif chemokine receptor 1	Chemokine receptor commonly secreted by neurons for glial migration (125).	Increased levels in human AD and may regulate microglial activation in models of AD (126).
CD64 (FcγRI)	Cluster of differentiation 64	Triggers macrophage immune response by binding to IgG (127). Can aid with phagocytosis of foreign materials (115).	Increased in AD, not associated with Aβ plaques (123).
CD16 (FcγRIII)	Cluster of differentiation 16	Marker of microglia, macrophages and monocytes that initiates an IgG mediated immune response (63).	Increased in dementia with Lewy bodies and may indicate a more reactive microglial subtype (128).
CD11b	Cluster of differentiation 11b	Part of the compliment receptor 3. Aids in recognition of foreign antigens. More associated with the reactive microglial phenotype (101).	Not necessarily increased in AD.
CD11c	Cluster of differentiation 11c	Integrin receptor X. Typically a dendritic cell marker, but also found in amoeboid microglial cells (129).	Associated with the DAM phenotype in AD (107).
CD45	Cluster of differentiation 45	Located on the membrane of microglial, as well as macrophages and T cells, and involved in cell differentiation and proliferation. Expressed by most subsets of microglia (120).	Higher expression of $CD45^+$cells in AD. Most being spread throughout the parenchyma, not associated with Aβ plaques (130).
CD68	Cluster of differentiation 68	Class of scavenging receptor (122). Present in microglia and macrophages. Lysosomal marker of phagocytic reactive microglia (118).	Increased in AD. Also associated with APOE ε4 genotype and cognitive decline (115).
CD163	Cluster of differentiation 163	Scavenging receptor in the macrophage lineage (120). Some phagocytic capabilities.	Increase in AD, specifically within Aβ plaques (131).
CD206 (Mannose receptor)	Cluster of differentiation 206	The mannose receptor is a marker of macrophages (132). Aids in endocytosis.	Increases in an acute manner for intracerebral haemorrhage (133). Unsure of its role in AD.

Finding microglial markers that are specific and can identify all functional subtypes is highly sought after in the field. There are some markers that aim to do this; however, these can be slightly controversial and results vary. One classic microglial marker is Iba1 which is cytoplasmic marker involved in motility and cytoskeletal organisation (115). There is conflicting evidence for this marker

in terms of its function in AD, with several papers showing a decrease of Iba1 (115) as the cells ability to be motile reduces. Other papers show an increase of Iba1 (134) in AD, so results may not be verified. An interesting result that supports the claim of Iba1 being present in both reactive and non-reactive microglia phenotypes, was its higher presence in an intermediate morphology rather than ramified (physiological/surveying) or amoeboid (reactive) microglia in an AD chimpanzee model (135). The other common target thought to be a pan-microglial marker is TMEM119, which has a currently unknown function and is found on the cell surface (109). It has been shown that expression of this marker does not change in response to inflammatory stimuli such as LPS, IL4 etc and that it is present in both ramified ($Iba1^+$) and amoeboid ($CD68^+$) morphologies (109). However, as with Iba1 there is data that demonstrates not all microglia express TMEM119, in both healthy and disease conditions such as AD (136), and that $TMEM119^+$ microglia decrease in AD (136), therefore making its use as a pan-microglial marker uncertain.

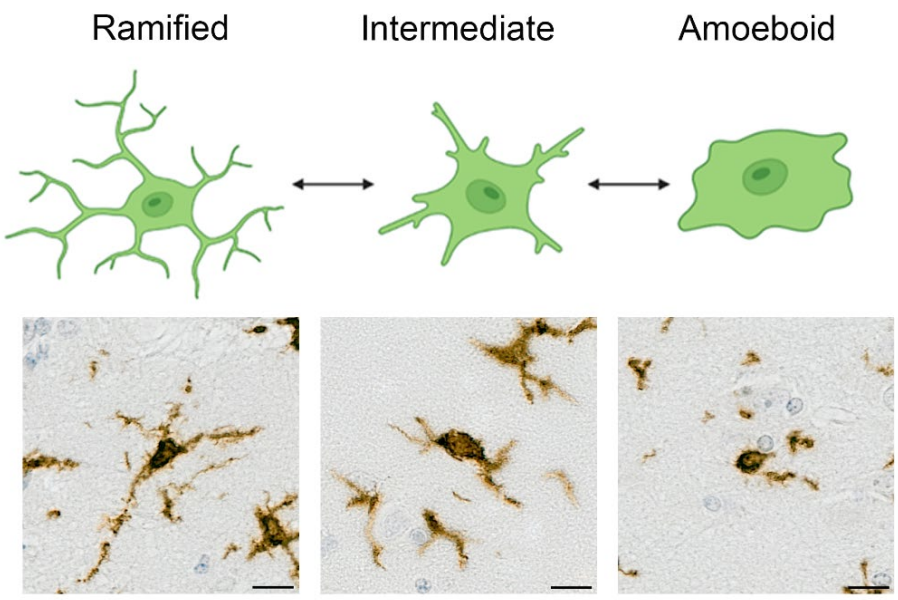

Figure 3 Figure depicting different microglial morphologies with corresponding DAB immunohistochemical staining using Iba1. 20X magnification. Scale bars = 20µm. Created with BioRender.com.

1.3 Neuroinflammation in Alzheimer's disease

1.3.1 Microglia

Microglia are heavily implicated in neurodegenerative diseases such as Alzheimer's and Parkinson's disease (PD), as discovered by GWAS analysis with risk factors related to microglia and the immune

response being highly enriched in AD (111, 137). Their exact role in this capacity is unknown and a large focus in current neuroimmunology research is to discover if microglia and other immune cells, such as macrophages, T and natural killer cells, are beneficial or detrimental in disease, or if these cells have the ability to both aid and hinder neurodegeneration. As mentioned in Section **1.2.2**, microglia contribute to neuroinflammation by release of cytokines; however, in AD, the chronic release of these cytokines becomes toxic and can cause damage to neurons and other cortical cells (**Figure 4**) (138). This further incites microglia to become reactive and exacerbates the neuroinflammatory process in disease (139). It has been suggested that there are two waves of microglial reactivity, an early protective peak and a later inflammatory peak, found via use of neuroinflammatory PET ligands in AD (12, 13, 140) (further discussed in Section **1.4**). The first protective peak was found to correlate to a slower cognitive decline (12) but the later peak, signalling microglial reactivity in AD, was associated with failure to clear Aβ and cognitive decline (12, 140).

There is evidence to suggest that microglia may lose motility in AD, as seen by a decrease in Iba1 immunostaining (115), which could impact their ability to survey the brain parenchyma. Also, microglial dystrophy, characterised by beading and fragmentation of the processes (141), has been observed in greater numbers in neurodegenerative diseases compared to normal ageing (142) (**Figure 4**). On the other hand, the cells clearance and phagocytic capabilities are increased in AD brains shown by an increase in the CD68 and MSR-A markers (115). This may suggest that the microglia are trying to clear AD related pathologies including Aβ plaques, whether this is successful is debatable. There is evidence to show that microglia can effectively clear plaques by phagocytosing the Aβ peptides (143) (**Figure 4**). However, if this was effective, AD symptoms would perhaps be reduced. A possible theory states as the disease progresses and the Aβ plaque level increases, this overwhelms the microglia and they are unable to clear this protein (140).

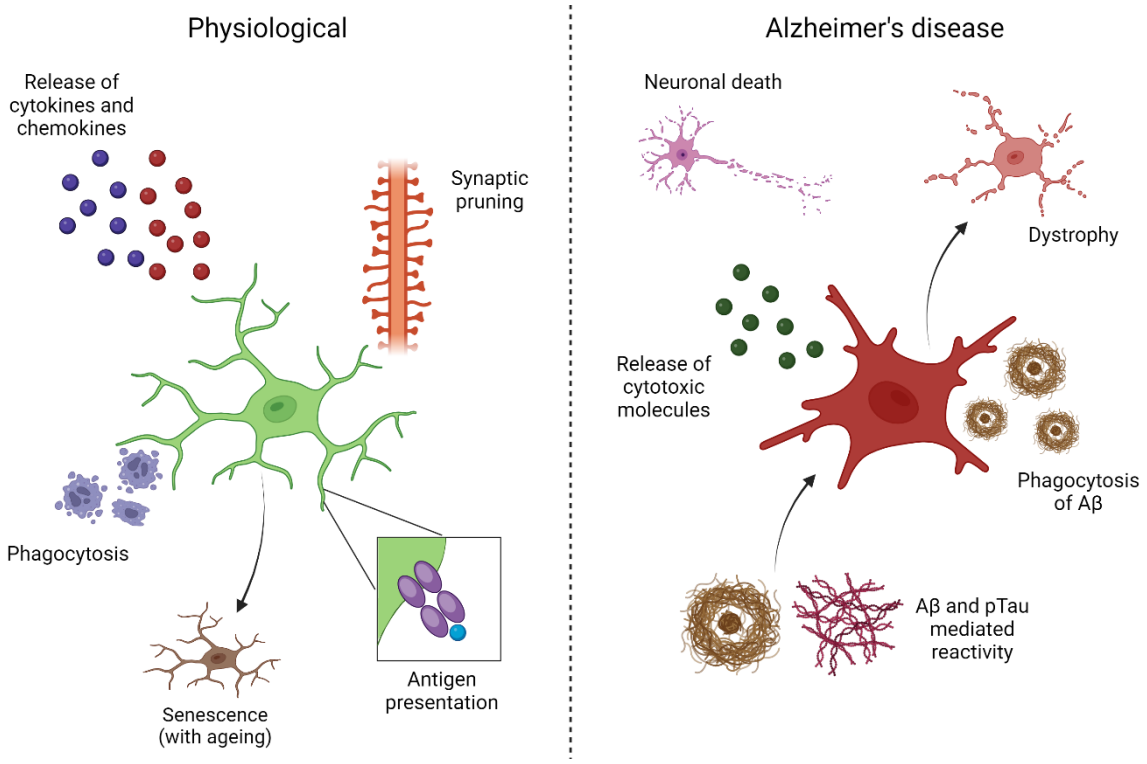

Figure 4 Diagram illustrating the normal physiological functions of microglia and how these cells are affected by/contribute to AD. Green microglial cell is homeostatic in nature and the red microglial cell indicates a reactive phenotype. Adapted from Amor et al, Acta Neuropathol (2021). Created with BioRender.com.

Likewise, the role toxic hyperphosphorylated tau plays in the disease may affect the microglia's ability to aid the CNS. It has been shown that microglia can further exacerbate tau pathology in AD (144). This may occur due to an increase in Interleukin-1 (IL-1) in the brain, which in turn causes the microglia to start a proinflammatory signal transduction (144). This appears to cause an increase in tau phosphorylation. Interestingly, this action reduces amyloid plaque distribution which may be due to an increase in the number of amyloid-associated microglia (144). Microglia may also contribute to the spread of tau via cell-cell transfer through exosomes. In a mouse model expressing human tau conformer 1N4R, depletion of microglia reduced the propagation of tau (145). Further preventing exosome synthesis by using the phagocytic inhibitor, cytochalasin D, reduced this also (145). Furthermore, it could be the tau itself being detrimental to microglial function. Evidence has shown that when microglia are in proximity to tau tangles, their morphology alters, and they may not be as effective in performing their normal functions (146) (**Figure 4**). These factors could be a consequence of the disease affecting the microglia and causing them to become dysfunctional. On the other hand, the microglia could be performing their normal function, but the disease progression is too severe for the cells to provide significant aid in toxic protein clearance. It is also likely that microglial response is

disease stage and brain region dependant. Microglial reactivity may occur in line, or just before, tau tangles arise in a specific region following the Braak stages when examining both translocator protein (TSPO), a marker of neuroinflammation, and tau *in vivo* PET scans (147). In areas such as the temporal lobe, that are pathologically affected by the disease early on, multiple CSF markers of pTau (p-tau181, p-tau231 and p-tau217) have been found to correlate with TSPO PET binding in MCI and AD patients (148). Interestingly, this relationship was dependant on the presence of tau tangles and therefore, this association may be most prevalent in later stage disease (148).

DAMs have been identified using single-cell RNA sequencing and are associated with neurodegenerative disease in AD models, where a two-step process is necessary to convert homeostatic microglia into this disease phenotype in a Trem2 dependant fashion (107). This subtype of cells are categorised by having a phagocytic capability but reduced expression of homeostatic genes such as *P2ry12* and *Tmem119* and an increase in disease associated genes including *Apoe* and *Trem2* (107). A subset of DAM genes has been identified in humans, but there is not a complete overlap (149), and DAMs where localised only to neuritic plaques in human AD (107), showing the difference between human AD and mouse models. Another classification for microglia, the MGnD phenotype, was found to be related to the Trem2/Apoe pathway after injection of apoptotic neurons in a mouse model of AD (106). The slight differences between the proposed reactive microglial phenotypic categorisations indicates further research is needed to create a collective phenotypic subset, which would also need to be confirmed in human disease.

Emerging evidence has shown that microglia begin to proliferate excessively at the onset of AD in an APP/PS1 mouse model which leads to microglial senescence (150). This may be due to new pathologies starting to accumulate in the brain and the response to try and clear these. This proliferation event can cause the cells to specify into DAMs (150, 151). It has been shown that when DAMs have been hindered from proliferating in this manner using the CSF1R proliferation inhibitor, key pathologies such as Aβ accumulation have been prevented (150). This suggests that preventing senescence of microglia could stop the onset of amyloidosis and be important in finding new microglia related AD treatments. However, it has been established that sole removal of Aβ does not have significant benefits in the reducing the symptoms/progression of AD (72-74). Therefore, it may be prudent to stop the microglial response to Aβ as a pathological consequence prior to its removal via these cells.

To explore this point further, it has been proposed that microglia fit into, and play a key part in, the sequence of progression of AD. For example, Aβ accumulation occurs in healthy human brains (152), however, when this transpires in AD it is followed closely by microglial activation. It is thought that this reaction may cause neurites to become dystrophic, which promotes the subsequent spread and

accumulation of tau (153). It has been shown that initial Aβ accumulation was deposited in a diffuse manner, with no presence of microglia or tau (153). This progressed to an amyloid plaque being surrounded by a cluster of microglia (in the form of HLA-DR positive cells) and also APP dystrophic neurites being present. Finally, the neuritic plaque contains the presence of microglia, APP and pTau, which then begins to spread in the form of tangles and neuropil threads to other neurons (153). This is a plausible explanation as, firstly, it is well established that Aβ is the first pathological protein to accumulate many years before disease symptoms (64). Also, dystrophic neurites have been observed in humans without the presence of tau (154), with tau being seen in conjunction with neurites later in the disease progression. The exact mechanism of how microglial involvement may contribute to disease progression is a salient question.

As mentioned, APOE is implicated in AD, especially in regard to microglial function. Microglia secrete this protein, and it has been shown to be involved in their ability to phagocytose Aβ plaques. When Aβ plaques were infused with Apoe ε3, a rapid microglial response occurred in an Alzheimer's mouse model (Cx3cr1) over a 24h period. The opposite was observed with infusion of Apoe ε4 (155). This shows that the APOE ε3 allele may indeed have a protective, or at least neutral, quality as it aids microglia immune function. Another protein that aids in this ability is TREM2. This protein is thought to be involved in microglial health and also may support the response to Aβ plaque pathology (156). With the *TREM2* R47H mutation, microglia cannot surround and breakdown Aβ plaques as efficiently. This leads to more phosphorylated tau and dystrophic neurites present (157). Furthermore, it is thought that APOE and TREM2 may interact to support microglial function. In a Trem2 knockout model, Apoe ε3 or Apoe ε4 were again infused into Aβ plaques, and results showed that there were a higher number of homeostatic genes in the *Trem2* knockout microglia when infused with Apoe ε4 and a decreased uptake of Aβ also (155). This could indicate that TREM2 disruption cause microglia to insufficiently remove Aβ, even with the presence of risk factor APOE ε4. However, as stated previously, TREM2 may identify monocytes rather that microglia in humans (36).

As mentioned in Section **1.1.1**, mitochondrial dysfunction is now thought to play an important role in AD, and in particular, within microglial cells. It has been proposed that this dysfunction occurs before microglia become reactive and cause subsequent neuroinflammation in AD, indicating that mitochondria play a crucial role in microglia's involvement with disease progression. For example, there may be a reduction in glucose metabolism in AD (158), and to compensate for this loss microglia recruit more GLUT-1 transporters to their membranes (159). A recent study has shown that mitochondrial DNA leaks into the microglial cytosol and this activates a DNA immune sensing pathway called cGAS-STING, which in turn causes inflammation and other neurodegenerative features during ageing (160). It was also shown that blocking cGAS-STING improved neurodegenerative symptoms in an aged mouse model (160), which could lead to therapeutic

targets. An interesting study by Fairley et al has demonstrated both TSPO and hexokinase-2 are heavily involved in microglial metabolism and the energy supply needed for phagocytosis (161). Genetic depletion of TSPO in microglial cell culture decreased ATP (impaired respiration) and enabled a switch to glycolysis, resulting in reduced phagocytosis of Aβ (161). The group also found that actin levels were decreased, and that phagocytosis could be impaired as a result of inadequate actin polymerisation within the cytoskeleton of microglia due to less ATP available (161). Mitochondrial dysfunction appears to be an important part of microglial involvement in AD pathogenesis, potentially early on in disease, meaning therapeutic targets for this could be a viable treatment option.

1.3.2 Astrocytes

Astrocytes are a star shaped cell that develop from radial glia in the ventricular zone during late embryogenesis (162) and contribute to brain immunity. They account for ~30% of CNS cells and their primary function is to maintain the BBB by using structures called endfeet to create a border around pericytes and endothelial cells (163). They are also crucial for modulating synapses (163). In the white matter, astrocytes are termed 'fibrous' and in the grey matter 'protoplasmic' (164). GFAP is an important astrocytic intermediate filament, whose role is critical within the cytoskeleton of the cells to maintain this structure (165). In neurodegenerative disease and neuronal injury, astrocytes become reactive, which is marked by a morphological change of process thickening, increased expression of GFAP and STAT3 signalling (165). Reactive astrocytes are characterised by either being 'A1', which causes synapse destruction and neurotoxicity, or 'A2', which promotes neuronal survival and synapse maintenance (163). However, like microglia, this categorisation may be too rigid as these cells also have dynamic phenotypic changes. Examining astrocytic reactivity, it has been observed that the deletion of STAT3 in a mouse model of spinal cord injury caused an inability of astrocytes to become reactive and form a glial scar around the injury site, leading to further inflammation (166). In addition, overexpression of a STAT3 inhibitor in a models of AD and Huntington's disease (HD) pathology caused a reduction in astrocytic reactivity, a decrease in microglial activation (suggesting a link between the two immune cells) and a rise in the neuropathological hallmark protein of HD (167). It is well established that Aβ plaques in AD are often surrounded by reactive astrocytes and that this phenomenon increases as the disease progresses (168, 169), further indicating a strong association between astrocytes and neurodegenerative disease.

Astrocytes often work in conjunction with other immune cells, namely microglia, and communicate with these cells via various mechanisms (170). This communication is bidirectional and requires a myriad of inflammatory signals such as toll-like receptors (TLRs) and TNF for the induction of

activation cascades and chemoattractants such as β chemokines (170). There is evidence for microglia and astrocytes responding preferentially to different stimuli. When exposed to lipopolysaccharide (LPS), microglia release chemokines such as CCL2, CCL3 and CCL4, whereas astrocytes do not. However, when stimulated with pro-inflammatory cytokines such as TNFα, both cell types subsequently release chemokines (171). This suggests that microglia react more strongly to pathogens, with astrocytes working in conjunction to cause inflammation. The communication between astrocytes and microglia can occur is many ways including the CD200 receptor. This receptor is found on microglia, and under physiological circumstances, astrocytes do not express the corresponding CD200 protein. However, in disease CD200 has been seen to localise with astrocyte protein GFAP (172). It is postulated that reactive astrocytes use CD200 to signal to microglia, which are the more motile cell, to move to the damaged area to initiate inflammation in an acute stress event or chronic neurodegenerative disease.

1.3.3 Other innate immune/CNS cells

Macrophages and monocytes are other immune cells that play important roles in the CNS. Monocytes are a subtype of white blood cell that circulate the vasculature. They can differentiate into macrophages and dendritic cells when contact is made with a foreign particle (173). Macrophages provide immunity primarily by phagocytosing these foreign bodies and can also signal to other immune cells to initiate a cascade immune response (173). Monocytes are derived from the bone marrow and express different subsets of CD14 and CD16 in humans (173). It has been observed that monocytes do enter the brain parenchyma at the site of injury, but not in the healthy CNS (174). In a mouse model of a seizure disorder, monocytes were seen to infiltrate the brain after seizure activity (174). Perivascular macrophages are seen in the space surrounding the blood vessels in the brain (174) and are identified by the markers CD163 and CD206 (120, 132) (**Table 1**). These cells also became involved subsequent to seizures (174), suggesting the contribution of many immune cells working in conjunction for a targeted neuroinflammatory problem.

Monocytes and macrophages/microglia work together in neurodegenerative diseases such as AD and autoimmune diseases such as MS. A proposed consequence of AD is the disruption of the BBB, primarily due to Aβ deposition in the vasculature and insufficient clearance of this protein with ageing (175), which may lead to cerebral amyloid angiopathy (CAA) (173). This leads to the infiltration of immune cells such as monocytes and macrophages to the brain space (176). It is unknown whether this is beneficial or harmful to the brain environment. In human cell culture, it was shown that $CD14^+$ non-inflammatory cells were decreased in AD compared to MCI patients when exposed to Aβ42, with the opposite being seen in $CD14^+$ inflammatory cells (177). This suggests that inflammation may increase in AD based on monocyte response to Aβ.

Endothelial cells make up 0.3% of CNS cells (178) but are vitally important to maintain structure in the blood vessel walls by creating intercellular junctions that allow permeability (179). They derive from the mesoderm (179) and are a crucial part of the BBB. Once developed they can be identified by platelet endothelial cell adhesion molecule 1 (PECAM1), also called CD31 (179). In AD, there is evidence that endothelial cells undergo changes that can lead to improper response to Aβ and CAA (180). If there is improper clearance of Aβ, this leads to the accumulation of the protein in AD. The toxicity of Aβ effects transporter expression on endothelial cells causing inability of the protein to cross the BBB and be cleared from the brain (181). On the other hand, dysfunctional endothelial cells could also allow Aβ to cross over the BBB and due to other mechanisms, such as extracellular matrix protein lysyl oxidase (LOX) inhibition, and therefore Aβ accumulates within the blood vessels and causes CAA (175).

1.4 TSPO radioligands for microglial identification

1.4.1 Overview of TSPO

TSPO is used as a marker of 'neuroinflammation' in PET studies of neurodegenerative disease such as AD. This marker is thought to detect microglial activation which is a hallmark of disease. There are certain prerequisites for a radioligand to be used successfully in PET studies: they should be able to cross the BBB, they should have good specificity, they should be small (<700 Da) and they should have high affinity for the target (182). TSPO was originally named peripheral benzodiazepine receptor (PBR) as it was found to be a binding site for the anxiety drug, diazepam, in the 1970s (183). TSPO is found on the outer mitochondrial membrane where its five transmembrane α-helices (made up of 169 amino acids) intercept the membrane to create a pore (184). It is thought to be involved with cholesterol transport into the inner mitochondria membrane for steroid synthesis (116) (**Figure 5**) via its cholesterol recognition amino-acid consensus (CRAC) found in transmembrane helix 5, starting with the amino acid residue A147 and ending at S159 (185). However, this function now has some conflicting data, as TSPO knock-out mouse models have demonstrated functioning steroid synthesis capabilities (186). This could mean that there are other compensatory mechanisms that aid with cholesterol transport for steroidogenesis. Other functions of the receptor may include an ability to be resistant to ROS (116), which can support mitochondrial homeostasis (**Figure 5**). Furthermore, TSPO may have a protective role as it controls the release of apoptotic factors, decreasing these to allow for better cell survival (116). TSPO is found in many tissues in the periphery but in the brain it is found primarily in microglia in very high levels and endothelial cells in lower amounts (187), making it a useful marker for these cells. There is evidence that shows increased TSPO expression in microglia

in response to infection or injury. In mice exposed to intracerebral haemorrhage, there was an amplification of TSPO in microglia up to 7 days after injury (188). Thus, supporting the theory that TSPO highlights reactive microglia.

These radioligands, and PET in general, are important tools for researching neurodegenerative diseases. TSPO ligands have been used to look at the microglial profiles of AD, MS, HD, PD and various psychiatric disorders (189). TSPO is increased in reactive microglia in response to injury or infection and expressed in lower levels in microglia performing their surveying function (190). A significant finding has been that the TSPO ligands' uptake is increased in AD patients compared to controls in brain regions that are known to contain the classic pathological hallmarks of the disease (12, 13, 191), showing that inflammation and microglia go hand in hand with AD. Alternatively, a recent study has proposed that in humans, increased TSPO may be linked with microglial cell number and not a direct increase in expression of this protein (192). It was found that the level of TSPO per microglia did not increase in AD, ALS or MS human *post-mortem* tissue compared to controls but microglia number increased in ALS and MS tissue, therefore the increase in overall TSPO levels was due to an increase in number of cells (192). However, as mentioned previously, the microglial cell population remains fairly stable in the brain (94), suggesting the expression level of TSPO within microglia may require further explanation.

Mitochondrial dysfunction plays a role in AD, specifically within microglia. Increase in ROS has been observed due to Aβ initiating nicotinamide adenine dinucleotide phosphate (NADPH) in microglia leading to toxicity (193). Cholesterol is also a point of interest in AD, as research has shown this lipid to become raised in AD, causing disruption to the mitochondrial membrane (194). As TSPO plays a role in cholesterol transport into the mitochondria, there may be a link between TSPO and this disruption. However, TSPO may be protective against ROS (116) so it could be feasible that the receptor may become dysfunctional in this role. TSPO PET scans are a fairly expensive way of examining neuroinflammation in the brain. Therefore, they are currently used in research or clinical trials and not routinely for diagnostic analysis in patients (195).

Interestingly, direct application of TSPO to 3xTg-AD mouse models has shown an improvement in memory and a reduction of Aβ deposition in the hippocampus of these animals (196). This could lead to potential therapeutic uses of TSPO in neurodegenerative disease as there is speculation surrounding this protein's ability to increase the reactivity of microglia. Leading on from this, TSPO may have a protective role in relation to mitochondrial dysfunction. As mention in Sections **1.1.1** and **1.3.1**, there is emerging research that mitochondrial dysfunction plays a role in AD. From this, it could be postulated that TSPO may have beneficial applications to counteract this. There is evidence that treatment with TSPO can improve mitochondrial health and functioning by boosting ATP

production via respiration and reducing ROS levels in cell models of AD (116, 197). TSPO could provide a new avenue for AD treatment strategies, but more research needs to be conducted before it could be applied to human AD.

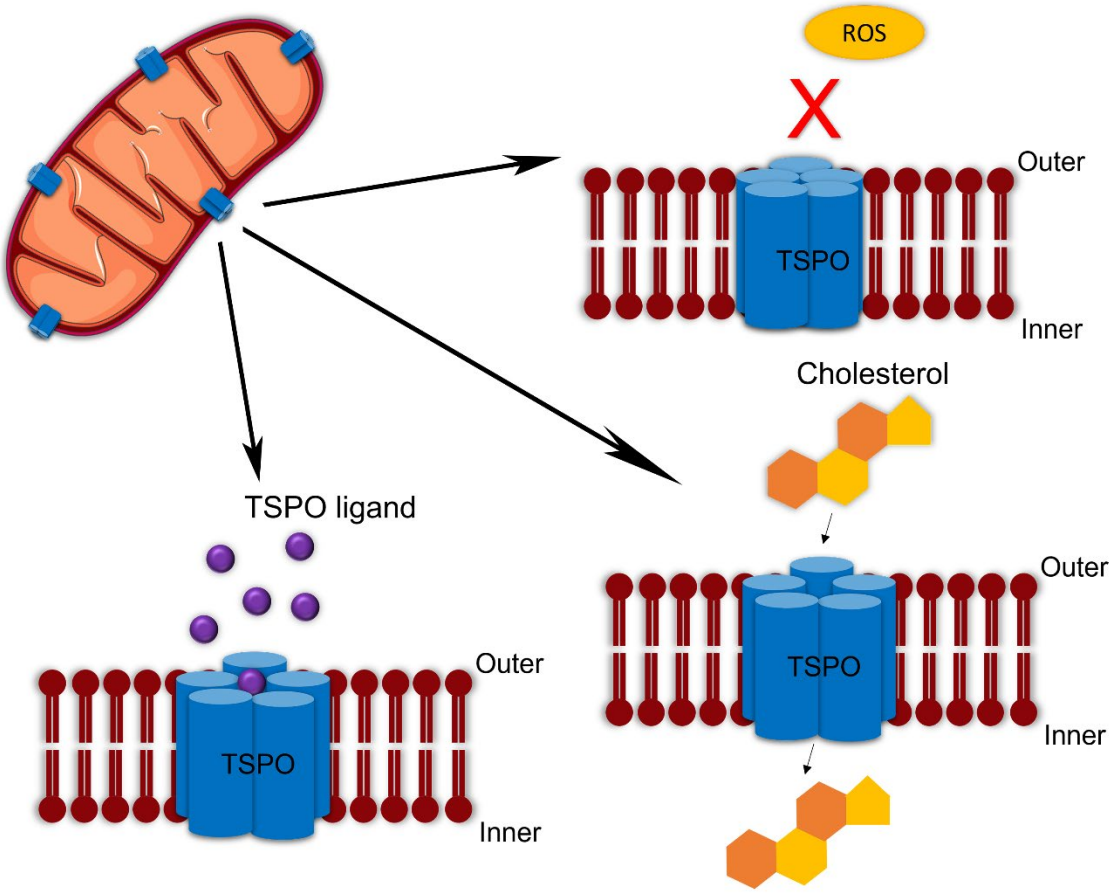

Figure 5 Locality of Translocator protein (TSPO) and its functions. TSPO has five transmembrane α-helices as depicted in blue and sits on the outer mitochondria membrane. Its normal function includes cholesterol transport into the organelle, as well as aiding mitochondrial homeostasis by supporting resistance to reactive oxygen species (ROS). Its associated PET ligand will bind to this receptor between all five α-helices.

1.4.2 First generation TSPO ligands

There are many different radioligands that can identify TSPO, including first generation ligand [C^{11}]PK11195, which was first described in 2001 (198) and has been commonly used in research since this date. This first generation ligand binds monomerically to the hydrophobic pocket between the bundle of five α-helix transmembrane proteins towards the outer side of the pore (184) (**Figure 5**). The ligand binds to amino acid residues: A23, V26, L49, A50, I52, W107, L114, A147 and L150 (184).

PK11195 is a [^{11}C] compound which has been shown to have a high uptake rate in AD patients compared with controls (199), indicating that TSPO, and therefore microglia, must play a key role in the disease in their reactive state. On the other hand, some research has shown a milder association between PK11195 and AD. One study showed that in MCI there was little PK11195 signal seen (199), concluding that this ligand may not be sensitive enough to detect microglia in earlier stages of the disease. Another study found small significant clusters of PK11195 in AD patients compared to controls but overall, found no significant difference (200). However, this ligand can label reactive microglia in *post-mortem* tissue of AD mouse models (201) and also show an increased expression level in human *post-mortem* AD tissue (202). There has been substantial research conducted with this radioligand, but there are limitations to its use. It has a low signal-to-noise ratio, meaning there is background signal which may confuse results, as well as a high non-specific binding ability (203). Furthermore, it can be difficult for the PK11195 ligand to discriminate between microglia, macrophages and astrocytes (201), meaning that its binding ability is broadly associated to the inflammatory response and not limited to microglia.

1.4.3 Second generation TSPO ligands

Second generation radioligands have been developed in order to combat some of the previous limitations. For example, [^{11}C]DPA-713, [^{18}F]PBR111, [^{11}C]PBR28 and [^{18}F]DPA-714 are all second generation ligands. However, [^{11}C] has a short half-life which is why [^{18}F] ligands are more popular in order to combat this problem (203). It is clear that second generation ligands are more reliable than the first generation. For example, a study applied both PK11195 and PBR28 on *post-mortem* tissue of MS patients, and while there was a 2-fold increase of PK11195 within MS lesions, there was a 7-fold increase in PBR28 compared to controls (204). Another comparison was performed between PK11195 and second generation ligand DPA-713. DPA-713 was found to have a higher binding ability than PK11195 and had a significant increase in expression levels in AD patients compared to controls (205). Also, DPA-713 binding correlated to clinical scores of patients (205), which could prove a link between AD symptom progression and neuroinflammation. This exhibits that second generation ligands may show increased binding to microglia and therefore, further reliability with use in PET scans for neuroinflammation. The second generation ligand DA11106 was proven to effectively label microglia in human *post-mortem* tissue using a combination of immunohistochemistry and autoradiography (206). This study showed that certain brain regions such as the thalamus, parietal and temporal lobes had increased TSPO binding compared to controls. This was matched with the presence of reactive microglia staining in the same regions (206). This provides good evidence for TSPO being highly related to reactive microglia and that this protein increases its expression in AD.

An issue that has arisen from second generation ligands is the sensitivity to a polymorphism that affects binding ability. Different patients can be low or high affinity binders which will affect who is eligible in the use of these TSPO ligands. This polymorphism will be discussed further in Section **1.4.4**.

When TSPO PET scans have been performed on AD patients, control subjects are often used as a comparison model. However, this provides challenges as there are person to person changes that will be present causing variability in results. Therefore, another method of standardising the TSPO binding in the brain is used in conjunction with arterial blood sampling called absolute quantitation (207). The disadvantage of this method is it takes time to perform as it requires blood samples to be drawn. To combat this, it has been proposed to use a brain region of lower TSPO expression as a pseudo-reference region, and while there is no brain region completely devoid of TSPO (207), this would negate the impact of patient differences. One such proposed region is the cerebellum as this area has been suggested to have less severe AD pathology (208, 209) and lower TSPO expression from other studies using the absolute quantitation method (210). One study used the cerebellum as a pseudo-reference area compared to temporal and parietal lobes (areas of high AD pathology) in controls, MCI and AD patients using standardized uptake value ratio (SUVR) and absolute quantitation (207) using [^{11}C]PBR28. Greater TSPO binding was observed in the temporal and parietal lobes using the SUVR of the cerebellum compared to the absolute quantitation method (207). Several other second generation TSPO studies have also used the cerebellar SUVR method with reliable results (12, 13).

1.4.4 [^{18}F]DPA-714

The TSPO ligand [^{18}F]DPA-714 was chosen for use in this thesis (**Chapter 6**) and will be reviewed here. Studies have shown that DPA-714 has the highest binding potential to microglia compared to DPA-713 and PK11195 in a rat model (211). DPA-714 has also been shown to be an effective biomarker for microglia and neuroinflammation in the APP/PS1 mouse model (212). This has similarly been recapitulated in both healthy and AD humans (213), showing that this radioligand is a better alternative to older isotopes of TSPO and that it could potentially be used to detect AD phenotypes in humans. However, there are conflicting results as one study states that DPA-714 cannot differentiate between AD patients and healthy controls when using this ligand in PET scans (213). This study had a small sample size and was followed up using a different parametric method of visualising the PET ligand. The follow up study showed that by looking at more brain regions there was a significant difference in the uptake of DPA-714 in AD patients versus controls (214). This may lead to the idea that the DPA-714 ligand could be used in a diagnostic capacity for AD.

Binding of TSPO has been shown to positively correlate with deteriorating cognition (13). Also, there are indications that in AD patients whose disease progression is slow, the microglia (identified with DPA-714) are increased in number and may play a protective role in the early stages of the disease (13). Putting these evidential pieces together could mean that somewhere along the disease progression the microglia become dysfunctional rather than protective. Although, it is not completely known whether TSPO identifies reactive microglia or another form of these cells. Further research needs to be conducted to confirm these findings.

As mentioned in Section **1.4.3**, there is a polymorphism that affects second generation radiotracer ligands such as DPA-714. This single nucleotide polymorphism (SNP) is denoted rs6971 and causes a substitution for Alanine(A)147Threonine(T) in the TSPO gene (215). As the A147 amino acid is one of the residues that is involved in binding to the ligand in the hydrophobic pocket of the transmembrane protein (184), this substitution contributes to issues in binding ability by altering the distance between transmembrane two and five which closes the pore size (216). Interestingly, the A147 residue is also involved in cholesterol transport (185), and therefore the SNP has been shown to alter this function (217). There is evidence for up to 50-fold binding difference between HABs (A/A) and LABs (T/T) (218), with another subtype being denoted as mixed affinity binders (MABs) (A/T). This polymorphism leads to problems in the clinical setting with genotyping being required for patients in order to get standardised results from second generation TSPO ligands. This increases time and cost and may not be a feasible option for all PET scans being performed.

The radioligand DPA-714 needs to be better explored in order to confidently explain exactly what microglial/neuroinflammatory profile it is identifying. The DPA-714 TSPO ligand in this project will be used in conjunction with known microglial markers to establish what state the cells are in, both in healthy and disease *post-mortem* tissue. This could lead to a better understanding of microglia in neurodegenerative disease and may even aid in developing ideas for diagnostic methods based on the neuroinflammatory profile.

1.4.5 Third generation TSPO and other neuroinflammatory ligands

To combat the rs6971 SNP that effects second generation PET tracers, third generation radioligands are currently being evaluated; but are still in the early stages of testing, with the aim of these to further improve specificity and binding ability. For example, initial research conducted using autoradiography on human *post-mortem* samples with the radiotracer [^{18}F]FEBMP showed no sensitivity to the polymorphism as known LABs and HABs displayed the same binding levels (219). This ligand would need to be used in human patients to be validated for clinical use. Another tracer, [^{18}F]GE-180 has been shown to be insensitive to the rs6971 polymorphism (220), however, there is

some debate about how accurate this ligand is, with possible ineffectiveness in crossing the BBB. Some research has shown that [^{18}F]GE-180 has a lower total volume of distribution than [^{11}C]PBR28, meaning that the later had a better penetrance into the vasculature (220). The development of new TSPO radioligands is a step in the right direction but their effectiveness and applicability need to be tested in more preclinical and clinical models.

Furthermore, there is some concern that TSPO is not microglia specific and is present in other cell types meaning alternative targets are being investigated. However, it is important to note that even though TSPO might bind to several cell types, this still shows levels of neuroinflammation as these would all be immune cells. Other targets include colony-stimulating factor 1 receptor (CSF1R), which is expressed by microglia and monocytes with good exclusivity, as found using human RNA-seq data (195). CSF1R radioligand [^{11}C]CPPC has been tested in a mouse model of AD, with good evidence for elevated binding and specificity (221). Cannabinoid receptor type 2 (CB2R) is another target being tested; however, this is also found in multiple cell types including microglia, monocytes, macrophages and endothelial cells so may present with the same problems as TSPO. While upregulation of the receptor has been seen in animal models of AD, in PET scans using human AD patients, [^{11}C]NE40 (a CB2R ligand) was decreased, and no relationship was observed with Aβ (222). This could indicate this receptor isn't the best target to determine microglial activity in AD. The authors highlight here that there is evidence that CB2R is expressed by neuronal cells and that the decrease seen could be due to neuronal loss rather than a decreased microglial response (222). Finally, purinergic receptors P2RX7 and P2RY12 have been tested as PET ligands, again due to their exclusive expression in microglia (195). P2RX7 is involved in the neuroinflammatory response of microglia and this receptor is upregulated in AD (223). P2RX7 ligand ([^{11}C]GSK1482160) has shown to be effective in a mouse model of neuroinflammation (224), but further testing in humans would be needed to validate this tracer. P2RY12 is associated with homeostatic microglia and decreases in AD (107). The ligands developed for this receptor have mainly been tested using autoradiography. [^{11}C]P2Y12R-ant was used for autoradiography on human MS tissue and exhibited a decrease in disease compared to control (225). Further experimentation is needed to confirm the use of P2RY12 ligands in human AD.

Currently, TSPO is still the most promising radioligand and provides the best evidence for neuroinflammatory changes in AD. However, more research is needed to produce ligands that are insensitive to the rs6971 polymorphism and to understand exactly which microglia are highlighted by TSPO ligands, which this thesis aims to elucidate.

1.5 Scope for project

Inflammation is an important component in many neurodegenerative diseases. Having a better understanding of the mechanisms involved can lead to improved diagnostic tools and treatments. Particularly in AD, microglia are a key cell type that influence the brain environment and how it deals with the disease. Early diagnosis of AD using microglial and neuroinflammatory markers may enable more brain function to be saved if accurate treatments become available. PET scans could be a useful early diagnostic tools to determine the level of neuroinflammation in the brains of AD patients, which could specify the stage and progression of the disease. Ligands for PET scans are being developed for pathological markers such as Aβ and tau, but also for neuroinflammation. Specifically, the TSPO marker is being studied to assess levels of microglial reactivity in AD and other neurodegenerative diseases. However, microglia are highly diverse cells and have interchangeable morphology and functions depending on the requirement of the CNS. It is currently unknown which type of microglia are most associated with TSPO, whether this is a specific phenotypic subset or all cells. This knowledge would aid clinicians' interpretation of the signal they observe from PET scans and give better insight into inflammation within the patient's brains, as well as provide further understanding of the role of microglia in AD.

Chapter 2 Project Hypothesis and Aims

This thesis aims to explore the microglial profile in Alzheimer's disease identified by the TSPO protein in two distinct brain regions and compare this with known microglial markers over the course of disease progression. This will elucidate if TSPO identifies a specific subset of microglia or can be used as a more generalised marker of neuroinflammation, and whether this is dependent on disease stage. Furthermore, the use of the cerebellum as a pseudo-reference region for TSPO PET scans will be clarified in this project.

2.1 Hypothesis

It is hypothesised that the TSPO signal highlights several, specific microglial phenotypes based on the stage and severity of Alzheimer's disease, with a more homeostatic phenotype present in early stages and more reactive phenotype in later stages; and this will differ between the pathologically affected temporal lobe and less severely affected cerebellum.

2.2 Aims

Using human *post-mortem* brain tissue, at different disease stages, from the South West Dementia Brain Bank and the TSPO protein, this project will explore:

i. The pathological and neuroinflammatory profiles of the temporal lobe and the cerebellum, and thus confirm whether the cerebellum can be used as a pseudo-reference region for TSPO PET scans.
ii. The prevalence of the rs6971 SNP in the cohort and the impact this has on the binding of the TSPO antibody.
iii. The microglial phenotypes recognised by TSPO from early to late stages of Alzheimer's disease.
iv. Whether other cells in the CNS express the TSPO signal.
v. Whether a fluorescently conjugated TSPO ligand ([^{18}F]DPA-714) can be used on the tissue compared to the TSPO antibody.

Chapter 3 Materials and Methods

3.1 Cases

Post-mortem brain tissue from 60 donors was used from the South-West Dementia Brain Bank (SWDBB), split into three groups: Braak stage 0-II, Braak stage III-IV and Braak stage V-VI (N=20 in each group) as marker of disease severity (**Table 2**). Cases in each group were closely matched for age (P=0.056), sex (P=0.515) and *post-mortem* delay (P=0.126) between Braak groups. *Post-mortem* delay was no more than 72 hours for most cases. Formalin-fixed paraffin embedded (FFPE) tissue from the middle/superior temporal gyrus and cerebellum were obtained for immunohistological analysis. Frozen tissue from the same brains and regions was also obtained to perform detection of the inflammatory environment by MesoScale Discovery (MSD) multiplex assays (**Table 2**).

Table 2 Demographic, clinical and *post-mortem* characteristics of cases from the South-West Dementia brain bank

Cases	*Braak stage 0-II*	*Braak stage III-IV*	*Braak stage V-VI*
Gender	7M:13F	11M:9F	9M:11F
Age at death (years, mean±sd)	84.95±8.94	86.20±6.40	80.45±7.60
Braak stage	0 = 4 I = 8 II = 8	III = 10 IV = 10	V = 8 VI = 12
APOE genotype	2/2 = 0 2/3 = 3 2/4 = 0 3/3 = 12 3/4 = 3 4/4 = 0 ? = 2	2/2 = 0 2/3 = 4 2/4 = 0 3/3 = 8 3/4 = 8 4/4 = 0	2/2 = 0 2/3 = 1 2/4 = 1 3/3 = 10 3/4 = 5 4/4 = 3
Post-mortem delay (hours, mean±sd)	54.00±32.00	42.56±19.59	37.00±22.03
Total	20	20	20

M male, *F* female, *SD* standard deviation, *APOE genotype* showing 2/3 as alleles or as unknown (?)

3.1.1 Ethical approval

The study is covered by the ethical approvals from the South-West Dementia Brain Bank (NRES Committee South West Central Bristol (REC reference: 08/H0106/28+5)) and is sponsored by the University of Southampton (ERGO 62445).

3.2 Immunohistochemistry

Table 3 Lists of antibodies used in the project, including their host species, primary antibody dilution (1°), secondary antibody dilution (2°), antigen retrieval buffer, supplier and product reference

Protein	*Species*	*1° Dilution*	*2° Dilution*	*Antigen retrieval*	*Supplier*	*Product number*
Pan-Aβ (4G8)	Mouse	1:2000 (DAB)	1:800 (DAB)	Citrate (pH6)	Covance-Biolegend	800708
pTau (AT8)	Mouse	1:500 (DAB)	1:800 (DAB)	Citrate (pH6)	Thermo Scientific	MN1020
TSPO	Rabbit	1:5000 (DAB) 1:2500 (Fluorescent)	1:800 (DAB) 1:200 (Fluorescent)	Citrate (pH6)	Abcam	Ab109497
Iba1	Rabbit	1:750 (DAB)	1:800 (DAB)	Citrate (pH6)	Wako	019-19741
Iba1	Goat	1:1000 (Fluorescent)	1:100 (Fluorescent)	Citrate (pH6)	Abcam	Ab5076
HLA-DR	Mouse	1:200 (DAB) 1:50 (Fluorescent)	1:800 (DAB) 1:200 (Fluorescent)	Citrate (pH6)	Dako	M0775
MSR-A	Goat	1:500 (DAB) 1:100 (Fluorescent)	1:600 (DAB) 1:200 (Fluorescent)	Citrate (pH6)	R&D Systems	AF2708
CD68	Mouse	1:250 (Fluorescent)	1:200 (Fluorescent)	Citrate (pH6)	Dako	M0876
CD64	Goat	1:100 (Fluorescent)	1:200 (Fluorescent)	Citrate (pH6)	R&D Systems	AF1257
CD31	Mouse	1:50 (Fluorescent)	1:200 (Fluorescent)	Citrate (pH6)	Abcam	Ab9498
CD163	Mouse	1:500 (Fluorescent)	1:200 (Fluorescent)	Citrate (pH6)	Serotec	MCA1853
GFAP	Mouse	1:1000 (Fluorescent)	1:200 (Fluorescent)	Citrate (pH6)	Abcam	Ab4648

3.2.1 Finding positive control brain sections

In order to ensure the consistency and specificity of staining for the protein of interest, positive control brain sections were identified. To find a good set of positive controls, 11 AD brains were tested with previously optimised antibodies, including Iba1 and TSPO using both DAB and immunofluorescence staining. The brains were AD1T, AD2T, AD5O, AD5CG, AD8CG, AD9T, AD10T, AD10MF, AD11OC, AD13-3 and AD13S and sourced from BRAIN UK. Of these brains, AD1T, AD2T, AD8CG and AD10T had the best and most uniform staining (**Figure 6**). Therefore, these were used as

positive controls throughout the project for antibody optimisation due to the presence of microglial cells.

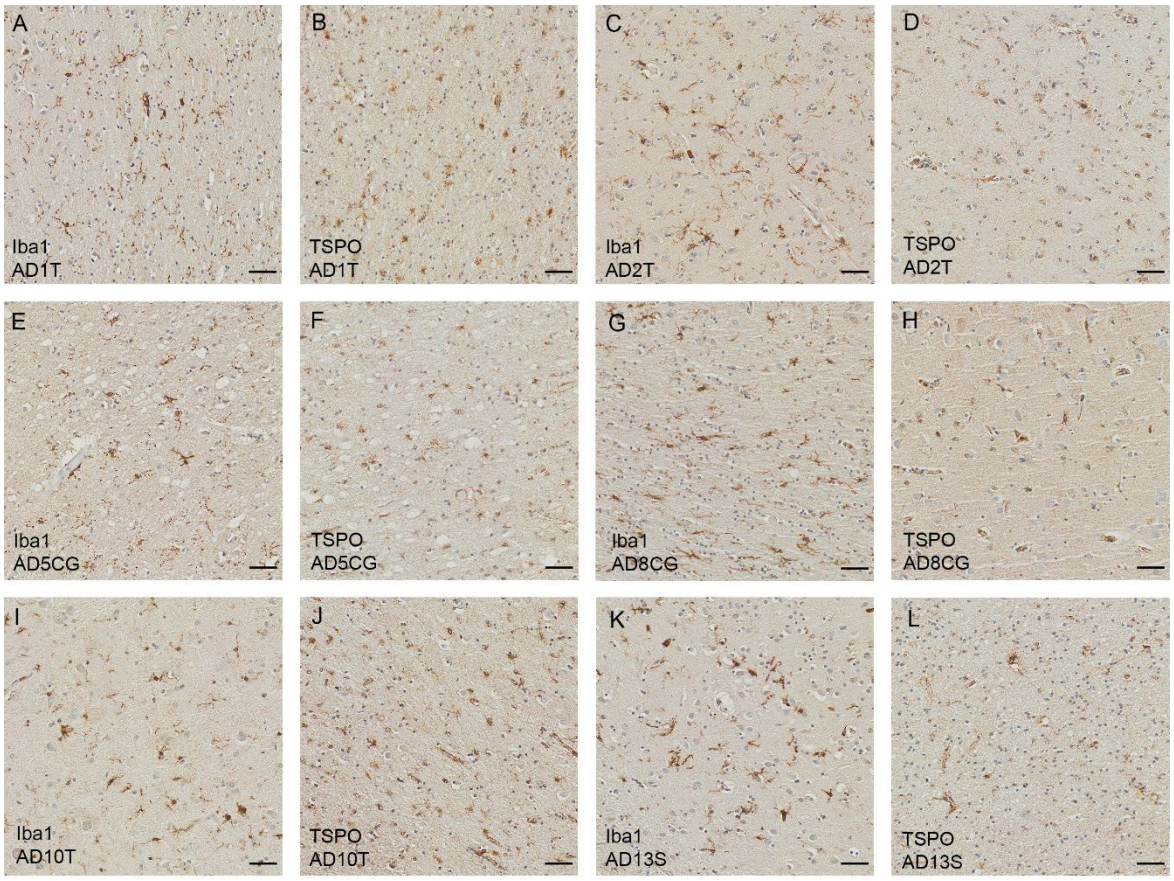

Figure 6 Establishing a positive control. Using Iba1 (019-19741) and TSPO (ab109497) to stain several AD brains in order to find a positive control. Counterstaining: Haematoxylin. Scale bars = 50µm.

3.2.2 DAB protocol

6µm tissue sections from formalin-fixed paraffin-embedded tissue were used to perform immunohistochemistry targeting two markers of AD pathology: pan-Aβ (Covance-Biolegend, 800708) and phosphorylated (p)Tau (Thermo Scientific, MN1020) (**Table 3**). The following markers: TSPO (Abcam, ab109497), Iba1 (Wako, 019-19741), HLA-DR (Dako, M0775) and MSR-A (R&D Systems, AF2708) were used to assess microglia (**Table 3**). Hydrogen peroxide was used in 70% ethanol to block endogenous peroxidase reactivity. Antigen retrieval was performed with EDTA (pH8) or Citrate (pH6) (**Table 3**), depending on previously validated preference of each antibody. Blocking endogenous proteins was achieved with a solution made in the lab containing bovine serum albumin (BSA) and foetal calf serum or a solution of 5% normal rabbit/goat/donkey serum (NR/G/DS). Antibodies were visualised using the avidin-biotin-peroxidase complex method (Vectastain Elite, Vector Laboratories) with 3,3'-diaminobenzidine (DAB) as the chromogen and 0.05% hydrogen

peroxide as the substrate (Vector Laboratories) (**Figure 7**). These sections were counterstained with haematoxylin, dehydrated and mounted with Pertex (Histolab Products AB). Optimisation of new antibodies was performed with a variety of antigen retrieval methods, primary antibody dilutions and other parameters, further described in **Appendix B**. A negative control with no primary antibody was included in all staining runs. DAB staining was carried out by the author of this thesis, except for Iba1 and HLA-DR in temporal lobe, which was performed by Rebecca Beardmore, a previous PhD student working on the same cohort.

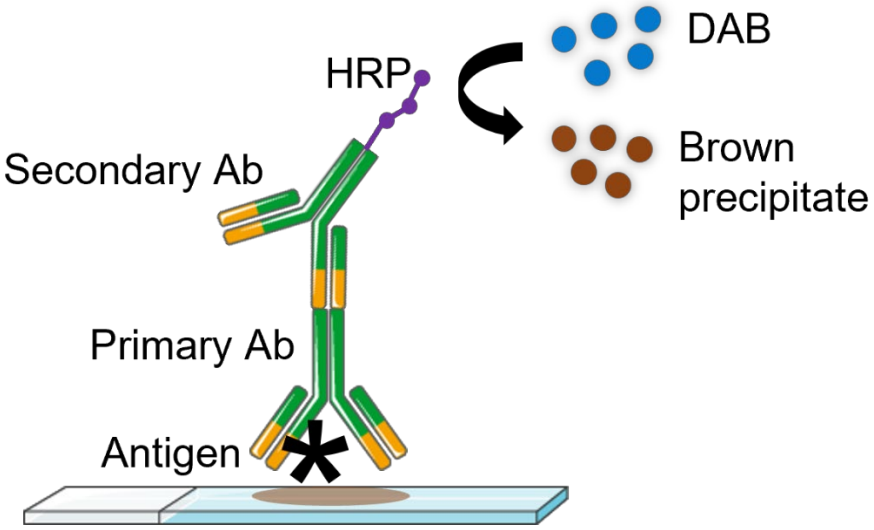

Figure 7 Schematic of immunohistochemistry method of staining FFPE tissue using the avidin-biotin-peroxidase complex and DAB chromogen. The primary antibody binds to the antigen. The HRP conjugated secondary antibody binds to the primary antibody and catalyses hydrogen peroxide in order to oxidise DAB into a brown precipitate. Ab = antibody. HRP = horseradish peroxidase.

3.2.3 Fluorescent protocol

A similar procedure was performed as in Section **3.2.2** for fluorescent immunohistochemistry of TSPO (Abcam, ab109497), Iba1 (Abcam, ab5076), HLA-DR (Dako, M0775), CD68 (Dako, M0876), MSR-A (R&D Systems, AF2708), CD64 (R&D Systems, AF1257), CD31 (Abcam, Ab9498), CD163 (Serotec, MCA1853) and GFAP (Abcam, Ab4648) (**Table 3**). Conjugated fluorescent secondary antibodies were used, dependant on the species the primary antibodies were raised in (ThermoFisher Highly Cross-Adsorbed Secondary Antibody, Alexa Fluor™ Plus 488/568/594) (**Figure 8**). 0.3% Sudan Black was used as a background autofluorescence quencher. Slides were counterstained with DAPI (1:500) to mark nuclei and mounted with Mowiol. Optimisation of new antibodies was performed with a variety of antigen retrieval methods, primary antibody dilutions and other parameters, further described in **Appendix B**. A negative control with no primary antibody was included in all staining runs. Double

staining for Iba1/TSPO, CD64/TSPO, CD31/TSPO, CD163/TSPO and GFAP/TSPO was performed by the author of this thesis, HLA-DR/TSPO was performed by students Laura Kulagowska and Thomas Scott, CD68/TSPO was performed by Henrike Antony and MSR-A/TSPO was performed by Charlotte Rogien, all MSc students co-supervised by the author of this thesis.

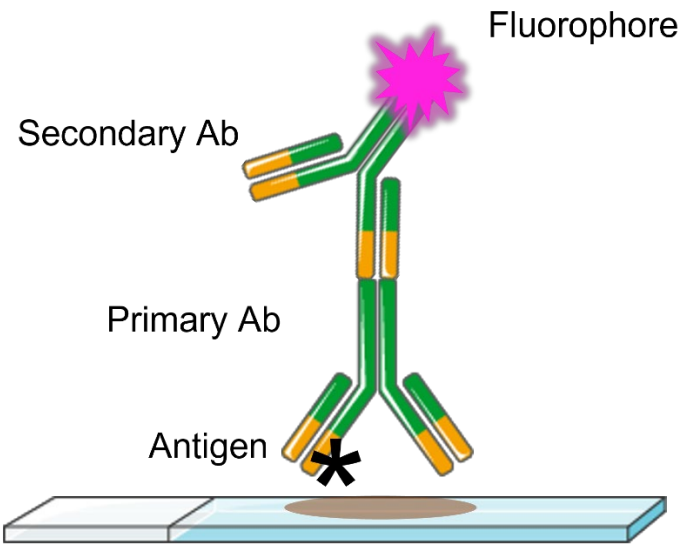

Figure 8 Schematic of immunofluorescent staining method of staining FFPE tissue. The primary antibody binds to the antigen. The fluorescently conjugated secondary antibody binds to the primary antibody. Ab = antibody.

3.3 Imaging and quantification

3.3.1 DAB analysis

To view the staining, the Olympus VS110 (Olympus America Inc.) automated slide scanner was used to take images for each run at 20X magnification. The digital images were visualised with the Olympus VS-Desktop software using the CSG add-in for extraction of regions of interest (ROI). For each slide, 30 ROIs of 500μmx500μm were selected in a pre-determined area of grey matter (**Figure 9**) and saved as a .tif format. Extracted ROIs were analysed with ImageJ/Fiji software using an automated macro, created by David Chatelet (BIU), to threshold and calculate protein load (%) of each antibody staining (**Figure 9**). This worked by separating out the colour channels (blue, green and brown) in the image in order to identify the brown DAB staining. To create an accurate threshold, images with high and low staining were analysed to get a threshold that would work for the majority of the images by capturing enough of the staining signal whilst keeping any background to a minimum. This was done using the thresholding tool in ImageJ/Fiji (**Figure 9**). All thresholding and analysis were done blinded to the case information. In total, for 60 cases and six markers used,

10,800 images were analysed for the DAB assessment. All DAB analysis was performed by the author of this thesis, except for Iba1 and HLA-DR in the temporal lobe, which was performed by Rebecca Beardmore, a previous PhD student in the Boche lab.

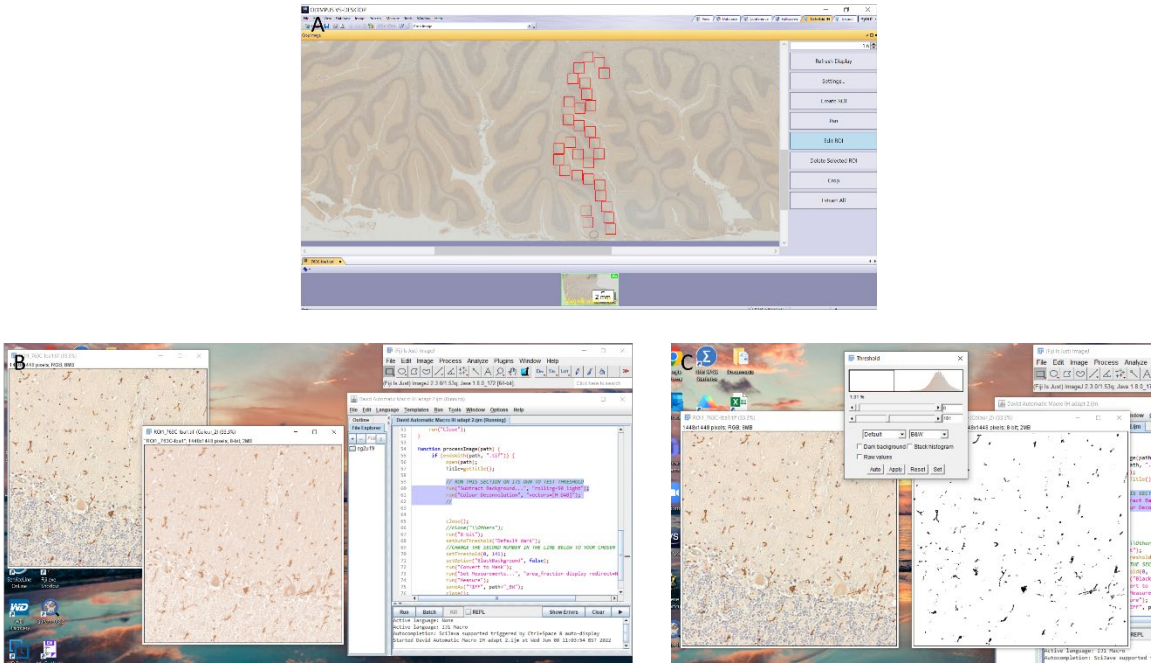

Figure 9 Quantitative analysis of DAB staining. (**A**) 30 regions of interest are placed in the grey matter, which the VS-Desktop software can crop and save. (**B**) A Fiji macro is used to separate the coloured channels so that just the brown DAB channel is selected. (**C**) The Fiji thresholding tool is used to find the best threshold for the staining, which is applied to all the cases and gives a readout of presence of staining per pixel (protein load %).

3.3.2 Fluorescent analysis

To quantify cell counts, the Olympus VS110 (Olympus America Inc.) automated slide scanner was used to take images at a 20X magnification with the fluorescent function. To visualise and analyse the slides, QuPath software (226) was used to select a section of pre-determined area of grey matter as the ROI and perform positive cell detection based on fluorescent thresholds for each marker (**Figure 10**). Thresholds were determined by selecting a test ROI and inputting different thresholds until an accurate number of positive cells were observed (227). This was performed in a blinded manner by two individuals on at least three cases to get an average threshold. The positive cell detection tool was used to ascertain the number of cells for each marker individually or the double staining (**Figure 10**). This used the nuclei stain DAPI to count total cells in the area as a baseline then, depending on the threshold settings, marked cells that were positive for FITC or CY3 fluorescent channels (**Figure 10**). The cell expansion measurement was determined based on the localisation of

the marker used. For example, Iba1 and HLA-DR are present on the cell membrane and therefore will be found close to the nucleus. This means the cell expansion can be set at 1µm around the nucleus. Whereas the TSPO is found in mitochondria and CD68 is found in the lysosomes, which may be located slightly further from the nucleus, thus a cell expansion of 2µm was ideal for these markers. The cell expansion was not set too large else other cells might intercept this and skew the number counted as positive. TSPO was typically stained with a corresponding secondary antibody conjugated with AF 568/594 and required the fluorescent channel CY3 in the Olympus slide scanner. The accompanying marker in the double staining was stained with the corresponding secondary antibody conjugated to AF 488 and required the fluorescent channel FITC.

When counting TSPO positive cells, the software could not differentiate between staining in the parenchyma or the blood vessels. Therefore, $TSPO^{+}$ endothelial cells had to be manually discounted from the total number of positive cells. For the double staining, there was no option for all three channels to be assessed (DAPI, FITC and CY3), therefore the software used the FITC channel as the baseline 'cell' and calculate how many CY3 'cells' were co-localised to this. If a 'cell' was marked as positive for both markers but did not have a nucleus associated, this was manually discounted from the total number of positive cells for the double staining. The threshold settings can be found in **Appendix A** and details of the optimisation of this analysis method can be found in **Appendix B - B.6**. In total, for 30 cases and five markers used in conjunction with TSPO, 150 images were analysed in the fluorescent assessment, with three channels examined in each image. Fluorescent cell counting analysis was performed by the author of this thesis, Thomas Scott, Henrike Antony and Charlotte Rogien.

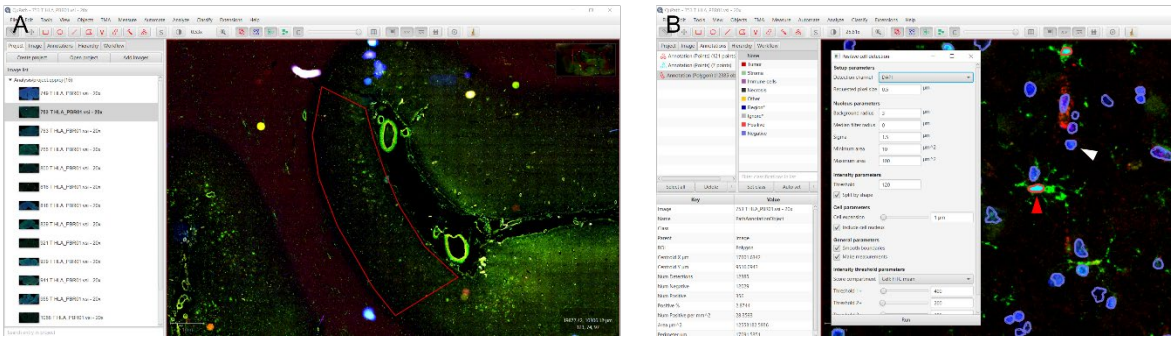

Figure 10 Qualitative analysis of fluorescent double staining. (**A**) QuPath software showing the ROI drawn using the polygon tool in a grey matter area of the temporal cortex. (**B**) Using the positive cell detection tool with predetermined thresholding parameters. The red arrow shows a positive cell detection, and the white arrow shows a negative cell detection in the FITC channel.

3.4 Multiplex assay

Inflammatory proteins were measured using the V-Plex MesoScale Discovery (MSD) multi-spot assay platform (MesoScale Diagnostics, Rockville USA) using the cohort of 60 cases. ~ 100mg of frozen grey matter from the temporal lobe (performed by Rebecca Beardmore) and cerebellum (performed by the author of this thesis) were homogenised at a 1:5 dilution with RIPA lysis buffer (Thermo Fisher Scientific), with protease and phosphatase inhibitors. Total protein concentration was found using the BCA Protein Assay Kit (Thermo Fisher Scientific). 25µl of brain homogenate was used for the V-Plex proinflammatory panel 1, chemokine panel 1 and cytokine panel 1, with each plate being read according to the manufacturer's instructions on Meso Quickplex SQ120. A serial dilution of the recommended diluent standards was used to create a calibration curve of known levels of cytokines/chemokines to standardise the samples against. Absolute target protein levels (pg/ml) were quantified and normalised in respect to the BCA assay total protein concentration. The preparation of tissue and BCA assay were performed by the author of this thesis, Oliver Dennett and Iain Hartnell. The MSD assay was carried out by Laurie Lau.

3.5 Genotyping

In order to assess which cases were LAB, MAB or HAB for the SNP rs6971, which causes an Ala147Thr substitution in the TSPO gene, a TaqMan genotyping assay was used (ThermoFisher, C___2512465_20).

3.5.1 DNA extraction

Genomic DNA was extracted from frozen cerebellum samples using the PureLink Genomic DNA Extraction Mini Kit (ThermoFisher, K182001). ~25mg of each sample was placed into 180µl of digestion buffer and 20µl of proteinase K for 3 hours at 55°C. After this time, samples were centrifuged for 3 minutes at 10,000xg. The supernatant was transferred to a new tube. 20µl of RNase A was added to remove RNA, then 200ul of PureLink Genomic Lysis/Binding buffer and 200ul of 100% ethanol was added to each sample. The lysate was placed into a spin column with a collection tube and centrifuged for 1 minute at 10,000xg. This collection tube was discarded, and the spin column was placed into a new collection tube. 500µl of wash buffer 1, pre-prepared with ethanol according to the instructions on the label, was added to the spin column. This was then centrifuged for 1 minute at 10,000xg. This collection tube was discarded, and the spin column was placed into a new collection tube. 500µl of wash buffer 2, pre-prepared with ethanol according to the instructions on

the label, was added and the spin column was centrifuged for 3 minutes at 10,000xg. Finally, the last collection tube was discarded. The spin column was placed in a microcentrifuge tube with 100µl of elution buffer and centrifuged for 1 minute at 10,000xg. The tube then contained purified genomic DNA, of which the concentration was calculated using 2µl of sample on the NanoDrop Microvolume Spectrophotometer. Samples were then diluted down, from their original stock, to 0.9ng/µl in DNAse free water.

3.5.2 PCR

The TaqMan SNP Genotyping assay kit contains forward and reverse primers and the VIC/FAM fluorescent probes the correspond to an A/G allele. 1.25µl of this assay is put into each well, along with 12.5µl of TaqMan Genotyping Master Mix (ThermoFisher, 4371353) and 11.25µl of the genomic DNA sample. DNA samples were run in duplicate on a 96 well plate along with two wells dedicated to no template controls (DNAse free water). A pre-PCR plate read was performed on the Applied Biosystems StepOnePlus RT PCR machine, followed by the PCR cycles (**Table 4**). Finally, a post-PCR plate read was performed. Results were visualised on the Applied Biosystems TaqMan Genotyping software.

Table 4 PCR cycle programme.

Step	*Temperature*	*Length*	*Cycles*
Polymerase activation	95°C	10mins	Ramp 1°C/sec
Denaturation	95°C	15secs	40
Annealing/extension	60°C	1min	40

3.6 Statistical analysis

Statistical analysis was carried out using the IBM SPSS v28 statistical software package (IBM Corp. Armonk, NY) and GraphPad Prism v9.2 (GraphPad Software. San Diego CA). The results were displayed as protein load (%) for DAB staining of Aβ, pTau, Iba1, TSPO, HLA-DR and MSR-A or the number of positive cells (% of total cells or % of microglial cells) for fluorescent staining of Iba1, HLA-DR, CD68, MSR-A and CD64 with TSPO. The data compared Braak stage groups or brain areas (temporal lobe and cerebellum) for analysis. The normality of distribution was assessed by the Shapiro-Wilk test for each set of staining in each brain area. If the data were found to be non-parametric, the Kruskal-Wallis test was used and median values were presented. Conversely, if the

data were found to be normally distributed, the parametric ANOVA U-test was performed, and mean values were presented. Correlations were performed using the Spearman's rank for non-parametric data and Pearson's correlation for parametric data. To account for multiple correlation testing, the two-stage step-up Benjamini, Kreiger and Yekutieli test was used to control for the false discovery rate (FDR) in *post-hoc* analysis. P values of <0.05 (*) were considered significant for the comparisons and P<0.01 (**) for the correlations. A P value of <0.001 may be denoted with (***) and P<0.0001 with (****).

Chapter 4 The Pathological and Neuroinflammatory Profile of the Temporal Lobe and Cerebellum

The temporal lobe and cerebellum exhibit vastly different environments in neurodegenerative disease. For example, in AD, the temporal lobe is affected by both amyloid and tau pathology early on in the disease progression as the first Braak stage is located to the entorhinal cortex (10). This differs to the cerebellum where amyloid pathology is not seen until later stages of the disease in Thal phase 5 (64), and practically no tau deposition is seen here (208). Furthermore, the cerebellum has been used in PET assessments of neuroinflammation as a pseudo-reference region to compare against the rest of the neocortex, without the need for arterial blood sampling (207) and to minimise patient-to-patient differences. Using this region as a pseudo-reference is applicable due to the cerebellum's lack of pathology and levels of neuroinflammatory marker (TSPO) remain consistent throughout the disease progression, hence the term 'pseudo' (207). However, there is a need to elucidate this finding, as some research suggests that other brain regions are more appropriate for this purpose (228). Classic pathological markers of AD: pan-Aβ and pTau, were used to immunostain the temporal lobe and cerebellum in order to clarify previous literature findings in which the cerebellum expresses lower levels of these proteins and therefore can be confirmed as a suitable pseudo-reference region.

As these two brain regions express different pathological environments, microglia, the main immune cells in the brain, are thought to contribute to the pathogenesis of AD differently in each area. However, there is still a lack of understanding as to how microglia promote or respond to neurodegeneration, and even less understanding of these cells in the cerebellar environment as this area has not been explored in depth in regard to its neuroimmune component. Different microglial markers are used in *post-mortem* studies to explore neuroinflammation in the brain after death, and the use of human tissue increases the relevance to clinical practice. There is evidence for microglial heterogeneity in AD (229), with diverse phenotypic expression seen in different brain regions and stages of the disease. This chapter aims to classify the immunophenotype of microglia seen during the progression of AD by using microglial markers in both the temporal lobe and cerebellum, to give insight into the differences, or similarities, of the neuroinflammatory phenotype of these cells in each region. Using PET analysis, TSPO levels appear to increase over the course of AD (12, 13), therefore, this thesis also aims to elucidate this finding.

This chapter presents results for the first two aims of this thesis (Section **2.2**). Using human *post-mortem* tissue, immunohistological techniques via DAB chromogenic reaction, and MSD assays, this chapter will explore the neuroinflammatory profiles of the temporal lobe and the cerebellum, and thus confirm whether the cerebellum can be used as a control region for TSPO PET scans (aim i). Furthermore, this chapter also reports the use of genotyping techniques to examine the prevalence of the TSPO rs6971 SNP in the cohort and the impact this had on the binding of the TSPO antibody (aim ii).

4.1 Pathological markers for AD

4.1.1 Aβ and pTau

Qualitative : Amyloid plaques in the temporal lobe appear neuritic in nature, with a dense core of dystrophic neurites and possible pTau and microglial involvement (230). There is a stark increase in spread of plaques between Braak stage 0 and Braak stage VI (**Figure 11A, B**). In the cerebellum, the plaques appear very diffuse, without the dense core, and are mainly found in the molecular layer of the cerebellum (**Figure 11D, E**). The pTau in temporal Braak stage VI is widespread in the form of neuropil threads throughout the parenchyma and also in tangles, presumably within the neuronal bodies (**Figure 11H**), whereas the cerebellum is mainly devoid of pTau (**Figure 11J, K**).

Quantitative: Both the Aβ and pTau antibody staining was quantified in the temporal lobe and cerebellum to ascertain levels of these proteins and whether there was a difference in AD pathology between the two brain areas. In the temporal tissue, a significant increase in pan-Aβ was observed in Braak stage V-VI compared to Braak stages 0-II (Braak 0-II: median 1.48%, Braak III-IV: median 5.88%, Braak V-VI: median 10.87%; $P<0.0001$). There were also significant increases between Braak stages 0-II and III-IV ($P=0.0275$), as well as Braak stages III-IV and V-VI ($P=0.0193$) (**Figure 11C**). In the cerebellum, there was a significant increase in pan-Aβ between Braak stages 0-II and V-VI (Braak 0-II: median 0.11%, Braak III-IV: median 0.15%, Braak V-VI: median 0.27%; $P=0.0005$) (**Figure 11F**). pTau was significantly increased across the Braak stages in temporal tissue (Braak 0-II: median 0.04%, Braak III-IV: median 0.75%, Braak V-VI: median 5.27%; $P<0.0001$), with significant increase observed between Braak stages 0-II and stages III-IV ($P=0.0053$) and between stages III-IV and V-VI ($P=0.0072$) (**Figure 11I**). However, no significant difference was seen in the cerebellum tissue for pTau (Braak 0-II: median 0.02%, Braak III-IV: median 0.03%, Braak V-VI: median 0.04%; $P=0.081$) (**Figure 11L**).

Differences between the pathology of the brain regions were also investigated, disregarding Braak stage, with Aβ (TL: median 6.19%, Cb: median 0.16%; $P<0.0001$) and pTau (TL: median 0.71%, Cb:

median 0.02%; P<0.0001) loads significantly higher in the temporal lobe than the cerebellum (**Figure 12A, B**). Finally, analysis was carried out to test for sex differences in pan-Aβ and pTau immunostaining, irrespective of Braak stage. There were no differences seen between male and female cases for Aβ (M: median 6.68%, F: median 4.99%; P=0.0599), or pTau (M: median 2.03%, F: 0.14%; P=0.0686) in the temporal lobe, and also no difference for Aβ (M: median 0.17%, F: median 0.15%; P=0.3643) or pTau (M: median 0.03%, F: median 0.02%; P=0.1474) in the cerebellum (**Figure A1A, G, B, H**).

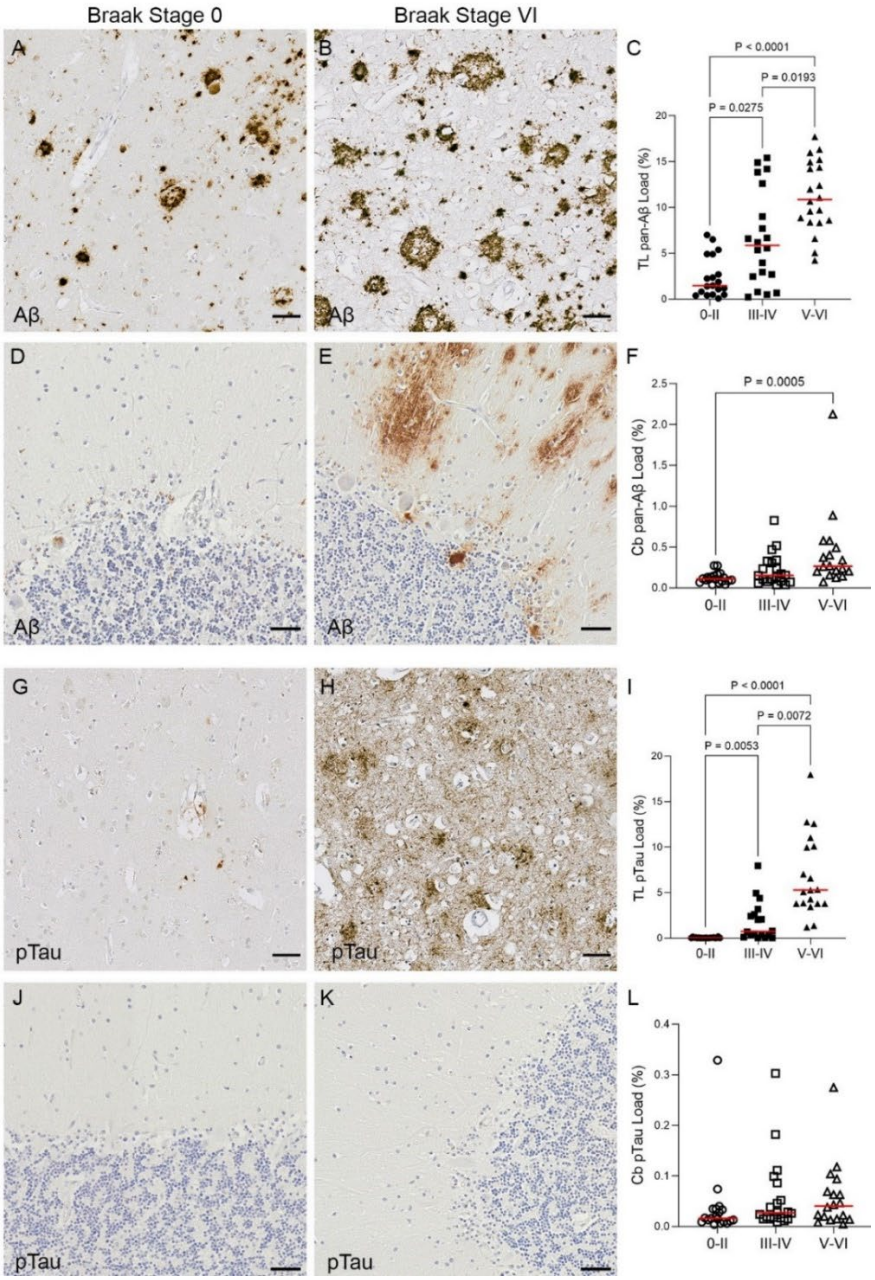

Figure 11 Illustrations and quantification of AD pathological markers pan-Aβ and pTau in the temporal lobe (**A, B, C, G, H, I**) and the cerebellum (**D, E, F, J, K, L**). Counterstain: Haematoxylin. Scale bars = 50μm. Graphs presented as individual values with median (**C, F, I, L**).

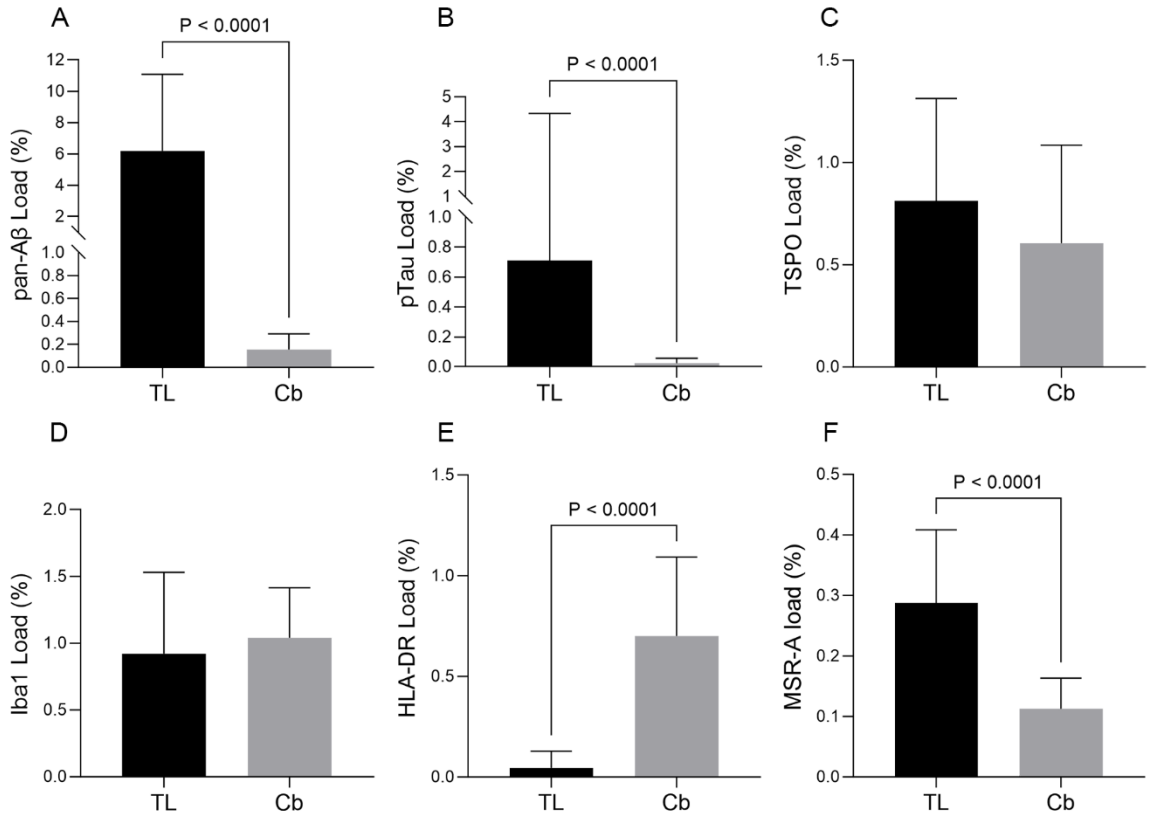

Figure 12 Comparisons between temporal lobe (TL) and cerebellum (Cb) for Aβ, pTau, TSPO, Iba1, HLA-DR and MSR-A protein loads. Graphs presented as median with range.

4.2 Microglial markers in AD

4.2.1 TSPO

TSPO is an outer mitochondrial membrane receptor thought to be responsible for cholesterol transport, protection against reactive oxygen species and general homeostatic maintenance in these organelles (116). In the periphery it is found in most tissues, but in the CNS it is primarily found in microglia and, to a lesser extent, macrophages and endothelial cells (187). The TSPO antibody used (ab109497) has been knock-out validated in mice and in control *vs* AD human brains (187).

Qualitative: TSPO staining was present in the endothelial cells as well as in microglial cells (**Figure 13E-H**, **Figure 14A, B** and **Figure 15A, B**). Temporal TSPO staining appeared in the parenchyma (within microglia) in Braak stage VI (**Figure 14B**). The TSPO in the cerebellum can be seen primarily between the molecular and granular layers, especially in Braak stage VI (**Figure 15B**). The overall appearance of TSPO immunostaining appeared punctate due to its presence within the mitochondria. Also, it can be seen surrounding the nucleus, as this is where the endoplasmic

reticulum is located, with which mitochondria have interactions (**Figure 13E, F**, **Figure 14A, B** and **Figure 15A, B**). It is important to note, that from qualitative pathological assessment, TSPO was not observed in neuronal or dendritic cells.

Quantitative: TSPO protein load was significantly increased across the Braak stages in the temporal lobe (Braak 0-II: mean 0.67%, Braak III-IV: mean 0.72%, Braak V-VI: mean 1.41%; P<0.0001), particularly between Braak stages III-IV and V-VI (P=0.0001) (**Figure 14C**). No difference was seen in the cerebellum for TSPO (Braak 0-II: median 0.57%, Braak III-IV: median 0.65%, Braak V-VI: median 0.64%; P=0.9249) (**Figure 15C**). Examining alteration between the temporal lobe and cerebellar TSPO load, there was no difference found (TL: median 0.81%, Cb: median 0.61%; P=0.0721) (**Figure 12C**). Finally, there was no difference between males and females TSPO load in either the temporal lobe (M: median 0.60%, F: median 0.85%; P=0.2887) or cerebellum (M: median 0.61%, F: median 0.61%; P=0.8171) (**Figure A1C, I**) was observed.

4.2.2 Iba1

Iba1 is a commonly used microglial marker due to its locality on the membrane, allowing for the full morphology of these cells to be detected. It is a calcium binding protein and is associated with actin in the cytoskeleton to enable microglia motility (119).

Qualitative: Qualitatively, Iba1 in the temporal lobe appeared to remain the same over the course of the disease, with cells exhibiting both ramified and some amoeboid morphology (**Figure 14D, E**). Clustering of $Iba1^+$ microglia was seen, which was postulated to be surrounding Aβ plaques (**Figure 13D**). This is corroborated with a large number of studies, discussed further in Section **4.6.1**. However, without an amyloid stain this could not be definitively proved. The Iba1 clustering seen in the cerebellum may be around dying Purkinje cells, rather than Aβ, as they are typically found at the junction of the cerebellar layers (**Figure 15D, E**). Also, the $Iba1^+$ microglia in this region showed slight thickening of processes, which may be the reason for the increase of this marker over the course of the Braak stages (**Figure 15E**).

Quantitative: No significant difference was found for Iba1 load in the temporal lobe (Braak 0-II: median 0.80%, Braak III-IV: median 1.10%, Braak V-VI: median 0.89%; P=0.6878) (**Figure 14F**). However, there was a significant increase in the protein load of this marker in the cerebellum (Braak 0-II: median 0.40%, Braak III-IV: median 1.07%, Braak V-VI: median 1.21%; P=0.0152) over the course of the disease (**Figure 15F**). Examining the difference between regions there was no difference in Iba1 load between the temporal lobe and cerebellum (TL: median 0.92%, Cb: median 1.04%; P=0.5367) (**Figure 12D**).There was no difference between the protein load of males and females in the temporal lobe (M: median 0.92%, F: median 0.97%; P=0.9789), but there was a significant

increase in male Iba1 protein load in the cerebellum (M: median 1.09%, F: median 0.79%; P=0.0469) (**Figure A1D, J**).

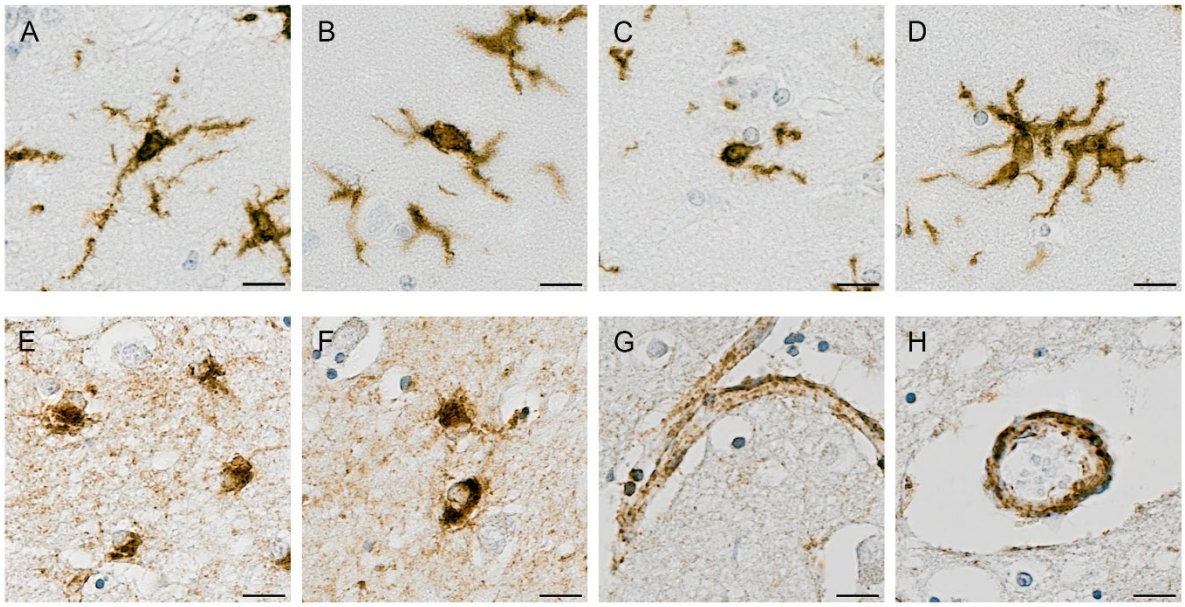

Figure 13 Illustrations of Iba1 and TSPO DAB staining. Iba1 identifies: (**A**) ramified microglia, (**B**) intermediate microglial morphology with shorter processes, (**C**) amoeboid microglia, and (**D**) microglial cluster. (**E-F**) shows TSPO$^+$ microglia, with TSPO primarily surrounding the nuclei but staining also seen in the processes. (**G-H**) TSPO expression in endothelial cells/smooth muscle cells of the blood vessel walls, in a (**G**) longitudinal and (**H**) horizontal plane. Counterstaining: Haematoxylin. Scale bars = 50µm.

4.2.3 HLA-DR

HLA-DR is associated with antigen presentation in microglial cells and is located on the cell surface. It is also present in monocytes and macrophages. HLA-DR aids the initiation of the inflammatory process by presenting antigens primarily to T cells (112).

Qualitative: The HLA-DR staining in the temporal lobe exhibited a stronger stain in Braak stage VI compared to Braak stage 0. Clustering was observed from the HLA-DR staining (**Figure 14H**). There were HLA-DR$^+$ cells present in both the granular and molecular layers of the cerebellum (**Figure 15G, H**).

Quantitative: No statistical difference was seen for HLA-DR protein load in the temporal lobe (Braak 0-II: median 0.06%, Braak III-IV: median 0.04%, Braak V-VI: median 0.05%; P=0.9681) or cerebellum (Braak 0-II: median 0.90%, Braak III-IV: median 0.63%, Braak V-VI: median 0.54%; P=0.0997) across

the disease progression, however a decreasing trend was seen in the cerebellum (**Figure 14I** and **Figure 15I**). Examining the difference between the brain regions there was a higher HLA-DR load in the cerebellum compared to the temporal lobe (TL: median 0.05%, Cb: median 0.70%; P<0.0001) (**Figure 12E**). Furthermore, no sex differences were seen for HLA-DR in the temporal lobe (M: median 0.05%, F: median 0.05%; P=0.9144) or cerebellum (M: median 0.63%, F: median 0.74%; P=0.3273) (**Figure A1E, K**).

4.2.4 MSR-A

MSR-A is a scavenging receptor, expressed on the cell surface, that contributes to macrophage adhesion to initiate inflammation and is typically associated with amyloid plaques in AD (115).

Qualitative: The MSR-A in the temporal lobe did exhibit more staining in Braak stage VI than Braak stage 0 and it appeared more amoeboid in morphology, with less processes, indicating a reactive phenotype. However, the staining is not abundantly present overall (**Figure 14J, K**). MSR-A is shown to be located around the Purkinje cells in the cerebellum, between the molecular and granular layers, but again shows low expression levels (**Figure 15K**).

Quantitative: Protein load of MSR-A did not reach significance across the Braak stages in the temporal lobe (Braak 0-II: median 0.23%, Braak III-IV: median 0.26%, Braak V-VI: median 0.31%; P=0.1263) or the cerebellum (Braak 0-II: median 0.12%, Braak III-IV: median 0.13%, Braak V-VI: median 0.10%; P=0.5308) (**Figure 14L** and **Figure 15L**). However, there was significant increase in the temporal lobe compared to the cerebellum (TL: median 0.29%, Cb: median 0.11%; P<0.0001) (**Figure 12F**). No sex differences were observed for this marker in the temporal lobe (M: median 0.26%, F: median 0.29%; P=0.6237) or cerebellum (M: median 0.12%, F: median 0.11%; P=0.9481) (**Figure A1F, L**).

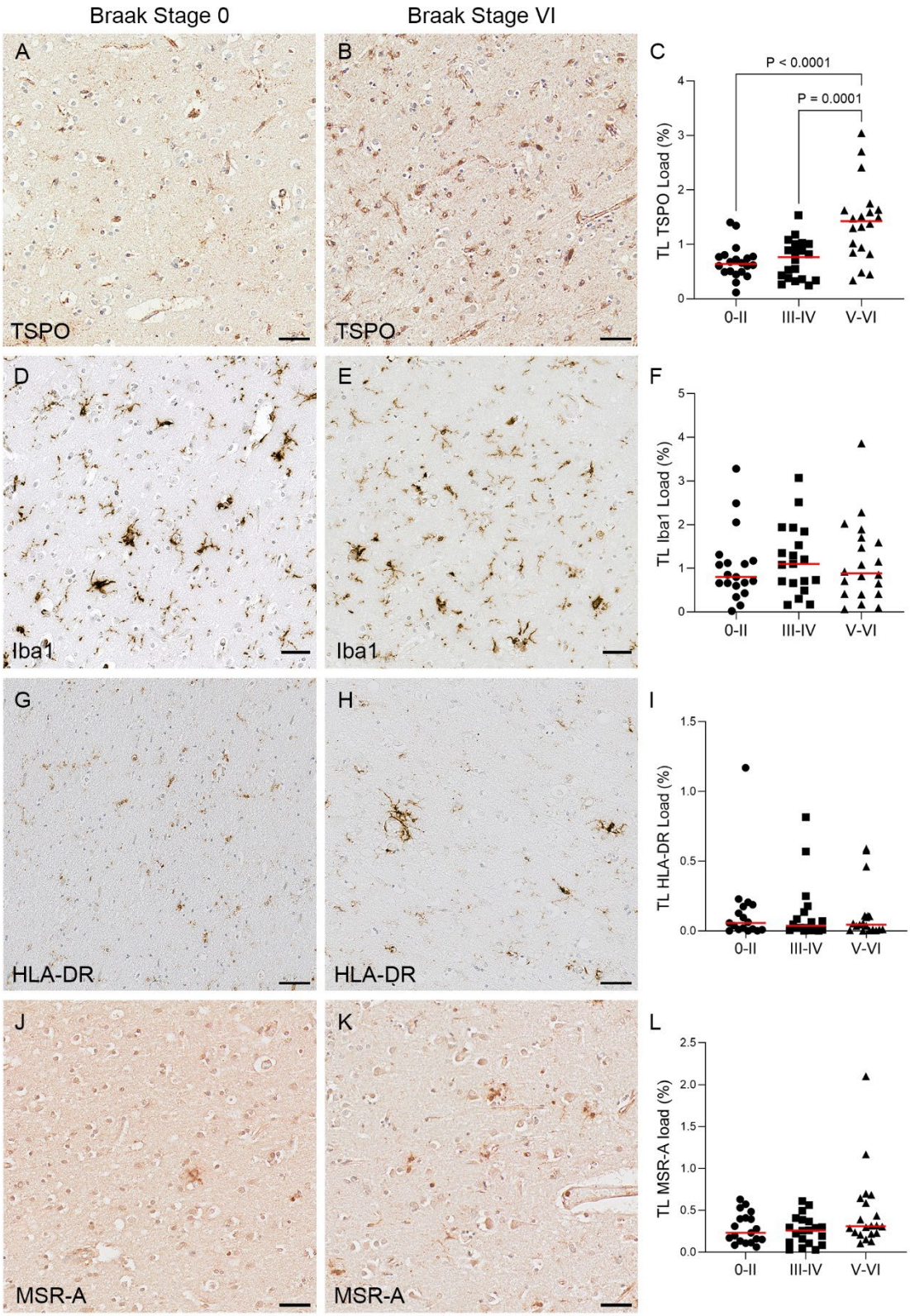

Figure 14 Illustrations and quantification of microglial markers TSPO (**A, B, C**), Iba1 (**D, E, F**), HLA-DR (**G, H, I**) and MSR-A (**J, K, L**) in the temporal lobe. Counterstain: Haematoxylin. Scale bar = 50µm. Graphs presented as individual values with mean (**C**) or median (**F, I, L**).

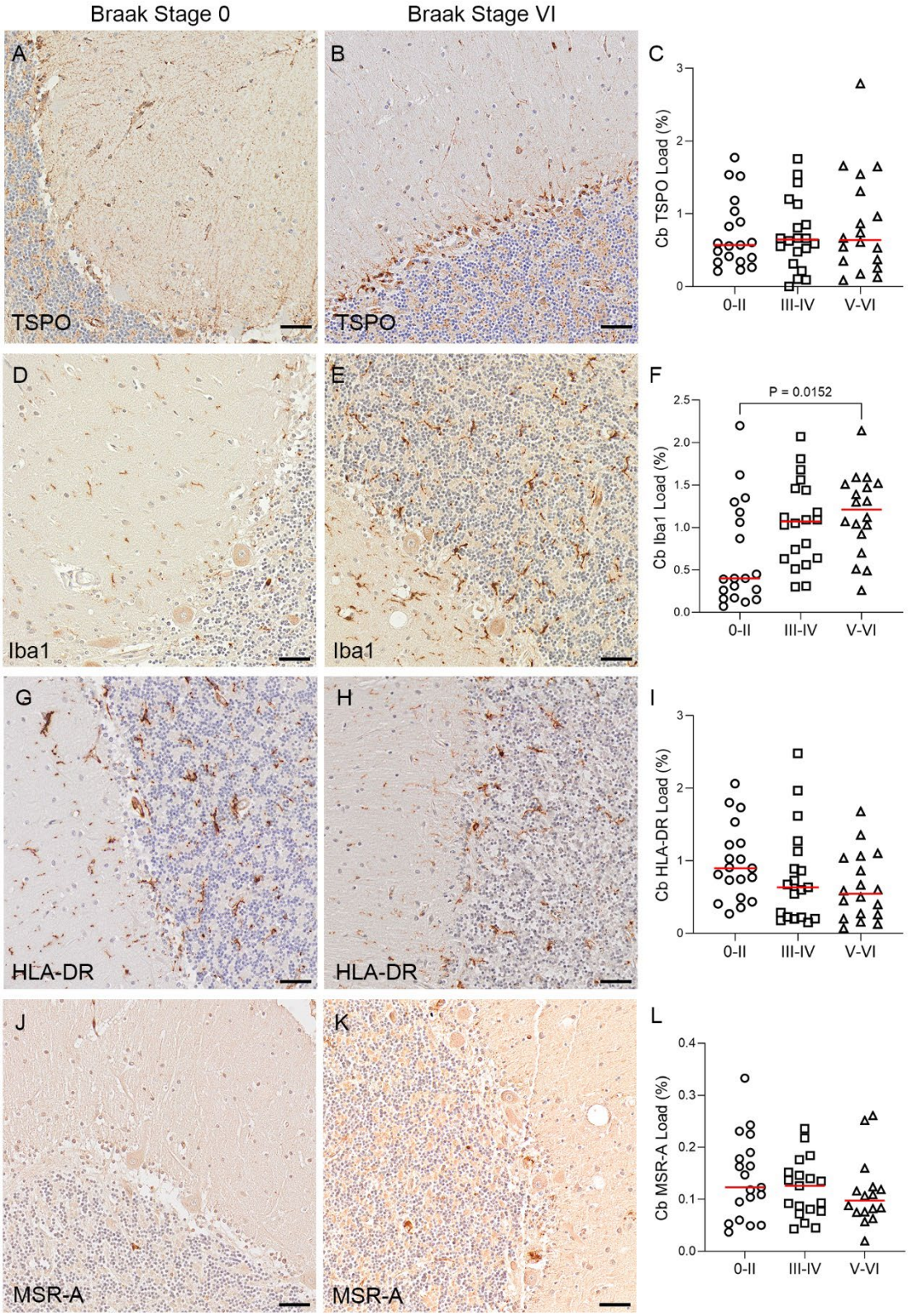

Figure 15 Illustrations and quantification of microglial markers TSPO (**A, B, C**), Iba1 (**D, E, F**), HLA-DR (**G, H, I**) and MSR-A (**J, K, L**) in the cerebellum. Counterstain: Haematoxylin. Scale bar = 50µm. Graphs presented as individual values with median (**C, F, I, L**).

4.3 Correlations between pathology and microglial markers

Pathology: Associations were seen for Aβ in temporal lobe and the cerebellum (P<0.001), as well as for Aβ and pTau the temporal lobe (P<0.001) and the cerebellum (P<0.001) using the whole cohort (**Table 5**). Splitting the cohort by Braak stage, only one association was observed for Aβ and pTau in Braak stage III-IV (P=0.004) (**Table 7**). Correlation analysis was performed between *post-mortem* delay and the Aβ and pTau markers to determine if the delay affected the immunostaining, and no significant associations were found (**Table A1**).

Microglial markers: Investigating correlations between the microglial markers and pathological protein loads, significant associations were detected in the temporal lobe between pTau and TSPO (P<0.001) and between TSPO and MSR-A (P=0.005) when all cases were included (**Table 5**). Splitting the cohort by Braak stage gives rise to different associations. In Braak stage 0-II, there was a positive correlation between TSPO in the temporal lobe and the cerebellum (P<0.01) (**Table 6**). In Braak stage V-VI, there is a positive correlation between TSPO in the cerebellum and HLA-DR in the temporal lobe (P=0.004) (**Table 8**). There were no associations for Iba1 when all cases were included in the correlation analysis (**Table 5**). However, when the correlations were split by Braak stage, there was a positive association between Iba1 in the temporal lobe and the cerebellum (P=0.009) at Braak stage 0-II (**Table 6**). An association was observed for HLA-DR between the temporal lobe and the cerebellum (P<0.001) including all cases (**Table 5**). When Braak stages were split, HLA-DR in the temporal lobe and the cerebellum were associated at Braak stage 0-II (P=0.002) (**Table 6**). In Braak stage III-IV there is again a positive correlation between HLA-DR in the temporal lobe and the cerebellum (P=0.004) (**Table 7**). Finally, an association was observed for MSR-A between the temporal lobe and the TSPO in the same area (P=0.005) including all cases (**Table 5**). There were no associations found between any of the microglial markers and *post-mortem* delay (**Table A1**).

Table 5 Correlation of AD pathological and microglial markers in temporal lobe and cerebellum in the whole cohort

	Aβ Cb	*pTau TL*	*pTau Cb*	*TSPO TL*	*TSPO Cb*	*Iba1 TL*	*Iba1 Cb*	*HLA-DR TL*	*HLA-DR Cb*	*MSR-A TL*	*MSR-A Cb*
Aβ TL	**r_s=0.505 *** P<0.001**	**r_s=0.751 *** P<0.001**	r_s=0.287 P=0.032	r_s=0.268 P=0.04	r_s=0.176 P=0.193	r_s=0.019 P=0.889	r_s=0.295 P=0.027	r_s=0.042 P=0.765	r_s=-0.118 P=0.392	r_s=0.061 P=0.646	r_s=-0.033 P=0.812
Aβ Cb		**r_s=0.516 *** P<0.001**	r_s=0.177 P=0.187	r_s=0.296 P=0.026	r_s=0.272 P=0.04	r_s=0.133 P=0.33	r_s=0.219 P=0.102	r_s=0.065 P=0.647	r_s=-0.143 P=0.294	r_s=0.121 P=0.37	r_s=-0.013 P=0.927
pTau TL			r_s=0.339 P=0.012	**r_s=0.465 *** P<0.001**	r_s=0.095 P=0.494	r_s=0.100 P=0.463	r_s=0.319 P=0.019	r_s=0.129 P=0.368	r_s=-0.23 P=0.098	r_s=0.099 P=0.465	r_s=-0.184 P=0.191
pTau Cb				r_s=0.081 P=0.547	r_s=0.141 P=0.297	r_s=0.079 P=0.561	r_s=-0.004 P=0.979	r_s=-0.036 P=0.802	r_s=-0.084 P=0.539	r_s=0.104 P=0.442	r_s=0.214 P=0.12
TSPO TL					r_s=0.220 P=0.101	r_s=0.010 P=941	r_s=0.284 P=0.033	r_s=0.139 P=0.316	r_s=0.083 P=0.544	**r_s=0.356 ** P=0.005**	r_s=-0.071 P=0.612
TSPO Cb						r_s=-0.091 P=0.507	r_s=0.230 P=0.085	r_s=0.274 P=0.05	r_s=0.164 P=0.228	r_s=0.204 P=0.129	r_s=0.015 P=0.913
Iba1 TL							r_s=0.256 P=0.057	r_s=0.082 P=0.556	r_s=-0.008 P=0.955	r_s=-0.103 P=0.436	r_s=-0.279 P=0.043
Iba1 Cb								r_s=0.119 P=0.402	r_s=-0.011 P=0.933	r_s=0.077 P=0.569	r_s=-0.071 P=0.61
HLA-DR TL									**r_s=0.548 *** P<0.001**	r_s=0.244 P=0.075	r_s=-0.08 P=0.583
HLA-DR Cb										r_s=0.088 P=0.518	r_s=0.087 P=0.536
MSR-A TL											r_s=0.043 P=0.759

r_s Spearman's rank correlation, significant P values are in bold (**<0.01, ***<0.001)
pTau phosphorylated tau, *TSPO* translocator protein
TL temporal lobe, *Cb* cerebellum

Table 6 Correlation of AD pathological and microglial markers in temporal lobe and cerebellum in Braak stages 0-II

	Aβ Cb	*pTau TL*	*pTau Cb*	*TSPO TL*	*TSPO Cb*	*Iba1 TL*	*Iba1 Cb*	*HLA-DR TL*	*HLA-DR Cb*	*MSR-A TL*	*MSR-A Cb*
Aβ TL	r_s = -0.391 P=0.108	r_s = -0.183 P=0.454	r_s = -0.022 P=0.932	r_s = -0.181 P=0.459	r_s = 0.119 P=0.639	r_s = -0.124 P=0.614	r_s = -0.278 P=0.264	r_s = -0.277 P=0.282	r_s = 0.04 P=0.874	r_s = 0.056 P=0.819	r_s = 0.23 P=0.358
Aβ Cb		r_s = -0.175 P=0.474	r_s = -0.191 P=0.433	r_s = 0.307 P=0.201	r_s = 0.088 P=0.721	r_s = 0.056 P=0.819	r_s = 0.224 P=0.357	r_s = 0.007 P=0.978	r_s = -0.004 P=0.989	r_s = 0.116 P=0.637	r_s = 0.316 P=0.188
pTau TL			r_s = 0.179 P=0.464	r_s = -0.356 P=0.124	r_s = -0.444 P=0.057	r_s = 0.192 P=0.417	r_s = -0.052 P=0.834	r_s = 0.201 P=0.44	r_s = -0.079 P=0.748	r_s = -0.414 P=0.069	r_s = -0.392 P=0.097
pTau Cb				r_s = 0.147 P=0.547	r_s = -0.133 P=0.586	r_s = -0.451 P=0.053	r_s = -0.054 P=0.828	r_s = -0.26 P=0.314	r_s = -0.3 P=0.212	r_s = 0.351 P=0.141	r_s = 0.432 P=0.065
TSPO TL					**r_s = 0.577** P<0.01**	r_s = -0.538 P=0.014	r_s = 0.125 P=0.611	r_s = 0.027 P=0.918	r_s = -0.037 P=0.881	r_s = 0.531 P=0.016	r_s = 0.053 P=0.831
TSPO Cb						r_s = -0.297 P=0.216	r_s = -0.118 P=0.629	r_s = 0.189 P=0.468	r_s = 0.228 P=0.348	r_s = 0.444 P=0.057	r_s = -0.033 P=0.892
Iba1 TL							**r_s = 0.584** P=0.009**	r_s = 0.337 P=0.186	r_s = 0.218 P=0.371	r_s = -0.424 P=0.062	r_s = -0.436 P=0.062
Iba1 Cb								r_s = 0.284 P=0.268	r_s = 0.287 P=0.234	r_s = 0.074 P=0.764	r_s = -0.202 P=0.407
HLA-DR TL									**r_s = 0.691** P=0.002**	r_s = 0.24 P=0.353	r_s = -0.265 P=0.305
HLA-DR Cb										r_s = 0.147 P=0.547	r_s = -0.177 P=0.468
MSR-A TL											r_s = 0.293 P=0.223

r_s Spearman's rank correlation, significant P values are in bold (**<0.01)
pTau phosphorylated tau, *TSPO* translocator protein
TL temporal lobe, *Cb* cerebellum

Table 7 Correlation of AD pathological and microglial markers in temporal lobe and cerebellum in Braak stages III-IV

	Aβ Cb	*pTau TL*	*pTau Cb*	*TSPO TL*	*TSPO Cb*	*Iba1 TL*	*Iba1 Cb*	*HLA-DR TL*	*HLA-DR Cb*	*MSR-A TL*	*MSR-A Cb*
Aβ TL	r_s = 0.456 P=0.043	**r_s = 0.648** P=0.004**	r_s = 0.143 P=0.548	r_s = -0.039 P=0.87	r_s = 0.165 P=0.468	r_s = 0.035 P=0.887	r_s = 0.075 P=0.753	r_s = 0.216 P=0.39	r_s = 0.018 P=0.943	r_s = -0.02 P=0.935	r_s = 0.067 P=0.786
Aβ Cb		r_s = 0.449 P=0.062	r_s = 0.164 P=0.49	r_s = 0.069 P=0.772	r_s = 0.43 P=0.058	r_s = 0.154 P=0.528	r_s = 0.041 P=0.865	r_s = 0.088 P=0.729	r_s = -0.056 P=0.819	r_s = 0.158 P=0.506	r_s = 0.146 P=0.552
pTau TL			r_s = 0.113 P=0.657	r_s = 0.215 P=0.392	r_s = 0.347 P=0.158	r_s = 0.162 P=0.535	r_s = 0.143 P=0.573	r_s = 0.109 P=0.688	r_s = 0.158 P=0.544	r_s = -0.313 P=0.206	r_s = 0.179 P=0.478
pTau Cb				r_s = 0.02 P=0.935	r_s = 0.32 P=0.169	r_s = 0.274 P=0.257	r_s = -0.105 P=0.661	r_s = -0.057 P=0.823	r_s = 0.012 P=0.96	r_s = -0.033 P=0.89	r_s = 0.142 P=0.562
TSPO TL					r_s = -0.072 P=0.762	r_s = 0.346 P=0.147	r_s = 0.213 P=0.368	r_s = 0.106 P=0.675	r_s = 0.533 P=0.019	r_s = 0.048 P=0.84	r_s = -0.158 P=0.519
TSPO Cb						r_s = -0.054 P=0.825	r_s = 0.488 P=0.047	r_s = 0.117 P=0.645	r_s = 0.16 P=0.514	r_s = 0.262 P=0.265	r_s = 0.539 P=0.017
Iba1 TL							r_s = -0.012 P=0.96	r_s = -0.255 P=0.323	r_s = 0.057 P=0.823	r_s = -0.03 P=0.904	r_s = 0.172 P=0.494
Iba1 Cb								r_s = 0.412 P=0.089	r_s = 0.204 P=0.403	r_s = -0.036 P=0.88	r_s = 0.488 P=0.055
HLA-DR TL									**r_s = 0.662** P=0.004**	r_s = 0.383 P=0.117	r_s = 0.01 P=0.97
HLA-DR Cb										r_s = 0.484 P=0.036	r_s = 0.007 P=0.977
MSR-A TL											r_s = 0.061 P=0.803

r_s Spearman's rank correlation, significant P values are in bold (**<0.01)
pTau phosphorylated tau, *TSPO* translocator protein
TL temporal lobe, *Cb* cerebellum

Table 8 Correlation of AD pathological and microglial markers in temporal lobe and cerebellum in Braak stages V-VI

	Aβ Cb	*pTau TL*	*pTau Cb*	*TSPO TL*	*TSPO Cb*	*Iba1 TL*	*Iba1 Cb*	*HLA-DR TL*	*HLA-DR Cb*	*MSR-A TL*	*MSR-A Cb*
Aβ TL	r_s = 0.201 P=0.423	r_s = 0.325 P=0.174	r_s = 0.474 P=0.047	r_s = -0.072 P=0.762	r_s = 0.381 P=0.119	r_s = 0.01 P=0.967	r_s = 0.123 P=0.627	r_s = 0.167 P=0.495	r_s = 0.41 P=0.091	r_s = -0.259 P=0.271	r_s = 0.041 P=0.88
Aβ Cb		r_s = 0.283 P=0.271	r_s = 0.118 P=0.642	r_s = 0.096 P=0.705	r_s = 0.234 P=0.349	r_s = 0.146 P=0.565	r_s = -0.201 P=0.423	r_s = 0.368 P=0.147	r_s = -0.053 P=0.836	r_s = -0.195 P=0.438	r_s = -0.4 P=0.125
pTau TL			r_s = 0.163 P=0.531	r_s = 0.176 P=0.472	r_s = 0.24 P=0.353	r_s = -0.078 P=0.75	r_s = 0.313 P=0.221	r_s = 0.138 P=0.586	r_s = -0.31 P=0.226	r_s = 0.462 P=0.046	r_s = -0.284 P=0.305
pTau Cb				r_s = -0.169 P=0.502	r_s = 0.332 P=0.178	r_s = 0.409 P=0.092	r_s = -0.155 P=0.539	r_s = 0.132 P=0.612	r_s = 0.319 P=0.197	r_s = -0.107 P=0.671	r_s = -0.015 P=0.957
TSPO TL					r_s = 0.238 P=0.341	r_s = 0.151 P=0.525	r_s = 0.182 P=0.47	r_s = 0.402 P=0.088	r_s = 0.061 P=0.81	r_s = 0.445 P=0.049	r_s = 0.006 P=0.983
TSPO Cb						r_s = 0.15 P=0.553	r_s = 0.314 P=0.205	**r_s = 0.662** P=0.004**	r_s = 0.15 P=0.553	r_s = -0.133 P=0.598	r_s = -0.282 P=0.289
Iba1 TL							r_s = -0.112 P=0.66	r_s = 0.095 P=0.7	r_s = -0.117 P=0.645	r_s = 0.136 P=0.567	r_s = -0.485 P=0.057
Iba1 Cb								r_s = -0.026 P=0.922	r_s = -0.092 P=0.717	r_s =0.174 P=0.489	r_s = -0.137 P=0.613
HLA-DR TL									r_s = 0.248 P=0.338	r_s = 0.184 P=0.45	r_s = 0.161 P=0.567
HLA-DR Cb										r_s = -0.319 P=0.197	r_s = 0.462 P=0.072
MSR-A TL											r_s = -0.009 P=0.974

r_s Spearman's rank correlation, significant P values are in bold (**<0.01)
pTau phosphorylated tau, *TSPO* translocator protein
TL temporal lobe, *Cb* cerebellum

4.4 Neuroinflammatory environment

From the Mesoscale Discovery experiment, 30 inflammatory markers were tested in the cohort of 60 brains in the temporal lobe and cerebellum (temporal lobe data was collected by a previous PhD student, Rebecca Beardmore). The markers were split into three groups: cytokines, proinflammatory and chemokines (n=10 each). Of these 30 markers, only one showed any significance; IL15 (P<0.024) from the cytokine group was significantly increased across the Braak stages in the temporal lobe (**Table 9**). Although no other markers were significantly changed over the course of the Braak stages (**Table 10** and **Table 11**), comparisons were performed between the temporal lobe and cerebellum including all cases (**Table 12**). The majority of markers were significantly higher in the temporal lobe, except for VEGF, IL8HA, IL10 and IL2 which were higher in the cerebellum (**Table 12**).

Table 9 Protein concentration of cytokines by Braak stage group in the temporal lobe and cerebellum

	Marker	*Braak 0-II*	*Braak III-IV*	*Braak V-VI*	*P value*
Temporal lobe	GM-CSF	$0.1x10^{-8}$ [$0.1x10^{-8}$ – $0.2x10^{-8}$]	$0.2x10^{-8}$ [$0.1x10^{-8}$ – $0.3x10^{-8}$]	$0.1x10^{-8}$ [$0.07x10^{-8}$ – $0.2x10^{-8}$]	0.254
	IL1α	$4.0x10^{-8}$ [$2.8x10^{-8}$ – $6.2x10^{-8}$]	$5.7x10^{-8}$ [$3.9x10^{-8}$ – $8.4x10^{-8}$]	$3.0x10^{-8}$ [$1.9x10^{-8}$ – $11.8x10^{-8}$]	0.424
	IL12/IL23p70	$1.3x10^{-8}$ [$1.1x10^{-8}$ – $1.9x10^{-8}$]	$1.6x10^{-8}$ [$1.1x10^{-8}$ – $2.0x10^{-8}$]	$1.2x10^{-8}$ [$1.0x10^{-8}$ – $1.8x10^{-8}$]	0.455
	IL15	**$6.7x10^{-8}$ [$6.0x10^{-8}$ – $8.1x10^{-8}$]**	**$7.5x10^{-8}$ [$6.4x10^{-8}$ – $9.5x10^{-8}$]**	**$9.3x10^{-8}$ [$7.6x10^{-8}$ – $10.7x10^{-8}$]**	**0.024***
	IL16	$4.2x10^{-6}$ [$3.9x10^{-6}$ – $6.9x10^{-6}$]	$6.0x10^{-6}$ [$3.7x10^{-6}$ – $8.4x10^{-6}$]	$6.3x10^{-6}$ [$4.3x10^{-6}$ – $7.7x10^{-6}$]	0.586
	IL17A	$1.3x10^{-8}$ [$1.1x10^{-8}$ – $1.7x10^{-8}$]	$1.5x10^{-8}$ [$0.9x10^{-8}$ – $1.8x10^{-8}$]	$1.7x10^{-8}$ [$1.3x10^{-8}$ – $1.9x10^{-8}$]	0.192
	IL5	$0.08x10^{-8}$ [$0.05x10^{-8}$ – $0.2x10^{-8}$]	$0.2x10^{-8}$ [$0.09x10^{-8}$ – $0.2x10^{-8}$]	$0.09x10^{-8}$ [$0.05x10^{-8}$ – $0.2x10^{-8}$]	0.188
	IL7	$0.4x10^{-8}$ [$0.3x10^{-8}$ – $0.6x10^{-8}$]	$0.6x10^{-8}$ [$0.4x10^{-8}$ –0.8 $x10^{-8}$]	$0.4x10^{-8}$ [$0.2x10^{-8}$ – $0.5x10^{-8}$]	0.070
	TNFβ	$0.1x10^{-8}$ [$0.09x10^{-8}$ – $0.2x10^{-8}$]	$0.1x10^{-8}$ [$0.1x10^{-8}$ – $0.2x10^{-8}$]	$0.1x10^{-8}$ [$0.1x10^{-8}$ – $0.2x10^{-8}$]	0.916
	VEGF	$2.0x10^{-8}$ [$1.0x10^{-8}$ – $3.7x10^{-8}$]	$2.5x10^{-8}$ [$1.2x10^{-8}$ – $4.9x10^{-8}$]	$2.2x10^{-8}$ [$0.7x10^{-8}$ – $4.1x10^{-8}$]	0.797
Cerebellum	GM-CSF	$5.9x10^{-10}$[$7.4x10^{-10}$ – $2.8x10^{-10}$]	$4.6x10^{-10}$ [$6.7x10^{-10}$ – $3.1x10^{-10}$]	$2.7x10^{-10}$[$4.2x10^{-10}$–$2.5x10^{-10}$]	0.447
	IL1α	$5.5x10^{-9}$[$6.8x10^{-9}$ – $4.4x10^{-9}$]	$6.6x10^{-9}$[$1.4x10^{-8}$ – $4.7x10^{-9}$]	$9.5x10^{-9}$[$1.2x10^{-9}$ – $4.6x10^{-9}$]	0.291
	IL12/IL23p70	$6.9x10^{-9}$[$1.6x10^{-8}$ – $3.6x10^{-9}$]	$1.1x10^{-8}$[$1.2x10^{-8}$ – $7.3x10^{-9}$]	$1.0x10^{-9}$[$1.3x10^{-8}$ – $5.9x10^{-9}$]	0.746
	IL15	$5.8x10^{-8}$[$6.3x10^{-8}$ – $5.2x10^{-8}$]	$5.8x10^{-8}$[$6.4x10^{-8}$ – $4.7x10^{-8}$]	$6.3x10^{-8}$[$5.5x10^{-8}$ – $7.2x10^{-8}$]	0.486
	IL16	$2.6x10^{-6}$[$4.6x10^{-6}$ – $1.8x10^{-6}$]	$4.7x10^{-6}$[$6.3x10^{-6}$ – $3.1x10^{-6}$]	$5.0x10^{-6}$[$5.7x10^{-6}$ – $3.3x10^{-6}$]	0.060
	IL17A	$1.5x10^{-8}$[$1.7x10^{-8}$ – $1.1x10^{-8}$]	$1.2x10^{-8}$[$1.6x10^{-8}$ – $1.1x10^{-8}$]	$1.4x10^{-8}$[$1.5x10^{-8}$ – $9.5x10^{-9}$]	0.700
	IL5	$4.8x10^{-10}$[$8.6x10^{-10}$ – $2.9x10^{-10}$]	$5.9x10^{-10}$[$7.9x10^{-10}$ – $3.88x10^{-10}$]	$6.8x10^{-10}$[$8.6x10^{-10}$ – $4.4x10^{-10}$]	0.356
	IL7	$5.2x10^{-10}$[$6.5x10^{-10}$ – $3.9x10^{-10}$]	$5.8x10^{-10}$[$8.6x10^{-10}$ – $2.11x10^{-10}$]	$5.4x10^{-10}$[$7.0x10^{-10}$ – $4.6x10^{-10}$]	0.996
	TNFβ	$4.8x10^{-10}$[$5.3x10^{-10}$ – $3.0x10^{-10}$]	$3.4x10^{-10}$[$5.22x10^{-10}$ – $2.0x10^{-10}$]	$3.1x10^{-10}$[$4.4x10^{-10}$ – $2.3x10^{-10}$]	0.513
	VEGF	$1.4x10^{-7}$[$2.3x10^{-7}$ – $5.0x10^{-8}$]	$9.6x10^{-8}$[$2.4x10^{-7}$ – $2.8x10^{-8}$]	$7.4x10^{-8}$[$1.7x10^{-7}$ – $5.4x10^{-8}$]	0.750

P values obtained using Kruskal-Wallis test with significant P value (*<0.05) in bold
Data displayed as - median [interquartile range]

Table 10 Protein concentration of proinflammatory proteins by Braak stage group in temporal lobe and cerebellum

	Marker	*Braak 0-II*	*Braak III-IV*	*Braak V-VI*	*P value*
Temporal lobe	IFNγ	$0.8x10^{-8}$ [$0.5x10^{-8}$ – $1.1x10^{-8}$]	$0.8\ x10^{-8}$ [$0.6x10^{-8}$ – $1.3x10^{-8}$]	$2.4x10^{-8}$ [$0.5x10^{-8}$ – $0.9x10^{-8}$]	0.241
	IL10	$0.1x10^{-8}$ [$0.09x10^{-8}$ – $0.2x10^{-8}$]	$0.2x10^{-8}$ [$0.1x10^{-8}$ – $0.2x10^{-8}$]	$0.1\ x10^{-8}$ [$0.08x10^{-8}$ – $0.2x10^{-8}$]	0.129
	IL12p70	$0.5x10^{-8}$ [$0.4x10^{-8}$ – $0.6x10^{-8}$]	$0.4\ x10^{-8}$ [$0.3x10^{-8}$ – $0.6x10^{-8}$]	$0.4\ x10^{-8}$[$0.3x10^{-8}$ – $0.5x10^{-8}$]	0.847
	IL13	$4.7x10^{-8}$ [$3.7x10^{-8}$ – $5.9x10^{-8}$]	$5.0x10^{-8}$ [$4.0x10^{-8}$ – $5.6x10^{-8}$]	$5.2\ x10^{-8}$ [$4.2x10^{-8}$ – $6.1x10^{-8}$]	0.885
	IL1β	$2.6\ x10^{-8}$ [$1.6x10^{-8}$ – $6.0x10^{-8}$]	$3.1x10^{-8}$ [$2.3x10^{-8}$ – $4.0x10^{-8}$]	$0.9\ x10^{-8}$ [$0.4x10^{-8}$ – $3.1x10^{-8}$]	0.592
	IL2	$0.3\ x10^{-8}$ [$0.2x10^{-8}$ – $0.4x10^{-8}$]	$0.3\ x10^{-8}$ [$0.3x10^{-8}$ – $0.4x10^{-8}$]	$0.2x10^{-8}$ [$0.2x10^{-8}$ – $0.4x10^{-8}$]	0.140
	IL4	$0.2x10^{-8}$ [$0.2x10^{-8}$ – $0.3x10^{-8}$]	$0.2x10^{-8}$ [$0.2x10^{-8}$ – $0.3x10^{-8}$]	$0.2x10^{-8}$ [$0.2x10^{-8}$ – $0.3x10^{-8}$]	0.628
	IL6	$5.1x10^{-8}$ [$1.9x10^{-8}$ –$19.9x10^{-8}$]	$8.3x10^{-8}$ [$3.6x10^{-8}$ – $17.4x10^{-8}$]	$5.0x10^{-8}$ [$2.7x10^{-8}$ – $14.7x10^{-8}$]	0.708
	IL8	$2.6x10^{-7}$[$1.6x10^{-7}$ – $7.0x10^{-7}$]	$2.9x10^{-7}$ [$1.8x10^{-7}$ – $8.6x10^{-7}$]	$2.3x10^{-7}$ [$1.5x10^{-7}$ – $5.7x10^{-7}$]	0.826
	TNFα	$0.6x10^{-8}$ [$0.5x10^{-8}$ – $0.7x10^{-8}$]	$0.6x10^{-8}$ [$0.4x10^{-8}$ – $0.8x10^{-8}$]	$0.5x10^{-8}$ [$0.4x10^{-8}$ – $0.7x10^{-8}$]	0.533
Cerebellum	IFNγ	3.6x10-9[4.5x10-9 – 2.9x10-9]	4.7x10-9 [5.6x10-9 - 3.7x10-9]	3.6x10-9[4.4x10-9 – 3.0x10-9]	0.173
	IL10	1.8x10-9[2.1x10-9 – 1.2x10-9]	1.9x10-9[2.6x10-9 – 1.7 x10-9]	1.8 x10-9[2.0x10-9 – 1.6x10-9]	0.265
	IL12p70	1.9x10-9[2.3x10-9 – 1.1x10-9]	2.5x10-9[3.2x10-9 – 1.8x10-9]	1.9x10-9[2.3x10-9 – 1.7x10-9]	0.093
	IL13	4.1x10-8[5.9x10-8 – 3.5x10-8]	4.2x10-8[6.7x10-8 – 2.8x10-8]	3.8x10-8[5.3x10-8 – 3.0x10-8]	0.545
	IL1β	5.8x10-8[1.6x10-8 – 3.9x10-9]	1.0x10-8[2.1x10-8 – 6.4x10-8]	4.9x10-9[1.1x10-8 – 4.2x10-9]	0.179
	IL2	4.6x10-9[5.4x10-9 – 3.5x10-9]	5.5x10-9[6x10-9 – 4.5x10-9]	4.7x10-9[5.4x10-9 – 4.1x10-9]	0.161
	IL4	1.2x10-9[1.4x10-9 – 8.5x10-10]	1.4x10-9[1.8x10-9 – 1.2x10-9]	1.4x10-9[1.4x10-9 – 1.2x10-9]	0.061
	IL6	5.1x10-8[9.6x10-8 – 2.2x10-8]	1.4x10-7[2.9x10-7 – 2.8x10-8]	2.5x10-8[1.3x10-7 – 2.0x10-8]	0.256
	IL8	1.9x10-7[3.7x10-7 – 9.3 x10-8]	1.4x10-7[5.6x10-7 – 9.3x10-8]	1.9x10-7[3.4x10-7 – 2.1x10-7]	0.845
	TNFα	3.6x10-9[4.0x10-9 – 2.3 x10-9]	3.5 x10-9[4.9x10-9 – 2.8 x10-9]	3.3 x10-9[3.7 x10-9 – 2.9 x10-9]	0.408

P values obtained using Kruskal-Wallis test with significant P value (*<0.05) in bold
Data displayed as - median [interquartile range]

Table 11 Protein concentration of chemokines by Braak stage group in temporal lobe and cerebellum

	Marker	*Braak 0-II*	*Braak III-IV*	*Braak V-VI*	*P value*
Temporal lobe	Eotaxin	$1.0x10^{-7}$ [$0.6x10^{-7}$ – $1.7x10^{-7}$]	$1.1x10^{-7}$ [$0.7x10^{-7}$ – $1.5x10^{-7}$]	$1.1x10^{-7}$ [$0.8x10^{-7}$ – $2.5x10^{-7}$]	0.510
	Eotaxin-3	$2.1x10^{-7}$ [$1.5x10^{-7}$ – $3.6x10^{-7}$]	$5.1x10^{-7}$ [$2.1x10^{-7}$ – $7.8x10^{-7}$]	$3.2x10^{-7}$ [$1.5x10^{-7}$ – $5.5x10^{-7}$]	0.105
	IL8 (HA)	$1.5x10^{-6}$ [$1.1x10^{-6}$ – $2.9x10^{-6}$]	$1.9x10^{-6}$ [$0.8x10^{-6}$ – $2.9x10^{-6}$]	$1.7x10^{-6}$ [$1.1x10^{-6}$ – $4.8x10^{-6}$]	0.924
	IP10	$2.7x10^{-7}$ [$1.7x10^{-7}$ – $4.3x10^{-7}$]	$4.3x10^{-7}$ [$2.3x10^{-7}$ – $12.3x10^{-7}$]	$4.7x10^{-7}$ [$3.0x10^{-7}$ – $7.3x10^{-7}$]	0.314
	MCP1	$6.0x10^{-7}$ [$3.3x10^{-7}$ – $10.3x10^{-7}$]	$7.3x10^{-7}$ [$4.4x10^{-7}$ – $14.1x10^{-7}$]	$11.3x10^{-7}$ [$7.3x10^{-7}$ – $16.3x10^{-7}$]	0.323
	MCP4	$2.0x10^{-7}$ [$1.6x10^{-7}$ – $2.5x10^{-7}$]	$1.7x10^{-7}$ [$1.6x10^{-7}$ – $2.5x10^{-7}$]	$2.4x10^{-7}$ [$1.6x10^{-7}$ – $2.5x10^{-7}$]	0.084
	MDC	$2.7x10^{-7}$ [$1.9x10^{-7}$ – $3.6x10^{-7}$]	$2.7\ x10^{-7}$ [$1.4x10^{-7}$ – $3.8x10^{-7}$]	$3.3\ x10^{-7}$ [$2.7x10^{-7}$ – $8.9x10^{-7}$]	0.174
	MIP1α	$1.3x10^{-7}$ [$1.0x10^{-7}$ – $1.6x10^{-7}$]	$1.7x10^{-7}$ [$1.0x10^{-7}$ – $3.0x10^{-7}$]	$1.5x10^{-7}$ [$1.3x10^{-7}$ – $2.9x10^{-7}$]	0.235
	MIP1β	$1.9\ x10^{-7}$ [$1.7x10^{-7}$ – $2.3x10^{-7}$]	$2.6\ x10^{-7}$ [$1.6x10^{-7}$ – $4.2x10^{-7}$]	$1.8\ x10^{-7}$ [$1.7x10^{-7}$ – $3.2x10^{-7}$]	0.242
	TARC	$2.2x10^{-8}$ [$0.9x10^{-8}$ – $3.6x10^{-8}$]	$2.9x10^{-8}$ [$2.1x10^{-8}$ – $4.7x10^{-8}$]	$2.4x10^{-8}$ [$1.2x10^{-8}$ – $4.1x10^{-8}$]	0.393
	Eotaxin	$1.9x10^{-9}$[$2.4x10^{-9}$ – $1.5x10^{-9}$]	$1.8x10^{-9}$[$2.5x10^{-9}$ – $1.6x10^{-9}$]	$2.2x10^{-9}$[$2.5x10^{-9}$ – $1.6x10^{-9}$]	0.965
Cerebellum	Eotaxin 3	$1.5x10^{-7}$[$3.5x10^{-7}$ – $8.3x10^{-8}$]	$1.1x10^{-7}$[$1.2x10^{-7}$ – $9.6x10^{-8}$]	$2.2x10^{-7}$[$3.7x10^{-7}$ – $9.2x10^{-8}$]	0.470
	IL8 (HA)	$5.7x10^{-6}$[$8.4x10^{-6}$ – $4.8x10^{-6}$]	$5.7x10^{-6}$[$7.6x10^{-6}$ – $4.8x10^{-6}$]	$7.2x10^{-6}$[$9.3x10^{-6}$ –$3.7x10^{-6}$]	0.912
	IP10	$2.1x10^{-7}$[$3.1x10^{-7}$ – $1.2x10^{-7}$]	$1.4x10^{-7}$[$3.5x10^{-7}$ – $1.1x10^{-7}$]	$2.3x10^{-7}$[$5.0x10^{-7}$ – $10.0x10^{-8}$]	0.734
	MCP1	$2.3x10^{-7}$[$4.3x10^{-7}$ – $1.5x10^{-7}$]	$2.3x10^{-7}$[$1.4x10^{-6}$ – $1.3x10^{-7}$]	$2.7x10^{-7}$[$4.0x10^{-7}$ – $1.9x10^{-7}$]	0.913
	MCP4	$1.5x10^{-7}$[$2.0x10^{-7}$ – $1.0x10^{-7}$]	$1.5x10^{-7}$[$1.8x10^{-7}$ – $1.2x10^{-7}$]	$1.2x10^{-7}$[$1.9x10^{-7}$ – $1.1x10^{-7}$]	0.861
	MDC	$2.4x10^{-7}$[$3.4x10^{-7}$ – $1.5x10^{-7}$]	$1.6x10^{-7}$[$2.7x10^{-7}$ – $1.1x10^{-7}$]	$2.1x10^{-7}$[$3.9x10^{-7}$ – $1.2x10^{-7}$]	0.487
	MIP1α	$7.0x10^{-8}$[$8.8x10^{-8}$ – $5.5x10^{-8}$]	$6.8x10^{-8}$[$1.3x10^{-7}$ – $6.1x10^{-8}$]	$6.9x10^{-8}$[$1.0x10^{-7}$ – $5.1x10^{-8}$]	0.625
	MIP1β	$9.9x10^{-8}$[$1.1x10^{-7}$ – $7.1x10^{-8}$]	$9.0x10^{-8}$[$1.4x10^{-7}$ – $7.3x10^{-8}$]	$7.1x10^{-8}$[$9.6x10^{-8}$ – $6.5x10^{-8}$]	0.352
	TARC	$2.8x10^{-8}$[$3.3x10^{-8}$ – $1.6x10^{-8}$]	$2.5x10^{-8}$[$3.3x10^{-8}$ – $1.6x10^{-8}$]	$2.2x10^{-8}$[$2.8x10^{-8}$ – $1.7x10^{-8}$]	0.744

P values obtained using Kruskal-Wallis test with significant P value (*<0.05) in bold
Data displayed as - median [interquartile range]

Table 12 Comparisons for protein concentration of cytokines, proinflammatory proteins and chemokines between temporal lobe and cerebellum in the whole cohort

Marker	*Temporal lobe*	*Cerebellum*	*P value*
GM-CSF	**$1.387x10^{-9}$ [$9.458x10^{-10}$-$1.804x10^{-9}$]**	**$4.240x10^{-10}$ [$2.465x10^{-10}$-$7.143x10^{-10}$]**	**<0.0001**
IL1α	**$4.184x10^{-8}$ [$2.660x10^{-8}$-$8.473x10^{-8}$]**	**$5.971x10^{-9}$ [$4.607x10^{-9}$-$1.163x10^{-8}$]**	**<0.0001**
IL12/IL23p70	**1.468e-008 [1.055e-008-1.781e-008]**	**9.353e-009 [5.434e-009-1.386e-008]**	**<0.0001**
IL15	**$7.555x10^{-8}$ [$6.237x10^{-8}$-$9.360x10^{-8}$]**	**$5.838x10^{-8}$ [$5.054x10^{-8}$-$6.649x10^{-8}$]**	**<0.0001**
IL16	**$5.706x10^{-6}$ [$3.960x10^{-6}$-$7.814x10^{-6}$]**	**$4.308x10^{-6}$ [$2.067x10^{-6}$-$5.509x10^{-6}$]**	**0.002**
IL17A	$1.449x10^{-8}$ [$1.095x10^{-8}$-$1.775x10^{-8}$]	$1.368x10^{-8}$ [$1.060x10^{-8}$-$1.715x10^{-8}$]	0.607
IL5	**$1.084x10^{-9}$ [$6.708x10^{-10}$-$1.868x10^{-9}$]**	**$5.870x10^{-10}$ [$3.850x10^{-10}$-$8.510x10^{-10}$]**	**<0.0001**
IL7	**$4.284x10^{-9}$ [$2.887x10^{-9}$-$6.229x10^{-9}$]**	**$5.740x10^{-10}$ [$3.070x10^{-10}$-$8.065x10^{-10}$]**	**<0.0001**
TNFβ	**$1.346x10^{-9}$ [$9.238x10^{-10}$-$1.686x10^{-9}$]**	**$3.470x10^{-10}$ [$2.240x10^{-10}$-$5.130x10^{-10}$]**	**<0.0001**
VEGF	**$2.112x10^{-8}$ [$1.119x10^{-8}$-$4.035x10^{-8}$]**	**$9.305x10^{-8}$ [$4.297x10^{-8}$-$2.316x10^{-7}$]**	**<0.0001**
Eotaxin	**$1.115x10^{-7}$ [$6.801x10^{-8}$-$1.767x10^{-7}$]**	**$1.885x10^{-8}$ [$1.594x10^{-8}$-$2.578x10^{-8}$]**	**<0.0001**
Eotaxin 3	**$2.889x10^{-7}$ [$1.529x10^{-7}$-$5.623x10^{-7}$]**	**$1.245x10^{-7}$ [$9.198x10^{-8}$-$2.551x10^{-7}$]**	**<0.0001**
IL8 (HA)	**$1.660x10^{-6}$ [$1.093x10^{-6}$-$2.921x10^{-6}$]**	**$5.730x10^{-6}$ [$4.496x10^{-6}$-$8.492x10^{-6}$]**	**<0.0001**
IP10	**$4.065x10^{-7}$ [$1.912x10^{-7}$-$7.324x10^{-7}$]**	**$1.929x10^{-7}$ [$1.073x10^{-7}$-$4.337x10^{-7}$]**	**0.0007**
MCP1	**$7.915x10^{-7}$ [$4.382x10^{-7}$-$1.468x^{10-6}$]**	**$2.311x10^{-7}$ [$1.393x10^{-7}$-$4.354x10^{-7}$]**	**<0.0001**
MCP4	**$2.036x10^{-7}$ [$1.631x10^{-7}$-$2.670x^{10-7}$]**	**$1.477x10^{-7}$ [$1.075x10^{-7}$-$1.936x10^{-7}$]**	**0.0001**
MDC	**$2.787x10^{-7}$ [$1.989x10^{-7}$-$4.191x^{10-7}$]**	**$2.052x10^{-7}$ [$1.211x10^{-7}$-$3.486x10^{-7}$]**	**0.012**
MIP1α	**$1.455x10^{-7}$ [$1.092x10^{-7}$-$2.208x^{10-7}$]**	**$6.897x10^{-8}$ [$5.467x10^{-8}$-$1.007x10^{-7}$]**	**<0.0001**
MIP1β	**$1.973x10^{-7}$ [$1.683x10^{-7}$-$3.086x10^{-7}$]**	**$8.807x10^{-8}$ [$6.698x10^{-8}$-$1.171x10^{-7}$]**	**<0.0001**
TARC	$2.706x10^{-8}$ [$1.248x10^{-8}$-$4.382x10^{-8}$]	$2.422x10^{-8}$ [$1.569x10^{-8}$-$3.234x10^{-8}$]	0.957
IFNγ	**$7.872x10^{-9}$ [$5.070x10^{-9}$-$1.064x10^{-8}$]**	**$3.941x10^{-9}$ [$2.936x10^{-9}$-$5.142x10^{-9}$]**	**<0.0001**
IL1b	**$2.728x10^{-8}$ [$1.786x10^{-8}$-$4.660x10^{-8}$]**	**$7.101x10^{-9}$ [$4.149x10^{-9}$-$1.846x10^{-8}$]**	**<0.0001**
IL10	**$1.230x10^{-9}$ [$9.295x10^{-10}$-$1.536x10^{-9}$]**	**$1.861x10^{-9}$ [$1.490x10^{-9}$-$2.279x10^{-9}$]**	**<0.0001**
IL12p70	**$4.220x10^{-9}$ [$3.027x10^{-9}$-$5.198x10^{-9}$]**	**$1.990x10^{-9}$ [$1.484x10^{-9}$-$2.597x10^{-9}$]**	**<0.0001**
IL13	$4.988x10^{-8}$ [$3.927x10^{-8}$-$5.827x10^{-8}$]	$4.117x10^{-8}$ [$3.240x10^{-8}$-$5.717x10^{-8}$]	0.097
IL2	**$2.901x10^{-9}$ [$2.237x10^{-9}$-$3.830x10^{-9}$]**	**$4.905x10^{-9}$ [$3.915x10^{-9}$-$5.640x10^{-9}$]**	**<0.0001**
IL4	**$2.134x10^{-9}$ [$1.676x10^{-9}$-$2.841x10^{-9}$]**	**$1.342x10^{-9}$ [$1.140x10^{-9}$-$1.564x10^{-9}$]**	**<0.0001**
IL6	$6.334x10^{-8}$ [$2.594x10^{-8}$-$1.506x10^{-7}$]	$5.288x10^{-8}$ [$2.046x10^{-8}$-$1.781x10^{-7}$]	0.644
IL8	**$2.589x10^{-7}$ [$1.647x10^{-7}$-$6.947x10^{-7}$]**	**$1.856x10^{-7}$ [$9.305x10^{-8}$-$4.485x10^{-7}$]**	**0.037**
TNFα	**$5.854x10^{-9}$ [$4.639x10^{-9}$-$6.918x10^{-9}$]**	**$3.423x10^{-9}$ [$2.507x10^{-9}$-$4.171x10^{-9}$]**	**<0.0001**

P values obtained using Mann-Whitney U test with significant P value (*<0.05, **<0.01, ***<0.001, ****<0.0001) in bold
Data displayed as - median [interquartile range]

4.4.1 Correlations

When the MSD data were correlated with the pathology and microglial data (Sections **4.1** and **4.2**), several associations were observed. In the temporal lobe, TSPO was negatively correlated with the cytokine GM-CSF (P<0.01) and HLA-DR was negatively correlated with macrophage derived chemokine (MDC) (P=0.007) (**Table 13**). Whereas, in the cerebellum, there was a positive correlation between Iba1 and the cytokine IL16 (P<0.001) (**Table 14**).

Table 13 Correlation of AD pathological and microglial markers in temporal lobe compared to inflammatory markers in the whole cohort

Marker	*Aβ TL*	*pTau TL*	*TSPO TL*	*Iba1 TL*	*HLA-DR TL*	*MSR-A TL*
GM-CSF	r_s = -0.145 P=0.312	r_s = -0.230 P=0.111	**r_s = -0.355**** **P<0.01**	r_s = -0.154 P=0.280	r_s = -0.088 P=0.554	r_s = -0.023 P=0.875

IL1α	r_s = 0.098 P=0.0499	r_s = -0.025 P=0.863	r_s = -0.136 P=0.337	r_s = -0.103 P=0.	r_s = 0.017 P=0.910	r_s = -0.065 P=0.652
IL12/IL23p70	r_s = -0.104 P=0.472	r_s = -0.192 P=0.187	r_s = -0.105 P=0.458	r_s = 0.060 P=0.676	r_s = 0.201 P=0.176	r_s = -0.084 P=0.560
IL15	r_s = 0.123 P=0.393	r_s = 0.268 P=0.063	r_s = 0.310 P=0.025	r_s = -0.094 P=0.513	r_s = -0.005 P=0.971	r_s = 0.044 P=0.757
IL16	r_s = 0.039 P=0.786	r_s = 0.060 P=0.682	r_s = 0.155 P=0.274	r_s = 0.267 P=0.059	r_s = 0.202 P=0.174	r_s = -0.161 P=0.260
IL17A	r_s = 0.016 P=0.915	r_s = 0.206 P=0.156	r_s = 0.134 P=0.344	r_s = -0.145 P=0.310	r_s = -0.239 P=0.106	r_s = -0.154 P=0.280
IL5	r_s = -0.117 P=0.417	r_s = -0.053 P=0.718	r_s = -0.107 P=0.451	r_s = 0.091 P=0.523	r_s = 0.160 P=0.283	r_s = -0.009 P=0.947
IL7	r_s = -0.297 P=0.036	r_s = -0.285 P=0.047	r_s = -0.013 P=0.925	r_s = -0.123 P=0.390	r_s = 0.144 P=0.334	r_s = 0.004 P=0.979
TNFβ	r_s = -0.069 P=0.632	r_s = -0.175 P=0.229	r_s = 0.042 P=0.767	r_s = -0.065 P=0.649	r_s = -0.007 P=0.962	r_s = -0.021 P=0.883
VEGF	r_s = -0.310 P=0.028	r_s = -0.081 P=0.578	r_s = -0.188 P=0.182	r_s = 0.010 P=0.945	r_s = 0.170 P=0.254	r_s = 0.152 P=0.286
Eotaxin	r_s = 0.005 P=0.974	r_s = 0.207 P=0.153	r_s = 0.019 P=0.895	r_s = 0.063 P=0.662	r_s = -0.256 P=0.083	r_s = -0.092 P=0.520
Eotaxin 3	r_s = 0.0003 P=0.998	r_s = 0.110 P=0.451	r_s = -0.014 P=0.923	r_s = -0.106 P=0.461	r_s = -0.209 P=0.158	r_s = 0.001 P=0.993
IL8 (HA)	r_s = -0.176 P=0.220	r_s = 0.092 P=0.531	r_s = 0.067 P=0.639	r_s = 0.016 P=0.914	r_s = -0.156 P=0.296	r_s = 0.036 P=0.800
IP10	r_s = 0.051 P=0.725	r_s = 0.192 P=0.186	r_s = 0.149 P=0.293	r_s = 0.251 P=0.075	r_s = 0.018 P=0.906	r_s = 0.059 P=0.682
MCP1	r_s = 0.186 P=0.196	r_s = 0.342 P=0.016	r_s = 0.119 P=0.400	r_s = 0.072 P=0.614	r_s = -0.054 P=0.718	r_s = -0.003 P=0.986
MCP4	r_s = -0.0004 P=0.998	r_s = 0.250 P=0.083	r_s = 0.335 P=0.015	r_s = -0.084 P=0.557	r_s = -0.219 P=0.139	r_s = -0.081 P=0.574
MDC	r_s = 0.011 P=0.942	r_s = 0.250 P=0.084	r_s = 0.152 P=0.281	r_s = -0.070 P=0.624	**r_s = -0.381**** **P=0.007**	r_s = -0.003 P=0.982
MIP1α	r_s = 0.002 P=0.991	r_s = 0.250 P=0.084	r_s = 0.054 P=0.702	r_s = 0.060 P=0.675	r_s = -0.150 P=0.315	r_s = 0.002 P=0.990
MIP1β	r_s = -0.188 P=0.192	r_s = 0.103 P=0.479	r_s = -0.010 P=0.944	r_s = 0.021 P=0.883	r_s = -0.140 P=0.350	r_s = -0.026 P=0.854
TARC	r_s = -0.015 P=0.919	r_s = 0.046 P=0754	r_s = -0.177 P=0.209	r_s = 0.0005 P=0.970	r_s = -0.075 P=0.618	r_s = 0.008 P=0.957
IFNγ	r_s = -0.030 P=0.835	r_s = -0.005 P=0.971	r_s = -0.123 P=0.386	r_s = 0.032 P=0.821	r_s = 0.019 P=0.897	r_s = 0.141 P=0.325
IL1b	r_s = -0.121 P=0.401	r_s = 0.039 P=0.791	r_s = -0.088 P=0.537	r_s = 0.088 P=0.537	r_s = -0.005 P=0.974	r_s = -0.025 P=0.864
IL10	r_s = -0.086 P=0.550	r_s = 0.049 P=0.741	r_s = -0.168 P=0.233	r_s = -0.023 P=0.873	r_s = -0.128 P=0.391	r_s = -0.058 P=0.684
IL12p70	r_s = -0.163 P=0.258	r_s = -0.049 P=0.739	r_s = 0.027 P=0.850	r_s = -0.236 P=0.095	r_s = -0.169 P=0.255	r_s = 0.002 P=0.990
IL13	r_s = -0.169 P=0.241	r_s = -0.016 P=0.914	r_s = 0.000 P=0.999	r_s = -0.273 P=0.053	r_s = -0.255 P=0.084	r_s = 0.155 P=0.276
IL2	r_s = -0.142 P=0.324	r_s = -0.095 P=0.515	r_s = -0.134 P=0.345	r_s = -0.061 P=0.669	r_s = -0.122 P=0.413	r_s = 0.126 P=0.337
IL4	r_s = -0.229 P=0.110	r_s = 0.016 P=0.912	r_s = 0.072 P=0.614	r_s = -0.125 P=0.382	r_s = -0.111 P=0.458	r_s = 0.159 P=0.266
IL6	r_s = -0.008 P=0.958	r_s = 0.033 P=0.820	r_s = 0.063 P=0.655	r_s = 0.032 P=0.823	r_s = -0.057 P=0.704	r_s = 0.115 P=0.421
IL8	r_s = -0.121 P=0.401	r_s = 0.008 P=0.954	r_s = -0.031 P=0.827	r_s = 0.000 P=0.998	r_s = -0.322 P=0.027	r_s = -0.025 P=0.860
TNFα	r_s = -0.273 P=0.055	r_s = -0.103 P=0.480	r_s = -0.118 P=0.406	r_s = -0.054 P=0.708	r_s = -0.221 P=0.135	r_s = -0.021 P=0.883

r_s Spearman's rank correlation, significant *P* values are in bold (**P<0.01)
pTau phosphorylated tau, *TSPO* translocator protein
TL temporal lobe

Table 14 Correlation of AD pathological and microglial markers in cerebellum compared to inflammatory markers in the whole cohort

Marker	*Aβ Cb*	*pTau Cb*	*TSPO Cb*	*Iba1 Cb*	*HLD-DR Cb*	*MSR-A Cb*
GM-CSF	r_s = 0.114 P=0.556	r_s = -0.163 P=0.398	r_s = -0.237 P=0.196	r_s = 0.031 P=0.873	r_s = 0.049 P=0.802	r_s = 0.136 P=0.498
IL1α	r_s = 0.060 P=0.674	r_s = 0.014 P=0.920	r_s = -0.121 P=0.392	r_s = 0.086 P=0.546	r_s = -0.189 P=0.179	r_s = 0.037 P=0.800
IL12/IL23p70	r_s = 0.006 P=0.969	r_s = -0.074 P=0.622	r_s = -0.037 P=0.807	r_s = 0.333 P=0.022	r_s = -0.194 P=0.191	r_s = -0.069 P=0.654
IL15	r_s = -0.005 P=0.974	r_s = 0.184 P=0.193	r_s = 0.241 P=0.086	r_s = 0.151 P=0.286	r_s = -0.118 P=0.403	r_s = 0.079 P=0.584
IL16	r_s = 0.189 P=0.179	r_s = -0.001 P=0.992	r_s = 0.121 P=0.391	**r_s = 0.438 P<0.001*****	r_s = 0.034 P=0.810	r_s = -0.018 P=0.902
IL17A	r_s = -0.180 P=0.202	r_s = -0.025 P=0.863	r_s = 0.058 P=0.682	r_s = 0.075 P=0.599	r_s = -0.239 P=0.088	r_s = -0.011 P=0.941
IL5	r_s = 0.255 P=0.094	r_s = 0.004 P=0.982	r_s = -0.364 P=0.015	r_s = 0.053 P=0.733	r_s = -0.177 P=0.249	r_s = 0.005 P=0.976
IL7	r_s = -0.223 P=0.464	r_s = 0.083 P=0.789	r_s = 0.586 P=0.035	r_s = 0.270 P=0.372	r_s = 0.193 P=0.528	r_s = -0.182 P=0.571
TNFβ	r_s = -0.296 P=0.049	r_s = -0.199 P=0.189	r_s = -0.088 P=0.567	r_s = 0.172 P=0.260	r_s = -0.220 P=0.146	r_s = -0.059 P=0.709
VEGF	r_s = -0.063 P=0.655	r_s = -0.088 P=0.537	r_s = -0.206 P=0.142	r_s = -0.070 P=0.622	r_s = -0.229 P=0.102	r_s = -0.096 P=0.507
Eotaxin	r_s = -0.129 P=0.361	r_s = -0.206 P=0.142	r_s = -0.226 P=0.108	r_s = 0.177 P=0.209	r_s = -0.212 P=0.131	r_s = -0.127 P=0.379
Eotaxin 3	r_s = 0.058 P=0.681	r_s = -0.097 P=0.493	r_s = -0.077 P=0.588	r_s = -0.156 P=0.269	r_s = 0.014 P=0.922	r_s = 0.109 P=0.449
IL8 (HA)	r_s = -0.089 P=0.532	r_s = 0.060 P=0.673	r_s = -0.023 P=0.870	r_s = 0.056 P=0.692	r_s = -0.316 P=0.023	r_s = 0.041 P=0.775
IP10	r_s = -0.059 P=0.679	r_s = -0.082 P=0.563	r_s = 0.059 P=0.680	r_s = -0.036 P=0.799	r_s = -0.016 P=0.911	r_s = 0.040 P=0.783
MCP1	r_s = -0.117 P=0.410	r_s = -0.043 P=0.760	r_s = -0.090 P=0.524	r_s = 0.058 P=0.658	r_s = -0.151 P=0.287	r_s = 0.129 P=0.373
MCP4	r_s = -0.153 P=0.280	r_s = -0.158 P=0.264	r_s = -0.166 P=0.240	r_s = 0.148 P=0.295	r_s = -0.222 P=0.114	r_s = -0.099 P=0.495
MDC	r_s = -0.135 P=0.341	r_s = -0.015 P=0.916	r_s = -0.083 P=0.557	r_s = 0.143 P=0.311	r_s = -0.233 P=0.096	r_s = 0.049 P=0.734
MIP1α	r_s = -0.137 P=0.332	r_s = -0.144 P=0.308	r_s = -0.184 P=0.191	r_s = 0.184 P=0.191	r_s = -0.253 P=0.070	r_s = -0.124 P=0.389
MIP1β	r_s = -0.299 P=0.031	r_s = -0.175 P=0.215	r_s = -0.193 P=0.171	r_s = 0.119 P=0.402	r_s = -0.238 P=0.090	r_s = 0.006 P=0.969
TARC	r_s = -0.303 P=0.029	r_s = -0.074 P=0.603	r_s = -0.169 P=0.231	r_s = -0.008 P=0.957	r_s = -0.142 P=0.316	r_s = -0.106 P=0.463
IFNγ	r_s = 0.010 P=0.946	r_s = -0.227 P=0.113	r_s = 0.164 P=0.257	r_s = 0.336 P=0.017	r_s = -0.165 P=0.251	r_s = -0.150 P=0.310
IL1b	r_s = -0.099 P=0.485	r_s = 0.028 P=0.843	r_s = 0.070 P=0.620	r_s = 0.011 P=0.940	r_s = 0.058 P=0.681	r_s = 0.178 P=0.216
IL10	r_s = 0.014 P=0.924	r_s = -0.226 P=0.107	r_s = -0.061 P=0.667	r_s = 0.321 P=0.020	r_s = -0.238 P=0.089	r_s = 0.026 P=0.858
IL12p70	r_s = -0.042 P=0.765	r_s = -0.232 P=0.098	r_s = -0.111 P=0.432	r_s = 0.287 P=0.039	r_s = -0.130 P=0.360	r_s = -0.019 P=0.895
IL13	r_s = -0.129 P=0.361	r_s = -0.146 P=0.301	r_s = -0.311 P=0.025	r_s = -0.137 P=0.333	r_s = -0.225 P=0.108	r_s = -0.010 P=0.947
IL2	r_s = -0.031 P=0.829	r_s = -0.242 P=0.087	r_s = -0.076 P=0.596	r_s = 0.340 P=0.015	r_s = -0.244 P=0.084	r_s = -0.050 P=0.734
IL4	r_s = 0.122 P=0.387	r_s = -0.030 P=0.834	r_s = -0.006 P=0.968	r_s = 0.192 P=0.174	r_s = -0.196 P=0.163	r_s = -0.104 P=0.473
IL6	r_s = -0.063 P=0.659	r_s = 0.032 P=0.823	r_s = 0.048 P=0.736	r_s = 0.055 P=0.699	r_s = -0.053 P=0.711	r_s = 0.174 P=0.228
IL8	r_s = 0.006 P=0.967	r_s = 0.029 P=0.836	r_s = -0.092 P=0.519	r_s = -0.031 P=0.829	r_s = -0.098 P=0.491	r_s = 0.159 P=0.271
TNFα	r_s = -0.143 P=0.312	r_s = -0.237 P=0.091	r_s = -0.200 P=0.154	r_s = 0.276 P=0.047	r_s = -0.163 P=0.247	r_s = -0.052 P=0.719

r_s Spearman's rank correlation, significant *P* values are in bold (**<0.01, ***<0.001)
4G8 pan-Aβ, *AT8* phosphorylated tau, *TSPO* translocator protein
TL temporal lobe

4.5 Rs6971 genotyping

In order to examine whether the rs6971 SNP in the TSPO gene affected the binding ability of the TSPO antibody, genotyping of the cohort was performed. This gave a result for the frequency of each allele and allowed for comparisons between the genotypes using the TSPO protein load. The allele frequency was 16.7% for A/A (low-affinity binders), 40.7% for A/G (mixed-affinity binders) and 42.6% for G/G (high-affinity binders) (**Figure 16A**). The protein load was not affected by the SNP as no significant difference was observed in either the temporal lobe (Braak 0-II: median 0.89%, Braak III-IV: median 0.84%, Braak V-VI: median 0.66%; P=0.7698) or the cerebellum (Braak 0-II: median 0.87%, Braak III-IV: median 0.61%, Braak V-VI: median 0.53%; P=0.3672) (**Figure 16B, C**).

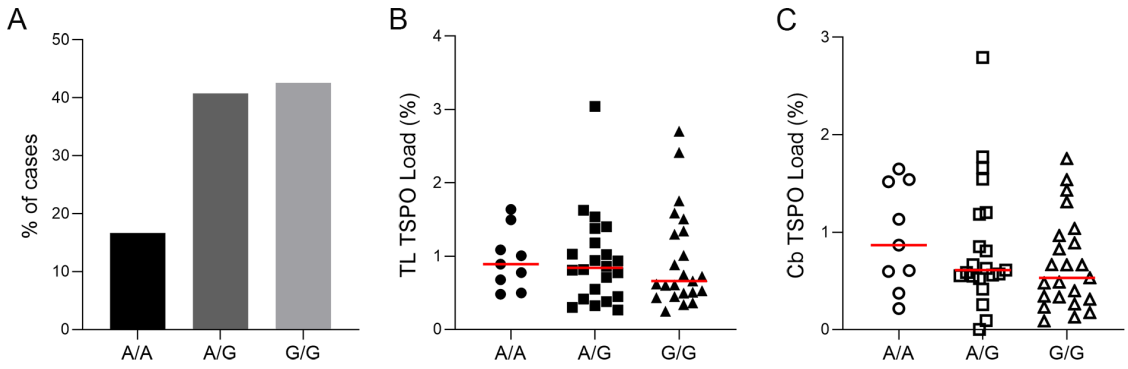

Figure 16 rs6971 genotyping showing percentage of cases with each genotype (A/A, A/G or G/G) (**A**). Comparisons between each genotype and TSPO protein load in the temporal lobe (TL) (**B**) and cerebellum (Cb) (**C**). Graphs presented as individual values with median (**B, C**).

4.6 Chapter discussion

4.6.1 Pathological and microglial markers

This chapter discussion explores the potential meaning of increased TSPO levels in the temporal lobe during AD progression, with relation to pathology, and the maintenance of a more homeostatic neuroinflammatory environment in the cerebellum. These results are novel and significant in that

they are fully quantitative using protein load as a proxy for expression, whereas the previous literature primarily uses semi-quantitative analysis (208).

Aβ and pTau: It is well established that Aβ and pTau are increased in AD, which are also shown unambiguously from these results (**Figure 11**) (10, 64, 208). Also, associations were seen between Aβ and pTau in these results (**Table 5**), which is supported by the literature indicating a spread of both proteins to the cerebral cortex in the late stages of AD and that both are required to drive the disease (153). The cerebellum exhibited significantly less pathology for both Aβ and pTau (**Figure 11**), which has been previously reported (208, 231). It is known that microglia react to Aβ and pTau in several different ways. For example, microglia have been shown to form barriers around amyloid plaques in mouse models of AD, with the aim to stop plaque spreading (232). This phenomenon is also seen in this thesis with $Iba1^+$ microglia clustering in the temporal lobe (**Figure 13**). This barrier formation role appears to be closely linked to the TREM2 protein. In humans with the R47H TREM2 mutation, which modifies the ligand-binding domain (138), there was a reduced ability to form these barriers and phagocytose Aβ (157). Although this project showed clustering of $Iba1^+$ microglia (**Figure 13**), it cannot be definitively said that this was around an amyloid plaque without the use of double staining for this pathological protein. $Iba1^+$ microglia have seen to form clusters or barriers around Aβ in previous research (233-235), making this phenomenon a plausible conclusion in these data.

TSPO: Microglial markers have been extensively studied in AD, with some degree of variability in both animal models and humans. The microglial profile in the temporal lobe showed differences to the cerebellum. The TSPO protein load was significantly increased in the temporal lobe (**Figure 14**), and due to the current hypothesis that TSPO highlights reactive microglia (13, 153), this may advocate for the temporal lobe indeed representing a reactive or disease associated subtype of microglia. There is substantial evidence that an increase in TSPO expression is a feature of AD and other neurodegenerative diseases, both from *in vivo* PET analysis (13, 198, 210) and *post-mortem* investigations (187, 204). Furthermore, examining different brain regions, it has been shown that TSPO expression is elevated in areas of high AD pathology, such as the temporal cortex (210). An interesting result was discovered when examining protein loads between the temporal lobe and cerebellum, which showed no statistical significance but a slightly higher TSPO load in the temporal lobe (TL: median 0.81%; Cb: median 0.61%) (**Figure 12**). Gui et al found a similar outcome to this, with the temporal cortex exhibiting higher TSPO but not at significant levels (187). This point on its own may lead to the notion that TSPO might not be important in AD, if the pathologically affected temporal lobe does not express significantly higher TSPO. However, there is the possibility that $TSPO^+$ microglia are associated with different phenotypes in different brain areas. This is discussed further in **Chapter 5**. Of note, TSPO expression using the DAB immunostaining was observed in microglia and endothelial cells. However, with microglia accounting for 10% (85, 86) and endothelial cells for 0.3%

(178) of cerebral cells, the TSPO protein load primarily represents microglia positive for this protein. It is important to note that there are blood vessel changes in AD, with CAA and BBB breakdown being components of disease (175, 236), which could affect the TSPO protein load also.

Iba1: When examining Iba1, thought to be a pan-microglial marker, some research has shown an increase in Iba1 in AD (237, 238), others have shown no difference (233) or a decrease compared to controls (35, 239). Therefore, it is difficult to definitively say how important Iba1 is in AD, especially as it is usually acknowledged as a general marker of microglia morphology. However, the role of Iba1 in physiology is to promote motility by aiding the formation of actin in the lamellipodia and filopodia of microglial processes and soma (119). This suggests Iba1 is crucial in the homeostatic functioning of microglia. These results showed an increase in Iba1 protein load in the cerebellum (**Figure 15**), which could suggest a higher expression level of the marker per cell or a change in microglial morphology such as process thickening, rather than an increased cell number itself. However, there is controversy in the literature, with some evidence for an increase in cell number in AD, and others suggesting that the cell number remains stable due to a synchronisation of proliferation and apoptosis (94). Qualitatively, the processes did appear to be thickening in the cerebellum as disease progression occurred (**Figure 15**), which could be a sign of the beginning stages of microglial reactivity. However, in the cerebellar region, no amoeboid microglia were seen (**Figure 15**), suggesting that the cells did not reach the final reactive state. Research has shown that in normal ageing, as well as in AD, microglial morphology is altered with thicker processes (240). Furthermore, this event of increased Iba1 has also been observed in the cerebellar region in previous research. A study found that Iba1 expression load increased significantly in the cerebellum of AD *post-mortem* tissue, with no change in $Iba1^+$ cell number (241). This corroborates the results in this thesis and provides good evidence for alteration of this microglial marker in the cerebellum during AD. The same study also observed a reduction in microglial process length and branching (241), again suggesting the altered phenotype is a present feature of AD in the cerebellum. Due to the Iba1 load being increased in the cerebellum, and no other reactive microglial marker being altered here (**Figure 15**), it could be proposed that while Iba1 is thought of as a general microglial marker, its increase in the cerebellum presents a more homeostatic environment than the temporal lobe and that the microglia in this region are more motile (119).

HLA-DR and MSR-A: Two markers of microglial reactivity, HLA-DR and MSR-A, did not change in protein load in the temporal lobe over the course of the disease (**Figure 14**). This could be considered an anomalous result as other research has shown an increase in these markers during AD progression (35, 242, 243). However, these markers were substantially different when comparing the temporal lobe with the cerebellum, with increased HLA-DR expression in the cerebellum (**Figure 12**). This is slightly different from the wider literature where there is evidence for HLA-DR being associated with

Aβ plaques and general disease progression, as well as being linked to a more activated microglial phenotype (120). However, the difference seen in this thesis could be due to the variability between human cohorts and the general heterogeneity of AD. MSR-A was discovered to be significantly higher in the temporal lobe (**Figure 12**), consistent with this marker's association with cognitive decline (115).

Associations: Further examining the importance of TSPO in AD, an interesting association between pTau and TSPO was discovered in the temporal lobe (**Table 5**). This could suggest that $TSPO^+$ microglia in the temporal lobe become reactive and may respond to pTau to a higher degree than Aβ in brain regions with high AD pathology, highlighting a longitudinal relationship between pTau and TSPO. A possible explanation for this is due to reactive microglia initiating the subsequent spread of pTau in AD progression (153). Further evidence for microglia triggering tau propagation comes from PET analysis of Aβ, tau and microglial activation, which revealed microglial activation and tau were associated through the Braak stages (147, 244, 245), and that having all three of these hallmarks gave the best indicator of AD (147). However, this theory also hinges on the response of microglia to Aβ initially, which is perhaps seen qualitatively with $Iba1^+$ microglia potentially clustering around Aβ plaques (**Figure 13**) but did not show in any associations. Tau is now thought to be the main driving force in microglial degradation in AD. Soluble pTau has proven to be toxic to microglia *in vitro* (246), and *in vivo* studies have shown a proximal relationship between microglia and pTau (247), further solidifying the stance that there is a possible detrimental connection between tau and microglia in AD.

Another positive association found was between TSPO and MSR-A in the temporal lobe (**Table 5**). This could be of interest as MSR-A is a marker of microglial reactivity and therefore could confirm that TSPO is also associated with this phenotypic type of microglia. MSR-A has been shown to closely associate with Aβ plaques in AD (123), which was observed via clustering of $MSR\text{-}A^+$ microglia but not with TSPO in this thesis (**Figure 14** and **Figure 15**). Also, MSR-A has been associated with decreased cognition in AD (115). When the associations were split by Braak stage, a positive association was found between HLA-DR in the temporal lobe and TSPO in the cerebellum at Braak stages V-VI (**Table 8**). This could provide further evidence that TSPO highlights reactive microglia as HLA-DR is a typical marker of microglial activation. It is surprising that this association was found in the cerebellum and not the temporal lobe as TSPO protein load was not increased in this region (**Figure 14**).

Neuroinflammatory microenvironment: Investigating the neuroinflammatory microenvironment in AD is crucial to understand key functions and communicative abilities of immune cells in the brain. The inflammatory status of the human brain presents a conflicting profile with some research suggesting that there are more inflammatory changes during ageing than in AD (248). In the CSF of

AD patients, higher levels of pro- and anti-inflammatory cytokines Eotaxin, IL1α, IL7, IL15 and MCP1 etc have been found compared to controls (249). In this project, only one molecule was seen to be significantly increased: IL15 in the temporal lobe (**Table 9**). IL15 is a cytokine which has been shown to be a chemoattractant to $CD4^+$ cells, such as microglia, and have an involvement in T cell recruitment (250, 251). In AD, the role of IL15 is becoming an increasingly significant topic. For example, IL15 was elevated in the CSF of AD and frontotemporal dementia patients, and this cytokine was associated with earlier age of onset (252). Also, when systemic infection occurred, both IL15 and T cell levels decreased in AD (63), further signifying a role of IL15 in T cell recruitment in disease. Higher levels of IL15 in AD have also been associated with tau. Increased IL15 in the CSF correlated with increased total and pTau, regardless of Aβ present (57). While this project found no association of IL15 with pTau (**Table 13** and **Table 14**), it is still an interesting notion to explore. Intriguingly, the majority of inflammatory markers were increased in the temporal lobe, however, four markers were increased in the cerebellum (**Table 12**). This again may reflect a regional difference of the neuroinflammatory environment in AD.

Two negative associations were seen between the inflammatory and microglial markers in the temporal lobe. The first was between HLA-DR and MDC, also called C-C motif chemokine ligand 22 (CCL22) (**Table 13**). MDC is a chemokine that has an anti-inflammatory effect (101) and acts on dendritic, natural killer (NK) cells and T cells (253). This molecule has been seen to be positively associated with HLA-DR in MS lesions (254). However, MS is an autoimmune disorder which has a different inflammatory profile to AD, meaning the negative association seen in this thesis could have altered implications in AD. In AD, T cell infiltration is a feature of the disease and $HLA\text{-}DR^+$ cells are known to interact with these immune cells (255). The negative association here could suggest impaired T cell activation in AD. The other negative association was between TSPO and Granulocyte-macrophage-colony-stimulating factor (GM-CSF) (**Table 13**). GM-CSF has been found to be increased in AD patients (256) and may have a role in stimulating microglial clearance of pathological proteins (257). The negative association between TSPO and GM-CSF could also further relate to TSPO's association with pTau; GM-CSF is implicated in microglial phagocytosis (257) and it could be suggested that this function is impaired as a result of the mitochondrial damage (increase in TSPO) in pathologically affected regions (258), and may contribute to spread of pTau seen in AD.

In the cerebellum, a positive association was discovered between Iba1 and IL16 (**Table 14**). IL16, like IL15, participates in T cell activation and has chemoattractive properties for $CD4^+$ cells (259). A study using human AD *post-mortem* tissue found that IL16, along with other inflammatory molecules, was increased compared to controls (124). A polymorphism in IL16 (rs4072111) has been shown to be decreased in AD patients, meaning this marker may provide a susceptibility to develop AD (260). Blood plasma data has demonstrated that IL16 is increased in early AD but not in the later stages of

the disease (261), which supports the finding in this thesis that the cerebellum exhibits an early AD pathology. Also, due to IL16 being chemoattractant (259), this may relate to Iba1's role in promoting microglial motility (119).

Overall, the microglial markers and microenvironment data showed a difference between the temporal lobe and the cerebellum. This may indicate that neuroinflammation in AD is region specific and varies depending on high or low levels of pathology, with microglia and other immune cells reacting accordingly. Also, that TSPO was significantly increased during disease progression in an area of high AD pathology indicated that it is indeed related to a reactive microglial phenotype. This could be an important finding to better understand the pathogenesis of AD in relation to the neuroinflammatory profile.

4.6.2 The cerebellum as a pseudo-reference region for TSPO PET scans

TSPO is used in a clinical setting as a neuroinflammatory PET marker in studies of neurodegenerative disease such as AD. TSPO is found in every brain region, however, the cerebellum may have lower amounts of the receptor present (207, 210), or a consistent level across the disease progression, as well as less Aβ and pTau (208). Therefore, this region has been proposed as a pseudo-reference region, rather than true reference region which would express zero TSPO, compared to the rest of the cortex in PET scans of neuroinflammation. This thesis corroborates this, as the results presented a much lower Aβ protein load in the cerebellum compared to the temporal lobe (~40-fold increase in the TL) (**Figure 11**). The results also showed very little pTau present in the cerebellum, whereas the temporal lobe showed a 35.5-fold increase compared to this region (**Figure 11**). This supports cerebellum exhibiting much lower levels of the typical AD pathological hallmarks. Additionally, from previous study of cerebellar Aβ, the majority of the plaques seen were diffuse and only found in the molecular layer of this region (208), which is supported by qualitative analysis in this thesis also (**Figure 11**). Furthermore, when examining TSPO, the cerebellum had a lower protein load (median 0.61%) than the temporal lobe (median 0.81%) (**Figure 14** and **Figure 15**). This difference was not stark, but it could suggest that the cerebellum is more devoid of TSPO than other brain areas. The cerebellum did not exhibit any changes in TSPO load across the disease progression, which permits it to be appropriately used as a pseudo-reference region, the definition of which states there should be a consistent level of TSPO, which is not necessarily at lower levels than other regions (262). Other research using the cerebellum as a pseudo-reference region has shown less TSPO binding in this region (13, 207, 263). The cerebellar cortex has been validated as a reference region when using a PET ligands for Aβ ([^{18}F]Florbetaben) and tau ([^{18}F]AV1451) deposition also (244, 264). Here, the term

'reference' is appropriate as the levels of these proteins were significantly lower in the cerebellum than other regions, as well as remaining low throughout the course of AD, which this thesis confirms (**Figure 11**). However, there is still some debate about the use of the cerebellum for this purpose. One study looking into amyotrophic lateral sclerosis used both the cerebellum and the occipital cortex as pseudo-reference regions, as well as testing the absolute quantitation. It was found that the SUV of the occipital lobe, rather than the cerebellum, provided the best regional group differences compared to pathologically affected areas (228). It could be proposed that difference reference regions are required for different neurodegenerative diseases, which would need to be verified by further study.

The data produced from the protein load analysis could advocate that the cerebellum appeared to produce a similar pathology to that of earlier stages of AD in the temporal lobe. For example, in Braak stage 0-II in the temporal lobe, the median Aβ load was 1.48%, whereas in the cerebellar Braak stage V-VI the protein load was 0.27%. While this was still much lower than the temporal lobe, it had increased from Braak stage 0-II in the cerebellum (median 0.11%), indicating that there could be delayed pathological progression here and if given enough time, would eventually become a similar level to areas affected earlier in the disease. Furthermore, the cerebellar Aβ plaques being diffuse in manner (**Figure 11**) further supports the stance that the cerebellum exhibits a more cognitively normal/early AD environment, as these types of plaques are found in non-demented individuals as they age (265). For pTau, there was a median protein load of 0.04% at Braak stage 0-II in the temporal lobe, which was almost identical to the pTau load in the cerebellum at Braak stage V-VI of 0.041%. Further suggesting a similar late pathological cerebellar environment to early stages in the temporal lobe. This again may support the use of the cerebellum being used as a pseudo-reference region in TSPO PET scans with lack/lesser amounts of AD pathology present.

4.6.3 Rs6971 genotyping

The rs6971 polymorphism impacts the binding ability of second generation TSPO radioligands such as DPA-714 and PBR28 (215). Therefore, it was imperative to observe how prevalent the SNP was in the cohort and whether the immunostaining of TSPO was dependent of the polymorphism. It was found that TSPO genotypes corresponding to high-affinity binders had the highest prevalence (42.59%), mixed-affinity binders had a prevalence of 40.74% and low-affinity binders had the least prevalence (16.67%) (**Figure 16**), as reported for other European population data (266). Also, TSPO immunostaining was not affected by the rs6971 polymorphism, as no difference was seen between allele groups for the TSPO protein load (**Figure 16**). These results confirm previous research showing

that rs6971 did not impact the TSPO immunoreactive burden (187). This could be explained by the difference in the binding site on the TSPO protein, with the radioligand recognising nine amino acid residues across all five transmembrane domains (184) whereas the antibody binding is between amino acid bases 76 and 169. It was important to distinguish whether the anti-TSPO antibody was affected by the SNP as this would impact the immunostaining results and could give inaccurate results. When rs6971 affected TSPO ligands are used, genotyping assessments allow for exclusion or control of participants that are low-affinity binders (12). This thesis confirms that the TSPO antibody used for immunostaining is appropriate and produced accurate results based on it being unaffected by the rs6971 SNP present.

4.7 Chapter conclusion

Based on the results from this chapter it appears that the cerebellum maintained a more homeostatic environment compared to the temporal cortex, due to the lower levels of AD pathology and lack of reactive microglial marker increase. Also, the observation of consistent levels of TSPO found in the cerebellum (and less pathology), may lend evidence for the use of this brain area as a pseudo-reference region for AD, confirming aim i. An interesting finding from this chapter demonstrated that TSPO microglial expression appeared to be associated with pTau and late stage AD in the temporal lobe. Furthermore, the prevalence of the rs6971 SNP was established in the cohort which reflected what has been seen in similar populations in other literature, and that the SNP did not impact the levels of TSPO immunostaining, verifying aim ii.

Chapter 5 Elucidating the Microglial Immunophenotype of TSPO

While TSPO PET ligands are used for assessing neuroinflammation in neurodegenerative diseases such as AD, its specific microglial association has yet to be defined. This receptor has been shown to increase in the brains of AD patients (13) and is postulated to have an early protective capacity in disease (12). It has been established that TSPO is found in a small number of cell types in the brain, primarily microglia and endothelial cells that line the blood vessel walls (187, 209), as well as some evidence for astrocytic TSPO (187). There is, however, very little quantitative research defining which phenotypic subtype of microglia express TSPO, whether expression is in all microglial cells or not. It is also important to note that TSPO is not exclusively expressed by microglia, which causes some debate in the ligand's efficacy as a neuroinflammatory marker for neurodegenerative disease. However, the other cell types that express TSPO are immune cells or cells that have implications within disease (267), therefore, while TSPO may not be specific to one cell type, it can still give an accurate picture of the overall neuroinflammatory process. It is theorised that due to TSPO levels increasing in disease (12, 13), this marker may be associated with a reactive microglial group. This is supported by microglial involvement in AD, whereby these cells develop increased reactivity to pathological proteins as the disease progresses (153) and could further the chronic neuroinflammatory process. It is important to accurately characterise the microglial/neuroinflammatory profile associated with TSPO as this could give clinicians a better understanding of TSPO PET scans, and further the knowledge of microglial involvement in AD.

This chapter seeks to address two aims of the thesis (Section **2.2**). Using human *post-mortem* tissue and double labelling immunofluorescence techniques, the microglial phenotypes recognised by TSPO from early to late stages of Alzheimer's disease were explored (aim iii), and whether other cells in the CNS expressed the TSPO signal (aim iv), using detailed qualitative and quantitative assessments.

5.1 Iba1 and TSPO

Qualitative: Iba1 is a cytoplasmic protein that is present in most microglial cells. It shows a range of morphologies in cells with elongated processes (ramified) and cells that are more spherical

(amoeboid). There was a wide distribution of the amoeboid Iba1$^+$ cells in the temporal lobe (**Figure 17A, B**), whereas the cerebellum exhibited cells that are more ramified (**Figure 18A, B**). In terms of co-localisation of Iba1 and TSPO, there was double labelling present in both areas but not every Iba1$^+$ cell was TSPO$^+$ also (**Figure 17G, H** and **Figure 18G, H**). TSPO was found in the parenchyma and in the blood vessel walls (**Figure 17D, E** and **Figure 18D, E**)

Quantitative: There was no significant difference found in positive cell count for Iba1$^+$ (Braak 0-II: median 22.83%, Braak III-IV: median 16.91%, Braak V-VI: median 25.07%; P=0.6740), TSPO$^+$ (Braak 0-II: median 2.92%, Braak III-IV: median 4.92%, Braak V-VI: median 4.34%; P=0.7850) or Iba1$^+$TSPO$^+$ (Braak 0-II: median 0.86%, Braak III-IV: median 1.30%, Braak V-VI: median 0.97%; P=0.5447) across the course of the disease in the temporal lobe when normalised to total cells (**Figure 17C, F, I**). There was a significant difference in positive cell count for Iba1$^+$TSPO$^+$ (Braak 0-II: median 0.09%, Braak III-IV: median 0.13%, Braak V-VI: median 0.33%; P=0.0377), but not Iba1$^+$ (Braak 0-II: median 0.86%, Braak III-IV: median 0.96%, Braak V-VI: median 1.66%; P=0.0543) or TSPO$^+$ (Braak 0-II: median 0.87%, Braak III-IV: median 0.72%, Braak V-VI: median 0.97%; P=0.3737) cells across the course of the disease in the cerebellum, normalised to total cells (**Figure 18I, C, F**). However, it is important to note the cell count for Iba1 in the cerebellum was close to reaching significance (P=0.0543) (**Figure 18C**). When normalised to Iba1$^+$ cells, no difference was found for Iba1$^+$TSPO$^+$ cell count in the temporal lobe (Braak 0-II: median 2.89%, Braak III-IV: median 8.09%, Braak V-VI: median 7.21%; P=0.5912) or cerebellum (Braak 0-II: median 13.33%, Braak III-IV: median 13.07%, Braak V-VI: median 19.05%; P=0.3123) through the Braak stages (**Figure 17J** and **Figure 18J** respectively).

Comparisons of Iba1$^+$TSPO$^+$ cell count between the temporal lobe and cerebellum showed a significant increase in the temporal lobe when normalised to total cells (TL: median 1.08%, Cb: median 0.18%; P<0.0001) (**Figure 27A**), but when normalised to Iba1$^+$ cell count this was significantly higher in the cerebellum (TL: median 5.59%, Cb: median 16.73%; P=0.0003) (**Figure 27F**). Finally, there were no sex differences for Iba1$^+$TSPO$^+$ count in either the temporal lobe (M: median 1.05%, F: median 1.53%; P=0.6516) or cerebellum (M: median 0.19%, F: median 0.18%; P=0.4672) when normalised to total cells (**Figure A2A, L**). There were also no sex differences in Iba1$^+$TSPO$^+$ cell count for the temporal lobe (M: median 7.83%, F: median 3.70%; P=0.2012) or cerebellum (M: median 19.96%, F: median 12.89%; P=0.3347) when normalised to Iba1$^+$ cells (**Figure A2F, Q**).

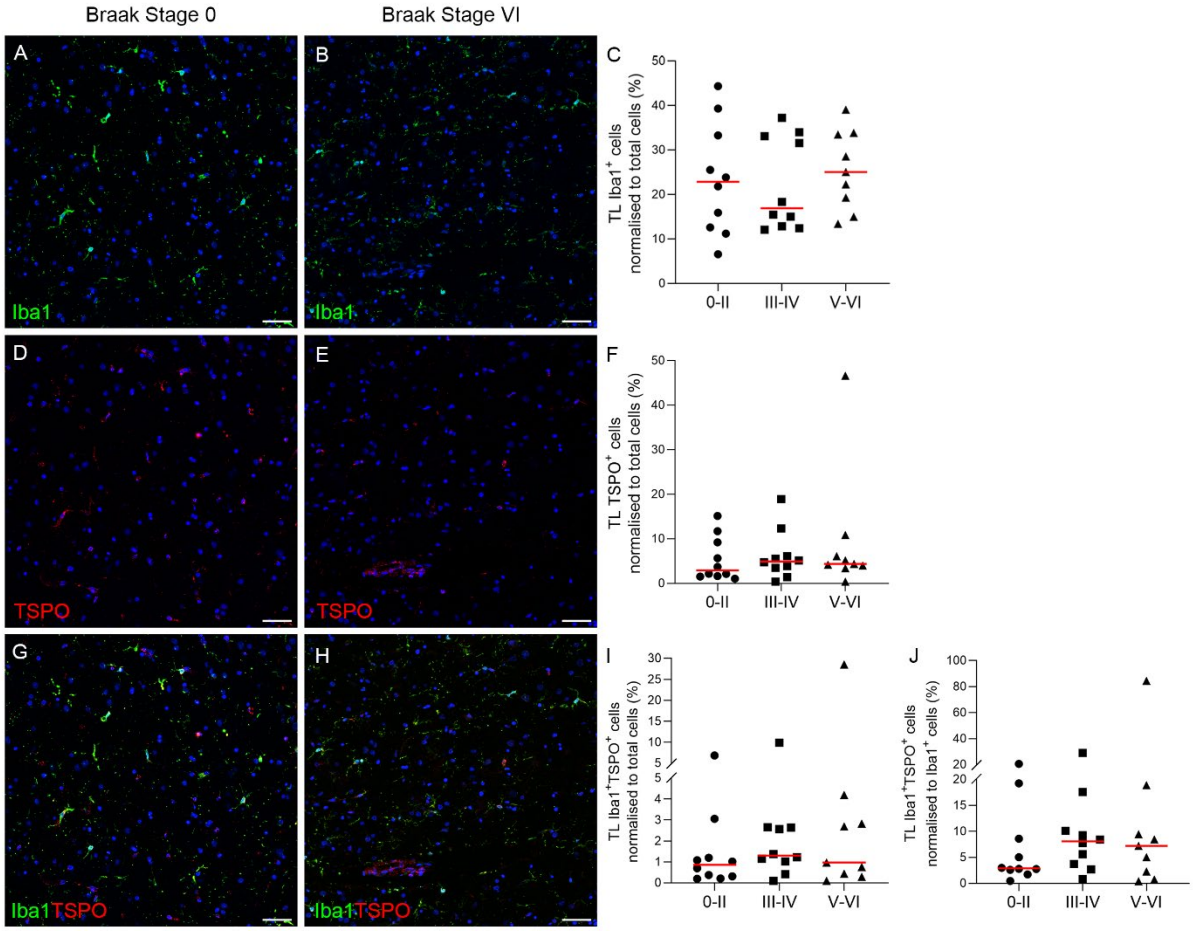

Figure 17 Fluorescent staining and quantification of Iba1$^+$ (green), TSPO$^+$ (red) and Iba1$^+$TSPO$^+$ cells in the temporal lobe over the course of the Braak stages, normalised to total cells (**C, F, I**) or Iba1$^+$ cells (**J**) (%). Counterstain: DAPI (blue). Scale bars = 50µm. Graphs presented as individual values with median (**C, F, I, J**).

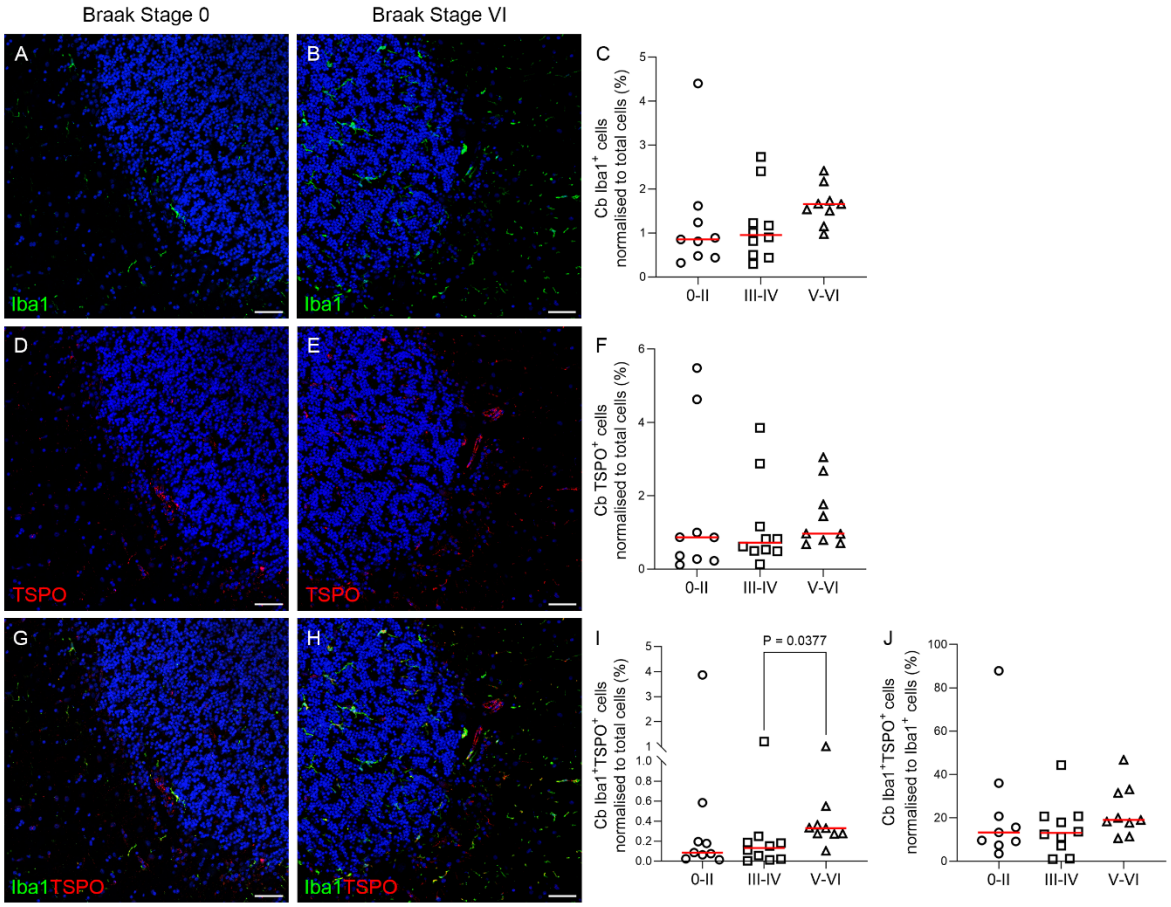

Figure 18 Fluorescent staining and quantification of Iba1$^+$ (green), TSPO$^+$ (red) and Iba1$^+$TSPO$^+$ cells in the cerebellum over the course of the Braak stages, normalised to total cells (**C, F, I**) or Iba1$^+$ cells (**J**) (%). Counterstain: DAPI (blue). Scale bars = 50µm. Graphs presented as individual values with median (**C, F, I, J**).

5.2 HLA-DR and TSPO

Qualitative: HLA-DR is typically thought to highlight a reactive subtype of microglia. It could be observed that the HLA-DR$^+$ cells in the temporal lobe exhibited clustering around a possible amyloid plaques in Braak stage VI (**Figure 19A**). There was TSPO present in the blood vessel walls and in the parenchyma (**Figure 19D, E**). Co-localisation of HLA-DR and TSPO was seen, but as with Iba1$^+$ cells, not every HLA-DR$^+$ cell was also TSPO$^+$ (**Figure 19G, H**). In the cerebellum, HLA-DR$^+$ cells seem to exhibit shorter, thicker processes at Braak stage VI compared to Braak stage 0. Both HLA-DR$^+$ and TSPO$^+$ cells were present in the granular and molecular layer of the cerebellar grey matter (**Figure 20B, E**).

Quantitative: In the temporal lobe, it was observed that HLA-DR$^+$ (Braak 0-II: median 5.30%, Braak III-IV: median 3.91%, Braak V-VI: median 6.12%; P=0.3539), TSPO$^+$ (Braak 0-II: median 4.30%, Braak III-

IV: median 1.53%, Braak V-VI: median 5.86%; P=0.0652) and HLA-DR$^+$TSPO$^+$ (Braak 0-II: median 0.69%, Braak III-IV: median 0.24%, Braak V-VI: median 0.52%; P=0.6839) cell number did not significantly change across the course of AD, normalised to total cells (**Figure 19C, F, I**). Interestingly, TSPO$^+$ cell number exhibited a high-low-high pattern which may corroborate with the theory of two waves of TSPO expression in AD (12, 140). In the cerebellum, the number of HLA-DR$^+$ (Braak 0-II: median 0.79%, Braak III-IV: median 0.50%, Braak V-VI: median 0.79%; P=0.9161), TSPO$^+$ (Braak 0-II: median 0.90%, Braak III-IV: median 1.24%, Braak V-VI: median 1.81%; P=0.0549) or double labelled cells (Braak 0-II: median 0.14%, Braak III-IV: median 0.05%, Braak V-VI: median 0.11%; P=0.4543) did not significantly change over the course of the disease, normalised to total cells (**Figure 20C, F, I**). Also, when normalised to HLA-DR$^+$ cell count, the double staining in the temporal lobe (Braak 0-II: median 14.08%, Braak III-IV: median 10.19%, Braak V-VI: median 11.44%; P=0.9782) and cerebellum (Braak 0-II: median 7.75%, Braak III-IV: median 8.37%, Braak V-VI: median 16.85%; P=0.5178) did not significantly change through the Braak stages (**Figure 19J** and **Figure 20J** respectively).

Comparisons of HLA-DR$^+$TSPO$^+$ cell count between the temporal lobe and cerebellum showed a significant increase in the temporal lobe when normalised to total cells (TL: median 0.52%, Cb: median 0.10%; P=0.0018) (**Figure 27B**), and no difference when normalised to HLA-DR$^+$ cell count (TL: median 11.44%, Cb: median 9.09%; P=0.6851) (**Figure 27G**). Also, there were no sex differences for HLA-DR$^+$TSPO$^+$ count in either the temporal lobe (M: median 0.35%, F: median 0.55%; P=0.3101) or cerebellum (M: median 0.07%, F: median 0.12%; P=0.8131) when normalised to total cells (**Figure A2B, M**), and no difference in HLA-DR$^+$TSPO$^+$ cell count for the temporal lobe (M: median 10.74%, F: median 15.18%; P=0.4509) or cerebellum (M: median 15.05%, F: median 8.05%; P=0.9582) when normalised to HLA-DR$^+$ cells (**Figure A2G, R**).

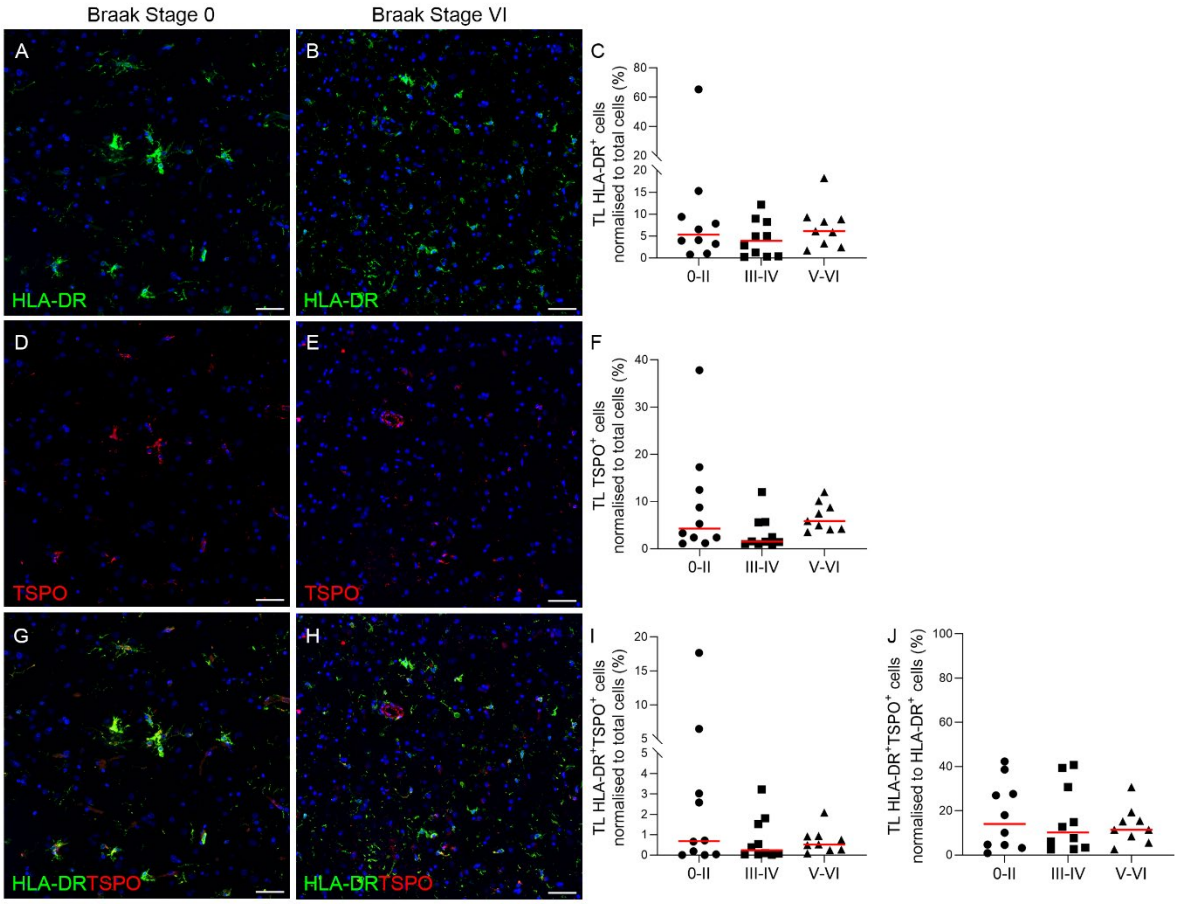

Figure 19 Fluorescent staining and quantification of HLA-DR$^+$ (green), TSPO$^+$ (red) and HLA-DR$^+$TSPO$^+$ cells in the temporal lobe over the course of the Braak stages, normalised to total cells (**C, F, I**) or HLA_DR$^+$ cells (**J**) (%). Counterstain: DAPI (blue). Scale bars = 50µm. Graphs presented as individual values with median (**C, F, I, J**).

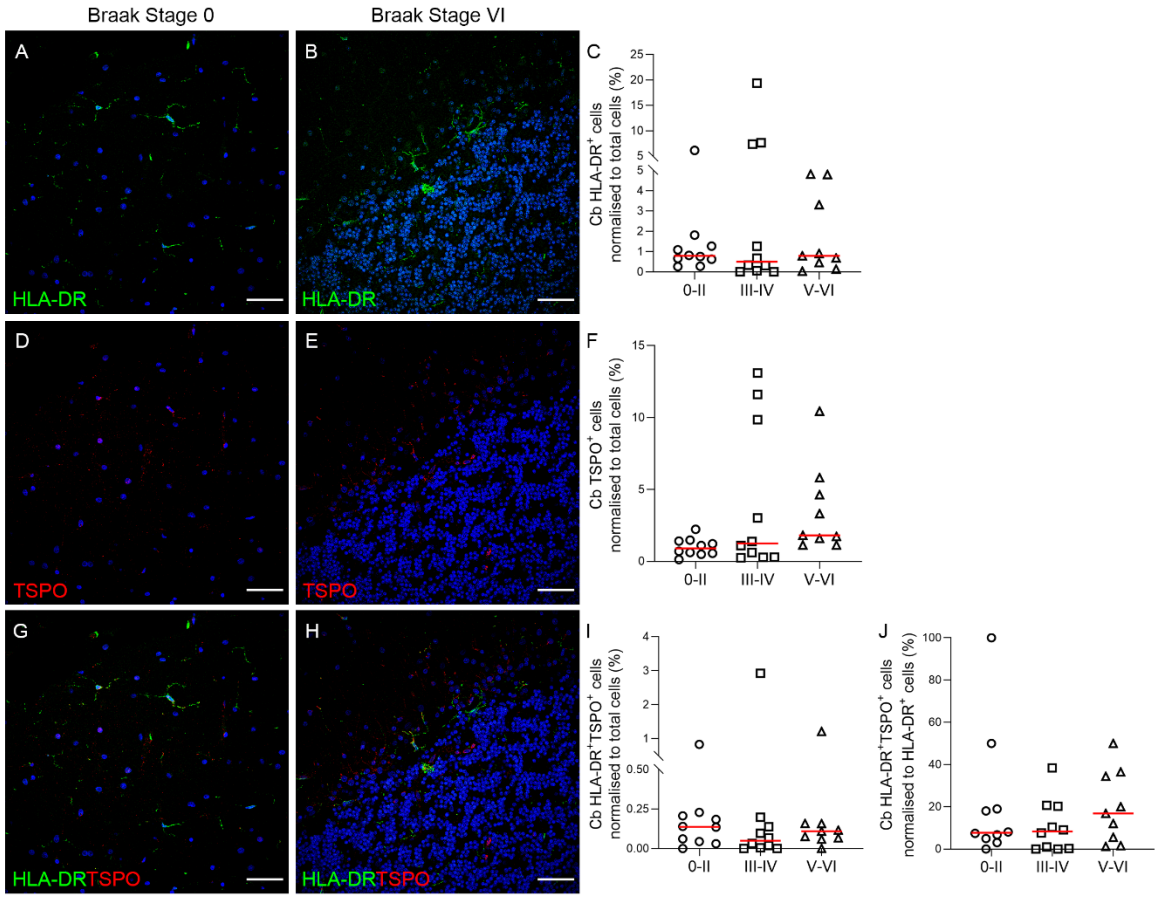

Figure 20 Fluorescent staining and quantification of HLA-DR$^+$ (green), TSPO$^+$ (red) and HLA-DR$^+$TSPO$^+$ cells in the cerebellum over the course of the Braak stages, normalised to total cells (**C, F, I**) or HLA-DR$^+$ cells (**J**) (%). Counterstain: DAPI (blue). Scale bars = 50µm. Graphs presented as individual values with median (**C, F, I, J**).

5.3 CD68 and TSPO

Qualitative: CD68 is a microglial marker associated with phagocytosis and is correlated with worsening cognitive decline in AD (115). From observation of the images, CD68 appeared as a punctate marker due to it being present in the lysosomes of the microglia, and there was clustering, potentially around Aβ plaques, seen in CD68$^+$ cells in the temporal lobe (**Figure 21B**). This marker was also found around blood vessels (**Figure 21A, B** and **Figure 22A, B**). The TSPO staining similarly appeared as small puncta, as it is found in the mitochondria. Although the two markers are not found within the same organelles, they did appear to co-localise/have some overlap within the same cell (**Figure 21G, H** and **Figure 22G, H**).

Quantitative: In the temporal lobe, no significant change was seen for CD68$^+$ cell count (Braak 0-II: median 3.20%, Braak III-IV: median 4.14%, Braak V-VI: median 4.83%; P=0.4312), TSPO$^+$ cell count

(Braak 0-II: median 8.94%, Braak III-IV: median 8.93%, Braak V-VI: median 11.25%; P=0.6558) or $CD68^+TSPO^+$ double staining cell count (Braak 0-II: median 1.40%, Braak III-IV: median 1.75%, Braak V-VI: median 1.06%; P=0.8467) when normalised to total cell count (**Figure 21C, F, I**). In the cerebellum, no significance was seen over the course of the Braak stages for $CD68^+$ (Braak 0-II: median 0.37%, Braak III-IV: median 0.26%, Braak V-VI: median 0.35%; P=0.9696), $TSPO^+$ (Braak 0-II: median 0.76%, Braak III-IV: median 0.97%, Braak V-VI: median 1.72%; P=0.3520) or $CD68^+TSPO^+$ (Braak 0-II: mean 0.18%, Braak III-IV: mean 0.26%, Braak V-VI: mean 0.17%; P=0.4189) positive cell counts, normalised to total cells (**Figure 22C, F, I**). No significant changes were seen for $CD68^+TSPO^+$ cell count in the temporal lobe (Braak 0-II: median 66.90%, Braak III-IV: median 37.43%, Braak V-VI: median 57.99%; P=0.5171) or cerebellum (Braak 0-II: mean 44.50%, Braak III-IV: median 45.98%, Braak V-VI: median 35.75%; P=0.7394) throughout the disease progression when normalised to $CD68^+$ cell count (**Figure 21J** and **Figure 22J** respectively).

Comparisons of $CD68^+TSPO^+$ cell count between the temporal lobe and cerebellum showed a significant increase in the temporal lobe when normalised to total cells (TL: median 1.40%, Cb: median 0.18%; P<0.0001) (**Figure 27C**), but no difference when normalised to $CD68^+$ cell count (TL: median 43.44%, Cb: median 42.15%; P=0.3597) (**Figure 27H**). There were no sex differences for $CD68^+TSPO^+$ count in either the temporal lobe (M: mean 2.17%, F: mean 1.55%; P=0.2266) or cerebellum (M: median 0.18%, F: median 0.17%; P=0.7461) when normalised to total cells (**Figure A2C, N**), and no difference in $CD68^+TSPO^+$ cell count for the temporal lobe (M: mean 55.02%, F: mean 46.63%; P=0.4645) or cerebellum (M: mean 49.73%, F: mean 35.62%; P=0.2202) when normalised to $CD68^+$ cells (**Figure A2H, S**).

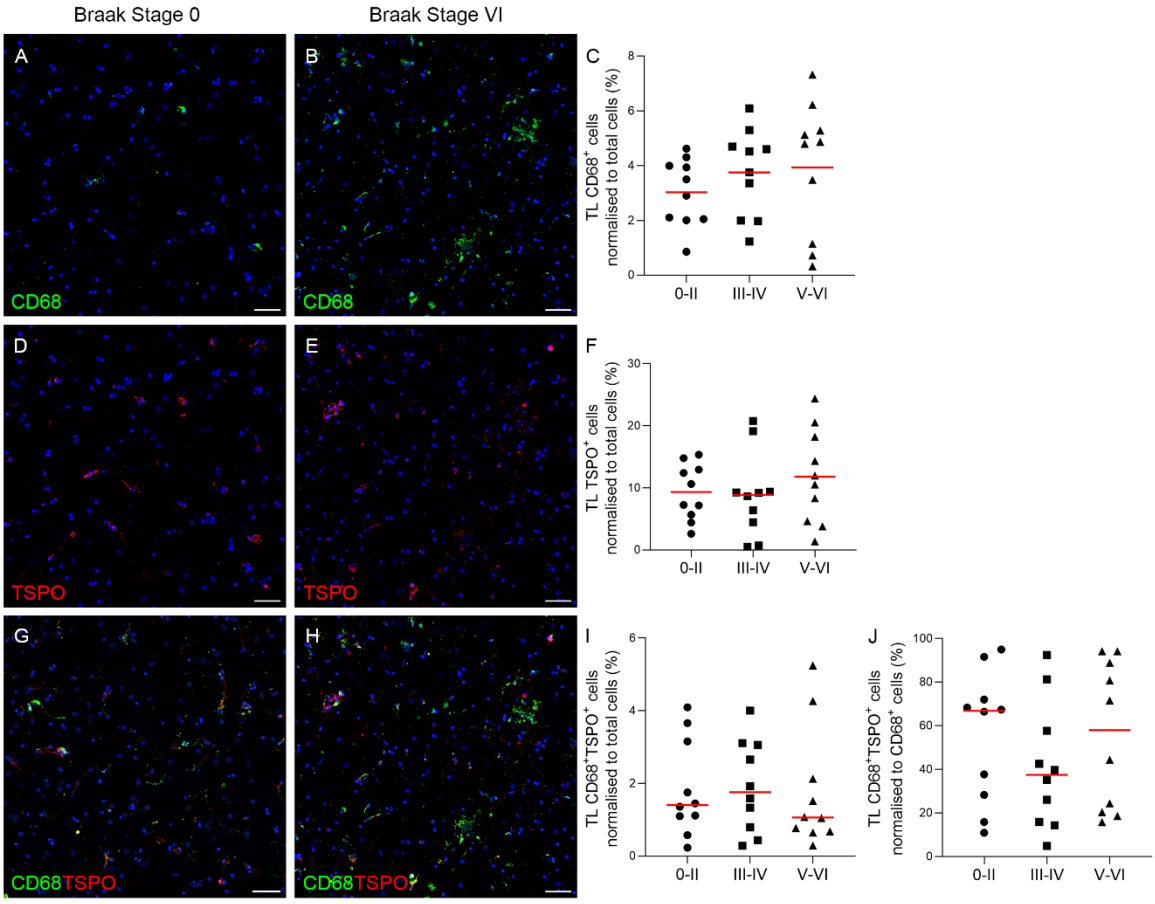

Figure 21 Fluorescent staining and quantification of CD68$^+$ (green), TSPO$^+$ (red) and CD68$^+$TSPO$^+$ cells in the temporal lobe over the course of the Braak stages, normalised to total cells (**C, F, I**) or CD68$^+$ cells (**J**) (%). Counterstain: DAPI (blue). Scale bars = 50µm. Graphs presented as individual values with median (**C, F, I, J**).

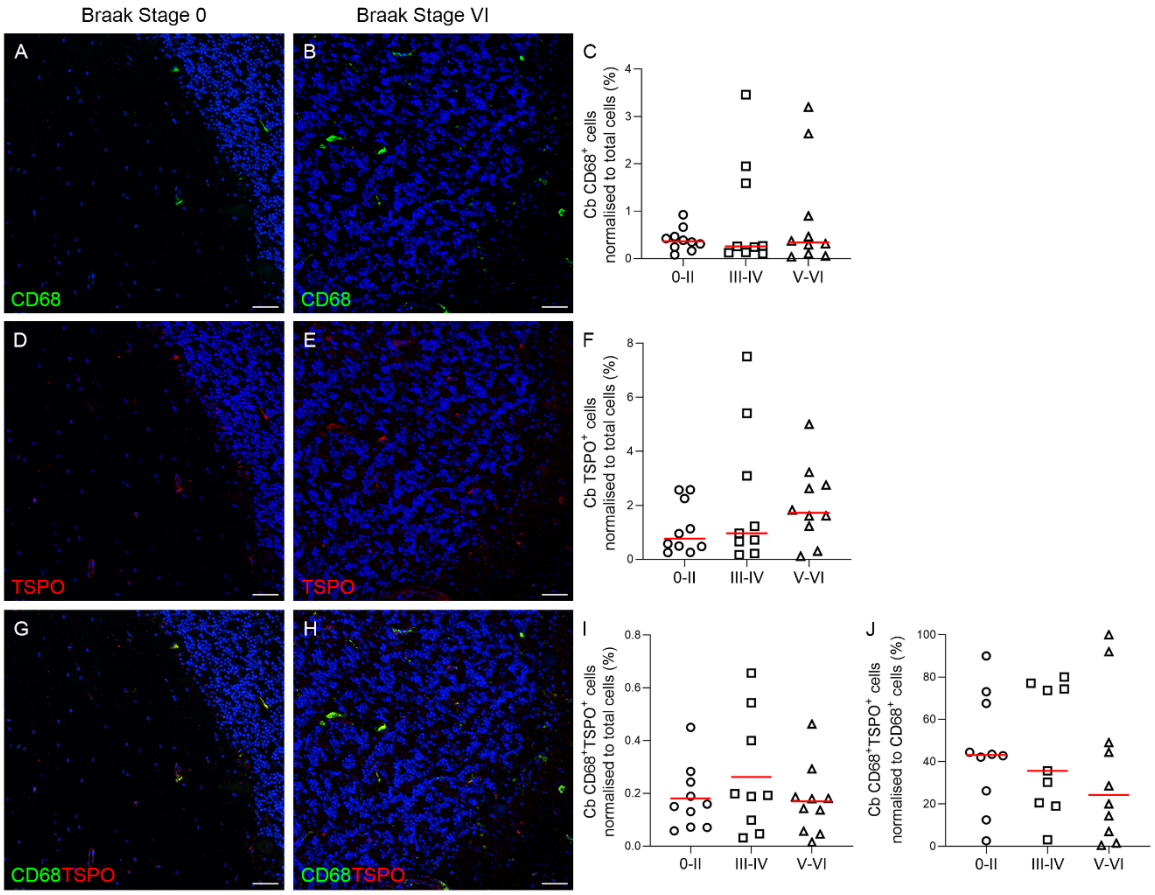

Figure 22 Fluorescent staining and quantification of CD68$^+$ (green), TSPO$^+$ (red) and CD68$^+$TSPO$^+$ cells in the cerebellum over the course of the Braak stages, normalised to total cells (**C, F, I**) or CD68$^+$ cells (**J**) (%). Counterstain: DAPI (blue). Scale bars = 50µm. Graphs presented as individual values with median (**C, F**) or mean (**I, J**).

5.4 MSR-A and TSPO

Qualitative: Very few microglial processes could be seen for microglia identified with MSR-A, the staining was primarily seen as spherical, amoeboid cells (**Figure 23A, B** and **Figure 24A, B**). There was clustering of MSR-A$^+$ microglia, which is feasibly around Aβ plaques due to their known association (115), in Braak stage VI in the temporal lobe (**Figure 23B**). The distribution of MSR-A was in both the granular and molecular areas of the cerebellum (**Figure 24A, B**). Co-localisation of TSPO and MSR-A was seen in both brain areas but, in line with the other markers, not every MSR-A$^+$ cell was TSPO$^+$ and *vice versa* (**Figure 23G, H** and **Figure 24G, H**).

Quantitative: There was no significant difference found over the course of the Braak stages for MSR-A$^+$ cells (Braak 0-II: mean 1.37%, Braak III-IV: mean 1.48%, Braak V-VI: mean 1.66%; P=0.7107), TSPO$^+$ cells (Braak 0-II: median 1.96%, Braak III-IV: median 2.50%, Braak V-VI: median 2.21%; P=0.7806) or

MSR-A$^+$TSPO$^+$ cells (Braak 0-II: mean 0.40%, Braak III-IV: median 0.43%, Braak V-VI: median 0.33%; P=0.6580) in the temporal lobe, normalised to total cells (**Figure 23C, F, I**). No significant difference was found across the disease for MSR-A$^+$TSPO$^+$ in the temporal lobe when normalised to MSR-A$^+$ cell count also (Braak 0-II: mean 29.08%, Braak III-IV: mean 29.00%, Braak V-VI: mean 22.08%; P=0.3713) (**Figure 23J**). In the cerebellum, no significant difference was found for MSR-A$^+$ (Braak 0-II: median 0.37%, Braak III-IV: median 0.39%, Braak V-VI: median 0.28%; P=0.9903), TSPO$^+$ (Braak 0-II: mean 1.05%, Braak III-IV: mean 0.78%, Braak V-VI: mean 1.69%; P=0.1265) or MSR-A$^+$TSPO$^+$ (Braak 0-II: median 0.08%, Braak III-IV: median 0.07%, Braak V-VI: median 0.07%; P=0.4541) cell counts when normalised to total cells (**Figure 24C, F, I**) or for MSR-A$^+$TSPO$^+$ when normalised to MSR-A$^+$ cells (Braak 0-II: median 18.33%, Braak III-IV: median 18.88%, Braak V-VI: median 23.81%; P=0.7106), across the course of the disease (**Figure 24J**).

Comparisons of MSR-A$^+$TSPO$^+$ cell count between the temporal lobe and cerebellum showed a significant higher cell number in the temporal lobe when normalised to total cells (TL: median 0.31%, Cb: median 0.07%; P<0.0001) (**Figure 27D**), but no difference when normalised to MSR-A$^+$ cell count (TL: median 23.62%, Cb: median 20.00%; P=0.118) (**Figure 27I**). Also, there were no sex differences for MSR-A$^+$TSPO$^+$ count in either the temporal lobe (M: mean 0.30%, F: mean 0.46%; P=0.0894) or cerebellum (M: median 0.07%, F: median 0.07%; P=0.5045) when normalised to total cells (**Figure A2D, O**), and no difference in MSR-A$^+$TSPO$^+$ cell count for the temporal lobe (M: mean 23.69%, F: mean 29.37%; P=0.2229) or cerebellum (M: median 20.33%, F: median 18.33%; P=0.6300) when normalised to MSR-A$^+$ cells (**Figure A2I, T**).

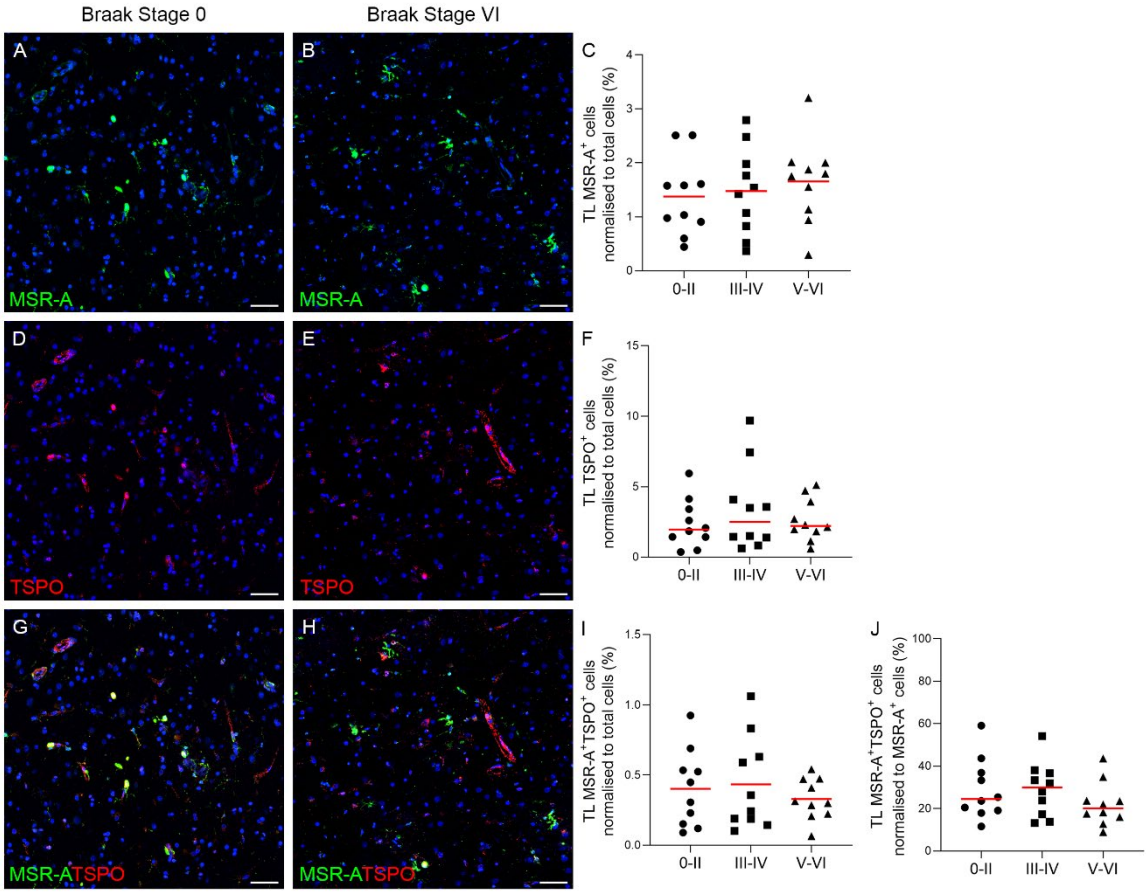

Figure 23 Fluorescent staining and quantification of MSR-A$^+$ (green), TSPO$^+$ (red) and MSR-A$^+$TSPO$^+$ cells in the temporal lobe over the course of the Braak stages, normalised to total cells (**C, F, I**) or MSR-A$^+$ cells (**J**) (%). Counterstain: DAPI (blue). Scale bars = 50µm. Graphs presented as individual values with mean (**C, I, J**) or median (**F**).

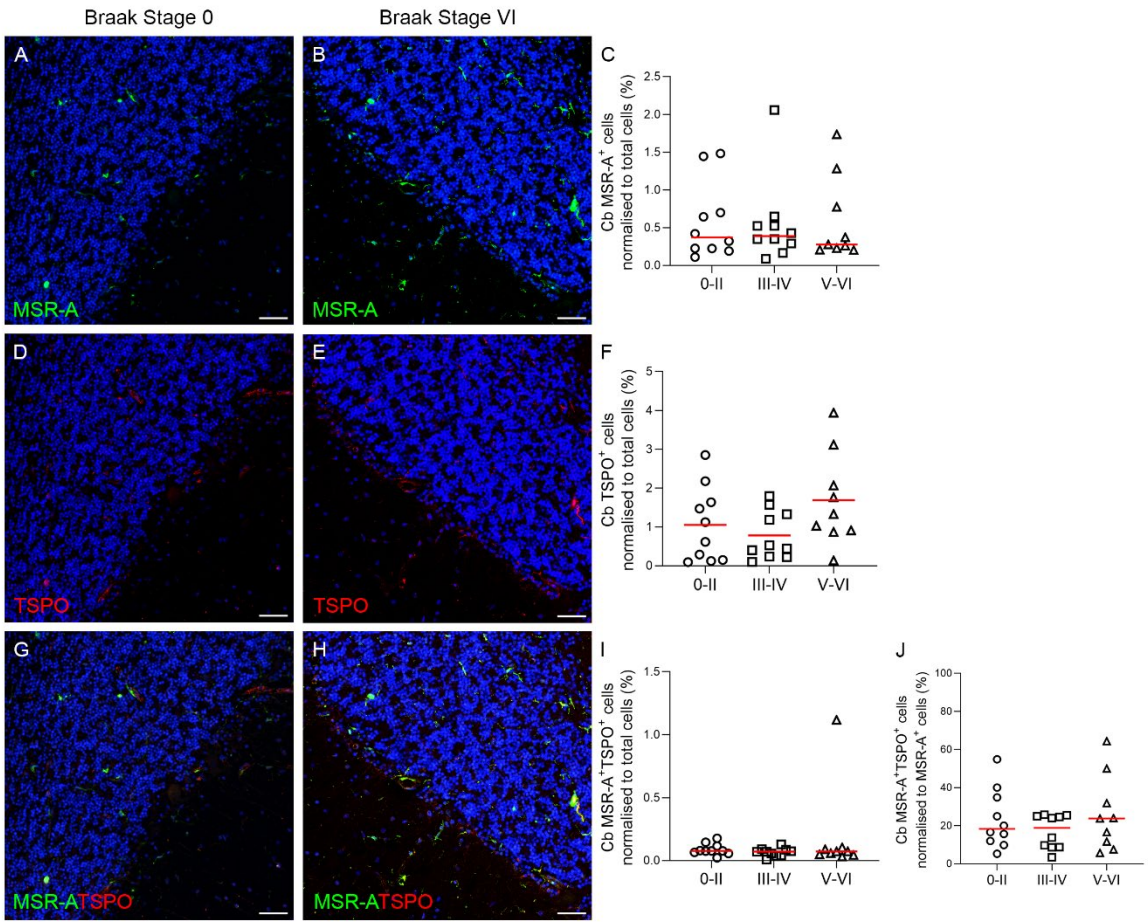

Figure 24 Fluorescent staining and quantification of MSR-A$^+$ (green), TSPO$^+$ (red) and MSR-A$^+$TSPO$^+$ cells in the cerebellum over the course of the Braak stages, normalised to total cells (**C, F, I**) or MSR-A$^+$ cells (**J**) (%). Counterstain: DAPI (blue). Scale bars = 50µm. Graphs presented as individual values with median (**C, I, J**) or mean (**F**).

5.5 CD64 and TSPO

Qualitative: CD64, also known as FcγRI, is a cell surface receptor which can trigger a macrophage immune response and is associated with the presence of immunoglobulins (63, 127). Like CD68, this marker is also associated with phagocytosis and has implication in neurodegenerative disease such as AD (118, 268). Microglial morphology can be seen as this marker is present on the cell membrane, as well as clustering of CD64$^+$ microglia (**Figure 25B** and **Figure 26B**). Co-localisation of CD64 and TSPO is observed, primarily in the cell soma (**Figure 25G, H** and **Figure 26G, H**).

Quantitative: There was no significant change over the course of the Braak stages for CD64$^+$ (Braak 0-II: mean 17.89%, Braak III-IV: mean 18.60%, Braak V-VI: mean 19.07%; P=0.0577), TSPO$^+$ (Braak 0-II: mean 3.84%, Braak III-IV: mean 6.25%, Braak V-VI: mean 8.13%; P=0.0654) or CD64$^+$TSPO$^+$ (Braak 0-II:

median 1.14%, Braak III-IV: median 0.99%, Braak V-VI: median 1.56%; P=0.6712) cells in the temporal lobe, normalised to total cells (**Figure 25C, F, I**). When normalised to $CD64^+$ cells, there was still no statistical change for $CD64^+TSPO^+$ cells (Braak 0-II: median 6.19%, Braak III-IV: median 5.84%, Braak V-VI: median 6.73%; P=0.6781) (**Figure 25J**). In the cerebellum, there was no significant differences for $CD64^+$ (Braak 0-II: median 6.53%, Braak III-IV: median 6.57%, Braak V-VI: median 3.26%; P=0.1054), $TSPO^+$ (Braak 0-II: median 0.74%, Braak III-IV: median 0.82%, Braak V-VI: median 0.84%; P=0.6941) or $CD64^+TSPO^+$ (Braak 0-II: median 0.20%, Braak III-IV: median 0.17%, Braak V-VI: median 0.19%; P=0.9078) cells, normalised to total cells (**Figure 26C, F, I**), or for $CD64^+TSPO^+$ (Braak 0-II: median 3.86%, Braak III-IV: median 2.48%, Braak V-VI: median 4.57%; P=0.5976) cells when normalised to $CD64^+$ cell count (**Figure 26J**).

Comparisons of $CD64^+TSPO^+$ cell count between the temporal lobe and cerebellum showed a significant higher cell number in the temporal lobe when normalised to total cells (TL: median 1.11%, Cb: median 0.20%; P<0.0001) (**Figure 27E**), and also a significant increase in the temporal lobe when normalised to $CD64^+$ cell count (TL: median 6.17%, Cb: median 3.53%; P=0.0296) (**Figure 27J**). Finally, there were no sex differences for $CD64^+TSPO^+$ count in either the temporal lobe (M: median 1.11%, F: median 1.08%; P=0.9185) or cerebellum (M: median 0.27%, F: median 0.13%; P=0.1103) when normalised to total cells (**Figure A2E, P**), and no difference in $CD64^+TSPO^+$ cell count for the temporal lobe (M: median 5.99%, F: median 7.76%; P=0.6971) or cerebellum (M: median 5.28%, F: median 2.45%; P=0.0925) when normalised to $CD64^+$ cells (**Figure A2J, U**).

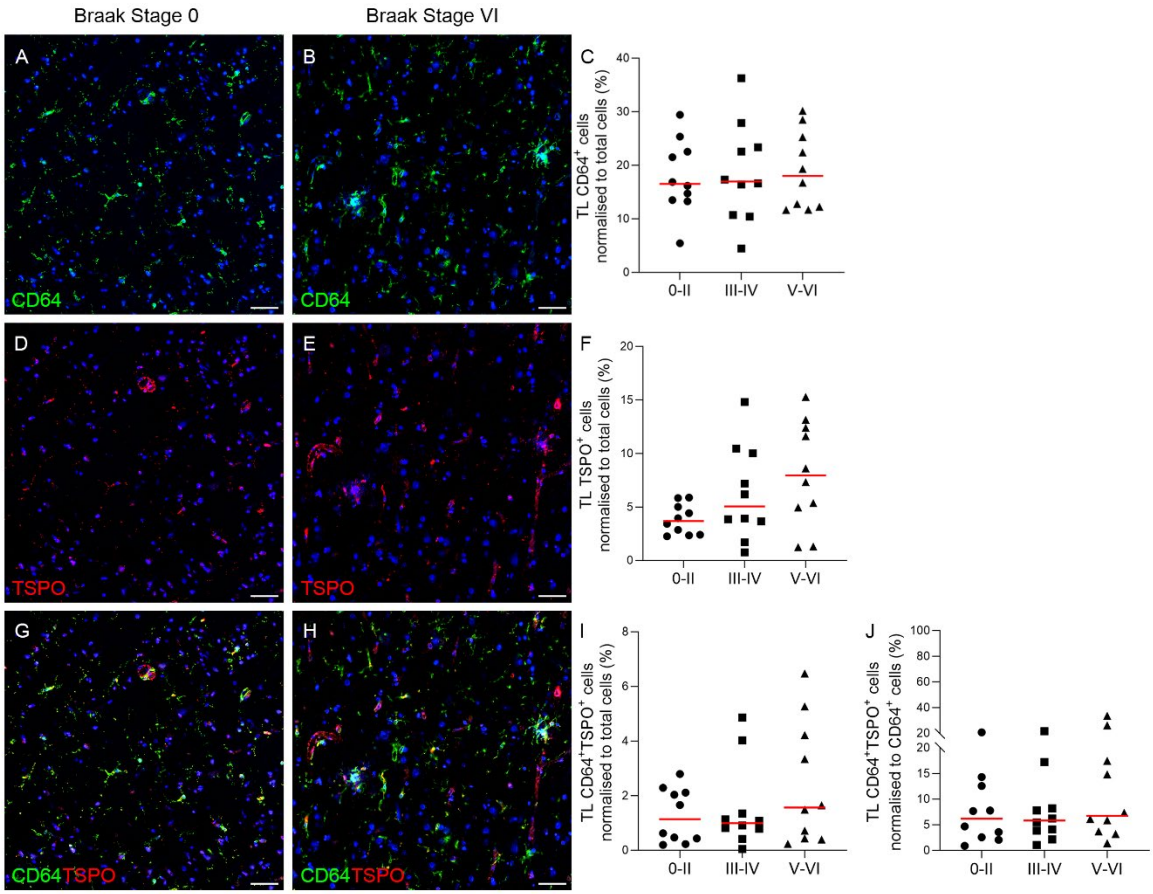

Figure 25 Fluorescent staining and quantification of CD64$^+$ (green), TSPO$^+$ (red) and CD64$^+$TSPO$^+$ cells in the temporal lobe over the course of the Braak stages, normalised to total cells (**C, F, I**) or CD64$^+$ cells (**J**) (%). Counterstain: DAPI (blue). Scale bars = 50µm. Graphs presented as individual values with mean (**C, F,**) or median (**I, J**).

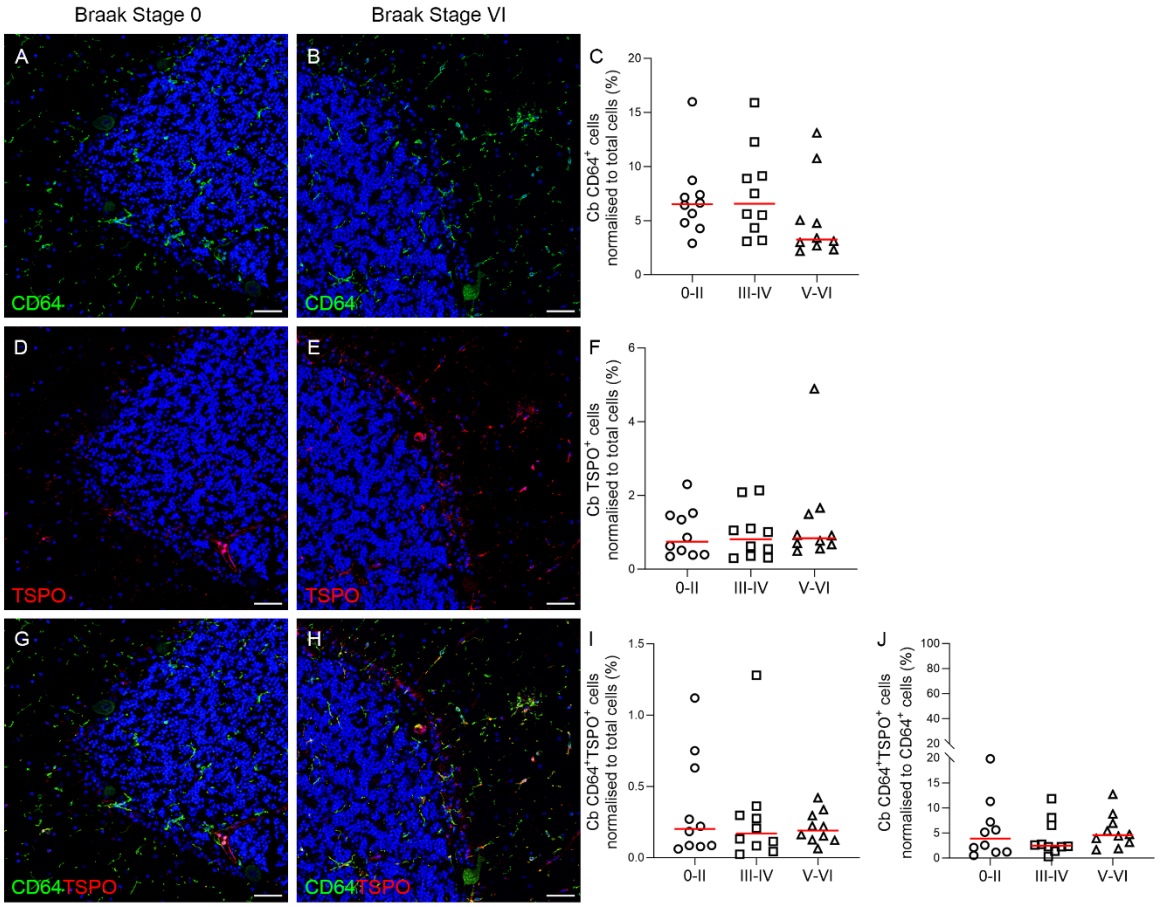

Figure 26 Fluorescent staining and quantification of CD64$^+$ (green), TSPO$^+$ (red) and CD64$^+$TSPO$^+$ cells in the cerebellum over the course of the Braak stages, normalised to total cells (**C, F, I**) or CD64$^+$ cells (**J**) (%). Counterstain: DAPI (blue). Scale bars = 50µm. Graphs presented as individual values with median (**C, F, I, J**).

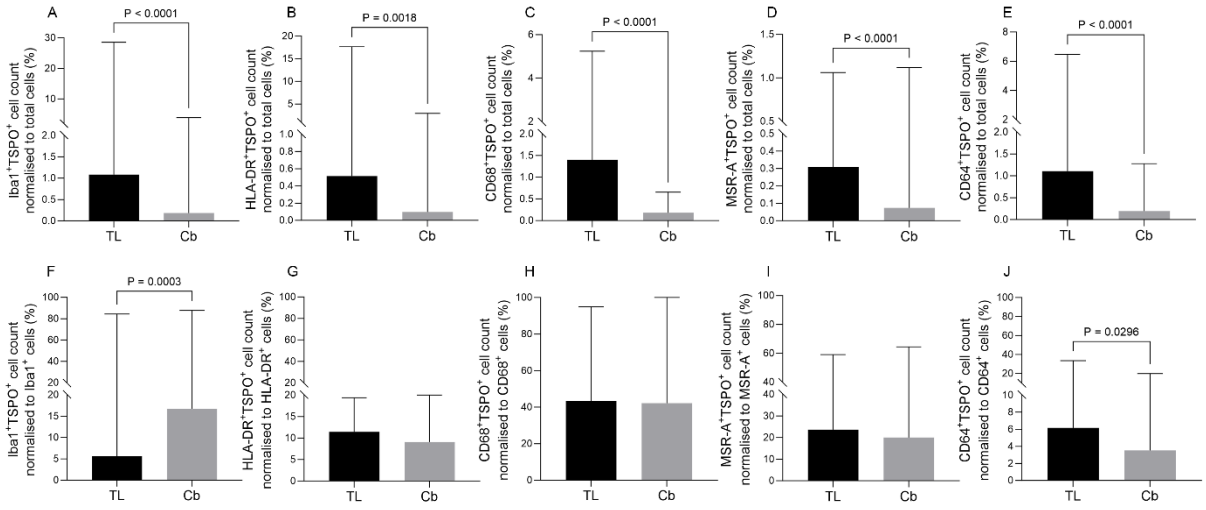

Figure 27 Comparisons between the temporal lobe (TL) and cerebellum (Cb) for double labelling of TSPO with Iba1, HLA-DR, CD68, MSR-A and CD64, normalised to total cell count (%) (**A-E**) or

corresponding microglial marker cell count (%) (**F-J**), including all cases. Graphs presented as median with range.

5.6 Marker comparisons

Whole cohort (total cell count): To understand the potential association of TSPO with known microglial markers, regardless of disease stage, double labelling of each stain was compared in the temporal lobe and cerebellum, first normalised to total cells and then normalised to the corresponding microglial marker (**Figure 28**). When all cases were included, normalised to total cell count, $CD68^{+}TSPO^{+}$ cell count was the highest in the temporal lobe (median 1.40%) and was significantly higher than $HLA\text{-}DR^{+}TSPO^{+}$ (median 0.60%; P=0.0294) and $MSR\text{-}A^{+}TSPO^{+}$ (median 0.31%; P<0.0001) (**Figure 28A**). Also in the temporal lobe, $Iba1^{+}TSPO^{+}$ (median 1.08%) and $CD64^{+}TSPO^{+}$ (median 1.11%) cell counts were significantly higher than $MSR\text{-}A^{+}TSPO^{+}$ (median 0.31%; P=0.0007 and P=0.0004 respectively) (**Figure 28A**). In the cerebellum, the highest cell count was $CD64^{+}TSPO^{+}$ (median 0.20%) and this was significantly higher than $MSR\text{-}A^{+}TSPO^{+}$ (median 0.07%; P=0.0012) (**Figure 28B**). $Iba1^{+}TSPO^{+}$ (median 0.18%) and $CD68^{+}TSPO^{+}$ (median 0.18%) cell counts were significantly higher than $MSR\text{-}A^{+}TSPO^{+}$ (median 0.07%; P=0.0147 and P=0.0233 respectively) in this region (**Figure 28B**).

Whole cohort (microglial marker count): Again when all cases were included in the analysis, but with the data normalised to corresponding microglial marker cell count, $CD68^{+}TSPO^{+}$ cell count was the highest in both brain regions (TL: median 43.44%, Cb: median 42.15%), and was significantly higher than $Iba1^{+}TSPO^{+}$ (median 5.59%; P<0.0001), $HLA\text{-}DR^{+}TSPO^{+}$ (median 11.40%; P<0.0001) and $CD64^{+}TSPO^{+}$ (median 6.17%; P<0.0001) cell counts in the temporal lobe (**Figure 28C**). $MSR\text{-}A^{+}TSPO^{+}$ (median 23.62%) cell count was also significantly increased compared to $Iba1^{+}TSPO^{+}$ (median 5.59%; P<0.0001), $HLA\text{-}DR^{+}TSPO^{+}$ (median 11.40%; P=0.0345) and $CD64^{+}TSPO^{+}$ (median 6.17%; P<0.0001) cell counts in this region (**Figure 28C**). In the cerebellum, $CD68^{+}TSPO^{+}$ cell count was significantly increased compared to $HLA\text{-}DR^{+}TSPO^{+}$ (median 8.57%; P=0.0012) and $CD64^{+}TSPO^{+}$ (median 3.53%; P<0.0001) (**Figure 28D**). $Iba1^{+}TSPO^{+}$ (median 16.73%) and $MSR\text{-}A^{+}TSPO^{+}$ (median 20.00%) counts were significantly higher than $CD64^{+}TSPO^{+}$ cell count (median 3.53%; P=0.0005 and P<0.0001 respectively) (**Figure 28D**).

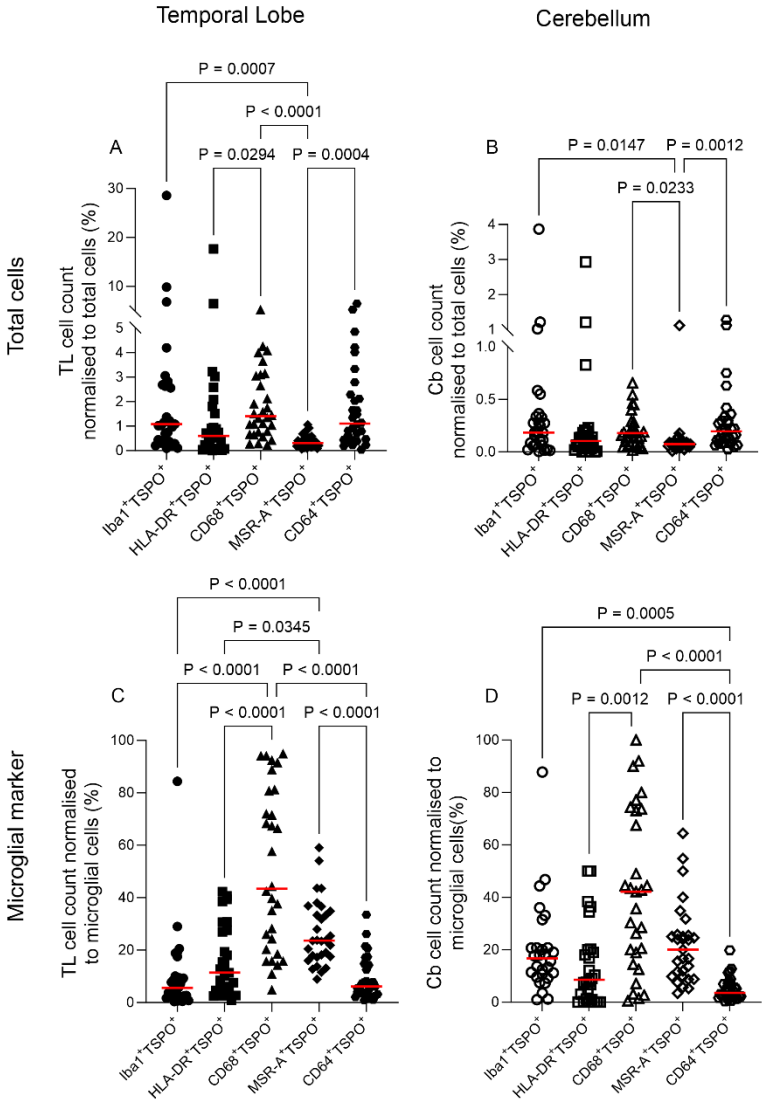

Figure 28 Comparisons between double labelling cell count of TSPO with Iba1, HLA-DR, CD68, MSR-A and CD64, normalised to total cell count (%) (**A, B**) or corresponding microglial marker cell count (%) (**C, D**), including all cases, in the temporal lobe (**A, C**) and cerebellum (**B, D**). Graphs presented as individual values with median.

Braak group (total cell count): This analysis was also performed with the Braak stages separated, in order to see how disease progression might affect the TSPO associated microglial phenotype (**Figure 29**). When normalised to total cell count, in the temporal lobe $CD68^+TSPO^+$ was the highest cell count in the first two Braak groups (Braak 0-II: median 1.40%, Braak III-IV: median 1.75%) and $CD64^+TSPO^+$ was the highest in the last Braak group (Braak V-VI: median 1.56%) (**Figure 29A**). Braak stage 0-II showed a significant increase in $CD68^+TSPO^+$ cell count compared to $MSR\text{-}A^+TSPO^+$ cell count (median 0.378%) (P=0.0412) (**Figure 29A**). Braak stage III-IV also had a significant increase $CD68^+TSPO^+$ compared to $MSR\text{-}A^+TSPO^+$ (P=0.0477) (**Figure 29A**). Finally, Braak stage V-VI exhibited a significant increase in $CD68^+TSPO^+$ (median 1.06%) and $CD64^+TSPO^+$ cell count (median 1.56%) compared to

MSR-A^{+}TSPO^{+} (median 0.31%) (P=0.0217 and P=0.0254 respectively) (**Figure 29A**). In the cerebellum, CD64^{+}TSPO^{+} was the highest marker in the first Braak group (Braak 0-II: median 0.20%), CD68^{+}TSPO^{+} is highest in the second Braak group (III-IV: median 0.19%) and Iba1^{+}TSPO^{+} was highest in the last Braak group (Braak III-IV: median 0.33%) (**Figure 29B**), but the only significantly increased marker was in Braak stage V-VI between Iba1^{+}TSPO^{+} (median 0.33%) and MSR-A^{+}TSPO^{+} (median 0.07%) cell count (P=0.0048) (**Figure 29B**).

Braak group (microglial marker count): Still classified by Braak stage, but normalised to microglial marker cell count, the temporal lobe Braak stage 0-II exhibited the highest cell count for CD68^{+}TSPO^{+} (median 66.9%) and was significantly increased compared to Iba1^{+}TSPO^{+} (median 2.89%; P=0.0004) and CD64^{+}TSPO^{+} (median 6.19%; P=0.0013) (**Figure 29C**). MSR-A^{+}TSPO^{+} (median 24.47%) was significantly higher than Iba1^{+}TSPO^{+} (median 2.89%; P=0.0251) in Braak 0-II also (**Figure 29C**). In Braak stage III-IV CD68^{+}TSPO^{+} also had the highest cell count (median 37.43%) and this was significantly increased compared to Iba1^{+}TSPO^{+} (median 8.09%; P=0.0205) and CD64^{+}TSPO^{+} (median 5.84%; P=0.005) (**Figure 29C**). MSR-A^{+}TSPO^{+} (median 29.91%) was significantly higher than CD64^{+}TSPO^{+} here also (median 5.84%; P=0.0166) (**Figure 29C**). In Braak stage V-VI the highest cell count was CD68^{+}TSPO^{+} (median 57.99%) as well and this was significantly higher than Iba1^{+}TSPO^{+} (median 7.21%; P=0.0017), HLA-DR^{+}TSPO^{+} (median 11.44%; P=0.0282) and CD64^{+}TSPO^{+} (median 6.72%; P=0.005) (**Figure 29C**). In the cerebellum, Braak stage 0-II exhibited CD68^{+}TSPO^{+} the highest cell count (median 43.17%) and was significantly increased compared to CD64^{+}TSPO^{+} (median 3.86%; P=0.0007) as well as MSR-A^{+}TSPO^{+} (median 18.33%) being significantly increased against CD64^{+}TSPO^{+} (median 3.86%; P=0.044) (**Figure 29D**). Braak stage III-IV demonstrated a similar pattern with CD68^{+}TSPO^{+} cell count being the highest (median 35.71%) and this was significantly increased compared to HLA-DR^{+}TSPO^{+} (median 8.37%; P=0.0168) and CD64^{+}TSPO^{+} (median 2.48%; P=0.0006) (**Figure 29D**). Finally, in Braak stage V-VI, CD68^{+}TSPO^{+} was again the highest cell count (median 24.29%) and was significantly increased compared with CD64^{+}TSPO^{+} (median 4.57%; P=0.0178) (**Figure 29D**).

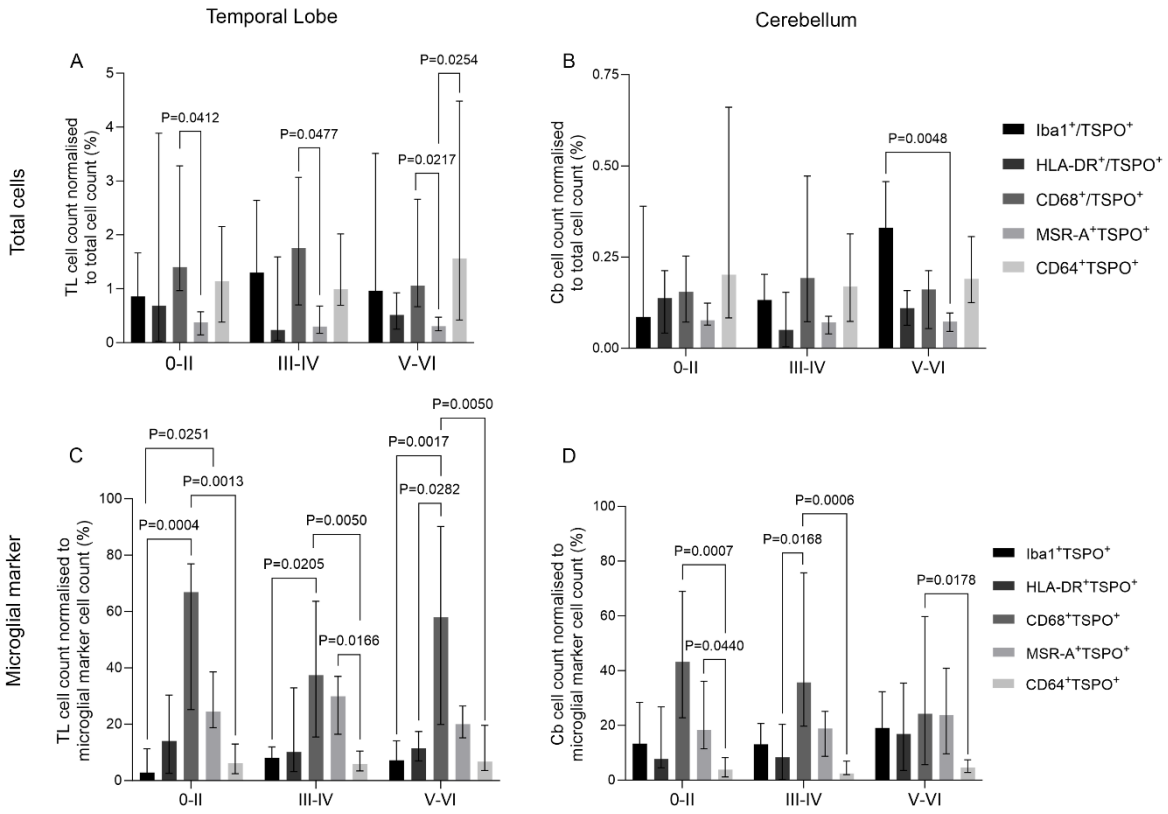

Figure 29 Comparisons between double labelling cell count of TSPO with Iba1, HLA-DR, CD68, MSR-A and CD64, normalised to total cell count (%) (**A, B**) or corresponding microglial marker cell count (%) (**C, D**), split by Braak stage, in the temporal lobe (**A, C**) and cerebellum (**B, D**). Key represents microglial marker double labelling with TSPO. Graphs presented as median with interquartile range.

5.7 CD31 and TSPO

CD31, or PECAM-1, is a marker of endothelial cells, present within the walls of the vasculature in the brain. This marker is involved in endothelial cell junction adhesion (269). TSPO has been suggested previously to be present in endothelial cells (187) and in order to confirm this, double immunofluorescence was performed in the temporal lobe and cerebellum (**Figure 30**). It appeared that CD31 and TSPO were co-localised to a certain degree, but there was more TSPO present in the outer blood vessel walls, with CD31 primarily present in the inner luminal area (**Figure 30**). TSPO could possibly be labelling the smooth muscle actin (SMA) as well as endothelial cells, however an antibody stain against SMA would be needed to confirm this.

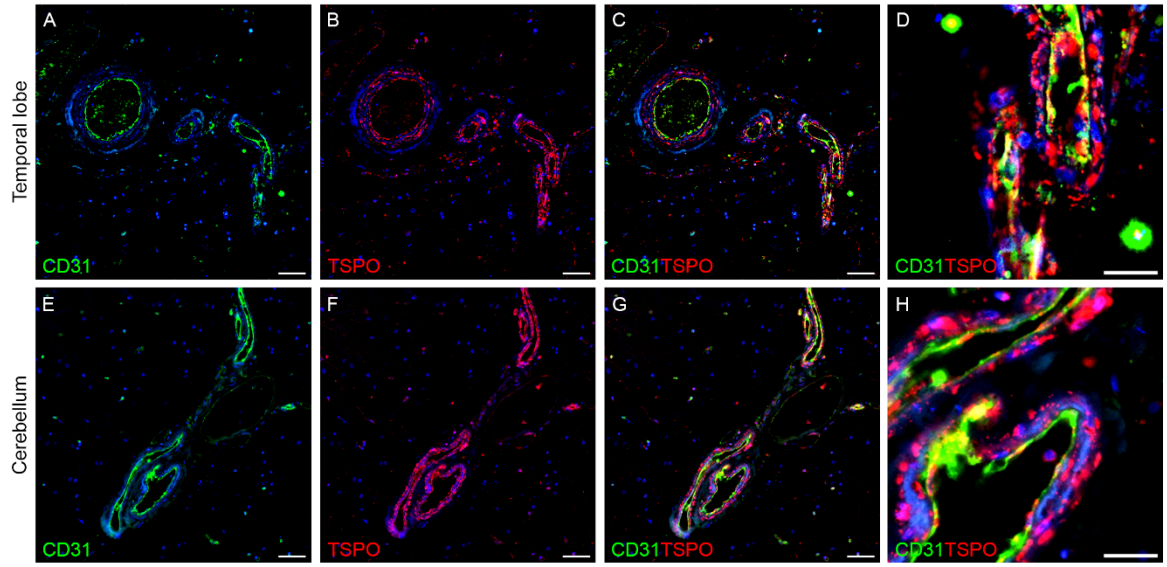

Figure 30 Double immunofluorescent staining of CD31 (green) and TSPO (red) in the temporal lobe (**A-D**) and cerebellum (**E-H**). (**D,H**) are cropped images of (**C,G**). Counterstain: DAPI (blue). Scale bars = 50µm (**A-C**, **E-F**)/20µm (**D,H**).

5.8 CD163 and TSPO

CD163 is a common marker for perivascular macrophages in the brain (270). From the staining images in **Figure 31**, there appeared to be very little, if any, TSPO present in perivascular macrophages (CD163), with the majority of TSPO staining seen in the blood vessel walls and microglial cells. There seemed to be potential overlap in the $CD163^{+}$ cells proximal to the blood vessels, however there was very little co-localisation of TSPO with this marker in both brain areas (**Figure 31**). There are other macrophage markers such as CD206 that could be used to assess the presence of TSPO in macrophages also.

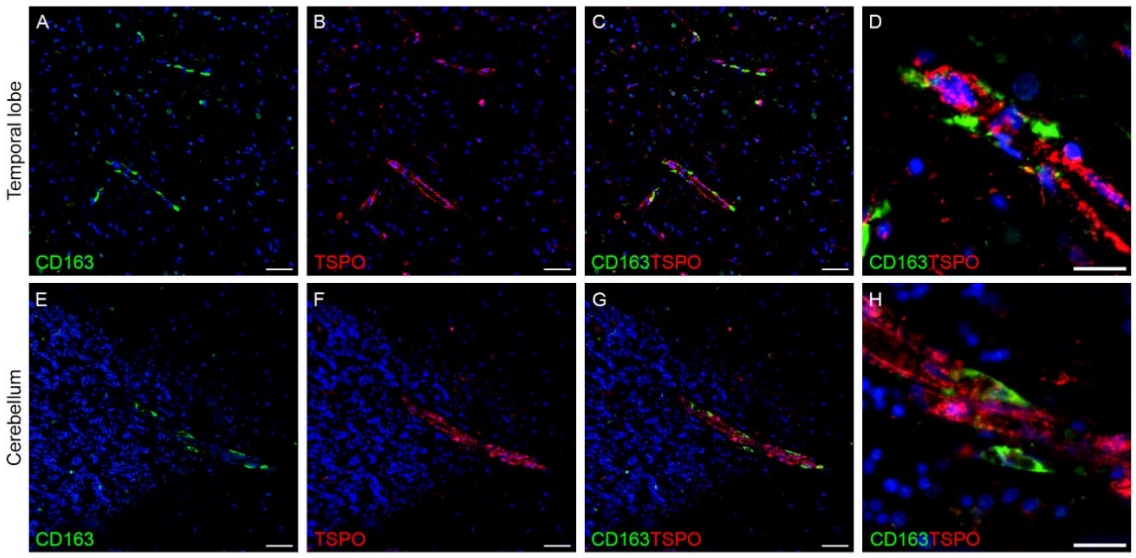

Figure 31 Double immunofluorescent staining of CD163 (green) and TSPO (red) in the temporal lobe (**A-D**) and cerebellum (**E-H**). (**D,H**) are cropped images of (**C,G**). Counterstain: DAPI (blue). Scale bars = 50μm (**A-C**, **E-F**)/20μm (**D,H**).

5.9 GFAP and TSPO

GFAP is an intermediate filament protein found in the astrocytic cellular cytoskeleton involved in motility and is upregulated in reactive astrocytes (165). Qualitative assessment of double labelling of GFAP and TSPO demonstrated very little, if any, TSPO present in $GFAP^+$ astrocytes. This was the case for both the temporal lobe and cerebellum (**Figure 32**). GFAP in the temporal lobe appeared to be present as both individual cells and clusters. As this was an AD brain (Braak stage VI), it could be likely that this was around neuritic plaques (**Figure 32**). In the cerebellum, the majority of astrocytes were found in the juncture between the granular and molecular layer (**Figure 32**), potentially where dying purkinje cells are located.

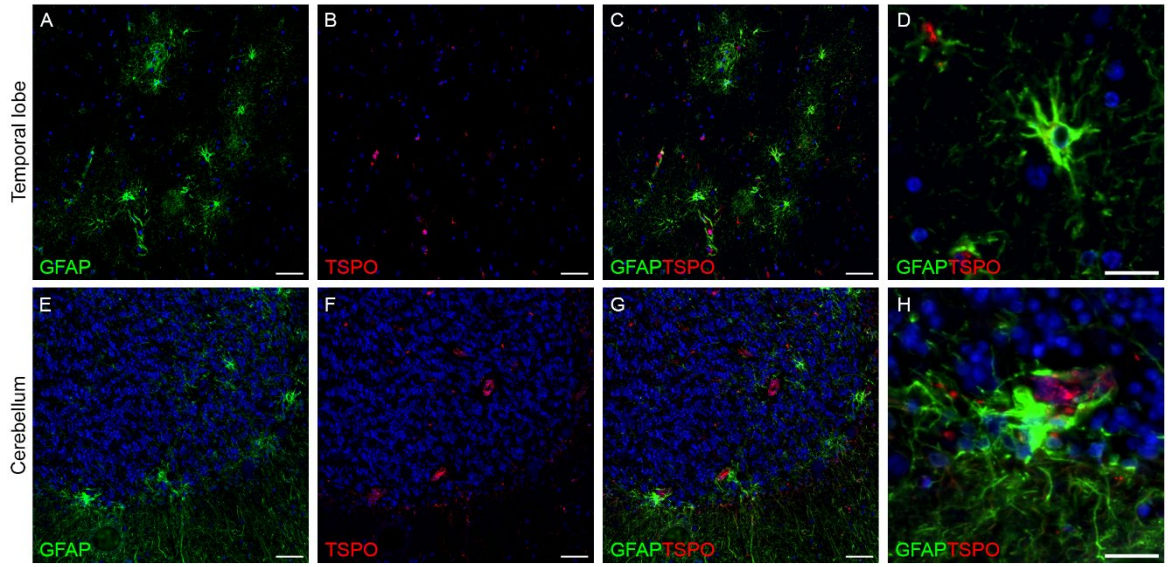

Figure 32 Double immunofluorescent staining of GFAP (green) and TSPO (red) in the temporal lobe (**A-D**) and cerebellum (**E-H**). (**D,H**) are cropped images of (**C,G**). Counterstain: DAPI (blue). Scale bars = 50µm (**A-C**, **E-F**)/20µm (**D,H**).

5.10 Chapter discussion

The results from this chapter demonstrate interesting revelations about microglial cell changes and their relation to TSPO expression also. Cell count analysis was chosen to assess the number of cells which were $TSPO^{+}$ rather than TSPO expression levels due to the nature of several of the microglial markers used. As TSPO is present within the mitochondria, there may not have been exact co-localisation with other markers, which were expressed in different areas of the cell, making double labelling protein load difficult to assess. Cell counts were deemed more appropriate because within one cell it could be established if both TSPO and the corresponding microglial marker were present or absent. Also, TSPO expression load was previously shown in **Chapter 4**. The method of analysis was performed in two ways to create a robust and well-rounded understanding of the changes that occurred in the cohort. One way sought to compare the cell counts (single and double) against total cells counted (DAPI). This gave an overall examination of the microglial environment and provided quantitative description of possible changes in cell number. The other form of analysis allowed for comparisons of the double label cell count against the corresponding microglial marker count, which was more reflective of the association between TSPO and each of the microglial markers. From this analysis it was clear to see the percentage of double labelled cells that related to the microglial marker, indicating a potential functional association for TSPO. It is important to consider the implications of both sets of data, which will be discussed below.

5.10.1 Microglial markers in relation to TSPO

As TSPO is commonly used in AD PET studies of neuroinflammation and it is imperative to understand what this ligand is presenting in terms of microglial phenotype. It has been shown previously, that within the brain, microglia can exhibit many different phenotypes/genotypes and that several subpopulations can co-exist (107, 271, 272). In disease, namely neurodegeneration, some of these subpopulations are DAMs which exhibit specific disease associated traits (107, 272), although this has mostly been shown in animal models. Therefore, recognizing the type of microglia TSPO identifies, whether this is specific or an array of phenotypes, could provide a better understanding of neuroinflammation in human AD.

The data from this thesis examining the co-localisation of TSPO with known microglial markers: Iba1, HLA-DR, CD68, MSR-A and CD64 provides unique information in exploring the microglial TSPO profile in AD. The $TSPO^+$ cell count exhibited no change across the course of the disease for any of the double labelling data in either the temporal lobe or cerebellum. In conjunction with the protein load data from Section **4.2.1**, where TSPO expression increased in the temporal lobe (**Figure 14**), this may indicate that TSPO is not necessarily associated with cell number, but rather each microglial cell may express more TSPO when they become reactive, as some of the literature would suggest (273). One study by Nutma and colleagues found that in the MS brain, the expression of TSPO per cell did not change between chronic lesions and normal appearing white matter, with the authors conclusion indicating that the increased TSPO in the disease is due to increased number of microglial cells (274). This is contradictory to the data found in this thesis, which may indicate that there could be different microglial profiles associated with different diseases based on brain environment as MS is an autoimmune disease. The same group have also examined TSPO in both mouse models and human AD. It was found that $TSPO^+$ cell number did not differ between AD and control hippocampal areas in human AD, as well as TSPO expression per cell not changing either (192). This partly confirmed in this thesis, with no change in $TSPO^+$ cell number across the Braak stages (Sections **5.1-5.5**), however, an increase in TSPO protein load was observed (**Figure 14**), which is a proxy for levels of TSPO expression. An interesting observation Nutma et al made showed that TSPO expression did not change in $Iba1^+$ microglia that were close to amyloid plaques or neurofibrillary tangles (NFTs) (192). The association between TSPO and pTau found in this thesis, presented in Section **4.3**, refutes this, but without more study of the relationship between TSPO and tau, this cannot be confirmed or denied. Nutma et al had a relatively small sample size of five control and five AD cases, which could be a limitation of the study (192). It is also important to note that when examining images in this thesis, clustering of several of the microglial markers (including Iba1, HLA-DR and MSR-A) can be observed, however, this is not seen in the TSPO staining. This may be due to the nature of the TSPO

staining being punctate and therefore it is difficult to see clustering. Furthermore, from qualitative observation of the pathology, TSPO expression was not observed in neurons or dendritic cells.

All double staining (%) was significantly higher in the temporal lobe than the cerebellum, when normalised to total cells (**Figure 27**). This could be due to the temporal lobe having a higher number of microglia in total (275), and with this region being more pathologically affected by the disease and may therefore require, or as a consequence has, more microglial reactivity. Furthermore, it is clear from the data that each marker is not 100% $TSPO^+$ (**Figure 28** and **Figure 29**), meaning that while one marker might be more related than the others, there is no one specific microglial phenotype fully associated with TSPO. This is an interesting revelation as much of the literature suggests that TSPO is highly expressed by microglia. However, an explanation for this could be that the cells that are not $TSPO^+$ are not as reactive as the ones that are $TSPO^+$.

Iba1 and TSPO: For the $Iba1^+TSPO^+$ staining, there was partial overlap of double labelling with these markers in both brain regions (**Figure 17**and **Figure 18**). This is supported by the evidence for an association of TSPO and Iba1 in human *post-mortem* AD tissue (187). It has been found that TSPO substantially overlaps with Iba1, with co-localisation particularly seen in the microglial processes (187). From the staining performed in this thesis, the qualitative images in **Figure 17** showed a similar staining pattern with TSPO present in the processes. Although, there appeared to be some TSPO present in the cell soma as well (**Figure 17**), which is something Gui and colleagues did not observe (187). However, as the $Iba1^+TSPO^+$ cell count didn't reach 100% when normalised to microglial marker (**Figure 17** and **Figure 18**), it can be concluded that not every $Iba1^+$ cell was also $TSPO^+$ in either the temporal lobe or cerebellum. Interestingly, the $Iba1^+TSPO^+$ cell count data shows a significant increase in the cerebellum (**Figure 18**), corroborating with the protein load increase in this region described in Section **4.2.2** (**Figure 15**). It is debated whether the number of cells changes in AD, however, the data here indicates that microglial cell number does not substantially change in AD. One study using Iba1 as a marker of general microglia found that markers of reactivity increased but Iba1 remained consistent over the course of AD (239). In line with data from Section **4.2.2**, which showed an increase in cerebellar Iba1 load, there is significantly more $Iba1^+TSPO^+$ in the cerebellum than the temporal lobe when normalised to $Iba1^+$ (**Figure 27**). This could indicate that while TSPO may not be specifically related to Iba1, there is an association, which appears to be stronger in the cerebellum then in the temporal lobe.

HLA-DR and TSPO: $HLA\text{-}DR^+$ cells have been shown to increase over the course of AD in other literature. A meta-analysis of *post-mortem* AD cases using microglial markers show consistent increases of HLA-DR in AD compared to controls (120). However, this thesis showed no increase in $HLA\text{-}DR^+$ cell number in the temporal lobe, which is in keeping with data from Section **4.2.3**. It has

been seen in previous studies that HLA-DR$^+$ cell number does not change over the course of AD in the temporal lobe (239), but there was an increase in the number of cells positive for this marker compared to controls (239). Another study examining cell number proved that there was no significant difference between HLA-DR$^+$ cell number in the cortex or cerebellum (276), which this thesis confirms (**Figure 27**), with no change in HLA-DR$^+$ cell number (**Figure 20**). Thus, maintaining consistency with data from Section **4.2.3** displaying no difference in protein load of HLA-DR in either brain region. Examining HLA-DR in the cerebellum, one study observed that the number of HLA-DR clusters was significantly lower in the cerebellum than in areas such as the frontal, parietal and occipital lobes in human AD cases (277). From examination of the images in this thesis, HLA-DR did appear to cluster in the later Braak stages of AD in the temporal lobe (**Figure 19**) but this was not seen in the cerebellum (**Figure 20**). This is supported by the presence of reactive microglia in neuritic plaques in the cortex but not the cerebellum (153). Not much substantial research has been conducted into the relationship between HLA-DR and TSPO in AD. However, this has been observed in MS. Using human *post-mortem* MS tissue, a 20-fold increase of co-localised TSPO and HLA-DR antibodies was seen in active MS lesions compared to normal white matter (204). However, as mentioned previously, MS has autoimmune components which could explain the increase in double labelling seen in the study. The data in this thesis showed low numbers of HLA-DR$^+$TSPO$^+$ cells in both brain regions and no change over the course of the disease (**Figure 19** and **Figure 20**), indicating that HLA-DR and TSPO may not be highly associated in AD. More research needs to be conducted in AD and other neurodegenerative diseases to be provide a conclusive result on the association of HLA-DR and TSPO. The number of HLA-DR$^+$TSPO$^+$ cells does not significantly differ between the temporal lobe or cerebellum when normalised to HLA-DR$^+$ cell count (**Figure 27**). This is interesting as HLA-DR is thought of as a reactive marker and to increase in areas affected by AD, however some studies have not seen any change in number of HLA-DR$^+$ microglia between these areas (276), supporting the finding in this thesis.

CD68 and TSPO: The number of CD68$^+$ or CD68$^+$TSPO$^+$ cells did not increase over the course of AD in either the temporal lobe or cerebellum (**Figure 21** and **Figure 22**). This marker has been seen to increase in AD (115) and is associated with cognitive decline and microglial phagocytosis (115, 118). However, most of this research has been done by protein expression rather than using cell counts. One explanation for the result in this thesis could indicate CD68$^+$ cell count may not be altered in disease, but the markers expression per cell could be increased. While CD68$^+$TSPO$^+$ cell count did not change over the course of the disease in this thesis, co-localisation was observed (**Figure 21** and **Figure 22**). Gui et al has qualitatively demonstrated the association of CD68 and TSPO in human AD tissue using similar techniques to this thesis, where it was shown that both of these markers were present within the same microglial cell (187). However, this assessment did not quantify the level of

this association. Further examining the relationship between CD68$^+$ microglia and TSPO in AD one study, using the autoradiography technique, found binding of the TSPO radioligand was more highly expressed in CD68$^+$ microglia compared to GFAP$^+$ astrocytes (278). In a study examining MS, CD68 was highly associated with TSPO in chronic active lesions (274), supporting the association between these two markers in another disease also. As with the other markers, not every CD68$^+$ cell was also TSPO$^+$, which suggests that, while TSPO may not be fully representative of just one microglial type, it still could be related more to one functional subpopulation than others. Notably, there is no difference between CD68$^+$TSPO$^+$ cell number in the temporal lobe and cerebellum, when normalised to CD68$^+$ cells (**Figure 27**). This is interesting due to the temporal lobe consisting of more reactive microglia and higher levels of TSPO seen from data in this thesis (**Chapter 4**). As CD68 is typically a marker for reactive microglial cells, it would be expected that there would be higher numbers here in the temporal lobe. However, this may further corroborate that there is not a change in microglial cell number but instead their expression levels of particular markers depending on functional requirements.

MSR-A and TSPO: There was no change in cell number for MSR-A$^+$, or MSR-A$^+$TSPO$^+$ cells over the course of disease in either the temporal lobe or cerebellum (**Figure 23** and **Figure 24**). MSR-A is linked to scavenging functions in microglia, specifically phagocytosis of Aβ (122, 170), but is not typically expressed by cells at high levels unless a severe immune response occurs. Co-localisation was seen between TSPO and MSR-A (**Figure 23** and **Figure 24**) but as with all the markers tested there was not a complete overlap between these. Little research has been conducted into the relationship between MSR-A and TSPO. However, MSR-A has been seen to be positively associated with presence of dementia (115), indicating this marker could have a role in the onset of AD or participate in late stage disease progression. There was clustering of MSR-A$^+$ microglia, particularly in the temporal lobe, (**Figure 23**) which is consistent with the wider literature (123). This could indicate clearance of, or reaction to, Aβ in this brain region, as is typical of MSR-A$^+$ microglia associated with neuritic plaques in AD (115), but this would need to be confirmed with an amyloid stain. The double labelling of MSR-A and TSPO was observed to be higher in the pathological temporal lobe compared to the cerebellum (**Figure 27**), which could confirm that MSR-A is related to a more reactive microglial phenotype.

CD64 and TSPO: Across the course of the disease, there was no change in number of CD64$^+$ cells or CD64$^+$TSPO$^+$ cells in either the temporal lobe or cerebellum (**Figure 25** and **Figure 26**). CD64 is involved in immune signalling as it is part of the FcγR family (127). As with MSR-A, this marker has been found to associate with impaired cognitive function in AD (115) and its gene expression to be upregulated in both ageing and AD (248). It could be theorised that as CD64 is increased in AD (118), and TSPO is thought to be associated with a reactive microglial phenotype, there could be a

relationship between the two markers. This was not seen across the course of the disease, however, there was a significant increase in $CD64^{+}TSPO^{+}$ cells in the temporal lobe compared to the cerebellum (**Figure 27**), which could indicate the double labelling of these markers were related to the area with higher pathology. Clustering of $CD64^{+}$ microglia can been seen and these clusters appeared to have a higher presence of TSPO (**Figure 25** and **Figure 26**), which is not something particularly observed for the other markers that exhibit clustering behaviour.

Marker comparisons: When normalised to total cells, the temporal lobe exhibited higher levels of double labelling than the cerebellum for all of the markers (**Figure 27** and **Figure 28**) This could be expected as this region is related to higher AD pathology and therefore would exhibit a more reactive microglial phenotype. Including the whole cohort, the highest cell count when comparing each set of double staining was $CD68^{+}TSPO^{+}$, both when normalised to total cells and corresponding microglial marker, in both brain regions (**Figure 28**). As mentioned, CD68 is associated with phagocytosis in microglial cells (118), meaning that TSPO may be more associated with this phenotypic subset than others. There is a plethora of evidence to support TSPO's association with CD68 in the literature using various techniques. One paper found a correlation between TSPO and CD68 expression in human AD hippocampal tissue (192). Using flow cytometry techniques on murine cells, it was found that $A\beta^{+}$ microglia were associated with not just TSPO but CD68 also (161). CD68 immunofluorescence has shown to co-localise with TSPO in both mouse and human brains (279) as well as in autoradiography data showing overlap with TSPO and CD68 in human AD tissue (278). These data add to the implication that TSPO is specifically associated with a phagocytic phenotype (CD68). Considering the data normalised to microglial cells, the second highest cell count was $MSR\text{-}A^{+}TSPO^{+}$ in the temporal lobe and cerebellum (**Figure 28**). MSR-A is primarily associated with scavenging (122), again relating TSPO to a phenotype which is involved in ridding the brain of foreign entities. This finding further validates the association previously found in this thesis between TSPO and MSR-A protein loads (Section **4.3**), providing substantial evidence that TSPO is related to this microglial phenotype. Both MSR-A and CD68 are classified as reactive markers and upregulated in disease (115), lending support for TSPO being associated with reactive cells of the phagocytic/scavenging phenotype.

When separated by Braak stage, in the temporal lobe $CD68^{+}TSPO^{+}$ double labelling was again the highest in every group apart from the Braak group V-VI normalised to total cells, for which $CD64^{+}TSPO^{+}$ cell count was the highest (**Figure 29**). Separating the analysis by Braak stage allows conception of the changes throughout the course of AD, which has shown that $CD68^{+}TSPO^{+}$ is consistently the highest set of double labelling compared to the other markers, regardless of disease stage. No other study, to the knowledge of the author, has conducted quantification of these markers over the course of AD. It is known that TSPO expression levels increase over the course of

the disease (12, 13), meaning that the increase seen in $CD68^{+}TSPO^{+}$cells compared to other markers may not be due to an increase in microglial cell number but an increase in TSPO expression per cell, and in particular cells that are $CD68^{+}$. Research suggests that microglial cell count remains stable during ageing and AD due to synchronised proliferation and apoptosis (94), which was corroborated by no change in the microglial cell number across the Braak stages for any marker in this thesis. In the cerebellum, there is a similar profile when normalised to corresponding microglial marker, with $CD68^{+}TSPO^{+}$ cell count being the most increased in each of the Braak stages (**Figure 29**). This could further confirm that the association of TSPO with a phagocytic phenotype is not related to disease stage in this area, and that this association is not necessarily dependant on brain region either. This is of interest as data from **Chapter 4** shows that the cerebellum exhibits a homeostatic neuroinflammatory nature, whereas CD68 is typically a marker of reactive microglia. However, while $CD68^{+}TSPO^{+}$ cell count was the highest set of double labelling in the cerebellum, the number of $CD68^{+}TSPO^{+}$ cells were lower in this region compared to the temporal lobe (**Figure 27**). This could imply that even with the double labelling of CD68 and TSPO being lower in the cerebellum this marker is still most related to TSPO, hence this association being independent of brain region.

5.10.2 Other CNS cell types in relation to TSPO

CD31 and TSPO: Endothelial cells are highly TSPO positive. This could be due to their shared developmental origin arising from the mesoderm (179). It is well established that endothelial cells express $TSPO^{+}$ mitochondria (187, 267). However, from the images in **Figure 30**, it could be suggested that there is more TSPO than CD31 staining and while there is some overlap in the staining, there is another cell type within the blood vessel walls that is expressing TSPO. It was postulated that this may be SMA cells expressing TSPO, which has been shown in other literature (187). Some data reports endothelial cells contribute to the baseline TSPO signal but not to the increase seen in this receptor during inflammation (280). Fluorescent activated cell sorting (FACS) on radioligand treated tissue demonstrated that injection of LPS in a mouse model increased the levels of TSPO in microglial cells and not astrocytes, endothelial cells or neurons (280). This may suggest that the increased binding signal seen for TSPO PET scans throughout the progression of neurodegenerative disease, in particular AD, is not due to endothelial cell contribution and still provides robust data for microglial reactivity.

CD163 and TSPO: Perivascular macrophages develop from the same lineage as microglia, originating from the yolk sac (281), therefore it would be prudent to assume these cells would also express TSPO. However, this did not seem to be the case from the double staining of CD163 and TSPO, which exhibited very little, if any, co-localisation of these markers (**Figure 31**). Other research has shown presence of $TSPO^{+}$ perivascular macrophages in diseases such as HIV, MS and AD (190); and

monocyte derived macrophages in a rat model of neuroinflammation (282). However, these studies used Iba1 as a marker for macrophages, not the specific macrophage marker CD163.

GFAP and TSPO: The presence of TSPO in $GFAP^+$ astrocytes is highly debated and not consistently observed. In this thesis it appeared that there was very little, if any, TSPO present in $GFAP^+$ astrocytes from observation of the qualitative data (**Figure 32**). Some of the literature has shown TSPO expression in astrocytes (187, 283), which is not something seen in this thesis. One study demonstrated an equal RNA expression level of TSPO in human astrocytes as in endothelial cells (195). However, other studies have performed double immunofluorescence of TSPO and GFAP in both murine models of AD (279) and human AD (190) with very little co-localisation of these markers observed. It may be that there are very low levels of TSPO present in astrocytes, which could be confirmed with a molecular assay such as an ELISA to measure absolute protein levels, and that the TSPO protein expressed in these cells is too low to be picked up by fluorescent microscopy. Another possibility to test the presence of TSPO in astrocytes could have been to use another astrocytic marker, such as ALDH1L1, which is thought to recognise all cells rather than purely reactive astrocytes. However, this qualitative data provides evidence for the TSPO marker remaining more appropriate for microglial cells and confirming TSPO PET scans results are primarily representative of microglia.

5.11 Chapter conclusion

It appears that no microglial marker was 100% positive for TSPO, which is a fascinating and novel finding, contributing to aim iii. The developmental lineage of the cell type may account for the presence of TSPO, as microglia, endothelial cells and smooth muscle cells all derive from the mesoderm, whereas neurons, astrocytes and dendritic cells develop from the neuroectoderm and did not appear to express TSPO (aim iv). TSPO presence is found most highly expressed in phagocytic/scavenging cells ($CD68^+$, $MSR\text{-}A^+$), which could be related to a reactive/disease associated phenotype, further supporting the results from **Chapter 4**, however this characteristic does not appear to be affected by brain region or disease stage (aim iii).

Chapter 6 Can a Fluorescently Labelled TSPO PET Ligand be used on *post-mortem* Tissue?

The rational for this chapter stands to compare the immunolabelling of the TSPO antibody with a fluorescently conjugated TSPO PET ligand. Using the ligand in *post-mortem* tissue could give a better understanding of the radiotracers use in PET scans *in vivo*, to provide information on which type of cells the ligand binds to and the localisation of this binding. Currently, TSPO PET radiotracers are used to classify general 'neuroinflammation' without detailed knowledge of which function/phenotype of microglial cells express this (12, 13, 267). The work done in **Chapter 5** aims to elucidate which microglial phenotype is associated with increased TSPO expression in AD, but the direct use of a TSPO ligand would give clinical relevancy to this study. For that reason, a fluorescently conjugated DPA-714 ligand was tested in human *post-mortem* tissue (aim v).

6.1 Optimisation

6.1.1 FFPE tissue

The DPA-714 ligand, supplied by Ambinter®, used in this project had a conjugated fluorescein isothiocyanate (FITC) fluorophore attached (Amb37787199). This was suggested by Ambinter® to be soluble up to 20µM in 25mM PBS buffer. The ligand solution was tested on human *post-mortem* FFPE tissue at a 20µM concentration and also at a diluted 1µM, 2nM, 1nM, 0.5nM and 0.1nM concentrations (**Figure 33**). Previous literature used a 0.1nM concentration on rat tissue (284). All images were taken on the Leica TCS-SP8/SP5 laser scanning confocal microscope at X40 magnification. The 20µM and 1µM test appeared to be too high a concentration (**Figure 33A, B**) and the 0.1nM test exhibited no staining, so was thought to be too low (**Figure 33D, E, F**). Initially, no pre-treatment was used to retrieve antigens or blocking step to prevent endogenous protein binding, but the tissue was still dewaxed prior to incubation in the ligand solution. Then different antigen retrieval methods were tested using citrate (pH6) or EDTA (pH8) buffer both with and without BSA. The use of EDTA and BSA appeared to decrease the background and thus were used subsequently (**Figure 33I**). Also, 1% Sudan black was applied to suppress autofluorescence in the tissue. It has been postulated

that Sudan black can supress staining signal, therefore a test was performed with a lower concentration of 0.3% Sudan black and also without any autofluorescence quencher (**Figure 33** and **Figure 34**). Comparing the staining of 1nM DPA-714 to a negative control, both in the absence of Sudan black, displayed the presence of lipofuscins and no apparent staining (**Figure 34A, C**), making it clear that Sudan black was necessary. The ligand was also tested on a positive control tonsil tissue that contained macrophages. This was applied at 0.5nM, 1nM and 2nM which yielded potential staining in the 0.5nM and 2nM concentrations(**Figure 33J, K, L**). The same conditions were also validated in AD brain tissue, and it could be said possible staining was seen in the 2nM concentration, primarily in the blood vessels, which may be perivascular macrophages or endothelial cells (**Figure 33O**). However, the appearance of signal did not exhibit the same extensive parenchymal staining as the TSPO antibody (ab109497) (Section **4.2.1** and **Chapter 5**), and it is therefore uncertain whether the fluorescent signal observed with the TSPO PET ligand is reliable and/or specific.

A protocol that effectively produced a reliable and specific fluorescent signal by the fluorescent DPA-714 ligand could not be established in the FFPE tissue, with many parameters tested (**Figure 33** and **Figure 34**). This could be due to several reasons discussed further in Section **6.2**, including the formalin fixation process interfering with ligand binding.

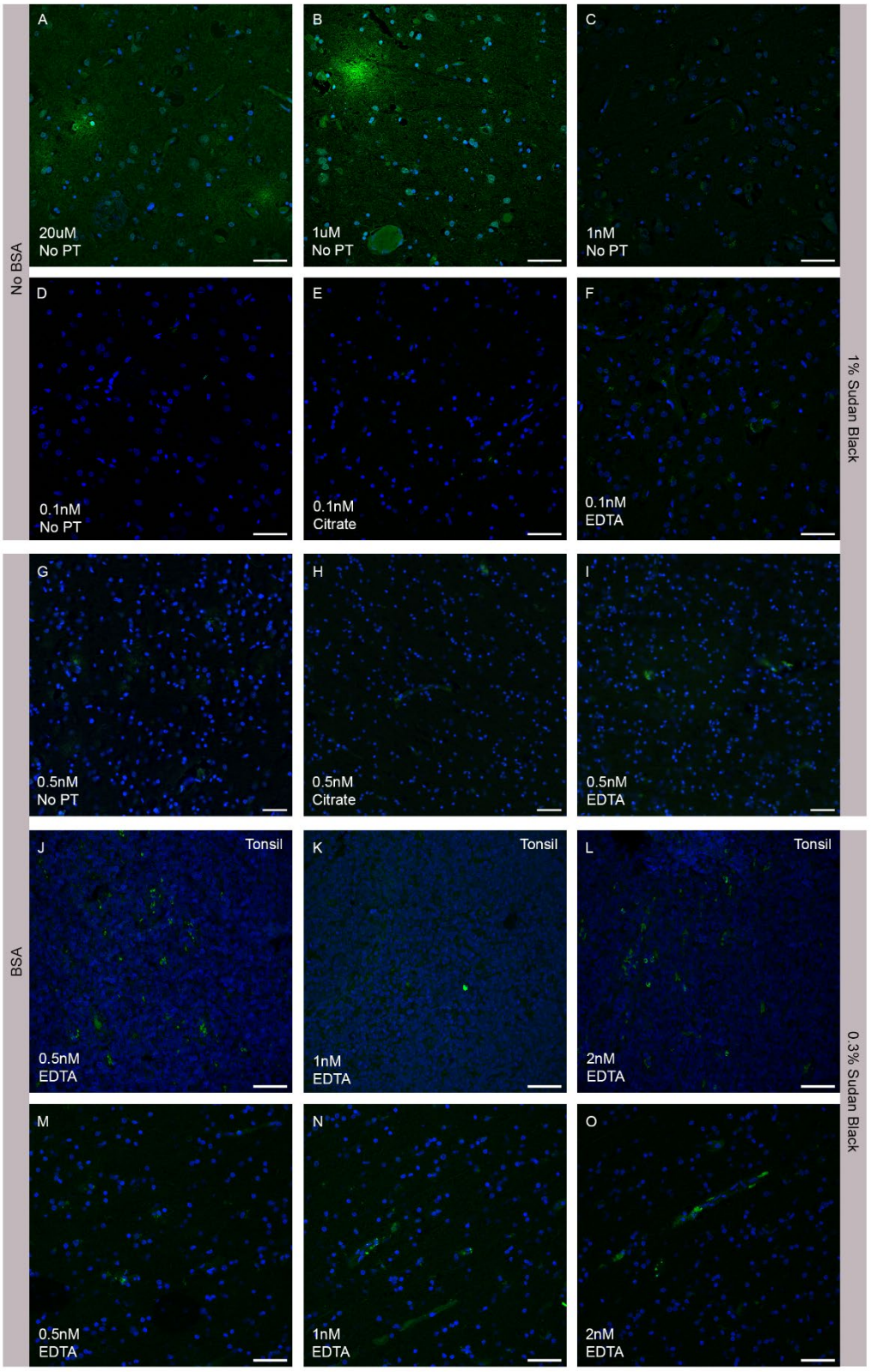

Figure 33 Parameters tested for fluorescently conjugated DPA-714 ligand on FFPE *post-mortem* tissue. (**A-D**) no BSA blocking medium step. (**G-O**) BSA blocking medium step. (**A-I**) 1% Sudan black applied. (**J-O**) 0.3% Sudan black applied as an autofluorescence quencher. Other parameters, such as antigen retrieval buffer (no PT = no pre-treatment, Citrate or EDTA) and ligand concentration

(0.1nM-20µM), are indicated on the image. Images taken at 40X magnification. Counterstain: DAPI (blue). Scale bar = 50µm.

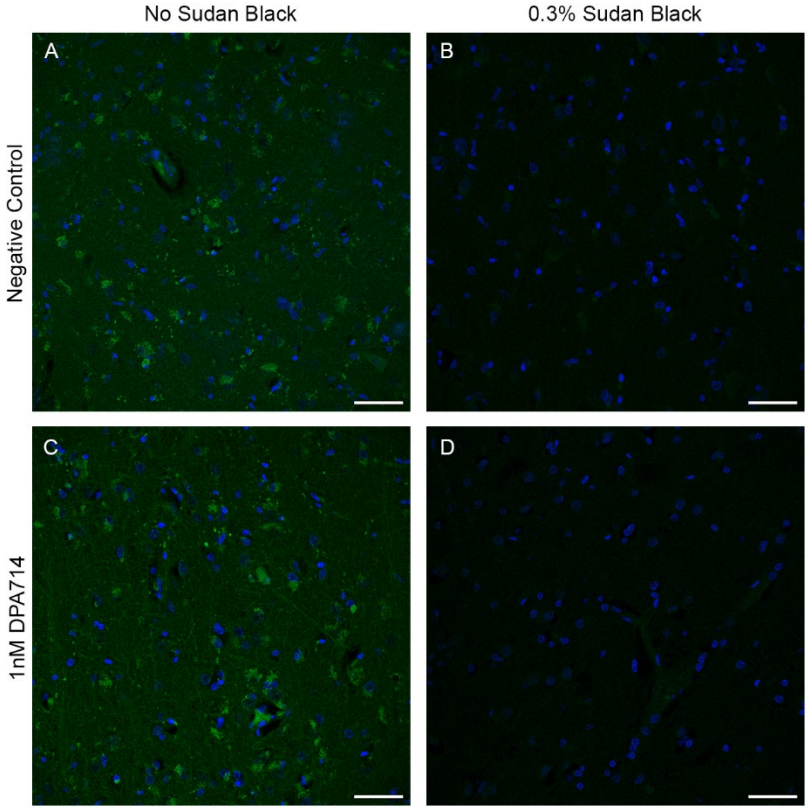

Figure 34 Negative control with (**B**) and without (**A**) 0.3% Sudan black compared to 1nM DPA-714 concentration with (**D**) and without (**C**) 0.3% Sudan black on FFPE *post-mortem* tissue. Images taken at 40X magnification. Counterstain: DAPI (blue). Scale bar = 50µm.

6.1.2 Frozen tissue

As the FFPE tissue did not appear to produce consistent staining, it was thought that frozen human *post-mortem* tissue could negate the possible formalin fixation problem, so this tissue was tested with the fluorescently conjugated DPA-714 ligand. As with the FFPE tissue, images were taken on the Leica TCS-SP8/SP5 laser scanning confocal microscope at X40 magnification. Assessments were conducted on cerebellum tissue initially, using 1nM concentration of the ligand (**Figure 35A-D**). Fixation was performed with acetone instead of formalin and therefore no cross-linking bonds were formed, potentially blocking the binding of the ligand. Testing was first conducted without Sudan black, and it was found that background autofluorescence and lipofuscins were present in both the negative control and stained tissue, making it impossible to identify specific staining (**Figure 35A, B**).

With 0.3% Sudan black, staining did appear in the cerebellum cases tested, at Braak stage 0 and Braak stage VI (**Figure 35C, D**). The same experiment was repeated in the temporal lobe, using same parameters, and possible staining was detected (**Figure 35E, F**). However, it was scarce, compared to the staining by the antibody (**Figure 35G, H**). Also, the quality of the tissue was poor as it was cut from a small cylindrical section of tissue which was primarily obtained for molecular assays. To ensure there was TSPO present in the samples and that frozen tissue was appropriate for this use, immunofluorescent staining with the already optimised TSPO antibody (ab109497) was performed. From the images in **Figure 35G, H**, TSPO staining with the antibody showed higher expression than the possible staining of the ligand, indicating again that the ligand staining might not have been optimal.

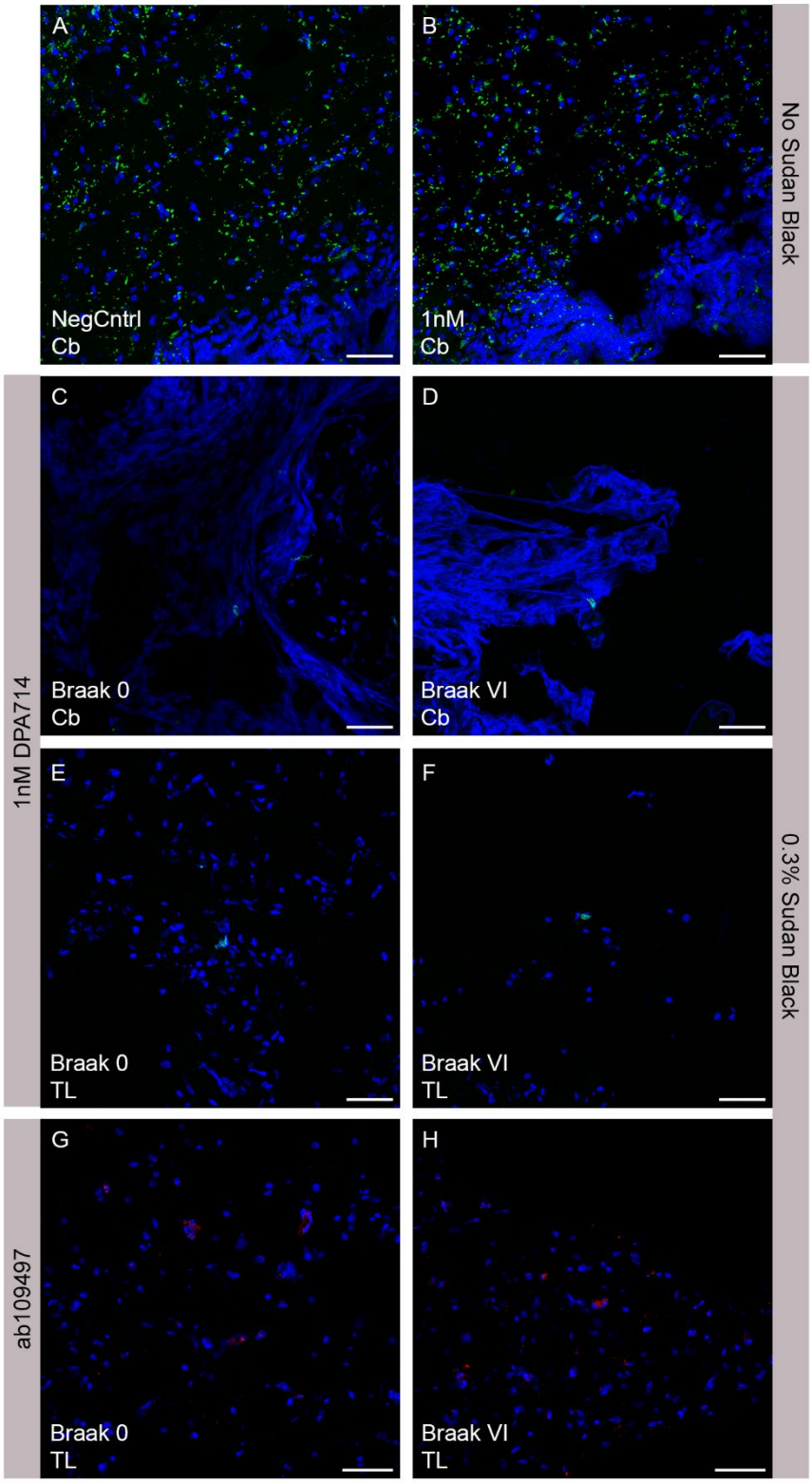

Figure 35 Parameters tested for fluorescently conjugated DPA-714 ligand (green) and TSPO antibody (ab109497) (red) on frozen *post-mortem* tissue. (**A,B**) no Sudan black. (**C-H**) 0.3% Sudan black applied and 1nM concentration of DPA-714 (**C-F**) or the TSPO antibody (**G,H**). Other parameters

indicated on image (Braak stage and brain region: TL = temporal lobe, Cb = cerebellum). Images taken at 40X magnification. Counterstain: DAPI (blue). Scale bar = 50μm.

6.2 Chapter discussion

The development of this novel methodology would have given clinical relevance to the project and allowed for direct comparison of the TSPO antibody with the fluorescent ligand. This would have ensured the cellular localisation of the antibody was the same as the ligand and provided confirmation of the immunofluorescent staining results. There have been fluorescent TSPO probes developed (285), however, as mentioned, this application of these to human *post-mortem* tissue had not been conducted as of the writing of this thesis. One study applied three different synthesized TSPO ligands, conjugated with fluorescent probes (including FITC), to brain tissue from Wistar rats (284). The brains had either been injected with LPS to chemically injure the tissue and create an immune response or were control brains. It was found that in the injured brains, but not the control brains, $TSPO^{+}$ staining was present in activated microglia, which were identified with isolectin B4 (284). Based on the type of injury, this suggests that a high microglial response might be needed to upregulate TSPO at a level for the fluorescently conjugated ligand to bind and produce a signal. Microglial response is a key hallmark of AD; therefore, it would be expected that the ligand would produce staining in the AD cohort used in this thesis, which was not the case. Fluorescent TSPO probes have been applied to cell culture (immunocytochemistry) with success (284, 286), indicating that this may be a better way to visualise TSPO than in FFPE tissue. There are possibilities as to why the ligand did not work in the human *post-mortem* tissue which will be discussed here.

The fluorescently conjugated DPA-714 ligand may not be appropriate for use on human FFPE *post-mortem* tissue due to a myriad of reasons, one being that the formalin fixation may impact the binding ability of the ligand as this alters the tissue state. The cross linking bonds created by formalin fixation (287) may have hindered the ligand from binding, potentially blocking binding sites. It could also be that the ligand does not bind in the same way as the antibody and therefore cannot bind effectively to this type of tissue. In the literature, the TSPO radioligands bind amino acid residues across all five α-helices of the protein, including lysine and arginine residues (184), which are affected by formaldehyde fixation (287). Whereas the TSPO antibody binds within residues 76-169 (supplied from Abcam). The potential difference between binding of these entities, and the effect of formaldehyde fixation, could give rise to complications when applying the ligand to the tissue.

When TSPO ligands have been applied to *post-mortem* tissue, it has often been in radioactive form and required the use of autoradiography to visualise the presence of the protein in the tissue (206).

This is a well-established protocol; however, it utilises radioactive components which are difficult to use and necessitates specific safety procedures in place. Consequently, using a fluorescently tagged ligand would be beneficial as these safety procedures would not be needed.

Lastly, the addition of the FITC fluorophore could have impacted the binding ability of the ligand to the tissue. FITC has a molecular weight of ~400 g/mol, making it a fairly small fluorophore when compared to another commonly used fluorophore, GFP which has a molecular weight of ~27,000 g/mol (288). Being a small molecule, it would be unlikely that FITC would interfere with binding of the ligand however, it is not out of the question. FITC is also sensitive to pH with a pH8 being optimal for this fluorophore (289). Citrate (pH6) and EDTA (pH8) were tested (**Figure 33**) and neither produced substantial staining on with the ligand.

There may be a possibility that the compound was not manufactured correctly and therefore would not be applicable/bind to the correct protein in the tissue. Unfortunately, there was no time to test the compound using facilities at the disposal of the author of this thesis. Therefore, the compound was sent to a collaborator (Michel Bottlaender) to assess the molecular composition of the ligand using mass spectroscopy, nuclear magnetic resonance (NMR) spectroscopy and further immunostaining techniques. The mass spectroscopy demonstrated the molecular weight is 869,04 g/mol, as expected.

6.3 Chapter conclusion

In this chapter, the fluorescently conjugated DPA-714 ligand was tested on human *post-mortem* tissue. Unfortunately, this method proved unsuccessful, and no adequate or reliable staining was produced. This may be due to a variety of reasons including inability to bind to this tissue type, fluorophore binding interference and variances in TSPO binding sites. Therefore, aim v cannot be confirmed. With more time, reliable staining might have been established.

Chapter 7 General Discussion and Conclusions

Microglia are a fairly well characterised immune cell of the brain, however there are still gaps in our knowledge about their function and phenotype, particularly in neurodegenerative disease. There is much evidence to support their role in diseases such as AD, therefore it is vital to understand more about the pathophysiological mechanisms they contribute to, which may lead to improved diagnosis and potential therapeutic targets.

Using PET scans to observe neuroinflammation are a promising way of examining the microglial contribution in AD, however, many of the radioligands used are not fully understood. For example, TSPO is the most commonly used tracer for neuroinflammation as it highlights 'activated microglia' and is seen to be increased in AD (13). Microglia are highly dynamic and perform many functions, so the statement 'activated' is not specific and can lead to an inaccurate interpretation of scan results. Therefore, understanding the exact microglial phenotype associated with TSPO can aid clinicians' interpretation of diagnostic results. This thesis has contributed to elucidating this question, by characterising which functional marker TSPO is most related to (one or multiple), over the course of AD using Braak staging as a marker of disease progression in two brains regions. The neuroinflammatory environments of these brain regions were also assessed to gain insight into the neuroimmune environment and how microglia respond at different stages of AD.

The way the study was conducted used established methods of immunostaining and subsequent analysis which provided good evidence for protein expression changes in the tissue. The detailed assessment of cell quantification proved an accurate and unbiased way of determining the relationship between TSPO and other markers. A strength of the study was the large sample size of good quality human *post-mortem* cases with a plethora of histological, pathological and genetic information provided by the SWDBB. A limitation of using *post-mortem* tissue is it provides information from one time point and could be considered undynamic. There also had to be care when selecting cases to ensure sex, age, co-morbidities, *post-mortem* delay and time in fixative is controlled for (290), which was done in the cohort used in this thesis. Another potential pitfall in the methodology of this thesis was the assumption that Braak staging gave an absolute measure of disease progression. While Braak staging is a well characterised and widely used method of characterising AD development, a small proportion of the cases used in this project had confounding Braak stages compared to their clinical diagnosis. For example, a Braak stage III case could either be classed as AD or control. However, for that reason, separating the cases by Braak staging, rather than clinical diagnosis, was chosen as it was a more quantifiable and robust approach to measuring AD

stage via tau tangles throughout the brain (10). Regarding the data analysis methods, both the protein load and fluorescent cell count analysis were reproducible and gave accurate results. A constraint of these analyses could lie in the thresholding of images. To keep the data comparable, the same threshold was used for all cases in each set of staining. However, this meant that some cases would not have the optimal threshold. To overcome this with the best accuracy possible, an average threshold was identified using several cases with high and low staining levels. Furthermore, it was noted that the TSPO protein load increase seen in the temporal lobe may have had contribution from endothelial cells. However, when observing the images, TSPO present in the blood vessels did not appear to change in intensity or number (although these were not directly analysed), whereas TSPO in the parenchyma increased. Allowing for the assumption that the increase seen in TSPO protein load comes primarily from microglia. Despite the possible limitations of this study, the immunohistochemistry techniques used provided reliable evidence about the neuroinflammatory changes seen in the brain during disease.

In quantifying the TSPO antibody, via protein load and cell counts, this study gains novelty as this type of quantitative analysis has not been done before. If the TSPO ligand had worked on *post-mortem* tissue this would have also provided insightful knowledge due to its clinical relevance. Furthermore, while the microglial markers used are all well established and have associated functions when these are upregulated in cells, it cannot be stated that each of these markers 100% recapitulates each function. For example, while CD68 expression is increased on phagocytic cells (115), there will also be other markers expressed by the microglia. This is why it was ensured that suggestions were made rather than absolute conclusions when regarding TSPO's association with each of the markers. Morphology can also be a proxy for functionality in microglia, with ramified cells conducive to motility and homeostasis, and amoeboid cells recapitulating reactivity (240). However, this is also not an exact measure for function and was only qualitatively assessed, not examined in detail in this thesis.

While the aims of this project have been addressed, more questions could be raised from the results found, as is the way with research. The use of autoradiography to examine the presence of TSPO in the cohort via radiotracers may have given a clinical insight, in light of the unsuccessful use of the conjugated TSPO ligand. Autoradiography is an *in vitro* x-ray imaging technique which can be quantified showing the density of binding sites, which would show the amount of TSPO expression in the tissue (291). However, the equipment needed for this technique was not available and it may not have been achievable to learn, optimise and perform in the timeframe of the project. Another question raised was how TSPO interacts with Aβ and pTau. The association found between pTau and TSPO in the temporal lobe provided evidence for this pathological protein to be a possible driver of increased microglial TSPO expression in AD. However, without quantitative staining this could not be

confirmed. Therefore, future work to examine the double labelling of TSPO with Aβ and pTau would provide comprehension of this. There is other evidence in the literature for an association between TSPO and tau progression in AD (147, 245), and there is also evidence for the association of certain microglial markers (MSR-A) and Aβ (115, 209), therefore further experimentation could clarify the association of TSPO with these pathological proteins.

Overall, the aims of the project have been addressed by showing increased TSPO over the course of AD in the temporal lobe, and this protein could be associated with a phagocytic microglial function in both the temporal lobe and cerebellum (**Figure 36**). This partially confirmed the hypothesis of this thesis by indicating TSPO is related to a specific microglial phenotype, however, rejects the second part of the hypothesis by finding this characteristic was not affected by brain region or disease stage, regardless of the overall increase in TSPO load in the pathologically affected temporal lobe. Furthermore, the cerebellum presented a more homeostatic neuroinflammatory profile, similar to that of early AD in other cortical areas, with lower and stable TSPO levels (**Figure 36**), confirming this area's use as a pseudo-reference region for TSPO PET scans. The findings from this project can help clarify the microglial profile present over the course of human Alzheimer's disease and give rise to a better understanding of microglia's neuroinflammatory role in the disease, with particular attention in regard to TSPO and the clinical implications this has.

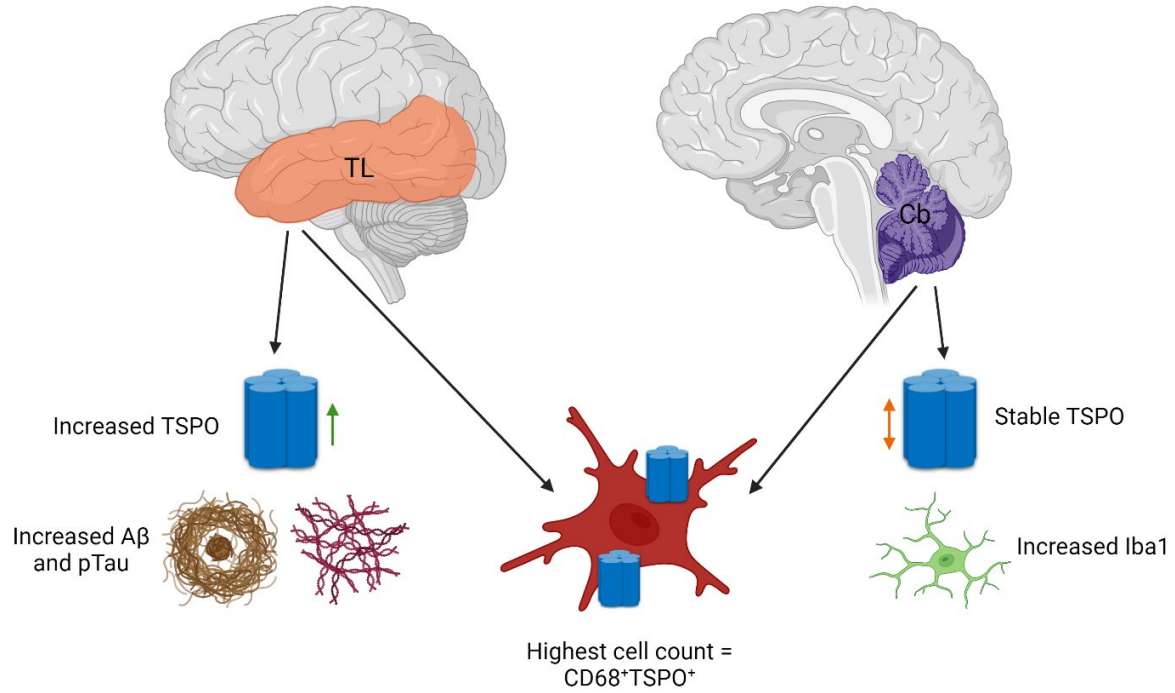

Figure 36 Thesis summary figure depicting increased protein load for TSPO, Aβ and pTau in the temporal lobe (TL), stable TSPO protein load and increased Iba1 load in the cerebellum (Cb) across the course of the disease (Braak stages). Also, the highest number of $TSPO^+$ double labelled cells was with $CD68^+$ cells in both brain regions and in all Braak stages. Created with BioRender.com.

Appendix A Supplementary Data

Table A1 Correlations between *post-mortem* delay and microglial markers (DAB data) in temporal lobe and cerebellum

	Marker	*r_s value*	*P value*
Temporal lobe	Aβ	-0.165	0.215
	pTau	-0.223	0.098
	TSPO	-0.093	0.485
	Iba1	-0.076	0.570
	HLA-DR	0.155	0.267
	MSR-A	0.060	0.649
Cerebellum	Aβ	-0.063	0.643
	pTau	-0.250	0.063
	TSPO	-0.085	0.533
	Iba1	-0.119	0.383
	HLA-DR	0.123	0.372
	MSR-A	0.009	0.946

r_s Spearman's rank correlation, significant P values are in bold (**<0.01)

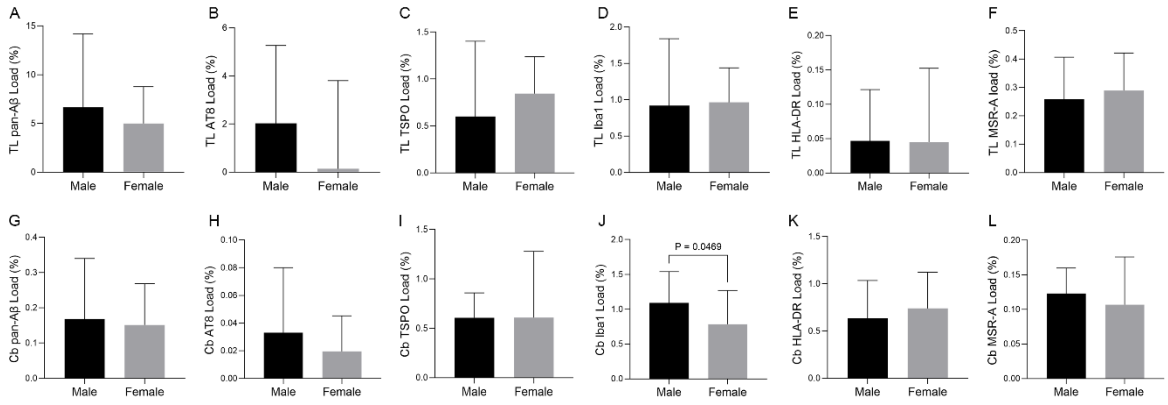

Figure A1 Sex differences for pan-Aβ (**A, G**), pTau (**B, H**), Iba1 (**C, I**), TSPO (**D, J**), HLA-DR (**E, K**) and MSR-A (**F, L**) in the temporal lobe (**A-F**) and in the cerebellum (**G-L**) (DAB data). Graphs presented as median with range.

Table A2 QuPath threshold information for positive cell counts of Iba1 (FITC) and TSPO (CY3)

Temporal	DAPI+FITC	DAPI+CY3	FITC+CY3	**Cerebellum**	DAPI+FITC	DAPI+CY3	FITC+CY3
Background radius	3µm	3µm	3µm	Background radius	3µm	3µm	3µm
Min area	10µm²	10µm²	10µm²	Min area	10µm²	10µm²	10µm²
Max area	100µm²	100µm²	100µm²	Max area	100µm²	100µm²	32µm²
DAPI threshold	80	80	250	DAPI threshold	80	80	200
Cell expansion	1µm	2µm	3µm	Cell expansion	1µm	2µm	3µm
Threshold +1	250	300	300	Threshold +1	200	1000	1000

Table A3 QuPath threshold information for positive cell counts of HLA-DR (FITC) and TSPO (CY3)

Temporal	DAPI+FITC	DAPI+CY3	FITC+CY3	**Cerebellum**	DAPI+FITC	DAPI+CY3	FITC+CY3
Background radius	3µm	3µm	5µm	Background radius	3µm	3µm	5µm?
Min area	10µm²	10µm²	10µm²	Min area	10µm²	10µm²	10µm²
Max area	100µm²	100µm²	100µm²	Max area	100µm²	100µm²	100µm²
DAPI threshold	120	120	250/400	DAPI threshold	100	100	400/300
Cell expansion	1µm	2µm	3µm	Cell expansion	1µm	2µm	3µm
Threshold +1	500/400	550/350	480/350	Threshold +1	600/400	550/350	480/350

Table A4 QuPath threshold information for positive cell counts of CD68 (FITC) and TSPO (CY3)

Temporal	DAPI+FITC	DAPI+CY3	FITC+CY3	**Cerebellum**	DAPI+FITC	DAPI+CY3	FITC+CY3
Background radius	3µm	3µm	3µm	Background radius	3µm	3µm	3µm
Min area	10µm²	10µm²	10µm²	Min area	10µm²	10µm²	10µm²
Max area	100µm²	100µm²	100µm²	Max area	100µm²	100µm²	100µm²
DAPI threshold	120	120	400	DAPI threshold	120	120	400
Cell expansion	2µm	2µm	3µm	Cell expansion	2µm	2µm	3µm
Threshold +1	400	650	650	Threshold +1	400	650	650

Table A5 QuPath threshold information for positive cell counts of MSR-A (FITC) and TSPO (CY3)

Temporal	DAPI+FITC	DAPI+CY3	FITC+CY3	**Cerebellum**	DAPI+FITC	DAPI+CY3	FITC+CY3
Background radius	3µm	3µm	3µm	Background radius	3µm	3µm	3µm
Min area	10µm²	10µm²	10µm²	Min area	10µm²	10µm²	10µm²
Max area	100µm²	100µm²	100µm²	Max area	100µm²	100µm²	100µm²
DAPI threshold	80	80	600	DAPI threshold	80	80	600
Cell expansion	1µm	2µm	3µm	Cell expansion	1µm	2µm	3µm
Threshold +1	600	450	450	Threshold +1	600	900	900

Table A6 QuPath threshold information for positive cell counts of CD64 (FITC) and TSPO (CY3)

Temporal	DAPI+FITC	DAPI+CY3	FITC+CY3	**Cerebellum**	DAPI+FITC	DAPI+CY3	FITC+CY3
Background radius	3µm	3µm	3µm	Background radius	3µm	3µm	3µm
Min area	10µm²	10µm²	10µm²	Min area	10µm²	10µm²	10µm²
Max area	100µm²	100µm²	100µm²	Max area	100µm²	100µm²	100µm²
DAPI threshold	80	80	450	DAPI threshold	80	80	450
Cell expansion	1µm	2µm	3µm	Cell expansion	1µm	2µm	3µm
Threshold +1	450	500	500	Threshold +1	450	550	550

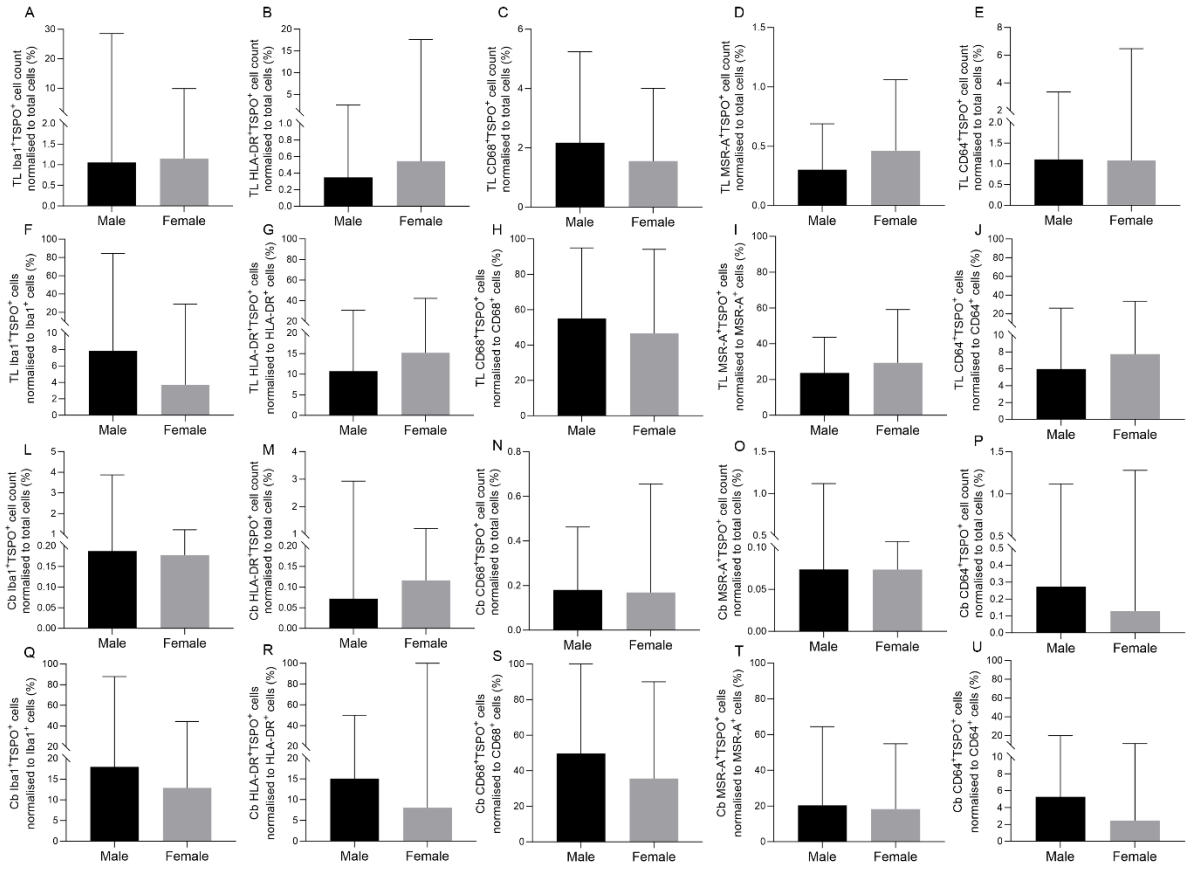

Figure A2 Sex differences for double labelling of TSPO with Iba1, HLA-DR, CD68, MSR-A and CD64, normalised to total cell count (%) (**TL: A-E, Cb: L-P**) or corresponding microglial marker cell count (%) (**TL: F-J, Cb: Q-U**), including all cases. Graphs presented as mean (**C, D, H, I, S**) or median (**A, B, E, F, G, J, K, L, M, N, O, P, Q, R, T, U**) with range.

Appendix B Optimisation

B.1 TSPO (DAB and Fluorescent)

Initial TSPO staining was performed using DAB as a chromogen on tonsil tissue (positive control), showing macrophages. Two Abcam antibodies (ab104546 and ab109497) were used at a 1:5000 dilution with citrate (pH6) as the antigen retrieval buffer, as per manufacturer guidelines. There did appear to be staining but also a lot of background so a higher dilution of 1:10,000 was used next. The ab109497 stained the tissue with better results than ab104546, using the 1:5000 dilution. Also, EDTA was tested alongside citrate to test if this affected the staining. The staining appeared to have more background with EDTA, therefore, it was confirmed that ab109497 works most effectively at a primary dilution of 1:5000 with a citrate (pH6) antigen retrieval buffer.

For fluorescent staining, the TSPO antibody (ab109497) was tested on human tissue at a 1:1000 primary dilution with the citrate antigen retrieval buffer as established previously. Three fluorescent secondaries from ThermoFisher, Donkey anti-rabbit (DAR) Alexa Fluor™ (AF) 488, 594 and 635, were tested at a secondary dilution of 1:200 (AF635 not pictured in **Figure B1**). As human brain tissue produces background autofluorescence, 1% Sudan Black was used to counteract this. The primary antibody dilution was possibly too low at 1:1000, this was adjusted to a 1:2500 dilution, which produced good staining (**Figure B1**).

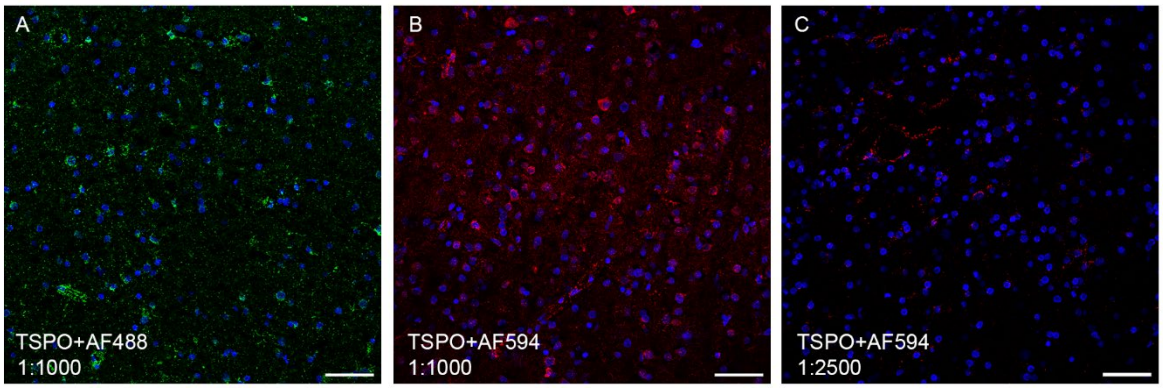

Figure B1 Testing fluorescent secondary antibodies with TSPO. Primary antibody dilution was tried at 1:1000 (**A, B**) and 1:2500 (**C**). Secondary antibody Alexa Fluor™ (AF) 488 (**A**) and 594 (**B, C**) were used at a dilution of 1:200. Counterstain: DAPI (blue) Scale bars = 50μm.

To negate the need for secondary antibodies, two conjugated Abcam antibodies (ab199779 and ab199836) for TSPO were tested at a primary dilution of 1:500. This produced a very week staining signal from both antibodies. Therefore, several different dilutions were tested (1:100, 1:500 and 1:2000) (**Figure B2**). None of these gave any substantial staining and was determined to be down to faulty antibodies or not appropriate for this kind of tissue. Another conjugated TSPO antibody from SAB Biotech (C48605) was tried with both citrate and EDTA as the antigen retrieval buffers but did not yield any promising results at either a 1:100 or 1:250 dilutions (**Figure B2**). Several autofluorescence quenchers were tested to eliminate background fluorescence, this is further discussed in Section **B.4.**

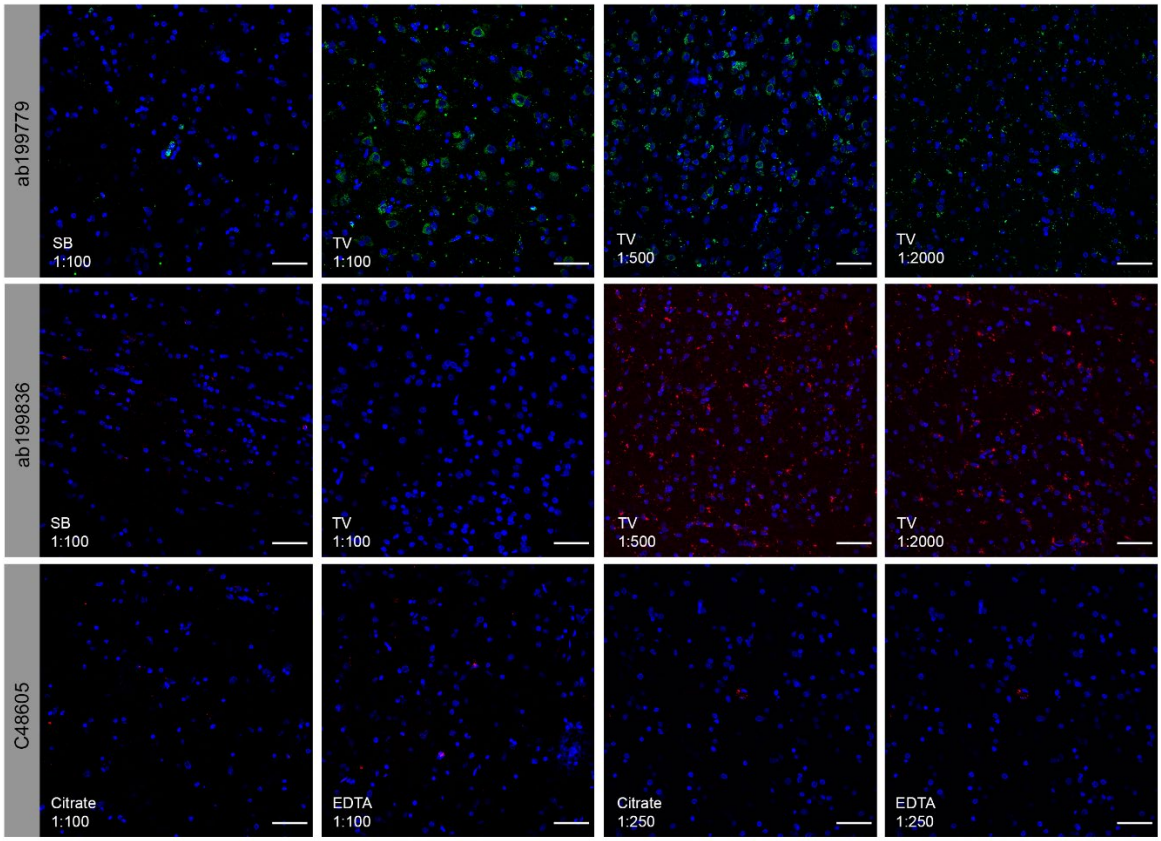

Figure B2 Testing conjugated TSPO antibodies. Three different antibodies were tested (ab199779, ab199836 and C48605) with varying antibody dilutions (1:100-1:2000) and different antigen retrieval buffers or autofluorescence quenching methods. Ab199799 was conjugated to Alexa Fluor™ (AF) 488 (green), ab199838 was conjugated to AF647 (red) and C48605 was conjugated to AF594 (red). SB = Sudan black, TV = Vector® TrueVIEW®. Counterstain: DAPI (blue). Scale bars = 50µm.

B.2 Iba1 (DAB and Fluorescent)

Iba1 (019-19741) has been used previously in the lab for DAB staining and was established to work at a 1:750 dilution with citrate (pH6) as the antigen retrieval method (**Table 3**). The same Iba1 antibody was tested for immunofluorescence at a 1:750 dilution for the primary antibody and a 1:200 dilution for the DAR AF488 secondary antibody. This produced adequate staining, with the signal possibly being too high. Therefore, the primary antibody dilution was increased to 1:1000 and the secondary antibody dilution was changed to 1:400. This produced good staining with minimal background.

When performing double staining, the anti-rabbit Iba1 (019-19741) could not be used in conjunction with the anti-rabbit TSPO (ab109497) as these were both raised in the same species and therefore, their secondaries would cross react (discussed further in Section **B.5.1**). In order to overcome this, an anti-mouse Iba1 antibody from Wako (013-272593) was tested using DAB staining. Several different dilutions, antigen retrieval methods and other parameters were used without successful staining (**Figure B3**). Therefore, another Iba1 was purchased, raised in goat from Abcam (ab5076). This antibody produced adequate staining using the DAB method but also produced a lot of background staining at a higher dilution. Therefore, the dilution was changed to 1:1000, which appeared to be optimal (**Figure B3**). However, different tests were conducted in order to eliminate more of the background staining, including using the antibody with and without Dako diluent. It was decided that using TBS was better than the Dako diluent. Furthermore, different incubation times were tested with 90minute room temperature giving the best results, although overnight room temperature also gave good staining results (**Figure B3**). Then the anti-goat Iba1 (ab5076) was tested in fluorescent staining, initially as a single marker and then for double staining (discussed further in **Section B.5.1**). It was tested at 1:250 and 1:500 dilutions, where it was established that the best results were using a 1:500 dilution, incubated overnight at room temperature (**Figure B3**).

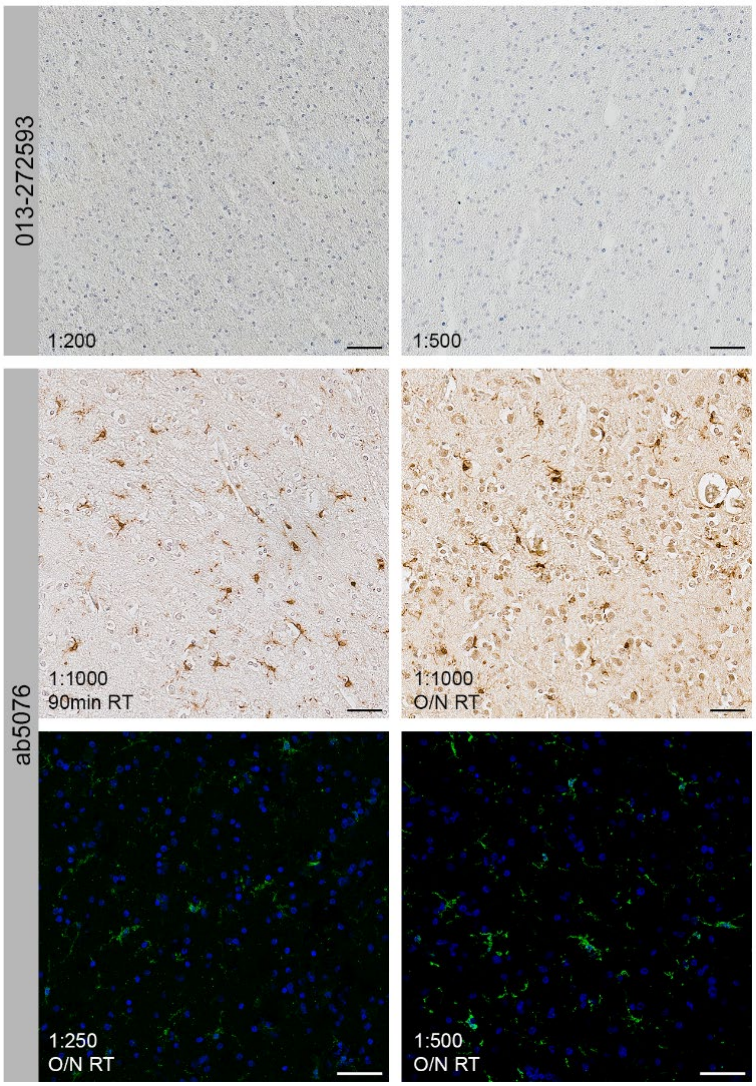

Figure B3 Testing new Iba1 antibodies. Two different antibodies were tested (Wako anti-mouse 013-272593 and Abcam anti-goat ab5076) and varying dilutions (1:100-1:1000) and incubation times (90min RT or O/N RT). Fluorescent secondary was DAG AF488 (1:100). Counterstain for DAB: Haematoxylin, counterstain for Fluorescent: DAPI (blue). Scale bars = 50μm.

B.3 TMEM119 and P2Y12

In order to have a well-rounded microglial marker panel, anti-mouse TMEM119 (Sigma-Aldrich, AMAB91528) and anti-mouse P2Y12 (Sigma-Aldrich, MABN2593) antibodies were tested. TMEM119 is thought to mark all subsets of microglia and does not change in expression when exposed to inflammatory stimuli (109). Manufacturer recommendations suggested the TMEM119 antibody be used at a 1:5000 dilution for standard immunohistochemistry but didn't recommend an antigen retrieval buffer, therefore both EDTA and citrate were tested. The staining produced was weak but there did appear to be some TMEM119^{+} cells present using the EDTA buffer. The dilution was lowered to 1:2500 and tested again with EDTA, however this test produced no staining at all on the

same tissue as before. It was decided to try this marker in fluorescent staining, so the dilution was lowered further to 1:500 and trialled with a corresponding secondary antibody conjugated to AF488. There was minimal staining present, and it was decided to stop the optimisation as this point.

P2Y12 is a marker present on the homeostatic subset of microglial cells and is thought to be microglia specific (no macrophage expression) (124), but there is controversy to this with conflicting evidence presented. Optimisation was carried out using a 1:250 dilution and citrate as the antigen retrieval buffer. This test did not produce any staining but there were high levels of background staining. In order to overcome this, the next test was performed using Dako diluent instead of TBS as a mixing constituent, due to its background reducing properties. This produced less background but still did not yield and substantial staining. Three dilutions were tried (1:50, 1:500 and 1:1000) with the P2Y12 antibody with no success. This antibody optimisation was also stopped due to time constraints.

B.4 Autofluorescence quencher

As mentioned previously, human brain tissue autofluoresces primarily due to the presence of lipofuscins (292). Therefore, an autofluorescence quencher is required when using this type of tissue. Several components were tested for this project including Sudan Black, Vector® TrueVIEW® Autofluorescence Quenching Kit (Vector Laboratories, SP8400) and Millipore Autofluorescence Eliminator Reagent (Sigma Aldrich, 2160). Sudan black was tested at 0.3%, 0.5% and 1%, with the 0.3% giving the best autofluorescence quenching while maintaining good fluorescent signal. The Vector® TrueVIEW® kit did eliminate autofluorescence but did not remove lipofuscin signal (**Figure B2**). This provided a problem as it hindered view of antibody staining. Lastly the Millipore reagent was found to stop autofluorescence relatively well, however when compared to Sudan Black, it was thought that this still gave the best result in terms of background fluorescence (**Figure B4**).

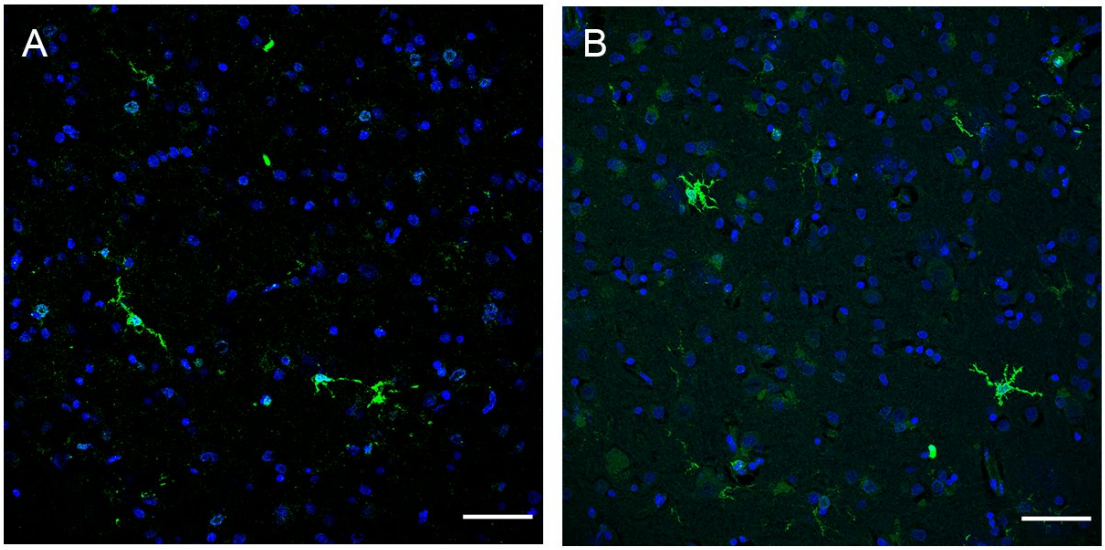

Figure B4 Testing the Merck autofluorescence quenching kit. Using Iba1 (019-19741) in green. (**A**) using 0.3% Sudan Black and (**B**) using Merck. In AD11 brain. Counterstain: DAPI (blue). Scale bars = 50µm.

B.5 Double staining

This section details the optimisation of TSPO with Iba1 and HLA-DR. TSPO with the remaining microglial markers (CD68, MSR-A and CD64) were tested before use on MTA148 tissue but did not require extended optimisation.

B.5.1 Iba1 and TSPO

The antibodies used for this staining were TSPO (ab109497) and two Iba1 antibodies (Wako 019-19741 and Abcam ab5076). TSPO parameters are always kept the same with a primary dilution of 1:2500 and DAR AF594 secondary used at a 1:200 dilution. As both the Wako Iba1 and TSPO were raised in rabbit, this provided a problem of cross-reactivity (**Figure B5**). Therefore, several tests were tried with varying methods to eliminate this problem, including conducting the staining over three days, incubating the monoclonal TSPO first followed by the polyclonal Iba1 and varying concentrations for both primary and secondary antibodies (**Figure B5**). Although there may have been accurate staining produced, there was still possible cross-reactivity between both antibodies raised in rabbit. Therefore, it was concluded that a new Iba1 antibody raised in a different species would be tested. When testing the new Iba1 antibody raised in goat (ab5076) individually, there appeared to be some punctate particles in the background tissue. It was thought that adding normal donkey serum (NDS) into both the primary and secondary antibody solutions could eliminate this.

However, this had no effect on the punctate issue (**Figure B5**). To overcome this, different antibody dilutions were assessed, 1:750 and 1:1000 with either 1:100 or 1:200 DAG AF488 secondary antibody dilutions. It was established that a primary Iba1 dilution of 1:1000 with a secondary dilution of 1:100 gave the best staining results (**Figure B5**).

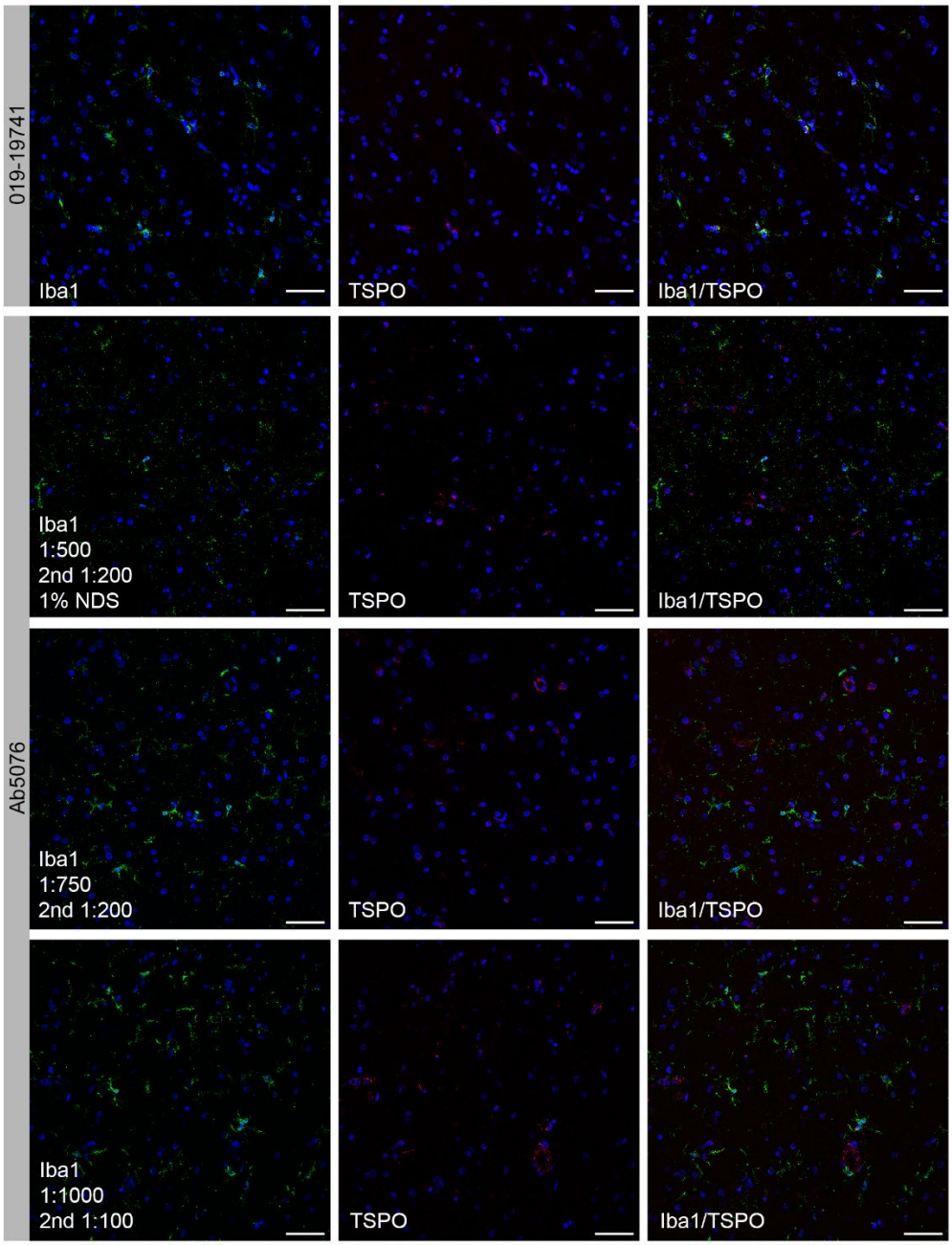

Figure B5 Tests for TSPO (ab109497) and two Iba1 antibodies (Wako 019-19741 and Abcam ab5076) double staining. TSPO was used at a primary dilution of 1:2500. Secondary antibodies used were DAG AF488 for Iba1 (green) and DAR AF594 for TSPO (red). Counterstain: DAPI (blue). Scale bars = 50μm.

B.5.2 HLA-DR and TSPO

The same TSPO antibody was used for this as previously mentioned (ab109497) with the same parameters. The HLA-DR antibody (M0775) was first tested at a 1:50 dilution, as previously established in DAB staining in the lab group. However, this first test did not yield adequate staining (**Figure B6**) and it was thought that the secondary antibody for HLA-DR was too old. Once a new secondary antibody was obtained, the staining was repeated with HLA-DR at a 1:100 and 1:50 primary dilution. It was seen that the 1:50 primary dilution gave the best staining results (**Figure B6**).

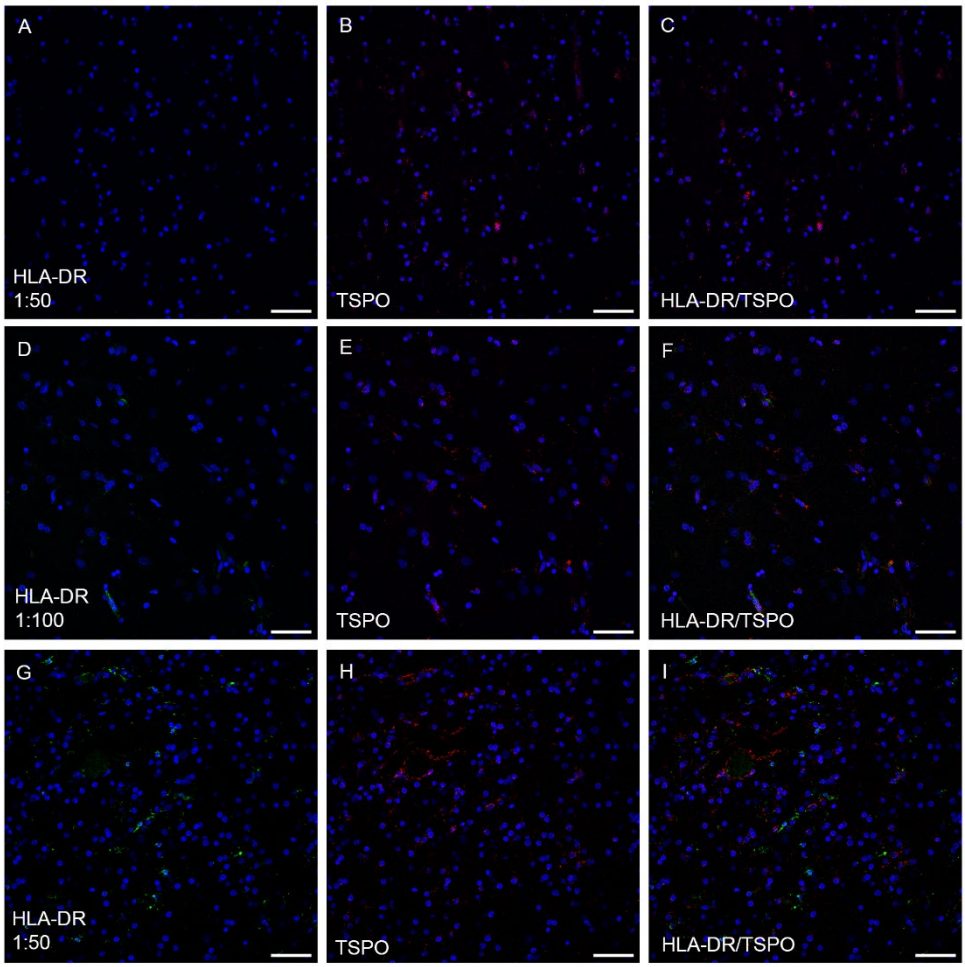

Figure B6 Tests for TSPO (ab109497) and HLA-DR (M0775) double staining. (**A, B, C**) show staining using old secondary antibody for HLA-DR. (**D-I**) HLA-DR staining with new secondary antibody. TSPO was used at a primary dilution of 1:2500. Secondary antibodies used were DAM AF488 for HLA-DR (green) and DAR AF594 for TSPO (red). Counterstain: DAPI (blue). Scale bars = 50μm.

B.6 Optimisation of fluorescent analysis

In order to perform cell counts, several options were tried. Initially, confocal microscopy (Leica SP8) was used to obtain images and ImageJ software to analyse these images. In order to get an accurate assessment of tissue, several ROIs would be needed to capture a large enough are of the tissue. This was difficult and time consuming to do on the confocal microscope as it required z-stacks image capture and careful manoeuvring as to ensure only grey matter was imaged. An ImageJ macro was created that would merge the fluorescent channels required and then using manual counts would be performed for each image. Firstly, this creates bias and unambiguous results as what is defined as a cell can differ between analysts and this method was extremely time consuming, therefore, other routes of analysis were subsequently explored.

Another software, QuPath, has been used previously in the lab group. It has the capability to analyse fluorescent images and perform automated cell counts based on thresholding inputs of each fluorescent channel compared to the nuclei. It took careful testing to ensure the software produced accurate results, with at least two people deciding the best thresholds to use. This proved a better and less time consuming method of counting cells. Protocol described in Section **3.3.2** and threshold parameters in **Appendix A**.

B.7 DPA-714

The ligand DPA-714 was purchased from Ambinter to have a conjugated FITC fluorophore (Amb37787199). This was suggested to be soluble in PBS up to 20µM in 25mM PBS buffer. However, when this was performed at this concentration the powder did not seem to fully dissolve into the solution. Regardless, the ligand solution was tested on human *post-mortem* FFPE tissue at a 20µM concentration and also at a diluted 0.1nM concentration (previous papers used this concentration). The 20µM test appeared to be too high a concentration and the 0.1nM test exhibited no staining, so was thought to be too low. The tissue was dewaxed, and tests were performed both with pre-treatment to retrieve antigens and no pre-treatment. Also, Sudan black was applied to suppress autofluorescence in the tissue. It was now thought that any accurate staining was obtained in any of the tests. Therefore, the ligand was not used in any quantification.

Further optimisation details and results can be found in Section **6.1**.

List of References

1. Guerreiro R, Bras J. The age factor in Alzheimer's disease. Genome Med. 2015;7:106.

2. Organization WH. Dementia 2023 [Available from: https://www.who.int/news-room/fact-sheets/detail/dementia.

3. Alzheimer A. Uber einen eigenartigen schweren Erkrankungsprozess der Hirninde. Neurologisches Centralblatt. 1906;25:1134.

4. Serrano-Pozo A, Frosch MP, Masliah E, Hyman BT. Neuropathological alterations in Alzheimer disease. Cold Spring Harb Perspect Med. 2011;1(1):a006189.

5. Wu Z, Peng Y, Hong M, Zhang Y. Gray Matter Deterioration Pattern During Alzheimer's Disease Progression: A Regions-of-Interest Based Surface Morphometry Study. Front Aging Neurosci. 2021;13:593898.

6. Hardy JA, Higgins GA. Alzheimer's disease: the amyloid cascade hypothesis. Science. 1992;256(5054):184-5.

7. Buxbaum JD, Christensen JL, Ruefli AA, Greengard P, Loring JF. Expression of APP in brains of transgenic mice containing the entire human APP gene. Biochem Biophys Res Commun. 1993;197(2):639-45.

8. Doody RS, Thomas RG, Farlow M, Iwatsubo T, Vellas B, Joffe S, et al. Phase 3 trials of solanezumab for mild-to-moderate Alzheimer's disease. N Engl J Med. 2014;370(4):311-21.

9. Vandenberghe R, Rinne JO, Boada M, Katayama S, Scheltens P, Vellas B, et al. Bapineuzumab for mild to moderate Alzheimer's disease in two global, randomized, phase 3 trials. Alzheimers Res Ther. 2016;8(1):18.

10. Braak H, Braak E. Neuropathological stageing of Alzheimer-related changes. Acta Neuropathol. 1991;82(4):239-59.

11. Kanaan NM, Morfini GA, LaPointe NE, Pigino GF, Patterson KR, Song Y, et al. Pathogenic forms of tau inhibit kinesin-dependent axonal transport through a mechanism involving activation of axonal phosphotransferases. J Neurosci. 2011;31(27):9858-68.

12. Hamelin L, Lagarde J, Dorothee G, Leroy C, Labit M, Comley RA, et al. Early and protective microglial activation in Alzheimer's disease: a prospective study using 18F-DPA-714 PET imaging. Brain. 2016;139(Pt 4):1252-64.

13. Hamelin L, Lagarde J, Dorothee G, Potier MC, Corlier F, Kuhnast B, et al. Distinct dynamic profiles of microglial activation are associated with progression of Alzheimer's disease. Brain. 2018;141(6):1855-70.

14. Lambert JC, Ibrahim-Verbaas CA, Harold D, Naj AC, Sims R, Bellenguez C, et al. Meta-analysis of 74,046 individuals identifies 11 new susceptibility loci for Alzheimer's disease. Nat Genet. 2013;45(12):1452-8.

15. Rak M, Benit P, Chretien D, Bouchereau J, Schiff M, El-Khoury R, et al. Mitochondrial cytochrome c oxidase deficiency. Clin Sci (Lond). 2016;130(6):393-407.

16. Elgenaidi IS, Spiers JP. Regulation of the phosphoprotein phosphatase 2A system and its modulation during oxidative stress: A potential therapeutic target? Pharmacol Ther. 2019;198:68-89.

17. Misrani A, Tabassum S, Yang L. Mitochondrial Dysfunction and Oxidative Stress in Alzheimer's Disease. Front Aging Neurosci. 2021;13:617588.

18. Raichle ME, Gusnard DA. Appraising the brain's energy budget. Proc Natl Acad Sci U S A. 2002;99(16):10237-9.

19. Zhu D, Montagne A, Zhao Z. Alzheimer's pathogenic mechanisms and underlying sex difference. Cell Mol Life Sci. 2021;78(11):4907-20.

20. Gaugler J, James B, Johnson T, Marin A, Weuve J, Assoc As. 2019 Alzheimer's disease facts and figures. Alzheimers & Dementia. 2019;15(3):321-87.

21. Thornton J. WHO report shows that women outlive men worldwide. BMJ. 2019;365:l1631.

22. Liu S, Seidlitz J, Blumenthal JD, Clasen LS, Raznahan A. Integrative structural, functional, and transcriptomic analyses of sex-biased brain organization in humans. Proc Natl Acad Sci U S A. 2020;117(31):18788-98.

23. Carroll JC, Rosario ER, Chang L, Stanczyk FZ, Oddo S, LaFerla FM, et al. Progesterone and estrogen regulate Alzheimer-like neuropathology in female 3xTg-AD mice. J Neurosci. 2007;27(48):13357-65.

24. Song YJ, Li SR, Li XW, Chen X, Wei ZX, Liu QS, et al. The Effect of Estrogen Replacement Therapy on Alzheimer's Disease and Parkinson's Disease in Postmenopausal Women: A Meta-Analysis. Front Neurosci. 2020;14:157.

25. Ramos-Cejudo J, Wisniewski T, Marmar C, Zetterberg H, Blennow K, de Leon MJ, et al. Traumatic Brain Injury and Alzheimer's Disease: The Cerebrovascular Link. EBioMedicine. 2018;28:21-30.

26. Livingston G, Huntley J, Sommerlad A, Ames D, Ballard C, Banerjee S, et al. Dementia prevention, intervention, and care: 2020 report of the Lancet Commission. Lancet. 2020;396(10248):413-46.

27. Kockx M, Traini M, Kritharides L. Cell-specific production, secretion, and function of apolipoprotein E. J Mol Med (Berl). 2018;96(5):361-71.

28. Verghese PB, Castellano JM, Holtzman DM. Apolipoprotein E in Alzheimer's disease and other neurological disorders. Lancet Neurol. 2011;10(3):241-52.

29. Hatters DM, Peters-Libeu CA, Weisgraber KH. Apolipoprotein E structure: insights into function. Trends Biochem Sci. 2006;31(8):445-54.

30. Aging NIo. Alzheimer's Disease Genetics Fact Sheet 2019 [Available from: https://www.nia.nih.gov/health/alzheimers-disease-genetics-fact-sheet.

31. Victor MB, Leary N, Luna X, Meharena HS, Scannail AN, Bozzelli PL, et al. Lipid accumulation induced by APOE4 impairs microglial surveillance of neuronal-network activity. Cell Stem Cell. 2022;29(8):1197-212 e8.

32. Ferrari-Souza JP, Lussier FZ, Leffa DT, Therriault J, Tissot C, Bellaver B, et al. APOEepsilon4 associates with microglial activation independently of Abeta plaques and tau tangles. Sci Adv. 2023;9(14):eade1474.

33. Hall-Roberts H, Agarwal D, Obst J, Smith TB, Monzon-Sandoval J, Di Daniel E, et al. TREM2 Alzheimer's variant R47H causes similar transcriptional dysregulation to knockout, yet only subtle functional phenotypes in human iPSC-derived macrophages. Alzheimers Res Ther. 2020;12(1):151.

34. Guerreiro R, Wojtas A, Bras J, Carrasquillo M, Rogaeva E, Majounie E, et al. TREM2 variants in Alzheimer's disease. N Engl J Med. 2013;368(2):117-27.

35. Korvatska O, Leverenz JB, Jayadev S, McMillan P, Kurtz I, Guo X, et al. R47H Variant of TREM2 Associated With Alzheimer Disease in a Large Late-Onset Family: Clinical, Genetic, and Neuropathological Study. JAMA Neurol. 2015;72(8):920-7.

36. Fahrenhold M, Rakic S, Classey J, Brayne C, Ince PG, Nicoll JAR, et al. TREM2 expression in the human brain: a marker of monocyte recruitment? Brain Pathol. 2018;28(5):595-602.

37. Larsson SC, Traylor M, Malik R, Dichgans M, Burgess S, Markus HS, et al. Modifiable pathways in Alzheimer's disease: Mendelian randomisation analysis. BMJ. 2017;359:j5375.

38. Armstrong NM, An Y, Doshi J, Erus G, Ferrucci L, Davatzikos C, et al. Association of Midlife Hearing Impairment With Late-Life Temporal Lobe Volume Loss. JAMA Otolaryngol Head Neck Surg. 2019;145(9):794-802.

39. Zanier ER, Bertani I, Sammali E, Pischiutta F, Chiaravalloti MA, Vegliante G, et al. Induction of a transmissible tau pathology by traumatic brain injury. Brain. 2018;141(9):2685-99.

40. Kandimalla R, Thirumala V, Reddy PH. Is Alzheimer's disease a Type 3 Diabetes? A critical appraisal. Biochim Biophys Acta Mol Basis Dis. 2017;1863(5):1078-89.

41. Nguyen TT, Ta QTH, Nguyen TKO, Nguyen TTD, Giau VV. Type 3 Diabetes and Its Role Implications in Alzheimer's Disease. Int J Mol Sci. 2020;21(9).

42. Stanciu GD, Bild V, Ababei DC, Rusu RN, Cobzaru A, Paduraru L, et al. Link Between Diabetes and Alzheimer's Disease due to the Shared Amyloid Aggregation and Deposition Involving both Neurodegenerative Changes and Neurovascular Damages. J Clin Med. 2020;9(6).

43. Huff FJ, Growdon JH, Corkin S, Rosen TJ. Age at onset and rate of progression of Alzheimer's disease. J Am Geriatr Soc. 1987;35(1):27-30.

44. Corder EH, Saunders AM, Strittmatter WJ, Schmechel DE, Gaskell PC, Small GW, et al. Gene dose of apolipoprotein E type 4 allele and the risk of Alzheimer's disease in late onset families. Science. 1993;261(5123):921-3.

45. Cacace R, Sleegers K, Van Broeckhoven C. Molecular genetics of early-onset Alzheimer's disease revisited. Alzheimers Dement. 2016;12(6):733-48.

46. Marshall GA, Fairbanks LA, Tekin S, Vinters HV, Cummings JL. Early-onset Alzheimer's disease is associated with greater pathologic burden. J Geriatr Psychiatry Neurol. 2007;20(1):29-33.

47. Stanley K, Walker Z. Do patients with young onset Alzheimer's disease deteriorate faster than those with late onset Alzheimer's disease? A review of the literature. Int Psychogeriatr. 2014;26(12):1945-53.

48. Wingo TS, Lah JJ, Levey AI, Cutler DJ. Autosomal recessive causes likely in early-onset Alzheimer disease. Arch Neurol. 2012;69(1):59-64.

49. Bateman RJ, Xiong C, Benzinger TL, Fagan AM, Goate A, Fox NC, et al. Clinical and biomarker changes in dominantly inherited Alzheimer's disease. N Engl J Med. 2012;367(9):795-804.

50. Arevalo-Rodriguez I, Smailagic N, Roque IFM, Ciapponi A, Sanchez-Perez E, Giannakou A, et al. Mini-Mental State Examination (MMSE) for the detection of Alzheimer's disease and other dementias in people with mild cognitive impairment (MCI). Cochrane Database Syst Rev. 2015(3):CD010783.

51. Basaia S, Agosta F, Wagner L, Canu E, Magnani G, Santangelo R, et al. Automated classification of Alzheimer's disease and mild cognitive impairment using a single MRI and deep neural networks. Neuroimage Clin. 2019;21:101645.

52. Calabrese M, Atzori M, Bernardi V, Morra A, Romualdi C, Rinaldi L, et al. Cortical atrophy is relevant in multiple sclerosis at clinical onset. J Neurol. 2007;254(9):1212-20.

53. Brodtmann A, Khlif MS, Egorova N, Veldsman M, Bird LJ, Werden E. Dynamic Regional Brain Atrophy Rates in the First Year After Ischemic Stroke. Stroke. 2020;51(9):e183-e92.

54. Ossenkoppele R, Jansen WJ, Rabinovici GD, Knol DL, van der Flier WM, van Berckel BN, et al. Prevalence of amyloid PET positivity in dementia syndromes: a meta-analysis. JAMA. 2015;313(19):1939-49.

55. Olsson B, Lautner R, Andreasson U, Ohrfelt A, Portelius E, Bjerke M, et al. CSF and blood biomarkers for the diagnosis of Alzheimer's disease: a systematic review and meta-analysis. Lancet Neurol. 2016;15(7):673-84.

56. Querol-Vilaseca M, Colom-Cadena M, Pegueroles J, San Martin-Paniello C, Clarimon J, Belbin O, et al. YKL-40 (Chitinase 3-like I) is expressed in a subset of astrocytes in Alzheimer's disease and other tauopathies. J Neuroinflammation. 2017;14(1):118.

57. Janelidze S, Mattsson N, Stomrud E, Lindberg O, Palmqvist S, Zetterberg H, et al. CSF biomarkers of neuroinflammation and cerebrovascular dysfunction in early Alzheimer disease. Neurology. 2018;91(9):e867-e77.

58. Simren J, Leuzy A, Karikari TK, Hye A, Benedet AL, Lantero-Rodriguez J, et al. The diagnostic and prognostic capabilities of plasma biomarkers in Alzheimer's disease. Alzheimers Dement. 2021;17(7):1145-56.

59. Cullen NC, Leuzy A, Janelidze S, Palmqvist S, Svenningsson AL, Stomrud E, et al. Plasma biomarkers of Alzheimer's disease improve prediction of cognitive decline in cognitively unimpaired elderly populations. Nat Commun. 2021;12(1):3555.

60. Ng TKS, Ho CSH, Tam WWS, Kua EH, Ho RC. Decreased Serum Brain-Derived Neurotrophic Factor (BDNF) Levels in Patients with Alzheimer's Disease (AD): A Systematic Review and Meta-Analysis. Int J Mol Sci. 2019;20(2).

61. Weinstein G, Beiser AS, Choi SH, Preis SR, Chen TC, Vorgas D, et al. Serum brain-derived neurotrophic factor and the risk for dementia: the Framingham Heart Study. JAMA Neurol. 2014;71(1):55-61.

62. Elahi FM, Casaletto KB, La Joie R, Walters SM, Harvey D, Wolf A, et al. Plasma biomarkers of astrocytic and neuronal dysfunction in early- and late-onset Alzheimer's disease. Alzheimers Dement. 2020;16(4):681-95.

63. Rakic S, Hung YMA, Smith M, So D, Tayler HM, Varney W, et al. Systemic infection modifies the neuroinflammatory response in late stage Alzheimer's disease. Acta Neuropathol Commun. 2018;6(1):88.

64. Thal DR, Rub U, Orantes M, Braak H. Phases of A beta-deposition in the human brain and its relevance for the development of AD. Neurology. 2002;58(12):1791-800.

65. Kovacs GG, Gelpi E. Clinical neuropathology practice news 3-2012: the "ABC" in AD-revised and updated guideline for the neuropathologic assessment of Alzheimer's disease. Clin Neuropathol. 2012;31(3):116-8.

66. Mirra SS, Heyman A, McKeel D, Sumi SM, Crain BJ, Brownlee LM, et al. The Consortium to Establish a Registry for Alzheimer's Disease (CERAD). Part II. Standardization of the neuropathologic assessment of Alzheimer's disease. Neurology. 1991;41(4):479-86.

67. Braak H, Braak E, Ohm T, Bohl J. Alzheimer's disease: mismatch between amyloid plaques and neuritic plaques. Neurosci Lett. 1989;103(1):24-8.

68. Sharma K. Cholinesterase inhibitors as Alzheimer's therapeutics (Review). Mol Med Rep. 2019;20(2):1479-87.

69. Rogers SL, Farlow MR, Doody RS, Mohs R, Friedhoff LT. A 24-week, double-blind, placebo-controlled trial of donepezil in patients with Alzheimer's disease. Donepezil Study Group. Neurology. 1998;50(1):136-45.

70. McShane R, Westby MJ, Roberts E, Minakaran N, Schneider L, Farrimond LE, et al. Memantine for dementia. Cochrane Database Syst Rev. 2019;3:CD003154.

71. Gilman S, Koller M, Black RS, Jenkins L, Griffith SG, Fox NC, et al. Clinical effects of Abeta immunization (AN1792) in patients with AD in an interrupted trial. Neurology. 2005;64(9):1553-62.

72. Nicoll JAR, Buckland GR, Harrison CH, Page A, Harris S, Love S, et al. Persistent neuropathological effects 14 years following amyloid-beta immunization in Alzheimer's disease. Brain. 2019;142(7):2113-26.

73. Salloway S, Sperling R, Fox NC, Blennow K, Klunk W, Raskind M, et al. Two phase 3 trials of bapineuzumab in mild-to-moderate Alzheimer's disease. N Engl J Med. 2014;370(4):322-33.

74. Woloshin S, Kesselheim AS. What to Know About the Alzheimer Drug Aducanumab (Aduhelm). JAMA Intern Med. 2022.

75. Salloway S, Chalkias S, Barkhof F, Burkett P, Barakos J, Purcell D, et al. Amyloid-Related Imaging Abnormalities in 2 Phase 3 Studies Evaluating Aducanumab in Patients With Early Alzheimer Disease. JAMA Neurol. 2022;79(1):13-21.

76. Plowey ED, Bussiere T, Rajagovindan R, Sebalusky J, Hamann S, von Hehn C, et al. Alzheimer disease neuropathology in a patient previously treated with aducanumab. Acta Neuropathol. 2022.

77. van Dyck CH, Swanson CJ, Aisen P, Bateman RJ, Chen C, Gee M, et al. Lecanemab in Early Alzheimer's Disease. N Engl J Med. 2023;388(1):9-21.

78. Company ELa. Lilly's Donanemab Significantly Slowed Cognitive and Functional Decline in Phase 3 Study of Early Alzheimer's Disease 2023 [Available from: https://investor.lilly.com/news-releases/news-release-details/lillys-donanemab-significantly-slowed-cognitive-and-functional.

79. Hampel H, Ewers M, Burger K, Annas P, Mortberg A, Bogstedt A, et al. Lithium trial in Alzheimer's disease: a randomized, single-blind, placebo-controlled, multicenter 10-week study. J Clin Psychiatry. 2009;70(6):922-31.

80. Wischik CM, Staff RT, Wischik DJ, Bentham P, Murray AD, Storey JM, et al. Tau aggregation inhibitor therapy: an exploratory phase 2 study in mild or moderate Alzheimer's disease. J Alzheimers Dis. 2015;44(2):705-20.

81. Slomski A. Anti-Tau Antibody Semorinemab Fails to Slow Alzheimer Disease. JAMA. 2022;328(5):415.

82. Mummery CJ, Borjesson-Hanson A, Blackburn DJ, Vijverberg EGB, De Deyn PP, Ducharme S, et al. Tau-targeting antisense oligonucleotide MAPT(Rx) in mild Alzheimer's disease: a phase 1b, randomized, placebo-controlled trial. Nat Med. 2023;29(6):1437-47.

83. von Bernhardi R, Cornejo F, Parada GE, Eugenin J. Role of TGFbeta signaling in the pathogenesis of Alzheimer's disease. Front Cell Neurosci. 2015;9:426.

84. Zhu M, Wang X, Hjorth E, Colas RA, Schroeder L, Granholm AC, et al. Pro-Resolving Lipid Mediators Improve Neuronal Survival and Increase Abeta42 Phagocytosis. Mol Neurobiol. 2016;53(4):2733-49.

85. Mittelbronn M, Dietz K, Schluesener HJ, Meyermann R. Local distribution of microglia in the normal adult human central nervous system differs by up to one order of magnitude. Acta Neuropathol. 2001;101(3):249-55.

86. Salter MW, Stevens B. Microglia emerge as central players in brain disease. Nat Med. 2017;23(9):1018-27.

87. Ginhoux F, Greter M, Leboeuf M, Nandi S, See P, Gokhan S, et al. Fate mapping analysis reveals that adult microglia derive from primitive macrophages. Science. 2010;330(6005):841-5.

88. Río-Hortega d. El “tercer elemento” de los centros nerviosos. I. La microglía en estado normal. Bol Soc Esp Biol 1919:67–82.

89. Spiteri AG, Wishart CL, Pamphlett R, Locatelli G, King NJC. Microglia and monocytes in inflammatory CNS disease: integrating phenotype and function. Acta Neuropathol. 2022;143(2):179-224.

90. Hutchins KD, Dickson DW, Rashbaum WK, Lyman WD. Localization of morphologically distinct microglial populations in the developing human fetal brain: implications for ontogeny. Brain Res Dev Brain Res. 1990;55(1):95-102.

91. Goldmann T, Wieghofer P, Muller PF, Wolf Y, Varol D, Yona S, et al. A new type of microglia gene targeting shows TAK1 to be pivotal in CNS autoimmune inflammation. Nat Neurosci. 2013;16(11):1618-26.

92. Reu P, Khosravi A, Bernard S, Mold JE, Salehpour M, Alkass K, et al. The Lifespan and Turnover of Microglia in the Human Brain. Cell Rep. 2017;20(4):779-84.

93. Lawson LJ, Perry VH, Gordon S. Turnover of resident microglia in the normal adult mouse brain. Neuroscience. 1992;48(2):405-15.

94. Askew K, Li K, Olmos-Alonso A, Garcia-Moreno F, Liang Y, Richardson P, et al. Coupled Proliferation and Apoptosis Maintain the Rapid Turnover of Microglia in the Adult Brain. Cell Rep. 2017;18(2):391-405.

95. Min B. Spontaneous T Cell Proliferation: A Physiologic Process to Create and Maintain Homeostatic Balance and Diversity of the Immune System. Front Immunol. 2018;9:547.

96. Boche D, Perry VH, Nicoll JA. Review: activation patterns of microglia and their identification in the human brain. Neuropathol Appl Neurobiol. 2013;39(1):3-18.

97. Paolicelli RC, Bolasco G, Pagani F, Maggi L, Scianni M, Panzanelli P, et al. Synaptic pruning by microglia is necessary for normal brain development. Science. 2011;333(6048):1456-8.

98. Wake H, Moorhouse AJ, Jinno S, Kohsaka S, Nabekura J. Resting microglia directly monitor the functional state of synapses in vivo and determine the fate of ischemic terminals. J Neurosci. 2009;29(13):3974-80.

99. Sipe GO, Lowery RL, Tremblay ME, Kelly EA, Lamantia CE, Majewska AK. Microglial P2Y12 is necessary for synaptic plasticity in mouse visual cortex. Nat Commun. 2016;7:10905.

100. Stoberl N, Maguire E, Salis E, Shaw B, Hall-Roberts H. Human iPSC-derived glia models for the study of neuroinflammation. J Neuroinflammation. 2023;20(1):231.

101. Jurga AM, Paleczna M, Kuter KZ. Overview of General and Discriminating Markers of Differential Microglia Phenotypes. Front Cell Neurosci. 2020;14:198.

102. Nimmerjahn A, Kirchhoff F, Helmchen F. Resting microglial cells are highly dynamic surveillants of brain parenchyma in vivo. Science. 2005;308(5726):1314-8.

103. Boche D. PVH, Nicoll V.A.R. Review: activation patterns of microglia and their identification in the human brain. Neuropathol Appl Neurobiol. 2013;39(1).

104. Mosser DM, Edwards JP. Exploring the full spectrum of macrophage activation. Nat Rev Immunol. 2008;8(12):958-69.

105. Edwards JP, Zhang X, Frauwirth KA, Mosser DM. Biochemical and functional characterization of three activated macrophage populations. J Leukoc Biol. 2006;80(6):1298-307.

106. Krasemann S, Madore C, Cialic R, Baufeld C, Calcagno N, El Fatimy R, et al. The TREM2-APOE Pathway Drives the Transcriptional Phenotype of Dysfunctional Microglia in Neurodegenerative Diseases. Immunity. 2017;47(3):566-81 e9.

107. Keren-Shaul H, Spinrad A, Weiner A, Matcovitch-Natan O, Dvir-Szternfeld R, Ulland TK, et al. A Unique Microglia Type Associated with Restricting Development of Alzheimer's Disease. Cell. 2017;169(7):1276-90 e17.

108. Boche D, Gordon MN. Diversity of transcriptomic microglial phenotypes in aging and Alzheimer's disease. Alzheimers Dement. 2022;18(2):360-76.

109. Satoh J, Kino Y, Asahina N, Takitani M, Miyoshi J, Ishida T, et al. TMEM119 marks a subset of microglia in the human brain. Neuropathology. 2016;36(1):39-49.

110. Zrzavy T, Hametner S, Wimmer I, Butovsky O, Weiner HL, Lassmann H. Loss of 'homeostatic' microglia and patterns of their activation in active multiple sclerosis. Brain. 2017;140(7):1900-13.

111. Efthymiou AG, Goate AM. Late onset Alzheimer's disease genetics implicates microglial pathways in disease risk. Mol Neurodegener. 2017;12(1):43.

112. Styren SD, Civin WH, Rogers J. Molecular, cellular, and pathologic characterization of HLA-DR immunoreactivity in normal elderly and Alzheimer's disease brain. Exp Neurol. 1990;110(1):93-104.

113. Xiang Z, Haroutunian V, Ho L, Purohit D, Pasinetti GM. Microglia activation in the brain as inflammatory biomarker of Alzheimer's disease neuropathology and clinical dementia. Dis Markers. 2006;22(1-2):95-102.

114. Parachikova A, Agadjanyan MG, Cribbs DH, Blurton-Jones M, Perreau V, Rogers J, et al. Inflammatory changes parallel the early stages of Alzheimer disease. Neurobiol Aging. 2007;28(12):1821-33.

115. Minett T, Classey J, Matthews FE, Fahrenhold M, Taga M, Brayne C, et al. Microglial immunophenotype in dementia with Alzheimer's pathology. J Neuroinflammation. 2016;13(1):135.

116. Lejri I, Grimm A, Halle F, Abarghaz M, Klein C, Maitre M, et al. TSPO Ligands Boost Mitochondrial Function and Pregnenolone Synthesis. J Alzheimers Dis. 2019;72(4):1045-58.

117. Ohsawa K, Imai Y, Kanazawa H, Sasaki Y, Kohsaka S. Involvement of Iba1 in membrane ruffling and phagocytosis of macrophages/microglia. J Cell Sci. 2000;113 (Pt 17):3073-84.

118. Walker DG, Lue LF. Immune phenotypes of microglia in human neurodegenerative disease: challenges to detecting microglial polarization in human brains. Alzheimers Res Ther. 2015;7(1):56.

119. Franco-Bocanegra DK, McAuley C, Nicoll JAR, Boche D. Molecular Mechanisms of Microglial Motility: Changes in Ageing and Alzheimer's Disease. Cells. 2019;8(6).

120. Hopperton KE, Mohammad D, Trepanier MO, Giuliano V, Bazinet RP. Markers of microglia in post-mortem brain samples from patients with Alzheimer's disease: a systematic review. Mol Psychiatry. 2018;23(2):177-98.

121. Autoimmunity: From Bench to Bedside. In: Anaya JM, Shoenfeld Y, Rojas-Villarraga A, Levy RA, Cervera R, editors. Bogota (Colombia): El Rosario University Press; 2013.

122. Wilkinson K, El Khoury J. Microglial scavenger receptors and their roles in the pathogenesis of Alzheimer's disease. Int J Alzheimers Dis. 2012;2012:489456.

123. Zotova E, Bharambe V, Cheaveau M, Morgan W, Holmes C, Harris S, et al. Inflammatory components in human Alzheimer's disease and after active amyloid-beta42 immunization. Brain. 2013;136(Pt 9):2677-96.

124. Franco-Bocanegra DK, George B, Lau LC, Holmes C, Nicoll JAR, Boche D. Microglial motility in Alzheimer's disease and after Abeta42 immunotherapy: a human post-mortem study. Acta Neuropathol Commun. 2019;7(1):174.

125. Chen P, Zhao W, Guo Y, Xu J, Yin M. CX3CL1/CX3CR1 in Alzheimer's Disease: A Target for Neuroprotection. Biomed Res Int. 2016;2016:8090918.

126. Merino JJ, Muneton-Gomez V, Alvarez MI, Toledano-Diaz A. Effects of CX3CR1 and Fractalkine Chemokines in Amyloid Beta Clearance and p-Tau Accumulation in Alzheimer's Disease (AD) Rodent Models: Is Fractalkine a Systemic Biomarker for AD? Curr Alzheimer Res. 2016;13(4):403-12.

127. Vogelpoel LT, Baeten DL, de Jong EC, den Dunnen J. Control of cytokine production by human fc gamma receptors: implications for pathogen defense and autoimmunity. Front Immunol. 2015;6:79.

128. Amin J, Holmes C, Dorey RB, Tommasino E, Casal YR, Williams DM, et al. Neuroinflammation in dementia with Lewy bodies: a human post-mortem study. Transl Psychiatry. 2020;10(1):267.

129. Benmamar-Badel A, Owens T, Wlodarczyk A. Protective Microglial Subset in Development, Aging, and Disease: Lessons From Transcriptomic Studies. Front Immunol. 2020;11:430.

130. Masliah E, Mallory M, Hansen L, Alford M, Albright T, Terry R, et al. Immunoreactivity of CD45, a protein phosphotyrosine phosphatase, in Alzheimer's disease. Acta Neuropathol. 1991;83(1):12-20.

131. Dal Bianco A, Bradl M, Frischer J, Kutzelnigg A, Jellinger K, Lassmann H. Multiple sclerosis and Alzheimer's disease. Ann Neurol. 2008;63(2):174-83.

132. Galea I, Palin K, Newman TA, Van Rooijen N, Perry VH, Boche D. Mannose receptor expression specifically reveals perivascular macrophages in normal, injured, and diseased mouse brain. Glia. 2005;49(3):375-84.

133. Shtaya A, Bridges LR, Williams R, Trippier S, Zhang L, Pereira AC, et al. Innate Immune Anti-Inflammatory Response in Human Spontaneous Intracerebral Hemorrhage. Stroke. 2021;52(11):3613-23.

134. Hendrickx DAE, van Eden CG, Schuurman KG, Hamann J, Huitinga I. Staining of HLA-DR, Iba1 and CD68 in human microglia reveals partially overlapping expression depending on cellular morphology and pathology. J Neuroimmunol. 2017;309:12-22.

135. Edler MK, Sherwood CC, Meindl RS, Munger EL, Hopkins WD, Ely JJ, et al. Microglia changes associated to Alzheimer's disease pathology in aged chimpanzees. J Comp Neurol. 2018;526(18):2921-36.

136. Kenkhuis B, Somarakis A, Kleindouwel LRT, van Roon-Mom WMC, Hollt T, van der Weerd L. Co-expression patterns of microglia markers Iba1, TMEM119 and P2RY12 in Alzheimer's disease. Neurobiol Dis. 2022;167:105684.

137. Jansen IE, Savage JE, Watanabe K, Bryois J, Williams DM, Steinberg S, et al. Genome-wide meta-analysis identifies new loci and functional pathways influencing Alzheimer's disease risk. Nat Genet. 2019;51(3):404-13.

138. Wang WY, Tan MS, Yu JT, Tan L. Role of pro-inflammatory cytokines released from microglia in Alzheimer's disease. Ann Transl Med. 2015;3(10):136.

139. Griffin WS, Stanley LC, Ling C, White L, MacLeod V, Perrot LJ, et al. Brain interleukin 1 and S-100 immunoreactivity are elevated in Down syndrome and Alzheimer disease. Proc Natl Acad Sci U S A. 1989;86(19):7611-5.

140. Fan Z, Brooks DJ, Okello A, Edison P. An early and late peak in microglial activation in Alzheimer's disease trajectory. Brain. 2017;140(3):792-803.

141. Streit WJ, Sammons NW, Kuhns AJ, Sparks DL. Dystrophic microglia in the aging human brain. Glia. 2004;45(2):208-12.

142. Shahidehpour RK, Higdon RE, Crawford NG, Neltner JH, Ighodaro ET, Patel E, et al. Dystrophic microglia are associated with neurodegenerative disease and not healthy aging in the human brain. Neurobiol Aging. 2021;99:19-27.

143. Bolmont T, Haiss F, Eicke D, Radde R, Mathis CA, Klunk WE, et al. Dynamics of the microglial/amyloid interaction indicate a role in plaque maintenance. J Neurosci. 2008;28(16):4283-92.

144. Ghosh S, Wu MD, Shaftel SS, Kyrkanides S, LaFerla FM, Olschowka JA, et al. Sustained interleukin-1beta overexpression exacerbates tau pathology despite reduced amyloid burden in an Alzheimer's mouse model. J Neurosci. 2013;33(11):5053-64.

145. Asai H, Ikezu S, Tsunoda S, Medalla M, Luebke J, Haydar T, et al. Depletion of microglia and inhibition of exosome synthesis halt tau propagation. Nat Neurosci. 2015;18(11):1584-93.

146. Streit WJ, Braak H, Xue QS, Bechmann I. Dystrophic (senescent) rather than activated microglial cells are associated with tau pathology and likely precede neurodegeneration in Alzheimer's disease. Acta Neuropathol. 2009;118(4):475-85.

147. Pascoal TA, Benedet AL, Ashton NJ, Kang MS, Therriault J, Chamoun M, et al. Microglial activation and tau propagate jointly across Braak stages. Nat Med. 2021;27(9):1592-9.

148. Alzforum. Microglia Conflicted: To Help, or to Hinder, Tau's March Across the Brain? 2023 [Available from: https://www.alzforum.org/news/conference-coverage/microglia-conflicted-help-or-hinder-taus-march-across-brain.

149. Mathys H, Davila-Velderrain J, Peng Z, Gao F, Mohammadi S, Young JZ, et al. Single-cell transcriptomic analysis of Alzheimer's disease. Nature. 2019;570(7761):332-7.

150. Hu Y, Fryatt GL, Ghorbani M, Obst J, Menassa DA, Martin-Estebane M, et al. Replicative senescence dictates the emergence of disease-associated microglia and contributes to Abeta pathology. Cell Rep. 2021;35(10):109228.

151. Mathys H, Adaikkan C, Gao F, Young JZ, Manet E, Hemberg M, et al. Temporal Tracking of Microglia Activation in Neurodegeneration at Single-Cell Resolution. Cell Rep. 2017;21(2):366-80.

152. Jagust W. Is amyloid-beta harmful to the brain? Insights from human imaging studies. Brain. 2016;139(Pt 1):23-30.

153. Boche D, Nicoll JAR. Invited Review - Understanding cause and effect in Alzheimer's pathophysiology: Implications for clinical trials. Neuropathol Appl Neurobiol. 2020;46(7):623-40.

154. Cras P, Kawai M, Lowery D, Gonzalez-DeWhitt P, Greenberg B, Perry G. Senile plaque neurites in Alzheimer disease accumulate amyloid precursor protein. Proc Natl Acad Sci U S A. 1991;88(17):7552-6.

155. Fitz NF, Nam KN, Wolfe CM, Letronne F, Playso BE, Iordanova BE, et al. Phospholipids of APOE lipoproteins activate microglia in an isoform-specific manner in preclinical models of Alzheimer's disease. Nat Commun. 2021;12(1):3416.

156. Ulland TK, Colonna M. TREM2 - a key player in microglial biology and Alzheimer disease. Nat Rev Neurol. 2018;14(11):667-75.

157. Yuan P, Condello C, Keene CD, Wang Y, Bird TD, Paul SM, et al. TREM2 Haplodeficiency in Mice and Humans Impairs the Microglia Barrier Function Leading to Decreased Amyloid Compaction and Severe Axonal Dystrophy. Neuron. 2016;90(4):724-39.

158. Kumar V, Kim SH, Bishayee K. Dysfunctional Glucose Metabolism in Alzheimer's Disease Onset and Potential Pharmacological Interventions. Int J Mol Sci. 2022;23(17).

159. Wang L, Pavlou S, Du X, Bhuckory M, Xu H, Chen M. Glucose transporter 1 critically controls microglial activation through facilitating glycolysis. Mol Neurodegener. 2019;14(1):2.

160. Gulen MF, Samson N, Keller A, Schwabenland M, Liu C, Gluck S, et al. cGAS-STING drives ageing-related inflammation and neurodegeneration. Nature. 2023;620(7973):374-80.

161. Fairley LH, Lai KO, Wong JH, Chong WJ, Vincent AS, D'Agostino G, et al. Mitochondrial control of microglial phagocytosis by the translocator protein and hexokinase 2 in Alzheimer's disease. Proc Natl Acad Sci U S A. 2023;120(8):e2209177120.

162. Akdemir ES, Huang AY, Deneen B. Astrocytogenesis: where, when, and how. F1000Res. 2020;9.

163. Liddelow SA, Barres BA. Reactive Astrocytes: Production, Function, and Therapeutic Potential. Immunity. 2017;46(6):957-67.

164. Kimelberg HK, Norenberg MD. Astrocytes. Sci Am. 1989;260(4):66-72, 4, 6.

165. Hol EM, Pekny M. Glial fibrillary acidic protein (GFAP) and the astrocyte intermediate filament system in diseases of the central nervous system. Curr Opin Cell Biol. 2015;32:121-30.

166. Herrmann JE, Imura T, Song B, Qi J, Ao Y, Nguyen TK, et al. STAT3 is a critical regulator of astrogliosis and scar formation after spinal cord injury. J Neurosci. 2008;28(28):7231-43.

167. Ben Haim L, Ceyzeriat K, Carrillo-de Sauvage MA, Aubry F, Auregan G, Guillermier M, et al. The JAK/STAT3 pathway is a common inducer of astrocyte reactivity in Alzheimer's and Huntington's diseases. J Neurosci. 2015;35(6):2817-29.

168. Itagaki S, McGeer PL, Akiyama H, Zhu S, Selkoe D. Relationship of microglia and astrocytes to amyloid deposits of Alzheimer disease. J Neuroimmunol. 1989;24(3):173-82.

169. Vehmas AK, Kawas CH, Stewart WF, Troncoso JC. Immune reactive cells in senile plaques and cognitive decline in Alzheimer's disease. Neurobiol Aging. 2003;24(2):321-31.

170. Garland EF, Hartnell IJ, Boche D. Microglia and Astrocyte Function and Communication: What Do We Know in Humans? Front Neurosci. 2022;16:824888.

171. Peterson PK, Hu S, Salak-Johnson J, Molitor TW, Chao CC. Differential production of and migratory response to beta chemokines by human microglia and astrocytes. J Infect Dis. 1997;175(2):478-81.

172. Koning N, Swaab DF, Hoek RM, Huitinga I. Distribution of the immune inhibitory molecules CD200 and CD200R in the normal central nervous system and multiple sclerosis lesions suggests neuron-glia and glia-glia interactions. J Neuropathol Exp Neurol. 2009;68(2):159-67.

173. Theriault P, ElAli A, Rivest S. The dynamics of monocytes and microglia in Alzheimer's disease. Alzheimers Res Ther. 2015;7(1):41.

174. Varvel NH, Neher JJ, Bosch A, Wang W, Ransohoff RM, Miller RJ, et al. Infiltrating monocytes promote brain inflammation and exacerbate neuronal damage after status epilepticus. Proc Natl Acad Sci U S A. 2016;113(38):E5665-74.

175. Kelly L, Sharp MM, Thomas I, Brown C, Schrag M, Antunes LV, et al. Targeting lysyl-oxidase (LOX) may facilitate intramural periarterial drainage for the treatment of Alzheimer's disease. Cereb Circ Cogn Behav. 2023;5:100171.

176. Fani Maleki A, Rivest S. Innate Immune Cells: Monocytes, Monocyte-Derived Macrophages and Microglia as Therapeutic Targets for Alzheimer's Disease and Multiple Sclerosis. Front Cell Neurosci. 2019;13:355.

177. Saresella M, Marventano I, Calabrese E, Piancone F, Rainone V, Gatti A, et al. A complex proinflammatory role for peripheral monocytes in Alzheimer's disease. J Alzheimers Dis. 2014;38(2):403-13.

178. Garcia FJ, Sun N, Lee H, Godlewski B, Mathys H, Galani K, et al. Single-cell dissection of the human brain vasculature. Nature. 2022;603(7903):893-9.

179. Dyer LA, Patterson C. Development of the endothelium: an emphasis on heterogeneity. Semin Thromb Hemost. 2010;36(3):227-35.

180. Bryant A, Li Z, Jayakumar R, Serrano-Pozo A, Woost B, Hu M, et al. Endothelial Cells Are Heterogeneous in Different Brain Regions and Are Dramatically Altered in Alzheimer's Disease. J Neurosci. 2023;43(24):4541-57.

181. Zhang YL, Wang J, Zhang ZN, Su Q, Guo JH. The relationship between amyloid-beta and brain capillary endothelial cells in Alzheimer's disease. Neural Regen Res. 2022;17(11):2355-63.

182. Mittal P, Singh N, Chaturvedi S, Jyoti A, Mishra AK, Hazari PP. Comprehensive review on design perspective of PET ligands based on β-amyloids, tau and neuroinflammation for diagnostic intervention of Alzheimer’s disease. Clinical and Translational Imaging. 2021;9(2):153-75.

183. Papadopoulos V, Baraldi M, Guilarte TR, Knudsen TB, Lacapere JJ, Lindemann P, et al. Translocator protein (18kDa): new nomenclature for the peripheral-type benzodiazepine receptor based on its structure and molecular function. Trends Pharmacol Sci. 2006;27(8):402-9.

184. Jaremko L, Jaremko M, Giller K, Becker S, Zweckstetter M. Structure of the mitochondrial translocator protein in complex with a diagnostic ligand. Science. 2014;343(6177):1363-6.

185. Lee Y, Park Y, Nam H, Lee JW, Yu SW. Translocator protein (TSPO): the new story of the old protein in neuroinflammation. BMB Rep. 2020;53(1):20-7.

186. Tu LN, Zhao AH, Stocco DM, Selvaraj V. PK11195 effect on steroidogenesis is not mediated through the translocator protein (TSPO). Endocrinology. 2015;156(3):1033-9.

187. Gui Y, Marks JD, Das S, Hyman BT, Serrano-Pozo A. Characterization of the 18 kDa translocator protein (TSPO) expression in post-mortem normal and Alzheimer's disease brains. Brain Pathol. 2020;30(1):151-64.

188. Bonsack Ft, Alleyne CH, Jr., Sukumari-Ramesh S. Augmented expression of TSPO after intracerebral hemorrhage: a role in inflammation? J Neuroinflammation. 2016;13(1):151.

189. Dupont AC, Largeau B, Santiago Ribeiro MJ, Guilloteau D, Tronel C, Arlicot N. Translocator Protein-18 kDa (TSPO) Positron Emission Tomography (PET) Imaging and Its Clinical Impact in Neurodegenerative Diseases. Int J Mol Sci. 2017;18(4).

190. Cosenza-Nashat M, Zhao ML, Suh HS, Morgan J, Natividad R, Morgello S, et al. Expression of the translocator protein of 18 kDa by microglia, macrophages and astrocytes based on immunohistochemical localization in abnormal human brain. Neuropathol Appl Neurobiol. 2009;35(3):306-28.

191. Suridjan I, Pollock BG, Verhoeff NP, Voineskos AN, Chow T, Rusjan PM, et al. In-vivo imaging of grey and white matter neuroinflammation in Alzheimer's disease: a positron emission tomography study with a novel radioligand, [18F]-FEPPA. Mol Psychiatry. 2015;20(12):1579-87.

192. Nutma E, Fancy N, Weinert M, Tsartsalis S, Marzin MC, Muirhead RCJ, et al. Translocator protein is a marker of activated microglia in rodent models but not human neurodegenerative diseases. Nat Commun. 2023;14(1):5247.

193. Agrawal I, Jha S. Mitochondrial Dysfunction and Alzheimer's Disease: Role of Microglia. Front Aging Neurosci. 2020;12:252.

194. Torres S, Garcia-Ruiz CM, Fernandez-Checa JC. Mitochondrial Cholesterol in Alzheimer's Disease and Niemann-Pick Type C Disease. Front Neurol. 2019;10:1168.

195. Zhou R, Ji B, Kong Y, Qin L, Ren W, Guan Y, et al. PET Imaging of Neuroinflammation in Alzheimer's Disease. Front Immunol. 2021;12:739130.

196. Christensen A, Pike CJ. TSPO ligand PK11195 improves Alzheimer-related outcomes in aged female 3xTg-AD mice. Neurosci Lett. 2018;683:7-12.

197. Grimm A, Lejri I, Halle F, Schmitt M, Gotz J, Bihel F, et al. Mitochondria modulatory effects of new TSPO ligands in a cellular model of tauopathies. J Neuroendocrinol. 2020;32(1):e12796.

198. Cagnin A, Brooks DJ, Kennedy AM, Gunn RN, Myers R, Turkheimer FE, et al. In-vivo measurement of activated microglia in dementia. Lancet. 2001;358(9280):461-7.

199. Wiley CA, Lopresti BJ, Venneti S, Price J, Klunk WE, DeKosky ST, et al. Carbon 11-labeled Pittsburgh Compound B and carbon 11-labeled (R)-PK11195 positron emission tomographic imaging in Alzheimer disease. Arch Neurol. 2009;66(1):60-7.

200. Schuitemaker A, Kropholler MA, Boellaard R, van der Flier WM, Kloet RW, van der Doef TF, et al. Microglial activation in Alzheimer's disease: an (R)-[(1)(1)C]PK11195 positron emission tomography study. Neurobiol Aging. 2013;34(1):128-36.

201. Venneti S, Lopresti BJ, Wang G, Hamilton RL, Mathis CA, Klunk WE, et al. PK11195 labels activated microglia in Alzheimer's disease and in vivo in a mouse model using PET. Neurobiol Aging. 2009;30(8):1217-26.

202. Kravitz E, Gaisler-Salomon I, Biegon A. Hippocampal glutamate NMDA receptor loss tracks progression in Alzheimer's disease: quantitative autoradiography in postmortem human brain. PLoS One. 2013;8(11):e81244.

203. Best L, Ghadery C, Pavese N, Tai YF, Strafella AP. New and Old TSPO PET Radioligands for Imaging Brain Microglial Activation in Neurodegenerative Disease. Curr Neurol Neurosci Rep. 2019;19(5):24.

204. Nutma E, Stephenson JA, Gorter RP, de Bruin J, Boucherie DM, Donat CK, et al. A quantitative neuropathological assessment of translocator protein expression in multiple sclerosis. Brain. 2019;142(11):3440-55.

205. Yokokura M, Terada T, Bunai T, Nakaizumi K, Takebayashi K, Iwata Y, et al. Depiction of microglial activation in aging and dementia: Positron emission tomography with [(11)C]DPA713 versus [(11)C](R)PK11195. J Cereb Blood Flow Metab. 2017;37(3):877-89.

206. Gulyas B, Makkai B, Kasa P, Gulya K, Bakota L, Varszegi S, et al. A comparative autoradiography study in post mortem whole hemisphere human brain slices taken from Alzheimer patients and age-matched controls using two radiolabelled DAA1106 analogues with high affinity to the peripheral benzodiazepine receptor (PBR) system. Neurochem Int. 2009;54(1):28-36.

207. Lyoo CH, Ikawa M, Liow JS, Zoghbi SS, Morse CL, Pike VW, et al. Cerebellum Can Serve As a Pseudo-Reference Region in Alzheimer Disease to Detect Neuroinflammation Measured with PET Radioligand Binding to Translocator Protein. J Nucl Med. 2015;56(5):701-6.

208. Braak H, Braak E, Bohl J, Lang W. Alzheimer's disease: amyloid plaques in the cerebellum. J Neurol Sci. 1989;93(2-3):277-87.

209. Garland EF, Dennett O, Lau LC, Chatelet DS, Bottlaender M, Nicoll JAR, et al. The mitochondrial protein TSPO in Alzheimer's disease: relation to the severity of AD pathology and the neuroinflammatory environment. J Neuroinflammation. 2023;20(1):186.

210. Kreisl WC, Lyoo CH, McGwier M, Snow J, Jenko KJ, Kimura N, et al. In vivo radioligand binding to translocator protein correlates with severity of Alzheimer's disease. Brain. 2013;136(Pt 7):2228-38.

211. Chauveau F, Van Camp N, Dolle F, Kuhnast B, Hinnen F, Damont A, et al. Comparative evaluation of the translocator protein radioligands 11C-DPA-713, 18F-DPA-714, and 11C-PK11195 in a rat model of acute neuroinflammation. J Nucl Med. 2009;50(3):468-76.

212. Hu W, Pan D, Wang Y, Bao W, Zuo C, Guan Y, et al. PET Imaging for Dynamically Monitoring Neuroinflammation in APP/PS1 Mouse Model Using [(18)F]DPA714. Front Neurosci. 2020;14:810.

213. Golla SS, Boellaard R, Oikonen V, Hoffmann A, van Berckel BN, Windhorst AD, et al. Quantification of [18F]DPA-714 binding in the human brain: initial studies in healthy controls and Alzheimer's disease patients. J Cereb Blood Flow Metab. 2015;35(5):766-72.

214. Golla SS, Boellaard R, Oikonen V, Hoffmann A, van Berckel BN, Windhorst AD, et al. Parametric Binding Images of the TSPO Ligand 18F-DPA-714. J Nucl Med. 2016;57(10):1543-7.

215. Owen DR, Yeo AJ, Gunn RN, Song K, Wadsworth G, Lewis A, et al. An 18-kDa translocator protein (TSPO) polymorphism explains differences in binding affinity of the PET radioligand PBR28. J Cereb Blood Flow Metab. 2012;32(1):1-5.

216. Li F, Liu J, Zheng Y, Garavito RM, Ferguson-Miller S. Protein structure. Crystal structures of translocator protein (TSPO) and mutant mimic of a human polymorphism. Science. 2015;347(6221):555-8.

217. Costa B, Pini S, Gabelloni P, Da Pozzo E, Abelli M, Lari L, et al. The spontaneous Ala147Thr amino acid substitution within the translocator protein influences pregnenolone production in lymphomonocytes of healthy individuals. Endocrinology. 2009;150(12):5438-45.

218. Owen DR, Gunn RN, Rabiner EA, Bennacef I, Fujita M, Kreisl WC, et al. Mixed-affinity binding in humans with 18-kDa translocator protein ligands. J Nucl Med. 2011;52(1):24-32.

219. Tiwari AK, Ji B, Yui J, Fujinaga M, Yamasaki T, Xie L, et al. [18F]FEBMP: Positron Emission Tomography Imaging of TSPO in a Model of Neuroinflammation in Rats, and in vitro Autoradiograms of the Human Brain. Theranostics. 2015;5(9):961-9.

220. Zanotti-Fregonara P, Pascual B, Rizzo G, Yu M, Pal N, Beers D, et al. Head-to-Head Comparison of (11)C-PBR28 and (18)F-GE180 for Quantification of the Translocator Protein in the Human Brain. J Nucl Med. 2018;59(8):1260-6.

221. Horti AG, Naik R, Foss CA, Minn I, Misheneva V, Du Y, et al. PET imaging of microglia by targeting macrophage colony-stimulating factor 1 receptor (CSF1R). Proc Natl Acad Sci U S A. 2019;116(5):1686-91.

222. Ahmad R, Postnov A, Bormans G, Versijpt J, Vandenbulcke M, Van Laere K. Decreased in vivo availability of the cannabinoid type 2 receptor in Alzheimer's disease. Eur J Nucl Med Mol Imaging. 2016;43(12):2219-27.

223. Francistiova L, Bianchi C, Di Lauro C, Sebastian-Serrano A, de Diego-Garcia L, Kobolak J, et al. The Role of P2X7 Receptor in Alzheimer's Disease. Front Mol Neurosci. 2020;13:94.

224. Territo PR, Meyer JA, Peters JS, Riley AA, McCarthy BP, Gao M, et al. Characterization of (11)C-GSK1482160 for Targeting the P2X7 Receptor as a Biomarker for Neuroinflammation. J Nucl Med. 2017;58(3):458-65.

225. Beaino W, Janssen B, Kooij G, van der Pol SMA, van Het Hof B, van Horssen J, et al. Purinergic receptors P2Y12R and P2X7R: potential targets for PET imaging of microglia phenotypes in multiple sclerosis. J Neuroinflammation. 2017;14(1):259.

226. Bankhead P, Loughrey MB, Fernandez JA, Dombrowski Y, McArt DG, Dunne PD, et al. QuPath: Open source software for digital pathology image analysis. Sci Rep. 2017;7(1):16878.

227. Courtney JM, Morris GP, Cleary EM, Howells DW, Sutherland BA. An Automated Approach to Improve the Quantification of Pericytes and Microglia in Whole Mouse Brain Sections. eNeuro. 2021;8(6).

228. Albrecht DS, Normandin MD, Shcherbinin S, Wooten DW, Schwarz AJ, Zurcher NR, et al. Pseudoreference Regions for Glial Imaging with (11)C-PBR28: Investigation in 2 Clinical Cohorts. J Nucl Med. 2018;59(1):107-14.

229. Bottcher C, Schlickeiser S, Sneeboer MAM, Kunkel D, Knop A, Paza E, et al. Human microglia regional heterogeneity and phenotypes determined by multiplexed single-cell mass cytometry. Nat Neurosci. 2019;22(1):78-90.

230. Dickson TC, Vickers JC. The morphological phenotype of beta-amyloid plaques and associated neuritic changes in Alzheimer's disease. Neuroscience. 2001;105(1):99-107.

231. Hu W, Wu F, Zhang Y, Gong CX, Iqbal K, Liu F. Expression of Tau Pathology-Related Proteins in Different Brain Regions: A Molecular Basis of Tau Pathogenesis. Front Aging Neurosci. 2017;9:311.

232. Condello C, Yuan P, Schain A, Grutzendler J. Microglia constitute a barrier that prevents neurotoxic protofibrillar Abeta42 hotspots around plaques. Nat Commun. 2015;6:6176.

233. Marlatt MW, Bauer J, Aronica E, van Haastert ES, Hoozemans JJ, Joels M, et al. Proliferation in the Alzheimer hippocampus is due to microglia, not astroglia, and occurs at sites of amyloid deposition. Neural Plast. 2014;2014:693851.

234. Streit WJ, Braak H, Del Tredici K, Leyh J, Lier J, Khoshbouei H, et al. Microglial activation occurs late during preclinical Alzheimer's disease. Glia. 2018;66(12):2550-62.

235. Paasila PJ, Davies DS, Sutherland GT, Goldsbury C. Clustering of activated microglia occurs before the formation of dystrophic neurites in the evolution of Abeta plaques in Alzheimer's disease. Free Neuropathol. 2020;1.

236. Cai Z, Qiao PF, Wan CQ, Cai M, Zhou NK, Li Q. Role of Blood-Brain Barrier in Alzheimer's Disease. J Alzheimers Dis. 2018;63(4):1223-34.

237. Lue LF, Schmitz CT, Serrano G, Sue LI, Beach TG, Walker DG. TREM2 Protein Expression Changes Correlate with Alzheimer's Disease Neurodegenerative Pathologies in Post-Mortem Temporal Cortices. Brain Pathol. 2015;25(4):469-80.

238. Rangaraju S, Gearing M, Jin LW, Levey A. Potassium channel Kv1.3 is highly expressed by microglia in human Alzheimer's disease. J Alzheimers Dis. 2015;44(3):797-808.

239. Serrano-Pozo A, Gomez-Isla T, Growdon JH, Frosch MP, Hyman BT. A phenotypic change but not proliferation underlies glial responses in Alzheimer disease. Am J Pathol. 2013;182(6):2332-44.

240. Davies DS, Ma J, Jegathees T, Goldsbury C. Microglia show altered morphology and reduced arborization in human brain during aging and Alzheimer's disease. Brain Pathol. 2017;27(6):795-808.

241. Singh-Bains MK, Linke V, Austria MDR, Tan AYS, Scotter EL, Mehrabi NF, et al. Altered microglia and neurovasculature in the Alzheimer's disease cerebellum. Neurobiol Dis. 2019;132:104589.

242. Mattiace LA, Davies P, Dickson DW. Detection of HLA-DR on microglia in the human brain is a function of both clinical and technical factors. Am J Pathol. 1990;136(5):1101-14.

243. Christie RH, Freeman M, Hyman BT. Expression of the macrophage scavenger receptor, a multifunctional lipoprotein receptor, in microglia associated with senile plaques in Alzheimer's disease. Am J Pathol. 1996;148(2):399-403.

244. Dani M, Wood M, Mizoguchi R, Fan Z, Walker Z, Morgan R, et al. Microglial activation correlates in vivo with both tau and amyloid in Alzheimer's disease. Brain. 2018;141(9):2740-54.

245. Malpetti M, Kievit RA, Passamonti L, Jones PS, Tsvetanov KA, Rittman T, et al. Microglial activation and tau burden predict cognitive decline in Alzheimer's disease. Brain. 2020;143(5):1588-602.

246. Navarro V, Sanchez-Mejias E, Jimenez S, Munoz-Castro C, Sanchez-Varo R, Davila JC, et al. Microglia in Alzheimer's Disease: Activated, Dysfunctional or Degenerative. Front Aging Neurosci. 2018;10:140.

247. Sanchez-Mejias E, Navarro V, Jimenez S, Sanchez-Mico M, Sanchez-Varo R, Nunez-Diaz C, et al. Soluble phospho-tau from Alzheimer's disease hippocampus drives microglial degeneration. Acta Neuropathol. 2016;132(6):897-916.

248. Cribbs DH, Berchtold NC, Perreau V, Coleman PD, Rogers J, Tenner AJ, et al. Extensive innate immune gene activation accompanies brain aging, increasing vulnerability to cognitive decline and neurodegeneration: a microarray study. J Neuroinflammation. 2012;9:179.

249. Taipa R, das Neves SP, Sousa AL, Fernandes J, Pinto C, Correia AP, et al. Proinflammatory and anti-inflammatory cytokines in the CSF of patients with Alzheimer's disease and their correlation with cognitive decline. Neurobiol Aging. 2019;76:125-32.

250. Huang Z, Ha GK, Petitto JM. IL-15 and IL-15R alpha gene deletion: effects on T lymphocyte trafficking and the microglial and neuronal responses to facial nerve axotomy. Neurosci Lett. 2007;417(2):160-4.

251. Broux B, Mizee MR, Vanheusden M, van der Pol S, van Horssen J, Van Wijmeersch B, et al. IL-15 amplifies the pathogenic properties of CD4+CD28- T cells in multiple sclerosis. J Immunol. 2015;194(5):2099-109.

252. Rentzos M, Zoga M, Paraskevas GP, Kapaki E, Rombos A, Nikolaou C, et al. IL-15 is elevated in cerebrospinal fluid of patients with Alzheimer's disease and frontotemporal dementia. J Geriatr Psychiatry Neurol. 2006;19(2):114-7.

253. Yamashita U, Kuroda E. Regulation of macrophage-derived chemokine (MDC, CCL22) production. Crit Rev Immunol. 2002;22(2):105-14.

254. Peferoen LA, Vogel DY, Ummenthum K, Breur M, Heijnen PD, Gerritsen WH, et al. Activation status of human microglia is dependent on lesion formation stage and remyelination in multiple sclerosis. J Neuropathol Exp Neurol. 2015;74(1):48-63.

255. Togo T, Akiyama H, Iseki E, Kondo H, Ikeda K, Kato M, et al. Occurrence of T cells in the brain of Alzheimer's disease and other neurological diseases. J Neuroimmunol. 2002;124(1-2):83-92.

256. Tarkowski E, Wallin A, Regland B, Blennow K, Tarkowski A. Local and systemic GM-CSF increase in Alzheimer's disease and vascular dementia. Acta Neurol Scand. 2001;103(3):166-74.

257. Kiyota T, Machhi J, Lu Y, Dyavarshetty B, Nemati M, Yokoyama I, et al. Granulocyte-macrophage colony-stimulating factor neuroprotective activities in Alzheimer's disease mice. J Neuroimmunol. 2018;319:80-92.

258. Strobel S, Grunblatt E, Heinsen H, Riederer P, Espach T, Meder M, et al. Astrocyte- and Microglia-Specific Mitochondrial DNA Deletions Levels in Sporadic Alzheimer's Disease. J Alzheimers Dis. 2019;67(1):149-57.

259. Cruikshank WW, Kornfeld H, Center DM. Interleukin-16. J Leukoc Biol. 2000;67(6):757-66.

260. Anvar NE, Saliminejad K, Ohadi M, Kamali K, Daneshmand P, Khorshid HR. Association between polymorphisms in Interleukin-16 gene and risk of late-onset Alzheimer's disease. J Neurol Sci. 2015;358(1-2):324-7.

261. Motta M, Imbesi R, Di Rosa M, Stivala F, Malaguarnera L. Altered plasma cytokine levels in Alzheimer's disease: correlation with the disease progression. Immunol Lett. 2007;114(1):46-51.

262. Wimberley C, Lavisse S, Hillmer A, Hinz R, Turkheimer F, Zanotti-Fregonara P. Kinetic modeling and parameter estimation of TSPO PET imaging in the human brain. Eur J Nucl Med Mol Imaging. 2021;49(1):246-56.

263. Toppala S, Ekblad LL, Tuisku J, Helin S, Johansson JJ, Laine H, et al. Association of Early beta-Amyloid Accumulation and Neuroinflammation Measured With [(11)C]PBR28 in Elderly Individuals Without Dementia. Neurology. 2021;96(12):e1608-e19.

264. Bullich S, Seibyl J, Catafau AM, Jovalekic A, Koglin N, Barthel H, et al. Optimized classification of (18)F-Florbetaben PET scans as positive and negative using an SUVR quantitative approach and comparison to visual assessment. Neuroimage Clin. 2017;15:325-32.

265. Neuropathology Group. Medical Research Council Cognitive F, Aging S. Pathological correlates of late-onset dementia in a multicentre, community-based population in England and Wales. Neuropathology Group of the Medical Research Council Cognitive Function and Ageing Study (MRC CFAS). Lancet. 2001;357(9251):169-75.

266. International HapMap C. The International HapMap Project. Nature. 2003;426(6968):789-96.

267. Nutma E, Ceyzeriat K, Amor S, Tsartsalis S, Millet P, Owen DR, et al. Cellular sources of TSPO expression in healthy and diseased brain. Eur J Nucl Med Mol Imaging. 2021;49(1):146-63.

268. Peress NS, Fleit HB, Perillo E, Kuljis R, Pezzullo C. Identification of Fc gamma RI, II and III on normal human brain ramified microglia and on microglia in senile plaques in Alzheimer's disease. J Neuroimmunol. 1993;48(1):71-9.

269. Lertkiatmongkol P, Liao D, Mei H, Hu Y, Newman PJ. Endothelial functions of platelet/endothelial cell adhesion molecule-1 (CD31). Curr Opin Hematol. 2016;23(3):253-9.

270. Kim WK, Alvarez X, Fisher J, Bronfin B, Westmoreland S, McLaurin J, et al. CD163 identifies perivascular macrophages in normal and viral encephalitic brains and potential precursors to perivascular macrophages in blood. Am J Pathol. 2006;168(3):822-34.

271. Friedman BA, Srinivasan K, Ayalon G, Meilandt WJ, Lin H, Huntley MA, et al. Diverse Brain Myeloid Expression Profiles Reveal Distinct Microglial Activation States and Aspects of Alzheimer's Disease Not Evident in Mouse Models. Cell Rep. 2018;22(3):832-47.

272. Rangaraju S, Dammer EB, Raza SA, Rathakrishnan P, Xiao H, Gao T, et al. Identification and therapeutic modulation of a pro-inflammatory subset of disease-associated-microglia in Alzheimer's disease. Mol Neurodegener. 2018;13(1):24.

273. Beckers L, Ory D, Geric I, Declercq L, Koole M, Kassiou M, et al. Increased Expression of Translocator Protein (TSPO) Marks Pro-inflammatory Microglia but Does Not Predict Neurodegeneration. Mol Imaging Biol. 2018;20(1):94-102.

274. Nutma E, Gebro E, Marzin MC, van der Valk P, Matthews PM, Owen DR, et al. Activated microglia do not increase 18 kDa translocator protein (TSPO) expression in the multiple sclerosis brain. Glia. 2021;69(10):2447-58.

275. Tan YL, Yuan Y, Tian L. Microglial regional heterogeneity and its role in the brain. Mol Psychiatry. 2020;25(2):351-67.

276. Wojtera M, Sobow T, Kloszewska I, Liberski PP, Brown DR, Sikorska B. Expression of immunohistochemical markers on microglia in Creutzfeldt-Jakob disease and Alzheimer's disease: morphometric study and review of the literature. Folia Neuropathol. 2012;50(1):74-84.

277. Giulian D, Haverkamp LJ, Li J, Karshin WL, Yu J, Tom D, et al. Senile plaques stimulate microglia to release a neurotoxin found in Alzheimer brain. Neurochem Int. 1995;27(1):119-37.

278. Venneti S, Wang G, Nguyen J, Wiley CA. The positron emission tomography ligand DAA1106 binds with high affinity to activated microglia in human neurological disorders. J Neuropathol Exp Neurol. 2008;67(10):1001-10.

279. Liu B, Le KX, Park MA, Wang S, Belanger AP, Dubey S, et al. In Vivo Detection of Age- and Disease-Related Increases in Neuroinflammation by 18F-GE180 TSPO MicroPET Imaging in Wild-Type and Alzheimer's Transgenic Mice. J Neurosci. 2015;35(47):15716-30.

280. Tournier BB, Tsartsalis S, Ceyzeriat K, Medina Z, Fraser BH, Gregoire MC, et al. Fluorescence-activated cell sorting to reveal the cell origin of radioligand binding. J Cereb Blood Flow Metab. 2020;40(6):1242-55.

281. Lee E, Eo JC, Lee C, Yu JW. Distinct Features of Brain-Resident Macrophages: Microglia and Non-Parenchymal Brain Macrophages. Mol Cells. 2021;44(5):281-91.

282. Vicente-Rodriguez M, Singh N, Turkheimer F, Peris-Yague A, Randall K, Veronese M, et al. Resolving the cellular specificity of TSPO imaging in a rat model of peripherally-induced neuroinflammation. Brain Behav Immun. 2021;96:154-67.

283. Tournier BB, Tsartsalis S, Ceyzeriat K, Fraser BH, Gregoire MC, Kovari E, et al. Astrocytic TSPO Upregulation Appears Before Microglial TSPO in Alzheimer's Disease. J Alzheimers Dis. 2020;77(3):1043-56.

284. Denora N, Laquintana V, Trapani A, Suzuki H, Sawada M, Trapani G. New fluorescent probes targeting the mitochondrial-located translocator protein 18 kDa (TSPO) as activated microglia imaging agents. Pharm Res. 2011;28(11):2820-32.

285. Wongso H. Recent progress on the development of fluorescent probes targeting the translocator protein 18 kDa (TSPO). Anal Biochem. 2022;655:114854.

286. Laquintana V, Denora N, Lopedota A, Suzuki H, Sawada M, Serra M, et al. N-benzyl-2-(6,8-dichloro-2-(4-chlorophenyl)imidazo[1,2-a]pyridin-3-yl)-N-(6-(7-nitrobenzo[c][1,2,5]oxadiazol-4-ylamino)hexyl)acetamide as a new fluorescent probe for peripheral benzodiazepine receptor and microglial cell visualization. Bioconjug Chem. 2007;18(5):1397-407.

287. Howat WJ, Wilson BA. Tissue fixation and the effect of molecular fixatives on downstream staining procedures. Methods. 2014;70(1):12-9.

288. Prasher DC, Eckenrode VK, Ward WW, Prendergast FG, Cormier MJ. Primary structure of the Aequorea victoria green-fluorescent protein. Gene. 1992;111(2):229-33.

289. Brelje TC, Wessendorf MW, Sorenson RL. Multicolor laser scanning confocal immunofluorescence microscopy: practical application and limitations. Methods Cell Biol. 2002;70:165-244.

290. Gomez-Nicola D, Boche D. Post-mortem analysis of neuroinflammatory changes in human Alzheimer's disease. Alzheimers Res Ther. 2015;7(1):42.

291. Griem-Krey N, Klein AB, Herth M, Wellendorph P. Autoradiography as a Simple and Powerful Method for Visualization and Characterization of Pharmacological Targets. J Vis Exp. 2019(145).

292. Gray DA, Woulfe J. Lipofuscin and aging: a matter of toxic waste. Sci Aging Knowledge Environ. 2005;2005(5):re1.